Max-Planck-Institut für Astrophysik

Type Ia Supernovae: Bolometric properties and new tools for photometric techniques

Maximilian Stritzinger

Vollständiger Abdruck der von der Fakultät für Physik der Technischen Universität München zur Erlangung des akademischen Grades eines

Doktors der Naturwissenschaften

genehmigten Dissertation.

Vorsitzender:	Univ.-Prof. Dr. L. Oberauer
Prüfer der Dissertation:	
	1. Hon.-Prof. Dr. W. Hillebrandt
	2. Univ.-Prof. Dr. M. Lindner

Die Dissertation wurde am 10. 10 2005 bei der Technischen Universität München eingereicht und durch die Fakultät für Physik am 17. 11. 2005 angenommen.

Contents

1. Introduction **1**

2. Observational and theoretical aspects of SNe Ia **3**
2.1. Historical perspective . . . 3
2.2. Classification of Supernovae . . . 4
2.3. Basic Observational Properties . . . 5
2.3.1. Spectra . . . 5
2.3.2. Light curves of SNe Ia . . . 7
2.4. Progenitor models . . . 9
2.5. SNe Ia, Cosmology and Implications . . . 10

3. Observational Data **13**
3.1. Light curve data . . . 13
3.2. Reddening . . . 13
3.3. Distances . . . 13

4. Bolometric light curves of SNe Ia **19**
4.1. The physics of a UVOIR bolometric light curve . . . 19
4.2. Construction of UVOIR light curves . . . 20
4.3. Results . . . 22
4.3.1. Maximum luminosity and ^{56}Ni mass . . . 23
4.3.2. Evolution of the post maximum UVOIR light curve . . . 27
4.3.3. γ-ray escape fraction . . . 29
4.4. Discussion . . . 30

5. Ejected masses of SNe Ia progenitor systems **33**
5.1. Introduction . . . 33
5.2. Method to determine the ejected mass . . . 33
5.3. Results . . . 38
5.4. Discussion . . . 42

6. Lower limits on the Hubble constant from models of SNe Ia **47**
6.1. Introduction . . . 47
6.2. Observational data . . . 48
6.3. ^{56}Ni yields from explosion models . . . 48
6.4. $H_\circ$ from model ^{56}Ni masses . . . 52

6.4.1. Connecting $H_\circ$ and the model luminosities . . . 52
6.4.2. Results . . . 53
6.5. $H_\circ$ through the Hubble diagram of SNe Ia . . . 55
6.5.1. Results . . . 57
6.6. Discussion . . . 57

7. New spectrophotometric standards stars useful for S-corrections 59
7.1. Introduction . . . 59
7.2. S-corrections . . . 60
7.3. Observations . . . 61
7.4. Spectroscopic reductions . . . 62
7.5. Results . . . 66
7.5.1. Program stars . . . 66
7.5.2. The Sun, Sirius and Vega . . . 69

8. Conclusion 87

A. An Atlas of *UVOIR* light curves 89

Bibliography 201

1. Introduction

Type Ia supernovae (hereafter SNe Ia) have become an exceptional tool in modern astronomy. Due to their large luminosity and apparent uniformity they can be used to constrain cosmological parameters and, as of yet, provide the only *direct* evidence for the existence of dark energy (Riess et al. 1998, Perlmutter et al. 1999). Besides their use as cosmological yardsticks, SNe Ia are of interests because they are thought to be the main contributors to the chemical enrichment of the universe. Additionally they also have a significant influence on the early evolution of galaxies as well as feedback effects upon the interstellar medium.

From a theoretical point of view SNe Ia offers one of the most challenging physical systems in astrophysics to model. Successful SN Ia explosion models require a combination of many disciplines in physics over a large range of scales. With advances in today's generation of supercomputers it has only recently become feasible to perform realistic 3-D simulations (see Hillebrandt & Niemeyer 2000). However, despite the progress in our understanding of SNe Ia, several key issues related to the nature of their progenitor systems and the physics of the explosion mechanisms have remained unsolved. In fact not one self-consistent explosion model has yet been presented that can account for the observed range in luminosity during maximum light. Our lack of understanding of both the progenitor systems and the exact nature of the explosion mechanisms is unsettling and must be addressed if we are to have confidence in the use of SNe Ia as distance indicators.

Due to their important role in astrophysics, a number of intensive research programmes (both observational and theoretical) throughout the world have worked diligently to increase our understanding of SNe Ia. As a result a large amount of observational data has become available with superb temporal coverage of the evolution of SNe Ia. With these data sets we are now in a position to conduct a systematic investigation of the photometric and spectroscopic properties of SNe Ia.

The main theme of this thesis is to use photometric observations of well-observed SNe Ia in order to gain further insight into the true nature of these stellar explosions. In particular we use broad-band photometry to derive bolometric light curves for a large number of events. With the bolometric light curves we are able to place constraints on a number of global parameters that relate to the elusive progenitor systems, explosion mechanisms, radiation physics and hence the temporal evolution of the luminosity. Additionally we couple the bolometric flux at maximum light with results obtained from the best available numerical models to place limits on the Hubble constant, independent of any external calibrators.

The most useful result of this thesis for the Astronomical community is not the study of SNe Ia, but rather the presentation of a comprehensive set of spectrophotometric Landolt standard stars. As the reader shall later see, this catalog will not only benefit researchers of supernovae, but anyone who wishes to obtain precise spectrophotometric observations of any celestial object.

Organization of this thesis

The ordering of this thesis is as follows. Chapter 2 gives an overview of SNe Ia's observational properties, their progenitor models and their use as distance indicators. References and basic information for all the SNe Ia that we have compiled for this study are given in Chapter 3. In Chapter 4 we present an analysis of the bolometric light curves and Chapter 5 presents the parameterized model to place constraints on the ejected mass for a number of SNe Ia. In Chapter 6 we proceed to place lower limits on the Hubble constant. In Chapter 7 we present an atlas of spectrophotometric Landolt standards stars while Chapter 8 contains the conclusions. Finally, the appendix contains 38 bolometric light curves useful for future studies.

2. Observational and theoretical aspects of SNe Ia

2.1. Historical perspective

There is little doubt that since the time of antiquity mankind has gazed at the heavens and witnessed the appearance of a "guest star" that brilliantly marks its place in the night sky. Bewildering and mystifying these objects must have led ancient people to ponder what lies out beyond in the heavens. Artifacts from several ancient civilizations provide historical evidence of man's observance of these transient phenomena. Chinese inscriptions on tortoise shells and bones dating back to $\sim$ 1500 B.C. are some of the first known objects which record such events. From 530 B.C. to 1064 A.D, Chinese astronomers made detailed observations of numerous ($\sim$ 75) such events (Mitton 1979). SN 1054 was one of them, which was also observed and recorded in rock paintings by the Anasazi people, who were natives of the great Sonoran desert (located in present-day Arizona and New Mexico).

A renaissance in the study of supernovae (hereafter SNe) occurred in Europe during the late sixteenth century, when two spectacular events were observed. On November 11, 1572, the first of these SNe appeared in the constellation Cassiopeia. Systematic observations of this "new star" were conducted by an eccentric Danish astronomer named Tycho Brahe (1545-1601) (Brahe 1573). These observations led him to suggest that the heavens were mutable. This was a revolutionary idea at the time that directly questioned the belief held by Aristotle. The Aristotelian viewpoint stated all changes in the heavens must occur close to Earth, within the lunar sphere, while the distant sphere containing all the fixed stars was immutable. Then on October 9, 1604, Jan Brunowski (who at this time was in Prague) discovered the last SN observed in the Milky Way. He notified Johannes Kepler (1571-1630), a student of Tycho Brahe, who a week later began detailed observations of this event. Kepler's observations led Galileo Galilei (1564-1642) to speak out and challenge the ideas of Aristotle and Ptolemy. He claimed that this SNe provided conclusive evidence which supported the Copernican theory that all planets revolve around the Sun. Needless to say his views were not supported by the Roman Catholic Church, who summoned him to Rome to stand trial as a heretic.

More than two hundred years later, on August 31, 1885, the German astronomer Ernst Hartwig (1851-1923) discovered (at the Dorpat Observatory in Estonia) the first SN to be observed outside our own galaxy. This SN was located in the Andromeda galaxy. Later studies by Knut Lundmark (1889-1958) showed that this event was nearly one thousand times brighter than a normal novae (Lundmark 1920). Soon after Lundmark's observations it became clear that there existed a distinction between ordinary novae and SNe (Baade & Zwicky 1934), and that the latter occurred in large stellar systems denoted as galaxies rather than "nebula". Baade & Zwicky (1934) and Zwicky (1935) were the first to suggest the extraordinary idea that SNe

were connected with the death of a star and the subsequent formation of some sort of compact object. It was Wilson (1939) and Zwicky (1939) who first suggested that –due to their extreme brightness– SNe offered to be an attractive tool to determine distances on cosmological scales.

Since the 1940's SNe have been observed by many astronomers throughout the world. The study of these cosmic explosions has allowed us to unravel many mysteries concerning the universe. However, as we learn more about SNe, we are confronted with deeper questions concerning their origins as well as the cosmological implications they yield.

2.2. Classification of Supernovae

With more detailed observations it became apparent that there existed large differences between SNe. Minkowski (1941) classified SNe into two categories, either (1) type II –those showing strong Hydrogen Balmer emission lines or (2) type I –those with broad emission features and no Hydrogen emission lines. With the proliferation of quality data it soon became clear that some events displayed trends that showed significant deviations from this simple taxonomy scheme.

Fig 2.1 displays a modern classification diagram that allows one to disentangle the different

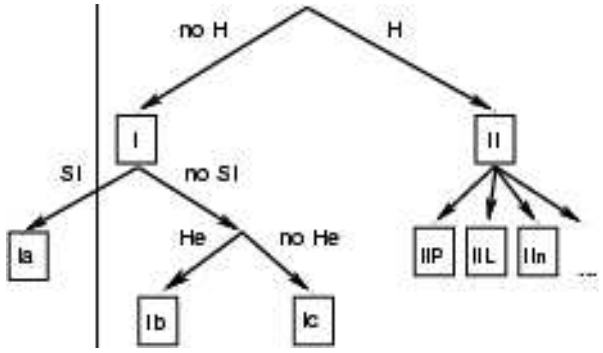

Figure 2.1.: Classification scheme of SNe

flavors of SNe.

The vertical line in Fig 2.1 separates thermonuclear SNe (type Ia) from core collapse SNe (CCSNe). All SNe right of the vertical line are believed to originate from the core collapse of a massive star ($M_{ZAMS} > 8\ M_{\odot}$)[1](see Arnett 1996, and references within). CCSNe are thought to lead to the formation of a neutron star or, in some cases, to a black hole (Brown & Bethe 1994). The variety of subclasses in the CCSN group can be attributed to differences in observed photometric and spectroscopic properties. These differences reflect the physical parameters that identify the progenitor star, e.g. the size of the progenitor's envelope, and/or interactions with the circumstellar medium. The majority of CCSNe occur in spiral galaxies and are often located

[1]ZAMS or *zero-age main sequence* refers to the mass of the progenitor star at the time when hydrogen burning is first initiated.

near star forming or H_2 regions. The reader is referred to Hamuy (2003) for a detailed review concerning the observed and physical characteristics of CCSNe, and van den Bergh et al. (2005) for a recent discussion on the host galaxies of all types of SNe.

The type I class of SNe is divided into two main groups. The first group –SNe Ia– displays a strong absorption feature in their spectra near 6150 Å. This absorption line is attributed to the blue-shifted Si II $\lambda\lambda$6347, 6371, also known as Si II λ6355. The second group of type I SNe are divided into type Ib and type Ic. The spectra of SNe Ib are characterized by having weak to nonexistent Si II $\lambda\lambda$6347, 6371 lines, and strong He I lines located at λ4471, λ5876, λ6678, and λ7065. Members of the type Ic class lack the Si II feature and have weak to absent He I lines. However, spectra of SNe Ic exhibit the Ca II H&K absorption feature, the Ca II near infrared triplet, and a O I λ7774 absorption line (Wheeler & Harkness 1990). With the first documentation of a shock wave breakout in the type Ib/c SN 1999ex (Stritzinger et al. 2002), it was established that these events are nothing more than a stripped version of a CCSN. In addition, van den Bergh et al. (2005) found no significant differences between the host galaxies of SNe Ib/c and CCSNe.

SNe Ia, on the other hand, are thought to originate from the thermonuclear disruption of a carbon oxygen (C-O) white dwarf that leaves no compact remnant (Hoyle & Fowler 1960). These events occur in all types of galaxies, ranging from old ellipticals to young spirals. The fact that some of these events occur in early type galaxies indicates that the progenitors are some sort of a highly evolved stellar system (see Chapter 2.4 for more details).

In the past few years a new class of SNe has emerged. These events (SN 1997ef, SN 1998bw, & SN 2002ap to name a few) have similar absorption features as SNe Ic, however, they are much more energetic as determined from their severely Doppler broadened absorption lines. With expansion velocities up to $\sim$ 30,000 km s^{-1} and hence explosion energies on the order of up to $E_K \sim 3 \cdot 10^{52}$ ergs, they have become known as *hypernovae*. Even more surprising, there is now conclusive evidence that these objects are related to the enigmatic γ-ray bursts.

2.3. Basic Observational Properties

This section provides a general review of the observational properties of SNe Ia. First the spectral properties are addressed. This is then followed by a discussion of their photometric behavior. A thorough review of SNe spectra is presented by Filippenko (1997). An excellent account of the photometric light curves of SNe Ia is given by Leibundgut (2000). See also Leibundgut & Suntzeff (2003), Meikle (2000) and Suntzeff (1996) for additional reviews.

2.3.1. Spectra

The detailed study of spectra provides a wealth of information. Most important of all, near maximum light spectra are the basis for the classification of SNe. In addition spectra allow us to place constraints on the energetics of the explosion, the nucleosynthesis of elements processed during nuclear burning, and the nature of the progenitor systems. Fig. 2.2 contains a temporal sequence of optical and infrared spectra for the well observed normal SN 1999ee (Hamuy et al. 2002).

Spectra of SNe Ia are (as seen in Fig. 2.2) generally characterized by containing strong absorption and emission lines imposed on top of a thermal pseudo-continuum. At early times the

optical portion of the spectra is dominated by intermediate mass elements (IMEs), e.g. O I, Mg II, Si II, S II and Ca II. There are also usually some weak Fe lines present. Absorption lines from the IMEs indicate expansion velocities of $\sim$ 10,000 km s^{-1} and are accompanied by P-Cygni profiles.[2] Some events (e.g. SN 1984A) have normal optical spectra, but have significantly larger expansion velocities of $\sim$ 20,000 km s^{-1}.

Infrared spectra display some IMEs such as Mg II, Ca II, Si II, and Fe group elements, e.g. Fe II, Co II and Ni II. There are several research groups that have been able to reproduce observed spectra rather well, however, detailed time-dependent NLTE codes have so far been difficult to construct. The modeling of infrared spectrophotometry is attractive, as this can provide an opportunity to learn more about the chemical structure of the ejecta, which may not be afforded in the optical due to line blending (see Marion et al. 2003).

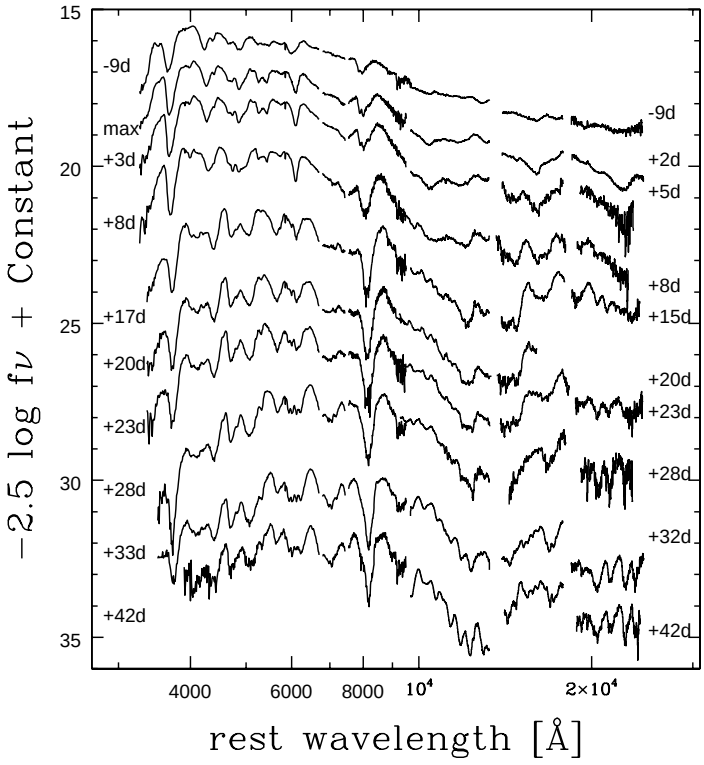

Figure 2.2.: Combined optical and infrared spectra of SN 1999ee (Hamuy et al. 2002).

As the ejecta transform to the nebular phase, both the optical and the infrared portions of the spectra become dominated by emission lines due to forbidden transitions of Fe and Co. It is evident in Fig. 2.2 that there is a depression of flux in the infrared portion compared to the optical (Meikle et al. 1997). This feature indicates that there is less flux emitted in the near infrared as opposed to optical wavelengths. At these epochs more flux is emitted in the optical

[2] A P-Cygni profile is formed from the resonant scatter of photons above the photosphere, and is consistent with an expanding atmosphere.

because there is a larger number of emitting spectral lines that efficiently radiate the thermalized photons trapped within the ejecta.

There are few ultraviolet (UV) observations of SNe Ia available, however, Kirshner et al. (1993) published IUE and HST observations of SN 1992A. In the UV there is a large suppression of flux due to severe line blanketing by Fe group elements. Early-time UV spectra may offer to be an extremely useful tool to probe the metallicity of the progenitor star.

Within the general framework just described several types of peculiar SN Ia exist that show recognizable differences compared to the 'Branch-normal' events (Branch et al. 1993). These SN Ia include the so called sub-luminous SN 1991bg-like events and the super-luminous SN 1991T-like events. Spectra of the SN 1991bg-like events typically exhibit a strong absorption line at 5700 Å, which may be due to Si II, and the presence of a wide absorption trough caused by Ti II extending from 4150 to 4400 Å. Spectra of SN 1991T-like events usually display (during the epochs prior to and during maximum light) weak Si II lines and high-excited Fe III absorption lines. Soon after maximum brightness their spectra transform to a normal SN Ia spectrum.

Li et al. (2000) used a sample of ~ 90 events and a Monte Carlo code to determine SNe Ia rates. They concluded that there is a high peculiarity rate of $> 30\%$. In addition they claim that there exists a flat luminosity function. In other words, the rate of sub-luminous to super-luminous is consistent with each other. They also noted that this high peculiarity rate suggests the existence of multiple types of progenitor systems. These could range from the Chandrasekhar mass model to the sub-Chandrasekhar mass model or the double degenerate scenario (see Chapter 2.4).

There have also been several well documented events (e.g. SN 2000cx and SN 2002cx) that display strong photometric and spectroscopic deviations from the three types of SNe Ia previously discussed. For a detailed discussion on these two SNe Ia see the following papers: Candia et al. (2003), Li et al. (2001), Thomas et al. (2004), Li et al. (2003), Branch et al. (2004a,b). See also Phillips et al. (2003) for a discussion on the abnormal SN 1999ac. Essentially these events can not be placed in either of the three SN Ia categories and/or do not conform to the luminosity-decline rate relation. The physical processes that lead to their peculiarities, the rate in which they occur, and the possible impact they may have on cosmological results are all open questions.

2.3.2. Light curves of SNe Ia

With increases in the sensitivity and linearity of modern CCDs, it has become relatively easy to assemble detailed light curves of nearby SNe Ia with meter class telescopes. Light curves from multi-band photometry prove to be a vital tool in the study of SNe Ia. All the information extracted from the light curves can be traced back to the energy inputs and subsequent radiation escape from the ejecta. With optical (and infrared) light curves it is possible to, among other things, measure the rise time to maximum light, trace the color evolution, make accurate extinction estimates, and normalize the peak luminosity in order to determine its distance from us.

Figure 2.3 displays the optical and near infrared photometry for the well observed SN 2002bo. Note that each light curve is offset with respect to the *V*-band for presentation purposes. One can immediately notice the characteristic bell shaped light curves. This is a telltale signature of SNe Ia and implies a compact sized progenitor. The time of maximum light generally occurs first in the near infrared followed by the optical passbands several days later (Contardo et al. 2000).

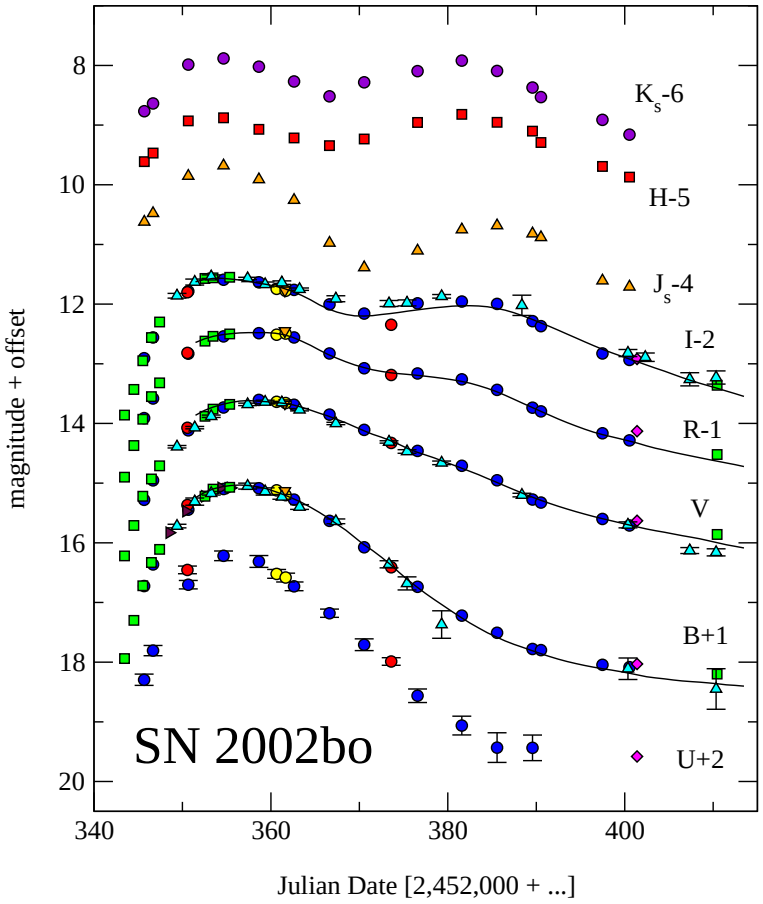

Figure 2.3.: Optical and near infrared light curves of SN 2002bo (Krisciunas et al. 2004c, Benetti et al. 2004). The different symbols in the optical light curves correspond to observations taken at different telescopes. The near infrared light curves are in the system of Persson et al. (1998) (see Chapter 7.5.2). The solid lines are the best fitted template light curves calculated using the Prieto et al. (2005) Δm_{15}(B) fitting program.

After ~ 30 days past maximum brightness the *UB* light curves quickly decline in luminosity until ~ 60 days when they reach a linear decline. As we move towards the red wavelengths there usually is an inflection point in the *V*-band light curve between +20 to +40 days past maximum brightness. In the *RI*-bands this feature is associate with a secondary maximum. It is even more pronounced in the near infrared where a prevalent secondary maximum is usually observed in the *zyJHK* light curves. This inflection point is thought to be caused by a redistribution of flux (Suntzeff 1996), however, the mechanism that leads to its presence has not yet been fully explained. Pinto & Eastman (2000b) have suggested that it is caused by the time dependence of the opacity. As the photosphere recedes into the ejecta there is a decrease in mean opacity, which leads to a shortened diffusion time. The net result is the release of 'stored energy' that has previously been trapped within the photosphere. A more detailed description of the physics that drives the evolution of the light curve is provided in Chapter 4.1.

The SN 1991T-like SNe Ia are usually somewhat more luminous compared to the normal

events, whereas SN 1991bg-like events can be significantly less luminous and always lack a secondary maximum. These differences are investigated in Chapter 4.3. From the detailed studies of several dozen objects we know that in the optical SNe Ia are indeed not a pure standard candle. However, recently, Krisciunas et al. (2004a,c) have shown that there is no decline rate relation in the near infrared. In other words SNe Ia appear to be true standard candles in the *JHK* passbands.

2.4. Progenitor models

"**WHAT IS THE PROGENITOR SYSTEM OF A SN Ia?**" This question can often lead a group of civilized scientists into a passionate and heated debate! The reasons why it is difficult to identify the true progenitor system is not as embarrassing as one may initially think. (Livio (2000) provides a complete (and readable) review of the most viable progenitor scenarios). The fact that some SN Ia occur in elliptical galaxies and that their spectra contain no H and He lines suggests that the progenitor systems are associated with an old stellar population. However, it appears that there exists a correlation between the host galaxy and the type of SN Ia. Van den Bergh et al. (2005) have shown that SN 1991bg-like events are more likely to occur in early-type E and E/Sa galaxies, while SN 1991T-like events occur in intermediate-type galaxies. They have found that this difference is significant at the 99.9% level! This evidence suggests that these events may possibly have different progenitor systems. Other difficulties that conspire against our efforts to determine the progenitor systems include the small rate of occurrence of SN Ia and the compactness of their proposed progenitor systems.

Each of the three models that are described below consists of some configuration of a binary system. Single stellar systems are ruled out based on physical arguments. Single stars that produce white dwarfs have no possibility to accrete enough matter to reach the Chandrasekhar mass and therefore can not ignite. In addition the lack of observed X-ray emission excludes the alternative that SN Ia are associated with the formation of either a neutron star or a black hole. Now we proceed to describe the three main progenitor scenarios.

Currently the favored view of a SN Ia's progenitor system is an accreting C-O white dwarf in a binary system that undergoes thermonuclear incineration at or near the Chandrasekhar mass (for reviews see Thielemann et al. 2004, Hillebrandt & Niemeyer 2000, Arnett 1996, Woosley & Weaver 1986, Nomoto et al. 1984). The energy released from burning to nuclear statistical equilibrium (NSE) at the densities and temperatures expected in these explosions completely disrupts the C-O white dwarf, while the subsequent light curve is powered by the Comptonization or "thermalization" of γ rays produced from the radioactive decay of $^{56}\mathrm{Ni} \rightarrow {}^{56}\mathrm{Co} \rightarrow {}^{56}\mathrm{Fe}$ (Pankey 1962, Colgate & McKee 1969).

Within this paradigm the C-O white dwarf accretes matter from an evolved massive star via Roche lobe overflow or through stellar winds before the explosion occurs. Recently the single degenerate model has become more favored over the double degenerate model. This is due to two recent discoveries. The first being the detection of Hα in the well observed SN 2002ic (Hamuy et al. 2003, Deng et al. 2004, Kotak et al. 2004), while more recently the companion star of Tycho Brahe's SN Ia has been identified Ruiz-Lapuente et al. (2004).

Another candidate for the progenitor system of a SN Ia is the so called sub-Chandrasekhar mass model. In this model the C-O white dwarf does not reach the necessary temperatures

and densities that leads to the formation of a flame that then causes a thermonuclear runaway. Therefore an outside catalyst is required to trigger the explosion. It has been suggested that this agent is associated with detonation(s) located at the base of a He layer that has accreted around the white dwarf (Weaver & Woosley 1980, Nomoto 1980, Sutherland & Wheeler 1984, Iben & Tutukov 1984). The He itself is thought to accrete from the white dwarf's companion star. The detonation(s) result in a compression wave that travels through the white dwarf causing the C-O core to ignite, whereupon a thermonuclear runaway ensues. This mechanism is known by several names which include: an edge lit detonation, a He ignitor, or an indirect double detonation.

Prior attempts to model sub-Chandrasekhar explosions (Woosley & Weaver 1994a, Livne & Arnett 1995, Höflich & Khokhlov 1996) have met with some success in reproducing observed light curves. However, these models typically predict a high velocity layer of ^{56}Ni and He above the IMEs, which is not observed in any spectra. It must be noted that, compared to Chandrasekhar mass models, there has been little effort made to conduct detailed 3-D simulations of sub-Chandrasekhar mass models (but, see García-Senz et al. (1999) and Benz (1997)). With more detailed modeling this progenitor channel may provide an attractive alternative to the Chandrasekhar mass models.

An alternative progenitor system that may account for the more luminous SN Ia is the so called double degenerate model. In this scenario two white dwarfs (which may vary depending on the scenario of a C-O and/or O-Ne-Mg white dwarf(s)) in a binary system merge due to the loss of gravitational wave radiation (Iben & Tutukov 1984, Webbink 1984). The smaller of the two white dwarfs is disrupted (via tidal stripping) and forms an accretion torus around the larger white dwarf. This material soon accretes onto the remaining white dwarf until it reaches a Chandrasekhar mass (Benz et al. 1990, Mochkovitch 1997). Two major problems exist with this progenitor model. The first is the difficulty for the remaining white dwarf to accrete matter at a rate in which shell flashes are suppressed. Frequent occurrence of pycnonuclear reactions on the surface of the white dwarf would lead to an insufficient amount of accreted matter necessary to ensure a thermonuclear runaway. Moreover, it has been suggested that the remaining white dwarf may collapse and lead to the formation of a neutron star rather than a SN Ia (Saio & Nomoto 1985).

In Chapter 6.3 we discuss in more detail the explosion mechanisms and results obtained from 1-D and recent 3-D simulations.

2.5. SNe Ia, Cosmology and Implications

Astronomers have long sought after a "standard candle" capable of determining accurate extragalactic distances. The quest was answered when it was realized that the extreme brightness of SNe Ia at maximum light appeared to be homogeneous for the bulk of events (see Leibundgut 2001, for a thorough review of the use of SNe Ia as distance indicators). The uncorrected peak *B*-band magnitude for *normal* SNe Ia displays a scatter of ~ 0.21 mag. If we include SN 1991bg-like events the range increases to ~ 2.5 mag! Phillips (1993) realized that the peak brightness correlates with the light curve shape. By using the so called Phillips relation (or Δm_{15}(B) method) to normalize the peak absolute magnitudes, SNe Ia have become the most accurate distance indicator past the Virgo cluster. Through application of the Phillips relation the scatter in *B*-band magnitudes reduces to ~ 0.13 mag (Parodi et al. 2000).

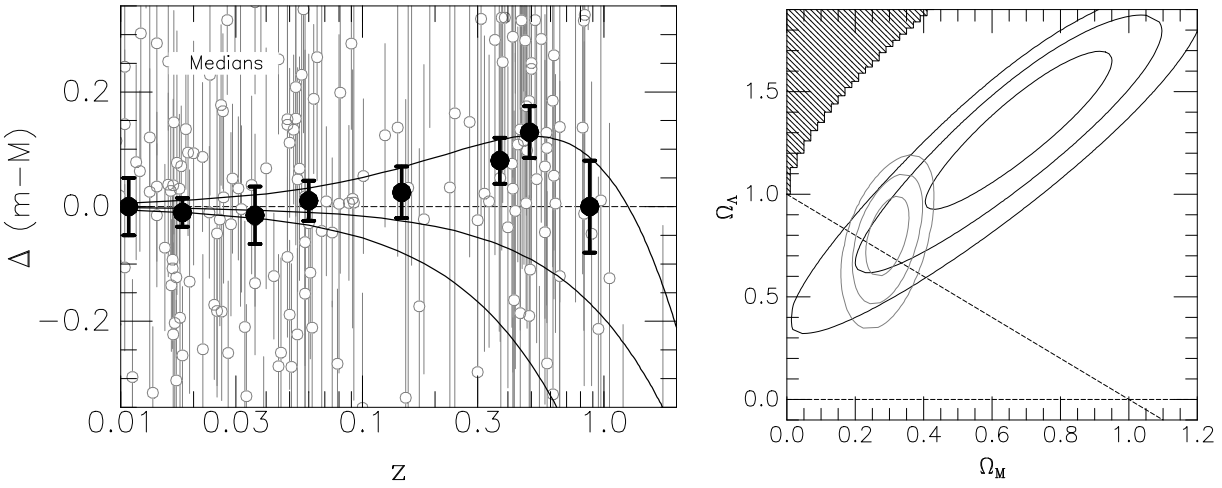

Figure 2.4.: Figure adopted from Tonry et al. (2003). *Left:* A residual Hubble diagram relative to an Einstein De-Sitter universe. Filled points are median redshift bins. The data clearly favors a universe with $\Omega_M = 0.3$, $\Omega_\Lambda = 0.7$ (top solid line). *Right:* Confi dence contours for different combinations of Ω_M and Ω_Λ. The smaller contours correspond to combined results from SNe Ia and the 2dF redshift survey (Percival et al. 2001).

Local SNe Ia are now used to determine the Hubble constant (see Chapter 6 and references within), while at high redshifts they are used to place constraints on a number of other cosmological parameters. In 1998 two independent teams reported that the high redshift SNe Ia appear to be 20% fainter compared to their nearby counterparts (Riess et al. 1998, Perlmutter et al. 1999). This result immediately implies that a large portion of the universe is dominated with a component that has a negative pressure, and thus causes cosmic acceleration. Fig. 2.4 sums up the main cosmological results obtained from observations of SNe Ia (Tonry et al. 2003). The left panel displays a modern Hubble diagram where the magnitudes have been normalized to an empty universe ($\Omega_M = 0$ and $\Omega_\Lambda = 0$). The filled circles are median values for eight redshift bins. The three solid lines correspond to different cosmological models. From top to bottom these models are (Ω_M, Ω_Λ) = (0.3, 0.7), (0.3, 0.0), and (1.0, 0.0), respectively. Clearly a flat universe dominated with a cosmological constant or a similar agent leading to an accelerated expansion best fits the data. The right panel displays 1 σ, 2 σ and 3 σ probability contours for different combinations of Ω_M and Ω_Λ. The black contours correspond to SN Ia data with a equation of state parameter equal to a negative one, i.e. $w = -1$.[3] This value is compatible with the simplest interpretation that the accelerated expansion of the universe is caused by the cosmological constant. The grey contours include SN Ia data and constraints based on results from the 2dF redshift survey (Percival et al. 2001). This figure coupled with recent results obtained from the cosmic microwave background (CMB) radiation measurements (Spergel et al. 2003), strongly suggests a universe with $\Omega_{tot} = 1$, where $\Omega_M = 0.3$ and $\Omega_\Lambda = 0.7$.

[3]The equation of state parameter is given by $w = p/(\rho c^2)$, where p is the pressure of the vacuum and ρ the energy density of the vacuum. With w = -1 the dark energy takes the form of Einstein's cosmological constant Λ. A universe with $w \neq -1$ implies an exotic form of dark energy. With $w < -1$ we obtain a dark energy that slowly decreases with the expansion of the universe. A $w > -1$ gives a universe that expands forever i.e. a "Big Rip."

With Ω_Λ being the dominant component in the universe one is forced to accept a discrepancy that has become known as the 'cosmological constant problem.' Quantum field theory calculations suggest that the energy density of the cosmological constant should be $\rho_\Lambda \sim 10^{76}$ GeV^4. This is 123 orders of magnitude larger than the observed value of $\rho_\Lambda \sim 10^{-47}$! Moreover, setting Ω_Λ in the early epochs of the universe to a very small value guarantees the acceleration to be a rather recent phenomena, but this results in the 'cosmic coincidence problem.' Why do we live at the time when Ω_Λ and Ω_M are about equal? If the cosmological constant (i.e. dark energy) had made its presences known in the early universe it would have interfered with structure formation while, if it occurred at a latter epoch, we would have not been able to observe its effects today. Currently there are many models that attempt to explain an accelerating universe. These range from Einstein's cosmological constant to dynamical models such as 'quintessence' models, which consist of time dependent scalar fields. Quintessence models are attractive because the time dependence of the dark energy addresses the fine tuning problem between the observed and predicted values of ρ_Λ. Today there is a rich literature of quintessence models that employ various forms of the Lagrangian.

Several astrophysical mechanisms have been proposed to explain why the distant sample of SNe Ia appears less luminous compared to the local sample (see Leibundgut 2001). These include novel forms of grey dust, evolution of both the progenitor systems and/or the sample, and effects due to gravitational lensing. Thus far, studies have shown that none of these mechanisms have a significant effect on the cosmological results obtained from SNe Ia, however, the statistics are still small.

3. Observational Data

3.1. Light curve data

There are a number of past (and present) dedicated monitoring programs located around the world that have assembled large collections of SNe Ia data. Programs which we have used here include: the Calán/Tololo Survey (Hamuy et al. 1995, 1996), the Center for Astrophysics (Riess et al. 1999b, Jha 2002), Supernovae Optical Infrared Survey (SOIRS) (Hamuy et al. 2001), and the European research training network on the physics of SN Ia explosions.[1]

In Table 3.1 we list the SNe Ia discussed in the next chapters as well as other pertinent information. This includes the references to the photometry, values of the color excess, and the assumed distances to each event. Appendix A contains a catalog of UVOIR light curves (in flux units) for all events listed in Table 3.1.

3.2. Reddening

Before we can analyze the bolometric light curves it is necessary to apply a reddening correction. The reddening of light emitted by extragalactic SNe Ia is not only caused by dust in our own Galaxy, but also by dust in the object's host galaxy.

Values listed for Galactic reddening were taken from the COBE dust maps of Schlegel et al. (1998), while host galaxy reddenings were procured from a variety of literature sources. To be as consistent as possible we used reddenings given in Phillips et al. (1999) for all SNe Ia that coincided with our sample. For those events not included in Phillips et al. (1999) we adopted values from the literature showing preference to those calculated via the Phillips method.

The Phillips method allows one to estimate the amount of extinction due to dust in the host galaxy of a SN Ia. This method makes use of the fact that the $B-V$ color evolution between 30 and 90 days past maximum is nearly identical for the majority of SNe Ia. With good sampling of the $B-V$ color evolution one can then calibrate the dependence of the $B_{\max}-V_{\max}$ and $V_{\max}-I_{\max}$ colors with the decline rate parameter (Δm_{15}(B), i.e. the number of B-band magnitudes that a SN Ia decreases fifteen days past maximum light). In turn Δm_{15}(B) can be used to determine the host galaxy extinction.

3.3. Distances

To place a SN Ia on an absolute flux scale requires the knowledge of an accurate distance to the host galaxy. For each event we used (if available) direct distance measurements e.g. Cepheid

[1] http://www.mpa-garching.mpg.de/ rtn/

distance (CH), Surface Brightness Fluctuations (SBF) distance or a Cepheid to cluster (CC) distance. Direct distance measurements are usually accurate to within 10%. If a direct distance measurement was not available we retrieved a redshift distance from the NASA/IPAC extragalactic database (NED) and transformed this to the CMB frame. Due to peculiar motions the redshift distances have $\sim$ 400 km s^{-1} uncertainty. Note throughout this work we assumed a Hubble constant of 72 km s^{-1} Mpc^{-1}(Freedman et al. 2001).

With the advent of the *Hubble Space Telescope* (HST) there has been a substantial effort from two groups (namely the HST Key Project (HKP) and the Saha, Tammann and Sandage (STS) group) to obtain accurate Cepheid distance measurements to galaxies that have hosted SNe Ia. Typically these two independent groups determine different distances for any one galaxy, even though they use the same data and similar data reduction software. These differences are a reflection of assumptions made in their analysis. The main factor that contributes to these discrepancies is the exact *P-L* relation used, and several other subtle nuances exacerbate the problem. These include: (1) the criteria adopted to select the Cepheids used to determine the distance, (2) if and how metallicity corrections are applied, and (3) anomalies related to the camera(s) on HST (see Parodi et al. 2000, Gibson et al. 2000, Riess et al. 2005).

In short, the HKP obtains a *short* distance scale that leads to a value of H$_\circ \sim$ 70 km s^{-1} Mpc^{-1} while the STS group determines a *long* distance scale that gives H$_\circ \sim$60 km s^{-1} Mpc^{-1}. Riess et al. (2005) have reviewed this issue, in order to reconcile the distances obtained by the two groups to galaxies that have hosted a SN Ia.

Six of the SNe Ia used in our study have a direct Cepheid distance to their host galaxy and one has a Cepheid distance to its galaxy cluster. Whether the distance scale is long or short will depend on which data (i.e. from which of these two groups) we use. This in turn will lead to either an under or over estimate of the distance. This uncertainty in the distance will affect the ^{56}Ni mass we determine and hence the ejected mass.

To illustrate the effect of this on our results, we consider the galaxy NGC 3982. This galaxy has three independent Cepheid distance measurements, one from each of the two teams just mentioned and one from Riess et al. (2005) who have used a new calibration of the *P-L* relationship and an elegant metallicity correction.

The STS group has published a distance modulus of $\mu = 31.72 \pm 0.14$ (Saha et al. 2001a), which is based on the Cepheid *P-L* relation published by Madore & Freedman (1991). Using a *P-L* relation based on ~650 Cepheids located in the Large Magellanic Cloud that were observed by the Optical Gravitational Lensing Experiment (OGLE) (Udalski et al. 2001) the HKP team concluded that $\mu = 31.56 \pm 0.08$ (Stetson & Gibson 2001). More recently Riess et al. (2005) used the Advanced Camera for Surveys on the HST to obtain a Cepheid distance. They used the *P-L* relation presented by Tammann & Reindl (2002) and Thim et al. (2003), based on only those Cepheids in the OGLE data set that have periods longer than 10 days. With this new *P-L* relation, and after applying a metallicity correction, Riess et al. found $\mu = 31.66 \pm 0.09$.

With the HKP distance modulus we obtain a ^{56}Ni mass that is 9% less compared to the STS distance modulus, and 4% less with the Riess et al. distance modulus. In turn the ejected mass derived with the HKP distance modulus is 22% greater compared to the STS distance modulus, and 13% greater compared to the Riess et al. distance modulus.

We have used a SBF distance for three SNe Ia in this sample. The zero-point for this method is based on an empirical relation derived from Cepheids, which can lead to a systematic under- or over- estimation of the distance, depending on whose Cepheids are used for the calibration. The

three SBF distances we have used are calibrated with the HKP Cepheid distances of Ferrarese et al. (2000). As pointed out by Tonry et al. (2001) the zero-point for the SBF distance scale is still being improved. With the application of the Cepheids determined with the complete set of OGLE data the SBF distances used here would be ~0.1 mag fainter. With this correction our derived ^{56}Ni masses would increase by ~8% and the ejected masses would decrease by ~16%.

Table 3.1. Well-observed SNe Ia

SN	Filters	Ref.	$E(B-V)^{a}_{gal}$	$E(B-V)_{host}$	v_{CMB} [b]	Ref[c]
SN1989B	*UBVRI*	1	0.032	0.340	797	CH 29
SN1990N	*UBVRI*	2	0.026	0.090	1604	CH 11
SN1991T	*UBVRI*	2	0.022	0.140	1012	CH 30
SN1991bg	*BVRI*	3	0.040	0.030	1322	SBF 31
SN1992A	*UBVRI*	5	0.017	0.000	1184	CC 32
SN1992bc	*BVRI*	5	0.022	0.000	5870	CMB
SN1992bo	*BVRI*	5	0.027	0.000	5151	CMB
SN1993H	*BVRI*	5	0.060	0.050	7112	CMB
SN1994D	*UBVRI*	6	0.022	0.000	1184	SBF 33
SN1994ae	*BVRI*	7	0.031	0.120	2067	CH 11
SN1995D	*BVRI*	7	0.058	0.040	2272	CMB
SN1995E	*BVRI*	7	0.027	0.740	3478	CMB
SN1995ac	*BVRI*	7	0.042	0.080	14651	CMB
SN1995al	*BVRI*	7	0.014	0.150	1776	CMB
SN1995bd	*BVRI*	7	0.495	0.150	4266	CMB
SN1996X	*UBVRI*	7, 8	0.069	0.010	2174	Δm_{15}[d] 8
SN1996bo	*BVRI*	7	0.078	0.280	4857	CMB
SN1997bp	*UBVRI*	9	0.044	0.132	2850	CMB
SN1997bq	*UBVRI*	9	0.024	0.200	2876	CMB
SN1997br	*UBVRI*	9, 10	0.113	0.237	1583	MV[e] 34
SN1998aq	*UBVRI*	11	0.014	0.002	1547	CH 11
SN1998bu	*UBVRI*	12	0.025	0.330	710	CH 35
SN1998de	*BVRI*	13	0.060	0.000	4653	CMB
SN1999aa	*UBVRI*	9, 14, 15	0.040	0.000	4546	CMB
SN1999ac	*UBVRI*	15, 16	0.046	0.120	294	CMB
SN1999aw	*BVRI*	15, 17	0.032	0.000	11754	CMB
SN1999by	*UBVRI*	18	0.016	0.000	1012	CMB
SN1999dq	*UBVRI*	3	0.024	0.139	4029	CMB
SN1999ee	*UBVRI*	19	0.020	0.280	3169	CMB
SN1999gp	*UBVRI*	9, 20	0.056	0.070	7783	CMB
SN2000E	*BVRI*	21	0.360	0.000	1281	CMB
SN2000cx	*UBVRI*	9,22	0.082	0.000	1727	SBF 31
SN2001bt	*BVRI*	23	0.065	0.256	4337	CMB
SN2001el	*UBVRI*	24	0.014	0.206	1053	CMB
SN2002bo	*UBVRI*	25	0.025	0.380	1579	CMB
SN2002cx	*BVRI*	26	0.032	0.000	7500	CMB
SN2002er	*UBVRI*	27	0.157	0.203	2577	CMB

Table 3.1 (cont'd)

SN	Filters	Ref.	$E(B-V)^{a}_{gal}$	$E(B-V)_{host}$	v_{CMB} [b]	Ref[c]
SN2003du	*UBVRI*	28	0.010	0.000	2011	CMB

[a]Taken from Schlegel et al. (1998) dust maps.

[b]Heliocentric velocities from NED transformed to the cosmic microwave background frame. Direct distance measurements are set to a Hubble scale of 72 km s^{-1} Mpc^{-1}(Freedman et al. 2001).

[c]CH – Cepheids to host galaxy, SBF– Surface Brightness Fluctuations, CC – Cepheids to cluster, CMB – cosmic microwave background, Δm_{15}[d] – Luminosity width decline rate relation, MV – mean recession velocity to group.

[d]See 8 for a detailed discussion on the distance to NGC 5061.

[e]See 10 for a detailed discussion on the distance to ESO 576-G40.

References. — (1) - Wells et al. 1994, (2) - Lira et al. 1998, (3) - Filippenko et al. 1992, Leibundgut et al. 1993, Turatto et al. 1996, (4) - Suntzeff 1996, (5) - Hamuy et al. 1996, (6) - Richmond et al. 1995, Patat et al. 1996, Meikle et al. 1996, Smith 2000, (7) - Riess et al. 1999b, (8) - Salvo et al. 2001, (9) - Jha 2002, (10) - Li et al. 1999, (11) - Riess et al. 2005, (12) - Hernandez et al. 2000, Jha et al. 1999, Suntzeff et al. 1999, (13) - Modjaz et al. 2001, (14) - Krisciunas et al. 2000, (15) - Regnault 2000, (16) - Phillips et al. 2003, (17) - Strolger et al. 2002, (18) - Garnavich et al. 2004, (19) - Stritzinger et al. 2002, (20) - Krisciunas et al. 2001, (21) - Vinkó et al. 2001, Valentini et al. 2003, (22) - Candia et al. 2003, Li et al. 2003, (23) - Krisciunas et al. 2004c, (24) - Krisciunas et al. 2003, (25) - Benetti et al. 2004, Krisciunas et al. 2004c, (26) - Li et al. 2003, (27) - Pignata et al. 2004, (28) - Stanishev 2005, (29) - Saha et al. 1999, (30) - Saha et al. 2001b, (31) - Tonry et al. 2001, (32) - Madore et al. 1999, (33) - Ajhar et al. 2001, (34) - Garcia 1993, (35) - Freedman et al. 2001.

4. Bolometric light curves of SNe Ia

This chapter addresses the overall bolometric properties of SNe Ia. In Sect. 4.1 we discuss the physical characteristics of a bolometric light curve as it evolves in time. Next we briefly discuss in Sect. 4.2 the method in which a bolometric light curve is constructed from broad-band photometry. Results are presented in Sect. 4.3 followed by a discussion in Sect. 4.4.

4.1. The physics of a UVOIR bolometric light curve

Here we provide a description of a typical bolometric light curve of a SN Ia and the physics driving its evolution and causing specific characteristics. Bolometric light curves constructed from photometric observations provide a simple and direct route to probe the complicated explosion physics and radiation transport. Bolometric light curves are well suited for this type of study because they are relatively easy to assemble from broad-band photometry (see below). As it is typically more straightforward to extract the total flux (hence luminosity) of a SN Ia from models rather than the flux for individual filters, which require complicated multi-group calculations (Leibundgut & Pinto 1992, Eastman 1997, Höflich & et al. 1997, Leibundgut 2000), bolometric light curves provide a unique tool to provide constraints on the progenitor systems.

Near the epoch of maximum light bolometric light curves reflect the fraction of "thermalized" γ rays. As $\sim$ 80% or more of the thermalized flux from γ rays is emitted at optical and near-infrared wavelengths (3000-10,000 Å) (Suntzeff 1996, 2003), what is manufacture from the observed photometry has been coined a UltraViolet Optical InfRared (*UVOIR*) light curve.

During maximum light the dynamical time (i.e. time since explosion) is approximately equal to the diffusion time for photons trapped within the expanding ejecta. Therefore, at the epoch of maximum light, the opacity is significantly reduced as compared to just after explosion. This allows an increasing fraction of photons to escape (Pinto & Eastman 2001). After maximum an ever increasing fraction of γ rays escapes freely and no longer deposits its energy in the ejecta. These γ rays are lost in the observed energy balance. We do not account for observations redward of 10,000 Å and therefore a small contribution of flux (no more than $\sim$ 5% near maximum light) is neglected in the construction of the UVOIR light curves (Contardo 2001). Right after maximum light, as both the $\gamma-$ray deposition rate and the temperature, hence opacity, decreases, it is believed that there is a release of 'old' photons. This causes the observed luminosity to briefly overshoot the energy input from the radioactive decays (see Sect. 6.3 for further discussion of this issue). With the release of stored energy the light curve declines in luminosity until an inflection point is reached (in most events) between 20 and 40 days after maximum light (see Suntzeff (1996) and Contardo et al. (2000)). After $\sim$ 60 days past maximum light as the energy input from radioactive decay decreases exponentially and less energy is deposited by escaping γ rays, the UVOIR light curve begins to follow a nearly linear decline out to $\sim$100 days past maximum of $\sim$ 0.026$\pm$0.002 mag/day (Contardo et al. 2000). At this time the infrared contribution

rises to around 10%

Only few late-time (t_{max} > 100 days) observations exist for SNe Ia. However, recently there has been an effort to increase the hitherto available data in order to gain a better understanding of the physical processes occurring during these epochs. At times greater than ∼ 150 days past maximum light the ejecta becomes completely transparent to the γ rays. At this epoch the light curve is powered entirely by the deposition of kinetic energy from positrons produced from the $^{56}Co \rightarrow {}^{56}Fe$ decay. It is still unclear whether the positrons are completely trapped within the ejecta by a strongly tangled magnetic field or freely escape along radially directed magnetic field lines (see Colgate et al. 1980, Ruiz-Lapuente & Spruit 1998, Milne et al. 1999, 2001).

Recently Sollerman et al. (2004) presented late-time observations of the peculiar SN 2000cx obtained with the VLT and HST telescopes covering phases 360 to 480 days past maximum light. Using a simple toy model they found that at these epochs the near-IR flux stays constant, contrary to the optical regime at late-times, which decays by ∼ 1.4 mag per 100 days. This implies that at late times the significance of the flux in the near-IR passbands upon the bolometric flux actually increases. Their light curve model was able to fit the observations, if all positrons were trapped within the ejecta. But their model suggests the existence of an infrared catastrophe, which was not supported by the observations.[1] They offer several explanations accounting for this discrepancy, but it will take further detailed modeling to arrive at a satisfactory explanation.

Today, with the large number of well-observed data sets covering the first ∼100 days of a SN, we are in the position to investigate the nature of SNe Ia using UVOIR light curves with the intent to gain a deeper understanding of the explosion mechanisms and the progenitor systems. Furthermore it is our hope that in the near future it will be possible to place constraints on explosion models with the UVOIR light curves presented in this work, as both the computational power and the sophistication of models increases.

4.2. Construction of UVOIR light curves

We constructed the UVOIR light curves in the same manner previously adopted by Vacca & Leibundgut (1996, 1997), Contardo et al. (2000), and Contardo (2001).The reader is referred to these papers for a detailed discussion of this empirical fitting method and previously attained results; here we briefly summarize the main points.

The fitting program models SNe Ia photometric light curves in a reliable way. Data for each filter is fitted with a ten parameter function. This function consists of a Gaussian, corresponding to the peak phase on top of a linear decline for the late time decay, an exponentially rising function for the initial rise to maximum, and a second Gaussian for the secondary maximum in the *VRI* light curves. The mathematical expression for this function is:

$$m = \frac{f_\circ + \gamma(t - t_\circ) + g_\circ \exp\left(\frac{-(t-t_\circ)^2}{2\sigma_\circ^2}\right) + g_1 \exp\left(\frac{-(t-t_1)^2}{2\sigma_1^2}\right)}{1 - \exp\left(\frac{\tau - t}{\theta}\right)} \,. \tag{4.1}$$

[1]The IR catastrophe refers to a thermal instability that occurs at late phases when the majority of emission makes a transition from optical and near-IR lines to mid- and far-IR lines.

Here γ is the slope of the linear decline and $f_\circ$ is the intercept of the linear decline. The third and fourth terms in the numerator correspond to the first and second maxima of the light curves that are both modeled by Gaussians. Each Gaussian is normalized to a phase ($t_\circ$ and t_1) and has amplitudes $g_\circ$ and g_1. Finally the widths of each Gaussian are represented by $\sigma_\circ$ and σ_1. The term in the denominator corresponds to the exponential rise to maximum, where θ is a characteristic time, and τ is a separate phase zero-point.

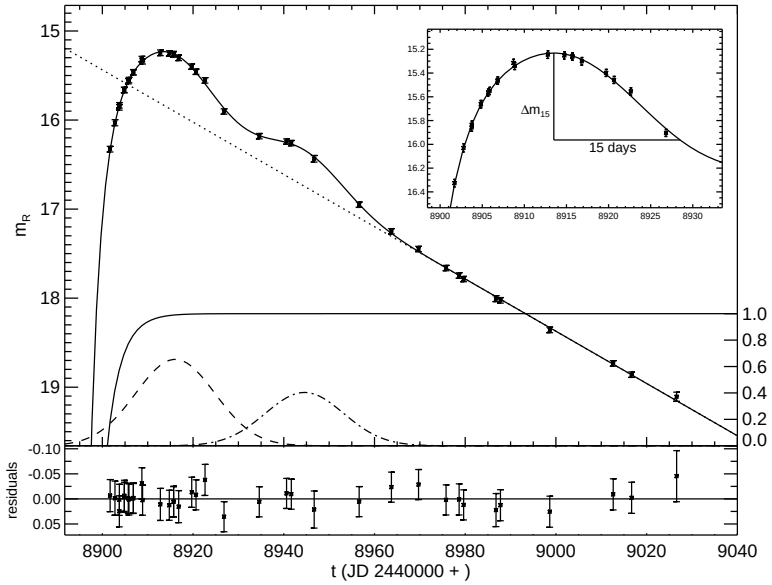

Figure 4.1.: Fit of Eq. (4.1) to the *R*-band photometry of SN 1992bc.

Fig. 4.1 presents a figure taken from Contardo (2001). This plot shows a fit of Eq. (4.1) to the *R*-band photometry of SN 1992bc. In addition to the modeled light curve this figure displays the different components used to generate the fit, e.g. the two Gaussians, the exponential rise to maximum, and the linear decline. The lower panel shows the residuals calculated from the program.

Fitting photometry in this manner is advantageous because a continuous representation of the light curves is produced without resorting to templates that do wash out subtleties of each filtered light curve. The ten fitted parameters and several other interesting quantities (such as Δm_{15} see inset of Fig. 4.1) can be used to explore the finer details of SNe Ia light curves (see Contardo et al. 2000, Contardo 2001).

To produce a UVOIR light curve we first fit the light curve of each filtered passband. Each magnitude is then converted to its corresponding flux at the effective wavelength and a reddening correction is applied. Afterwards the flux for each filter at a given epoch is integrated over wavelengths to get the total flux. Note, corrections are employed to account for overlaps and gaps between passbands.

We also have included a compensation in a manner similar to Contardo et al. (2000) for those SNe Ia that have no *U*-band photometry. Contardo et al. used a correction based on SN 1994D (Richmond et al. 1995, Patat et al. 1996, Meikle et al. 1996, Smith 2000), however, this event had an unusually blue color at maximum. For this reason corrections based on SN 1994D tend to

overestimate the fraction of flux associated with the *U*-band photometry. Instead we employed a correction derived from SN 1992A (Suntzeff 1996), which is the only well observed *normal* SN Ia with no host galaxy reddening. In Fig. 4.2 we plot the bolometric light curve of SN 1999ee (solid black line) based on *UBVRI*-band data along with what we obtain using the *U*-band compensations based on SN 1992A (red dash line) and SN 1994D (blue dot line). In the lower panel we plot the difference between the two UVOIR light curves with original *U*-band photometry compared to the light curves obtained with the two different *U*-band compensations. An additional 2% error is incurred on each UVOIR light curve that has the *U*-band correction based on SN 1992A. This difference is several percent less than if we would have used SN 1994D.

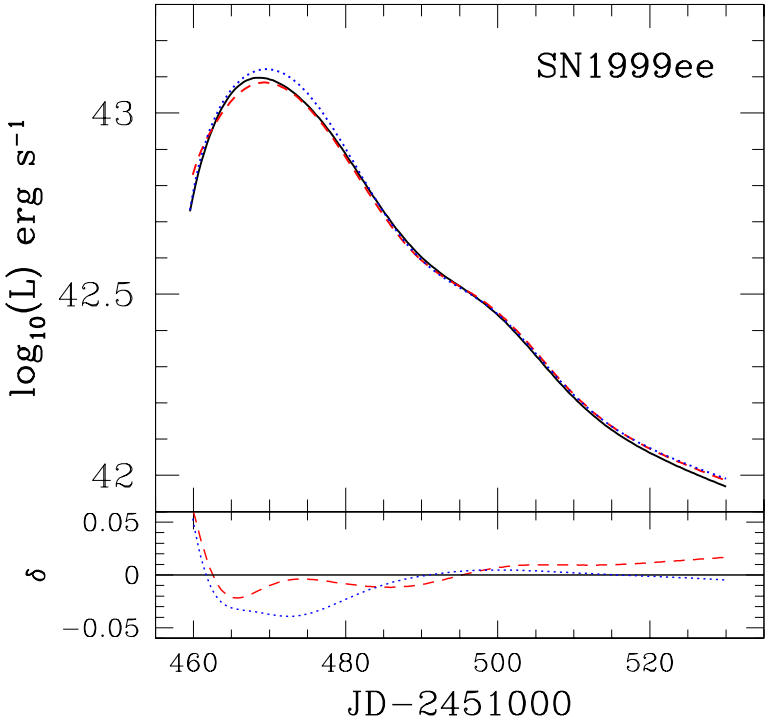

Figure 4.2.: UVOIR light curve of SN 1999ee (black solid line) plotted along with what we obtain using a *U*-band compensation based on SN 1992A (red dash line) and SN 1994D (blue dot line). Plotted in the lower panel is the difference between the UVOIR light curve with "real" *U*-band photometry and those based on the compensations. Dashed red line is the SN 1992A compensation and the dotted blue line is the SN 1994D compensation.

4.3. Results

Fig. 4.3 displays the UVOIR light curves of a selection of the SNe Ia listed in Table 3.1. In this section we proceed to address several features displayed in these light curves, and attempt to extract information that allows us to understand the physical properties that lead to these

observed characteristics. In Sect. 4.3.1 the UVOIR light curve is combined with Arnett's Rule[2] in order to determine a ^{56}Ni mass for each event. Next in Sect. 4.3.2 a quantitative analysis of the light curve shape is presented. Finally constraints are placed on the γ-ray escape fraction in Sect. 4.3.3.

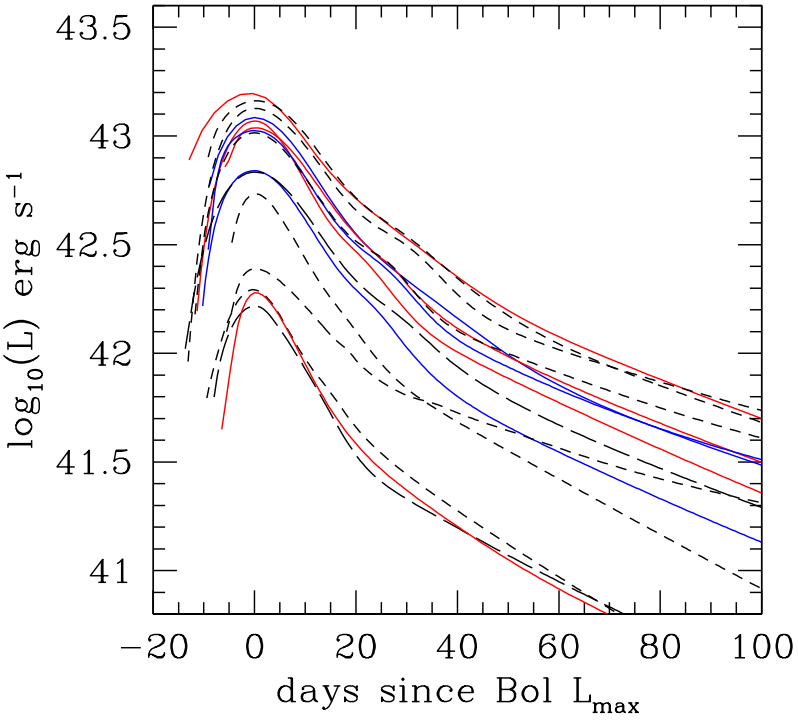

Figure 4.3.: UVOIR light curves for a selection of SNe Ia from Table 3.1. Solid lines are events with a direct distance measurement and dashed lines are redshift distances transformed to the CMB reference frame.

4.3.1. Maximum luminosity and ^{56}Ni mass

At maximum light the peak luminosity of a SN Ia is related, to first order, to the amount of ^{56}Ni produced during the explosion. The amount of ^{56}Ni synthesized from burning to NSE is itself thought to be largely dependent on the explosion mechanism. Thus with the ^{56}Ni mass we are directly probing the most sensitive part of the explosion and can therefore use observations to place constraints on the explosion mechanism.

With the UVOIR light curve and an accurate distance we are able to obtain a measure of the total luminosity and, through application of Arnett's Rule, the ^{56}Ni mass.

At maximum light the luminosity produced by the radioactive ^{56}Ni can be expressed as

$$L_{max} = \alpha E_{\mathrm{Ni}}(t_R) \; . \tag{4.2}$$

[2] Arnett's Rule simply states that during the epoch of maximum light the luminosity of a SN Ia is equal to the instantaneous energy deposition rate from the radioactive decays within the expanding ejecta (Arnett 1982, Arnett et al. 1985).

Here $E_{\rm Ni}(t_R)$ is the energy input from the decay of ^{56}Ni, evaluated at the time of bolometric maximum (rise time t_R), and α accounts for any deviations from Arnett's Rule (where α=1). An expression for $E_{\rm Ni}(t_R)$ can be found in Nadyozhin (1994)

$$E_{\rm Ni}(t_R) \;=\; \frac{\lambda_{\rm Ni}\lambda_{\rm Co}}{\lambda_{\rm Ni}-\lambda_{\rm Co}} \cdot \left\{ \left[Q_{\rm Ni}\left(\frac{\lambda_{\rm Ni}}{\lambda_{\rm Co}} - 1\right) - Q_{\rm Co}\right] \cdot e^{-\lambda_{\rm Ni}t} + Q_{\rm Co}e^{-\lambda_{\rm Co}t}\right\} M_{\rm Ni} \;=\; \epsilon(t_R)M_{\rm Ni} \;, \quad (4.3)$$

where $\lambda_{\rm Ni}$ and $\lambda_{\rm Co}$ are e-folding decay times of 8.8 and 111.3 days for ^{56}Ni and ^{56}Co, respectively, and $Q_{\rm Ni}$ and $Q_{\rm Co}$ correspond to the mean energy released per decay of 1.75 and 3.73 MeV. For 1 $M_\odot$ of ^{56}Ni, Eq. (4.3) turns into

$$E_{\rm Ni}(t_R)[1\ M_\odot] = 6.45\times10^{43}e^{-t_R/8.8} + 1.45\times10^{43}e^{-t_R/111.3} \;. \quad (4.4)$$

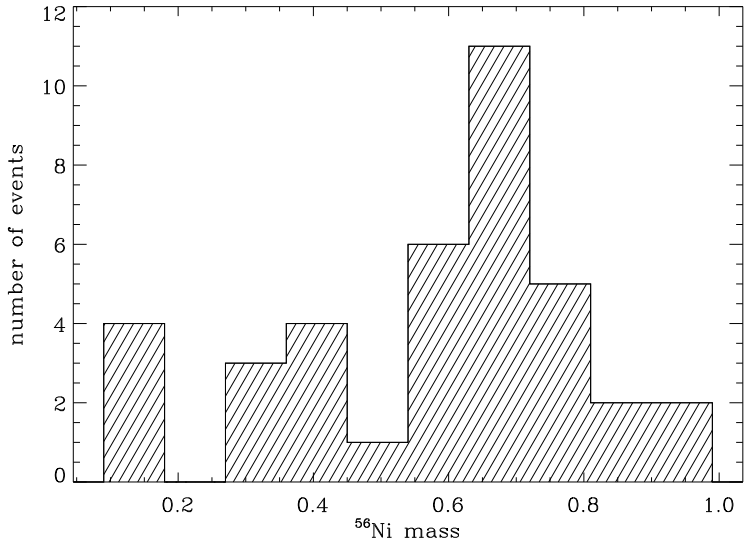

Figure 4.4.: Histogram of ^{56}Ni masses for all SNe Ia listed in Table 3.1.

Riess et al. (1999a) found, for a normal SN Ia (e.g. $\Delta m_{15}(B)$=1.1 mag) with a peak magnitude $M_V = -19.45$, a rise time to B maximum of ~19.5 days. Contardo et al. (2000) found the bolometric rise time to be within one day of the B-band for nearly all SNe Ia in their sample. Throughout this work we assume a bolometric rise time of 19±3 days. The adopted uncertainty should be adequate to account for intrinsic differences between the rise times of different SNe Ia. Using this rise time and assuming α=1.0 (Arnett's Rule) we can combine Eq. (4.2) and Eq. (4.4) and obtain the simple relation that gives for 1 $M_\odot$ of ^{56}Ni a total luminosity at maximum light of

$$L_{\rm max} \;=\; (2.0\pm0.3)\;\times\;10^{43}\;\frac{M_{\rm Ni}}{M_\odot}\;\;{\rm erg\;s^{-1}}\;, \quad (4.5)$$

where the error corresponds to the 3 day uncertainty in the adopted bolometric rise time.

As approximately 10% of the total flux at maximum light is emitted outside the optical regime each ^{56}Ni mass derived from Eq. (4.5) has been increased by a factor of 1.1. The dominant errors in the derived ^{56}Ni mass are associated with the adopted distance to the host galaxy and the total extinction (see Contardo et al. 2000).

Fig. 4.4 presents a histogram of the ^{56}Ni mass for all SNe Ia listed in Table 3.1 (determined using Eq. (4.5)) and Table 4.1 contains these values. For the SNe Ia considered in this study the ^{56}Ni mass ranges from ~ 0.10 M$_\odot$ to ~ 0.93 M$_\odot$. Note that the most and least luminous events have their absolute flux scale set by a Cepheid distance. We find that the ^{56}Ni mass (hence luminosity) ranges from ~ 0.1 to ~ 1.0 M$_\odot$. From Fig. 4.4 it is clear that the majority of events in this sample have ^{56}Ni masses larger than a half a solar mass. It is also interesting to note that there are no SNe Ia with a ^{56}Ni mass larger than 1 M$_\odot$.

These findings confirm results previously attained by several other similar and independent methods that set limits on the ^{56}Ni mass of SNe Ia (Bowers et al. 1997, Cappellaro et al. 1997, Contardo et al. 2000, Strolger et al. 2002, Suntzeff 2003). The fact that there exists a factor of 10 range in the ^{56}Ni mass is quite startling considering that SNe Ia were once thought to be an exquisite standard candle.[3] If all SNe Ia do indeed originate from a Chandrasekhar mass white dwarf, an immediate question then is: What physical mechanism(s) can explain this range in luminosity? This issue will be addressed in Sect.4.4.

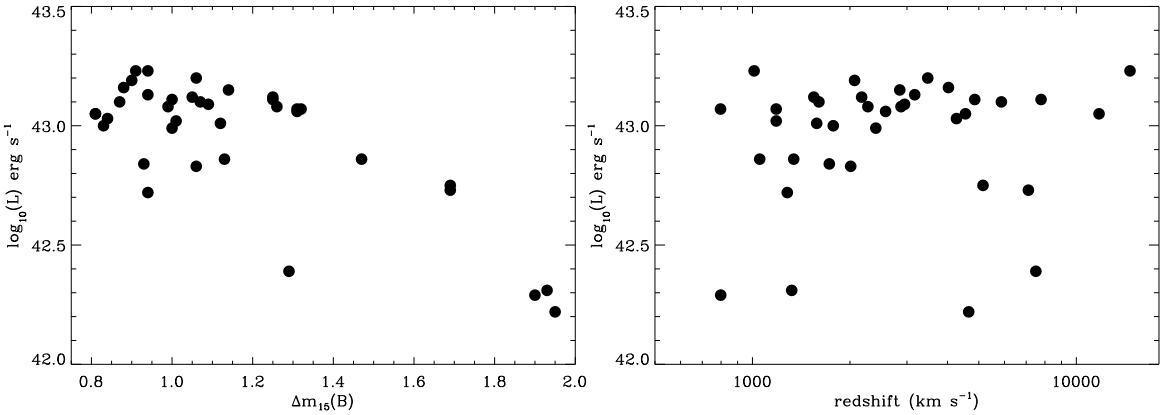

Figure 4.5.: *Left:* Luminosity at maximum light plotted vs. Δm$_{15}$(B). *Right:* Luminosity at maximum light plotted vs. redshift.

The reader will find differences between our ^{56}Ni masses and those derived in Contardo et al. for events that do not have a direct distance measurement. This is simply due to the fact that we have: (1) assumed a Hubble scale of 72 km s^{-1} Mpc^{-1}rather than 65 km s^{-1} Mpc^{-1}, (2) used CMB frame velocities instead of heliocentric velocities, and (3) assumed a slightly longer bolometric rise time. Also, note that a handful of the events with a direct distance measurement are updated compared to values used in Contardo et al. and Strolger et al. (2002).

[3] Although SNe Ia maybe be standardized through the luminosity-width relation, Krisciunas et al. (2004a) has recently present evidence of nearly no decline rate relation in the near-infrared (*JHK*-bands).

Table 4.1. Parameters describing bolometric light curves

SN	$\log_{10}(L_{max})$ (erg s^{-1})	M_{Ni} $M_\odot$	t^{I}_{2ndmax}	t^{1stdev}_{max}	t^{1stdev}_{min}	t^{1stdev}_{2ndmax}
SN1989B	43.07	0.64	···	11.43	···	···
SN1990N	43.10	0.69	···	···	···	···
SN1991T	43.23	0.93	25.42	11.16	30.78	33.91
SN1991bg	42.31	0.11	···	15.16	···	···
SN1992A	42.86	0.40	21.50	8.81	18.40	26.80
SN1992bc	43.09	0.68	33.06	12.95	28.27	40.67
SN1992bo	42.74	0.31	···	···	···	···
SN1993H	42.73	0.30	···	···	···	···
SN1994D	43.07	0.64	21.21	9.01	20.59	26.99
SN1994ae	43.19	0.84	28.76	12.69	24.98	36.37
SN1995D	43.08	0.66	29.19	11.99	25.73	37.62
SN1995E	43.20	0.88	···	···	···	···
SN1995ac	43.23	0.93	25.47	20.43	26.23	33.83
SN1995al	43.00	0.56	28.23	10.42	23.12	33.92
SN1995bd	43.03	0.59	31.32	14.12	27.12	40.22
SN1996X	43.12	0.73	25.66	10.50	22.80	30.80
SN1996bo	43.11	0.71	22.92	9.96	20.26	29.86
SN1997bp	43.15	0.78	27.40	10.81	23.11	33.69
SN1997bq	43.08	0.66	24.16	9.81	23.96	33.71
SN1997br	42.99	0.54	···	11.36	30.0	37.43
SN1998aq	43.08	0.67	26.78	12.54	···	···
SN1998bu	43.02	0.58	25.37	10.65	23.12	32.12
SN1998de	42.22	0.09	···	11.76	···	···
SN1999aa	43.05	0.61	28.85	12.26	25.93	36.11
SN1999ac	43.09	0.67	22.76	11.93	24.48	34.52
SN1999aw	43.05	0.62	36.45	13.82	30.09	44.93
SN1999by	42.29	0.11	···	14.76	19.61	34.66
SN1999dq	43.16	0.80	29.50	11.4	29.13	37.62
SN1999ee	43.13	0.74	29.76	13.43	26.57	36.74
SN1999gp	43.11	0.71	33.07	13.95	29.84	41.88
SN2000E	42.72	0.29	···	9.26	···	···
SN2000cx	42.84	0.38	26.00	10.43	22.23	29.16
SN2001bt	43.16	0.79	23.35	17.68	20.92	29.85
SN2001el	42.86	0.40	25.41	10.01	23.32	32.62
SN2002bo	43.01	0.57	26.68	14.50	24.37	31.64
SN2002cx	42.39	0.13	17.91	12.71	43.00	55.02
SN2002er	43.06	0.63	25.36	9.83	21.08	31.03
SN2003du	42.83	0.38	25.92	12.18	···	···

In Fig. 4.5 the luminosity at maximum light is plotted versus (left panel) Δm_{15}(B) and (right panel) the redshift. The left panel confirms previous results obtained by Suntzeff (2003) that there is no luminosity decline rate relation as seen in the *BV*-bands. In addition, the left panel suggests that for a look back time of ~0.5 Gyrs there is no correlation between the maximum luminosity and redshift.

4.3.2. Evolution of the post maximum UVOIR light curve

Another impressive feature displayed in the UVOIR light curves in Fig. 4.3 is the location and strength of the inflection point located between ~20 and 40 days after maximum light. Originally pointed out by Suntzeff (1996, 2003), this feature is associated with the *V*-band inflection point, and the secondary maximum observed in the *RIyzJHK*-bands. This feature indicates a redistribution of flux and is thought to appear in the IR-window due to the rapidly changing time dependence of the mean opacity (Pinto & Eastman 2000a,b). At these wavelengths there exists a large number of spectral lines associated with Fe group elements that emit stored flux via fluorescence. Most SNe Ia display this feature, albeit it maybe small for some events, however, it is clearly not evident in the subluminous events including the 'most peculiar' SN 2002cx (Li et al. 2003). In addition the red events such as SN 1992bo and SN 1993H also lack this inflection point. Curiously in some cases the strength (and placement) of the inflection point appears not to be dependent on the luminosity. This is evident in several cases as displayed in Fig 4.3.

Parameters that most likely effect the size and placement of this feature include the radial distribution of Fe group elements (i.e. mixing) which effects the mean opacity and the explosion energy (Pinto & Eastman 2001). It should be emphasized that currently there is not a complete explanation of the secondary maximum and why it varies between SNe Ia.

To obtain a more quantitative feeling of the morphology of the post maximum light curve we turn our attention to the derivative of Eq. (4.1) (see Contardo (2001) for an in depth analysis on this issue). As SN 1992A is representative of the majority of SN Ia we have adopted it for the present discussion. The right panel of Fig. 4.6 displays the UVOIR light curve and the left panel contains the associated derivative. In both panels the location of the maxima and minma are marked with vertical solid lines. As clearly seen in the left panel after maximum light the slope of the derivative increases until the first maxima is reached at 8.81 days past maximum luminosity. The slope of the derivative then decreases until a minima is reached at 18.40 days past maximum luminosity. The minimum is associated with the epoch when there is a redistribution of flux in the UVOIR light curve. Next the slope of the derivative again increases until it reaches a second maximum at 26.80 days past maximum luminosity. Finally the slope of the derivative again decreases until around 60 days past maximum light when it evolves to a constant slope of ~ 0.028 mag day^{-1}.

To illustrate the evolution of the derivative of Eq. (4.1) for our whole sample of SNe Ia light curves we present Fig. 4.7. Both panels contain the epochs of the maxima and minimum of the first derivative of Eq. (4.1). In the left panel the maximum luminosity is plotted versus the maxima and minima. In the right panel the position of the *I*-band secondary maximum is plotted versus the maxima and minima. The epochs of the maxima and minimum appear to be only roughly correlated to the maximum luminosity. This is not unexpected as we have already shown that the maximum luminosity does not appear to be correlated with Δm_{15}(B). However, there is a much stronger dependence between the maxima and minimum with respect to the time

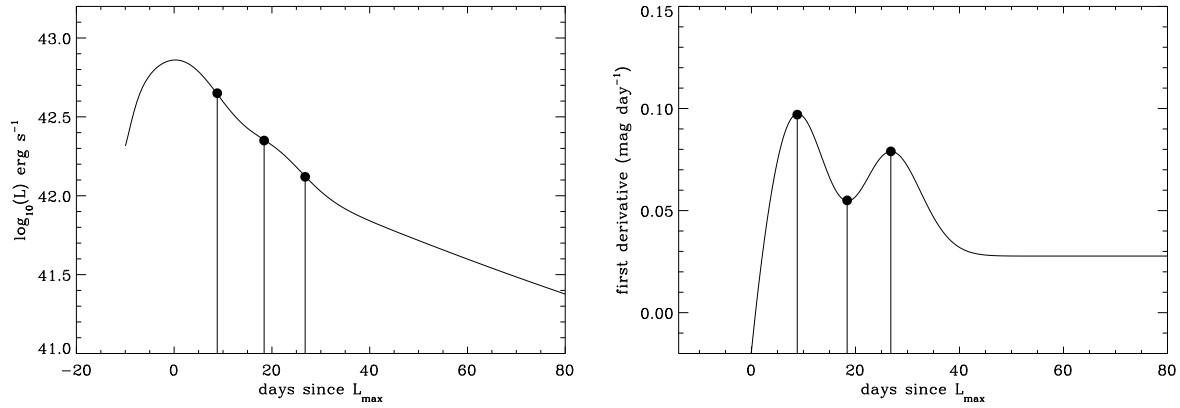

Figure 4.6.: *Left:* UVOIR light curve of SN 1992A. *Right:* The first derivative of the UVOIR light curve. Position of maxima and minima are indicated by solid vertical lines.

of the secondary maximum in the *I*-band. It should be noted that there are several events such as SN 1989B and SN 1998aq that are relatively bright, however, they lack both the first minimum and second maxima. In other words there seems to be little to no redistribution of flux in their UVOIR light curve.

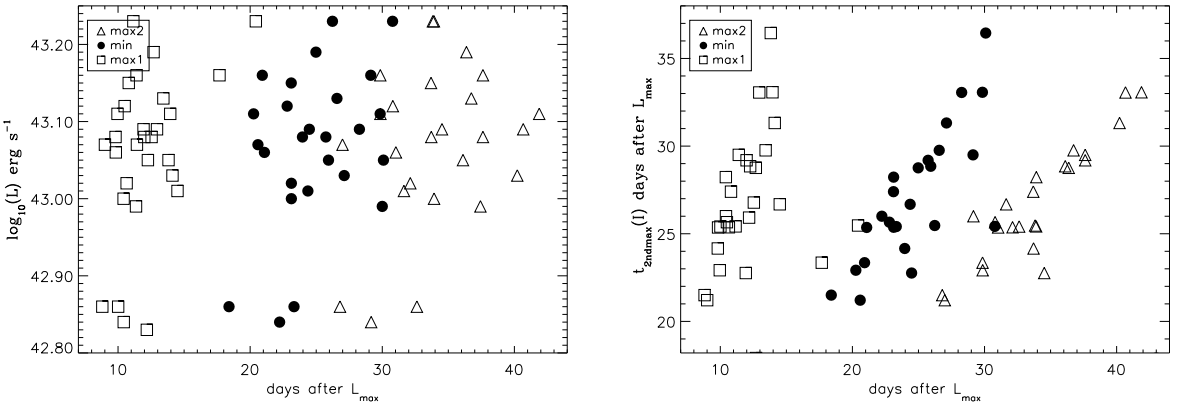

Figure 4.7.: *Left:* Maximum luminosity vs. the epochs of maxima and minimum of the first derivative of Eq. (4.1). *Right:* Position of the *I*-band secondary maximum with respect to time of bolometric maximum vs. the maxima and minimum of the first derivative.

Another remarkable feature of Fig. 4.3 is the difference in luminosity between the late-time UVOIR light curves. It is evident in the post maximum UVOIR light curve (i.e. > 50 days past L_{max}) that the difference in luminosity between the luminous and least luminous events actually increases!

In Fig. 4.8 we present a plot of the total time integrated luminosity versus the ^{56}Ni mass. The total energy radiated has been determined by integrating the UVOIR light curve from -6 to 100 days with respect to maximum light. The error bars that accompany the ^{56}Ni mass for each event accounts for uncertainties associated with the distance and the adopted reddening. It is evident that there is a strong correlation between these two parameters. This correlation fits in with the luminosity-width relation. Brighter SNe Ia evolve more slowly with time and hence have a larger total time integrated luminosity as compared to fainter ones that evolve rapidly.

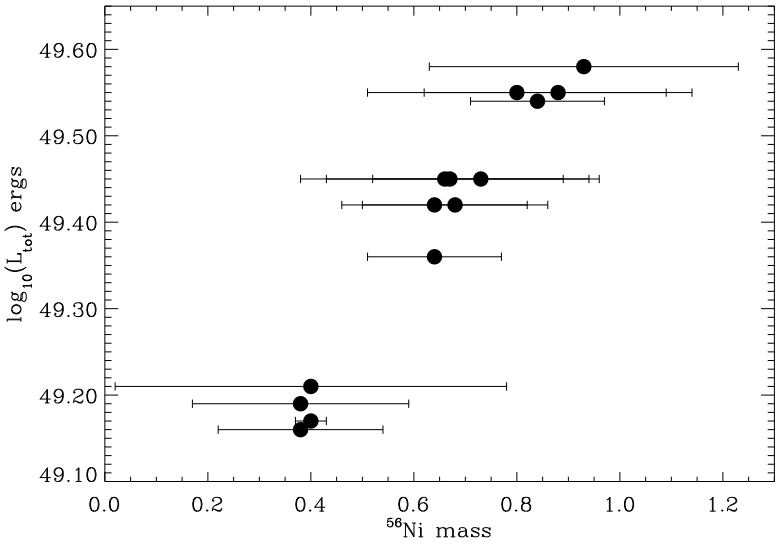

Figure 4.8.: Time integrated UVOIR luminosity vs. ^{56}Ni mass.

4.3.3. γ-ray escape fraction

By comparing the UVOIR light curve to the energy input from the radioactive decays –for both cases of complete trapping of γ rays and complete escape of γ rays– we can obtain a quantitative description of the γ-ray escape fraction.

An expression for the UVOIR light curve based on this prescription can be written as

$$LC(t)_{\rm obs} = (1 - \gamma(t))LC(t)_{\tau>>1} + \gamma(t)LC(t)_{\tau<<1} \ . \tag{4.6}$$

In this expression $LC(t)_{obs}$ is the UVOIR light curve, $LC(t)_{\tau>>1}$ represents the energy input from the radioactive decays assuming complete trapping of γ rays, $LC(t)_{\tau<<1}$ represents the case of complete escape of γ rays, and $\gamma(t)$ is the γ-ray escape fraction. Solving Eq. 4.6 for $\gamma(t)$ we obtain

$$\gamma(t) = \frac{LC(t)_{\tau>>1} - LC(t)_{\rm obs}}{LC(t)_{\tau>>1} - LC(t)_{\tau<<1}} \ . \tag{4.7}$$

In Fig. 4.8 we present the γ-ray escape fraction as a function of time (determined from Eq. (4.7)) for five of the SNe Ia in our sample. As the ejecta of the supernova expands there is an increase in the γ-ray escape fraction. This can be attributed to a decrease in the column density, which is accompanied with the expansion of the ejecta. Most of the curves in this figure are accompanied by a 'bump' between 20 and 40 days past maximum light. Also included in Fig. 4.8 is the γ-ray escape fraction calculated from W7 (red dash line) (Nomoto et al. 1984). W7 is a 'standard' 1-D explosion model that has been able to produce synthetic spectra that match well with the observations of several SN Ia. The agreement between W7 and our calculated γ-ray escape fraction curves is encouraging, considering that we are not adjusting any parameters.[4]

[4]Note that we have assumed a rise time to bolometric maximum of 19 days.

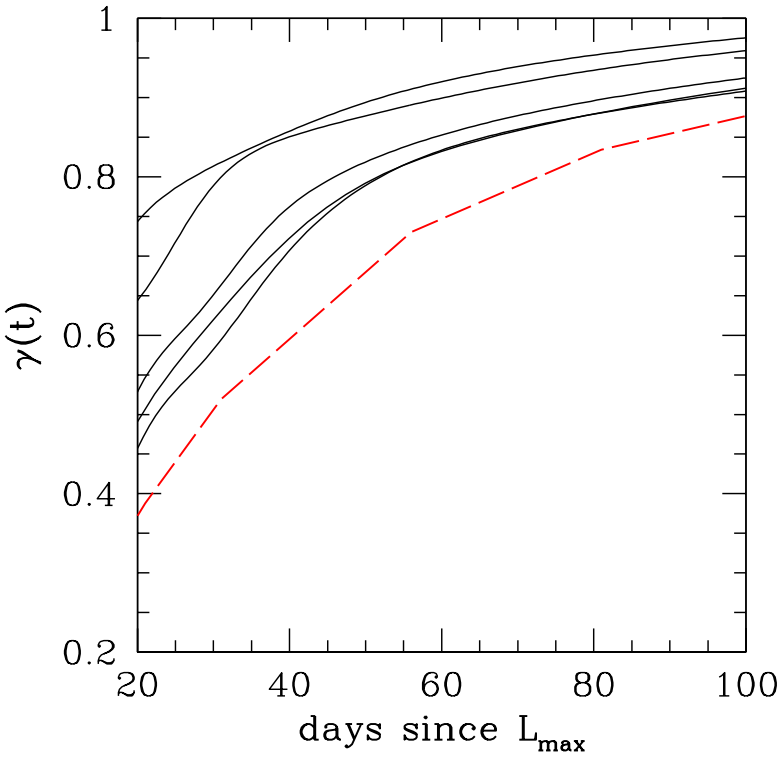

Figure 4.9.: γ-ray escape fraction as a function of time since maximum light for five SN Ia in our sample. These include (from top to bottom) SN 1991bg, SN 1994D, SN 2003du, SN 1991T, and SN 1999dq. The red dash line corresponds to W7. For W7 we have assumed a rise time to bolometric maximum of 19 days.

For the first three weeks after maximum light the γ-ray escape fraction from the UVOIR light curves is unreliable, as it is based on the assumption of $\tau << 1$, which clearly is not the case for $t < t_\circ$, where $t_\circ$ is the epoch when the ejecta becomes optically thin.

From Fig. 4.8 it is clear that the γ-ray escape fraction evolves faster in time for less luminous events. This is confirmed by Fig. 4.9 where we plot the γ-ray escape fraction at sixty days past bolometric maximum light versus Δm_{15}(UVOIR). At this epoch $\sim$ 10% more γ rays escape in the least luminous SNe Ia than in the brightest events. However, between 20 and 40 days past maximum light the differences are even more pronounced. This is expected, as at these epochs the UVOIR light curve has not yet reached its linear decline. In addition, as previously discussed the morphology of the secondary maximum can vary radically from SN to SN (see also Suntzeff 2003). This may then have a significant effect on the evolution of the γ-ray escape fraction during these phases.

4.4. Discussion

We now address possible explanations that may lead to the large range in the values of the amount of ^{56}Ni.

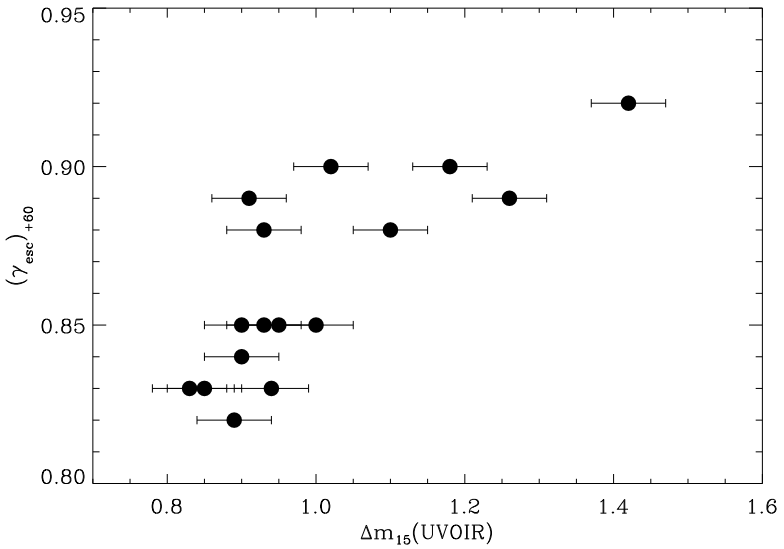

Figure 4.10.: γ-ray escape fraction at sixty days past maximum light vs. Δm_{15}(UVOIR).

There has been considerable effort on the part of modelers to address this question. Yet they have been met with little success to identify what parameter(s) can be tuned in order to account for a factor of ten in ^{56}Ni mass. Obvious candidates that may affect the production of ^{56}Ni are the initial parameters prior to explosion, e.g. metallicity, central density and ignition mechanism(s). Recently, Röpke & Hillebrandt (2004) have shown that the C-O ratio has essentially no effect on the amount of ^{56}Ni produced from burning to NSE. If prior to explosion there is a significant amount of alpha elements within the white dwarf, one may reasonably expect the production of more stable isotopes, thus reducing the amount of ^{56}Ni synthesized (Brachwitz et al. 2000). Moreover it has been shown that changes in the central density of the white dwarf can effect the strength of the explosion. Nevertheless, it is unrealistic that any one of these parameters, or even a combination of the three, can account for a factor of ten range in the ^{56}Ni mass. In reality these parameters affect the production of ^{56}Ni by no more than $\sim$ 20%.

More likely to influence the amount of ^{56}Ni synthesized is the explosion mechanism itself (see also Chapter 6.6). Currently the explosion mechanism and the subsequent evolution of the burning front is in open debate, and varies from a subsonic deflagration to a supersonic delayed detonation. Today the best Chandrasekhar mass models predict a ^{56}Ni mass that ranges between $\sim$ 0.40 to 0.60 $M_{\odot}$. Due to computational limitations the state-of-the-art 3-D deflagration models (Reinecke et al. 2002a,b) do not produce copious amounts of ^{56}Ni (Travaglio et al. 2004), and have appreciable amounts of unburned carbon and oxygen left over in the inner ashes (Kozma et al. 2005). The delayed detonation models (Woosley 1990, Khokhlov 1991, Woosley & Weaver 1994b, Höflich & Khokhlov 1996), on the other hand, can account for some of the more luminous events, but this class of models requires an additional free parameter. This parameter is essential to force the transition of the flame propagation from a deflagration to a detonation, and is physically not understood (however, see Gamezo & Khokhlov (2004) and Golombek & Niemeyer (2005)).

The fact that there does not exist a single class of Chandrasekhar mass models that can account for the complete population of SNe Ia is quite dissatisfying and should be seriously

addressed by theorists, if we are to insist that a Chandrasekhar size white dwarf accounts for the progenitor system of *all* SNe Ia.

An alternative progenitor model that has recently gained consideration is the super-Chandrasekhar mass white dwarf (Piersanti et al. 2003, Saio & Nomoto 2004, Yoon et al. 2004, Yoon & Langer 2005). If matter accreted on to the white dwarf carries a large amount of angular moment, one could expect the white dwarf to spin up, and hence acquire an ejected mass greater than 1.4 $M_{\odot}$ prior to the onset of thermonuclear combustion (Langer et al. 2000).

In the next chapter we provide evidence that suggests the existence of a sub-Chandrasekhar size white dwarf as the progenitor of some SN Ia.

5. Ejected masses of SNe Ia progenitor systems

5.1. Introduction

From the results presented in the previous chapter it is clear that SNe Ia do not consist of a homogeneous group of stellar explosions, but rather display a range in luminosity of a factor of ten or more (Contardo et al. 2000, Suntzeff 2003). In fact not one self-consistent explosion model has yet been proposed that can successfully account for this observed range in luminosity. This lack of understanding of the progenitor systems is unsettling, and must be addressed, if we are to have confidence in the cosmological results provided by SNe Ia. In this chapter we present an analysis of sixteen well-observed SNe Ia with the intent to place constraints on the ejected mass.

(*U*)*BVRI*-band observations for sixteen of the SNe Ia listed in Table 3.1 were used to determine the ejected mass (see Table 5.1). These events have photometric observations that extend to ~ 100 days past maximum light.

5.2. Method to determine the ejected mass

To place constraints on the ejected mass we perform a least-squares fit of a radioactive beta decay energy (RDE) deposition function to the post maximum phase UVOIR light curve. Prior works that discuss this method include the pioneering investigations of Colgate et al. (1980), followed by the more sophisticated treatment presented by Jeffery (1999); (see also Cappellaro et al. 1997 and Milne et al. 1999, 2001 for similar methods and techniques.) However, as of yet, no attempt has been made to apply such a method to UVOIR light curves derived from real observations.

An expression for the energy deposition of N_{Ni0} atoms of ^{56}Ni in the optically thin limit (i.e. when $\tau << 1$) is represented by

$$\begin{aligned} E_{\rm dep} &= E_{\rm Ni} + E_{\rm Co\ e^+} + [1-\exp(-\tau)]E_{\rm Co\ \gamma} \\ &= \lambda_{\rm Ni} N_{\rm Ni0}\ \exp(-\lambda_{\rm Ni} t) Q_{\rm Ni\ \gamma} + \lambda_{\rm Co} N_{\rm Ni0} \frac{\lambda_{\rm Ni}}{\lambda_{\rm Ni}-\lambda_{\rm Co}} [\exp(-\lambda_{\rm Co} t) - \exp(-\lambda_{\rm Ni} t)] \\ &\quad \times \{Q_{\rm Co\ e^+} + Q_{\rm Co\ \gamma}[1-\exp(-\tau)]\}\ . \end{aligned} \quad (5.1)$$

$\lambda_{\rm Ni}$ and $\lambda_{\rm Co}$ are the respective e-folding decay times of 8.8 and 111.3 days for ^{56}Ni and ^{56}Co. $Q_{\rm Ni\ \gamma}$ (1.75 MeV) is the energy released per $^{56}{\rm Ni} \rightarrow {}^{56}{\rm Co}$ decay. $Q_{\rm Co\ e^+}$ (0.12 MeV) and $Q_{\rm Co\ \gamma}$ (3.61 MeV) are the positron and γ-ray energies released per $^{56}{\rm Co} \rightarrow {}^{56}{\rm Fe}$ decay. Note that

throughout this work we assume that all neutrinos produced from the radioactive decays escape the ejecta entirely and do not contribute to the observed UVOIR flux.

As Eq. (5.1) is only applicable in the optically thin limit, when the thermalized photons can freely escape, it is safe to assume that at these epochs the majority of ^{56}Ni has decayed to ^{56}Co, and therefore the remaining amount of ^{56}Ni provides a negligible contribution to the energy deposition. At these epochs the UVOIR light curve (in flux units) appears to be nearly first order exponential, however it is more accurately described as 'quasi-exponential' (see Jeffery 1999, for a detailed discussion).

The Jeffery's Model

We now examine the comprehensive derivation provided in Jeffery (1999) for the parametrized SN Ia model, which is used in the next section to place limits on the ejected mass. To relate the ejected mass with the UVOIR light curve this model makes use of the γ-ray opacity parameter τ in Eq. (5.1) (see below).

In case of homologous expansion[1] the density profile of an exponential model is given by

$$\rho(v,t) = \rho_{\mathrm{ce},\circ}\left(\frac{t_\circ}{t}\right)^3 \exp(-v/v_e) = \rho_{\mathrm{ce},\circ}\left(\frac{t_\circ}{t}\right)^3 \exp(-z)\ . \tag{5.2}$$

In this equation the central density at fiducial time $t_\circ$ is given by $\rho_{\mathrm{ce},\circ}$, while v_e is the e-folding velocity, and the radial velocity is z.

Furthermore during homologous expansion an expression for the optical depth of the beam path traveled by a photon can be expressed either in physical space s or velocity space v_s:

$$\tau = \int_{em}^{sur} ds\ \kappa\rho[\vec{v}(s),t] = \left(\frac{t_\circ}{t}\right)^2 \int_{em}^{sur} dv_s\ t_\circ\kappa\rho_\circ[\vec{v}(v_s)]\ . \tag{5.3}$$

Here κ is the effective absorption opacity while the limits of integration refer to the location where the photon is originally emitted ('em') and the point where it emerges from the surface ('sur').

By replacing the density ρ in Eq. (5.3) with Eq. (5.2) and assume κ is constant, we obtain an exponential model for the γ-ray optical depth from the emission point of the photon to the surface z (where $z = \infty$), i.e.

$$\tau = \tau_{\mathrm{ce},\circ}\left(\frac{t_\circ}{t}\right)^2 \int_0^\infty dz_s \exp(-z')\ . \tag{5.4}$$

The variable $\tau_{\mathrm{ce},\circ}$ is the radial optical depth to the center at the fiducial time $t_\circ$, dz_s is the beam path velocity (in units of the e-folding velocity) and z' is given by

$$z' = (z^2 + z_s^2 + 2zz_s\mu)^{\frac{1}{2}}\ , \tag{5.5}$$

[1] Homologous expansion implies that the mean radius of the expanding ejecta scales with the velocity i.e. $\vec{v} \propto \vec{r}$ or $\vec{dv}/\vec{dr}$ = constant.

where μ is the cosine of the angle at the place of emission between the outward radial direction and the direction the beam propagates.

If a beam of photons is pointed in the radial outward direction (i.e. $\mu = 1$) Eq. (5.5) reduces to

$$\tau_r = \tau_{\mathrm{ce},\circ}\left(\frac{t_\circ}{t}\right)^2 \exp(-z)\ . \tag{5.6}$$

During the optically thin limit when the energy deposition is powered by only ^{56}Co we can rewrite Eq. (5.6) from a radial optical depth to a mean optical depth explicitly as

$$\bar{\tau} = \tau_{\mathrm{ce},\circ}\left(\frac{t_\circ}{t}\right)^2 q\ . \tag{5.7}$$

Here q is a general form factor that describes the distribution of ^{56}Ni in the ejecta (see the Jeffery's paper for the mathematical form of this parameter). From Eq. (5.7) it is evident that when the ejecta of a SN Ia reaches the optically thin limit the mean optical depth can be represented by a simple t^{-2} dependence.

Before we obtain the final expression from Eq. (5.7) we need to know $\tau_{\mathrm{ce},\circ}$. The radial optical depth from radius z to ∞ (assuming constant opacity κ) is defined as

$$\tau(z) = \kappa\rho_{\mathrm{ce},\circ} v_e t\left(\frac{t_\circ}{t}\right)^3 \exp(-z) = \frac{\kappa M}{8\pi v_e^2 t_\circ^2}\exp(-z) = \tau_{\mathrm{ce},\circ}\left(\frac{t_\circ}{t}\right)^2 \exp(-z)\ . \tag{5.8}$$

Hence $\tau_{\mathrm{ce},\circ}$ is

$$\tau_{\mathrm{ce},\circ} = \frac{\kappa M}{8\pi v_e^2 t_\circ^2}\ . \tag{5.9}$$

Substituting Eq. (5.9) into Eq. (5.7) and then evaluating Eq. (5.7) at the fiducial time $t_\circ$, we obtain a relationship between $t_\circ$ and a fiducial characteristic optical depth $\tau_{\mathrm{ch},\circ}$. At the fiducial time $t_\circ$, $\tau_{\mathrm{ch},\circ}$ becomes the optically thin $\bar{\tau}$. Since $t_\circ$ is defined to occur when the ejecta makes the transition from optically thick to optically thin we obtain

$$t_\circ = \left(\frac{M_{ej}\kappa q}{8\pi\tau_{\mathrm{ch},\circ}}\right)^{\frac{1}{2}}\frac{1}{v_e}\ . \tag{5.10}$$

Because $\tau_{\mathrm{ch},\circ}$ is conveniently equal to one at the epoch of $t_\circ$ Eq. (5.10) reduces to

$$t_\circ = \left(\frac{M_{ej}\kappa q}{8\pi}\right)^{\frac{1}{2}}\frac{1}{v_e}\ . \tag{5.11}$$

Here M_{ej} is the total ejected mass, κ is the γ-ray mean opacity, v_e is the e-folding velocity of an exponential model's density profile, and q describes the distribution of ^{56}Ni.

During the optically thin phase for an all-metal ejecta ($\mu_e = 2$), κ is expected to be in the range 0.025 to 0.033 cm^2 g^{-1} (see Swartz et al. 1995, Jeffery 1999, and references therein for a detailed discussion). We adopted the value of 0.025 cm^2 g^{-1} as our fiducial γ-ray mean opacity.

Jeffery (1999) compiled model e-folding velocities of several successful 1-D explosion models consisting of 1.4 $M_\odot$ Chandrasekhar size white dwarfs. These e-folding velocities are $\sim$ 2700 km s^{-1} for W7 (Nomoto et al. 1984), 2750 km s^{-1} for DD4[2]

More recently Röpke & Hillebrandt (2005) published two full-star 3-D explosion models of a 1.4 $M_\odot$ white dwarf; with different ignition conditions: a centrally ignited configuration (c3_4π) and a foamy multi-bubble flame structure ($f1$). Using Eq. (A10) of Jeffery (1999) and parameters given in Table 1 of Röpke & Hillebrandt (2005), we have calculated the e-folding velocities for these two models. The e-folding velocities correspond to $\sim$ 1611 km s^{-1} for the c3_4π simulation and $\sim$ 1842 km s^{-1} for the $f1$ simulation. These values are substantially smaller than the previously cited 1-D models and reflect the difference between the density profiles generated by 1-D and 3-D simulations. In the calculations presented below we arbitrarily adopted 3000 km s^{-1} as our 'average' fiducial e-folding velocity.

The parameter q is equal to one for high concentrations of ^{56}Ni at the center of the ejecta, small for low concentrations within the center, and one-third for the case when the ^{56}Ni is evenly distributed throughout the ejecta (see Jeffery 1999, for a detailed discussion). There is mounting evidence that an appreciable amount of ^{56}Ni is moderately mixed within the ejecta. However, it is likely that the amount of mixing may vary significantly from supernova to supernova.

An analysis of early-time spectra of SN 1991T (Ruiz-Lapuente et al. 1992, Mazzali et al. 1995) indicates the existence of an outer shell of ^{56}Ni. In contrast, Georgii et al. (2002) presented observations of SN 1998bu obtained with COMPTEL. They concluded that their non-detection of γ rays from the ^{56}Co$\rightarrow^{56}$Fe decay chain is a sign that there is no appreciable mixing of radioactive nuclides within the ejecta in the context of current models. More recently Stehle et al. (2005) have presented "abundance tomography" of SN 2002bo. With their unique technique they determined that the vast majority of ^{56}Ni was distributed between 3000 to 11,000 km s^{-1} for this particular event. Jeffery (1999) showed that for W7, the parameter q was equal to approximately one-third. As W7 has been able to quite successfully fit observed spectra for normal to bright SNe Ia (Harkness 1991, Mazzali et al. 1995, Mazzali 2001), we have adopted a q value of one-third in the calculations presented below.

As we previously saw during the optically thin limit the mean opacity has a simple t^{-2} dependence. Therefore we can replace τ in Eq. (5.1) with $\frac{t_\circ^2}{t^2}$, and then perform a least squares fit of Eq. (5.1) to the UVOIR light curve between 50 and 100 days past maximum light (when Eq. (5.1) is valid) in order to determine $t_\circ$.

With values of $t_\circ$, derived from the least squares fit of Eq. (5.1) to the UVOIR light curve during the quasi exponential phase, along with the adopted fiducial values for all the parameters in Eq. (5.11), we can proceed to place constraints on the ejected mass for all of the SN Ia in our sample.

[2]DD is the acronym for a delayed detonation model (see Section 6.3 for a discussion on this class of explosion model. (Woosley & Weaver 1994b), and 3000 km s^{-1} for M36 (Höflich 1995). In addition Jeffery et al. (1992) found that the DD2 model of Woosley (1991) has an e-folding velocity of $\sim$ 3160 km s^{-1}.

Table 5.1. Well-observed SNe Ia

SN	M_{Ni} ($M_\odot$)	$t_\circ$[a] (days)	M_{ej}[a] ($M_\odot$)	M_{IME} ($M_\odot$)
SN1989B	0.64(0.18)	32.23(0.12)	1.06(0.32)	0.42
SN1991T	0.93(0.30)	34.44(0.23)	1.21(0.36)	0.28
SN1991bg	0.11(0.03)	21.62(0.11)	0.48(0.14)	0.37
SN1992A	0.40(0.03)	26.58(0.10)	0.72(0.22)	0.32
SN1994D	0.64(0.13)	25.31(0.11)	0.65(0.20)	0.01
SN1994ae	0.84(0.13)	32.33(0.13)	1.07(0.32)	0.23
SN1995D	0.66(0.23)	35.15(0.12)	1.26(0.38)	0.60
SN1995E	0.88(0.26)	31.49(0.11)	1.01(0.30)	0.13
SN1996X	0.73(0.21)	28.70(0.10)	0.84(0.25)	0.11
SN1998aq	0.68(0.18)	28.88(0.17)	0.85(0.25)	0.17
SN1998de	0.09(0.03)	27.80(0.10)	0.68(0.20)	0.59
SN1999ac	0.67(0.29)	33.24(0.11)	1.13(0.34)	0.46
SN1999dq	0.80(0.29)	34.91(0.14)	1.24(0.37)	0.44
SN2000cx	0.38(0.16)	25.40(0.09)	0.66(0.20)	0.28
SN2001el	0.40(0.38)	31.94(0.12)	1.04(0.31)	0.64
SN2003du	0.38(0.21)	32.16(0.13)	1.05(0.32)	0.67

[a]Errors are listed in paraenthesis.

5.3. Results

In Fig. 5.1 we present the least squares fits of Eq. (5.1) to several UVOIR light curves. The four events shown in Fig. 5.1 are representative of the complete population of SN Ia, ranging from the bright SN 1991T to the subluminous SN 1991bg. Also plotted are the energy deposition curves corresponding to the ^{56}Ni $\rightarrow$ ^{56}Co $\rightarrow$ ^{56}Fe decay chain for the cases of complete γ-ray trapping (dash dotted line) and complete γ-ray escape (dashed line). Table 5.1 lists the ^{56}Ni mass calculated for each event through Eq. (4.5), as well as the determined values of $t_\circ$. For this sample of SNe Ia, the ^{56}Ni mass varies by a factor of $\sim$10, while $t_\circ$ varies by a factor of 1.6.

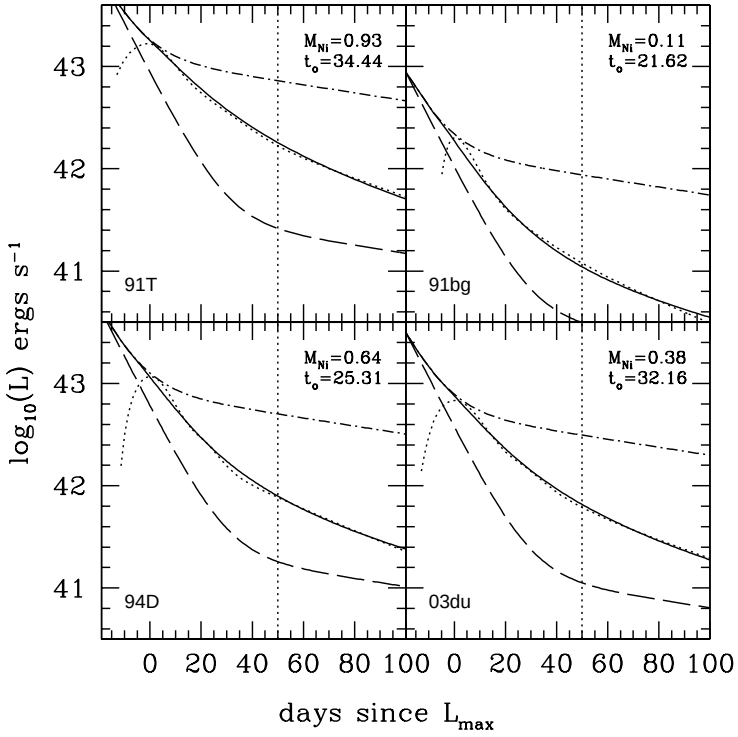

Figure 5.1.: Fit of Eq. (5.1) (solid line) to the UVOIR bolometric light curve (dotted curve) between 50 and 100 days past maximum light. The dotted dashed line is the energy deposition of γ rays and positrons from the ^{56}Ni to ^{56}Co to ^{56}Fe decay, assuming complete trapping (i.e. $\tau >> 1$). Dashed line is the case for complete escape of γ rays (i.e. $\tau << 1$). The vertical dotted line indicates the epoch (+50 days) when the fi t begins.

In order to give the reader a more intuitive feeling of how the RDE deposition curve depends on the value of $t_\circ$, we present Fig. 5.2. This figure contains the UVOIR light curve of SN 2003du, along with the energy deposition curves for different values of $t_\circ$ that vary, from top to bottom: ∞, 45, 40, 35, 32.16, 25, 20, 15, and 0 days. As expected for a fixed ^{56}Ni mass, when $t_\circ$ is increased, the energy RDE deposition function evolves more slowly with respect to time. Physically this effect is associated with an increase in the diffusion time of the photons trapped within the ejecta.

In Fig. 5.3 we plot $t_\circ$ versus Δm_{15}(UVOIR). Values for Δm_{15}(UVOIR) have been taken

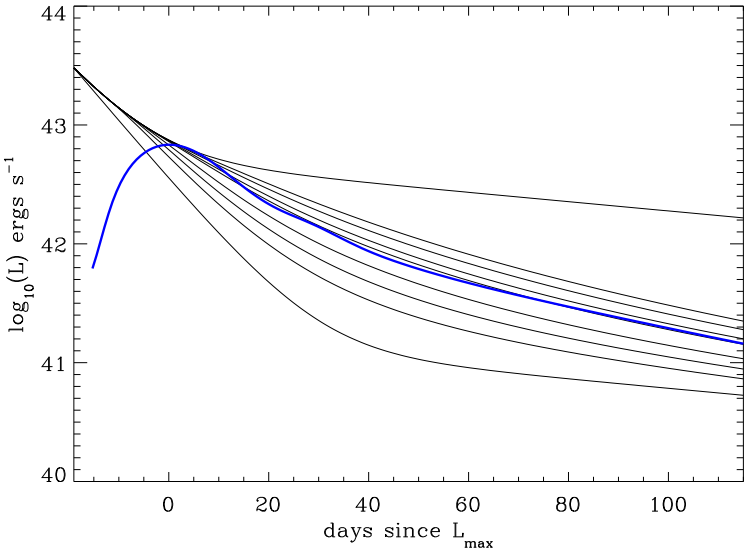

Figure 5.2.: Plot of Eq. (5.1) for a fixed ^{56}Ni mass of 0.38 $M_\odot$ while varying $t_\circ$ (solid lines). Here $t_\circ$ ranges (from top to bottom) ∞,45, 40, 35, 32.16, 25, 20, 15, and 0 days. The light curve (thick blue line) corresponds to SN 2003du.

directly from the UVOIR light curve.[3] From this figure it is clear that there exists a correlation between these two parameters. This correlation is in accord with our expectations, as it is well established that more luminous SNe Ia have smaller decline rates, and thus the epoch in which their ejecta transform to the nebular phase occurs at a later time (see Pinto & Eastman 2001, and references within for a detailed discussion of the physics that describes the luminosity-width relation).

Armed with our values of $t_\circ$, we can now proceed to place constraints on the total ejected mass. Fig. 5.4 is a plot of our calculated ejected mass versus the ^{56}Ni mass and Table 5.1 contains these values. For the calculation of the ejected mass we have used q = 1/3, v_e = 3000 km s^{-1} and κ = 0.025 cm^2 g^{-1}.

The error bars that accompany each ^{56}Ni mass account for uncertainties in host galaxy reddening and the adopted distance. For events with a CMB distance we have assumed 300 km s_s uncertainty for (random) peculiar velocities.

The ejected mass error bars include: (1) the uncertainty listed in Table 5.1 for each value of $t_\circ$, (2) a 300 km s^{-1} i.e. 10% uncertainty in v_e, (3) a 10% uncertainty in κ and (4) a 30% uncertainty in the adopted value of q. These '1-σ' error bars are not statistical but rather a sensible estimation of the possible range of each parameter.

Figure 5.4 displays several striking features that are worthy of comment. First, this figure suggests that there exists a range in the ejected mass of about a factor of two. Three events (SN 1992A, SN 1994D, and SN 2000cx) that have *moderate* amounts of M_{ej} (i.e. 0.4 - 0.6 $M_\odot$) are of particular interest. These events are located nearly 3-σ below the most massive events, which lie near the canonical value of 1.4 $M_\odot$. In order to increase the ejected mass of these three

[3] By plotting Δm_{15}(UVOIR) rather than the ^{56}Ni mass, we bypass the effect upon the luminosity (hence ^{56}Ni mass) associated with the uncertainty in the adopted distance to each event.

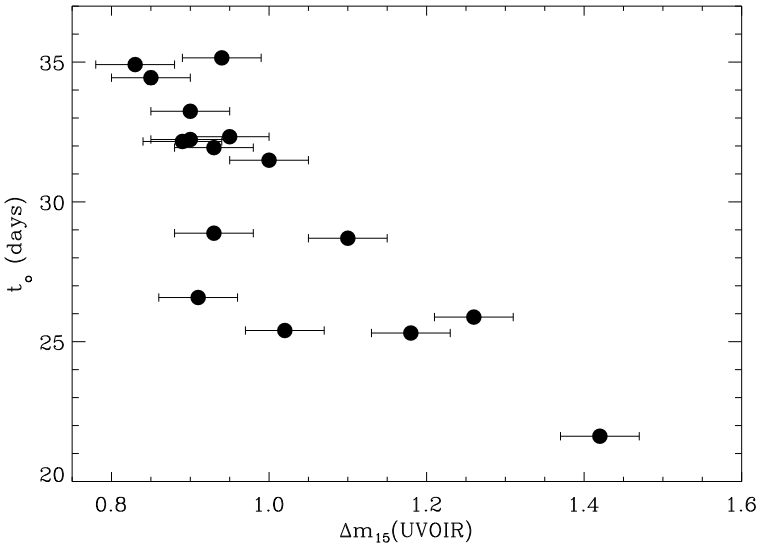

Figure 5.3.: Fiducial time, $t_\circ$ plotted versus Δm_{15}(UVOIR). Note the error bars associated with the values of $t_\circ$ are smaller than the size of the circles.

events to a Chandrasekhar mass, it is necessary to reduce either q (which is highly unlikely) or our fiducial value of κ by a factor of two, or increase either the value of $t_\circ$ by a factor of ~ 1.3 or v_e by a factor of ~ 1.4 or more. Implementing any of these changes results in ejected masses for all the other 'normal' SN Ia to be comparable to that of a neutron star mass. In other words, if we change any one of the parameters in Eq (5.11) while keeping all others constant, there will always exist a relative difference in the ejected mass of ~ 2 between these three events shown in Fig. 5.4, as compared to the more massive ones. Of course this is the case if the changes are applied uniformly to the whole sample. In reality some events may have different values for the parameters listed in Eq (5.11) when compared to each other.

The problem can, of course be inverted to derive mean values of q, κ, and v_e for a fixed ejected mass. With an ejected mass of 1.4 $M_\odot$ we find mean values $<v_e>$ =3762 km s^{-1}, $<q>$ = 0.224, and $<\kappa>$ = 0.0080 cm^2 g^{-1}. If the two subluminous events (i.e. SN 1991bg and SN 1998de) are excluded, these parameters change to $<v_e>$ =3626 km s^{-1}, $<q>$ = 0.236, and $<\kappa>$ = 0.0084 cm^2 g^{-1}.

This e-folding velocity may be slightly on the high side compared to what is predicted from 1-D explosion models that produce synthetic spectra that match observations. However, it is not radically different from our adopted e-folding velocity. An explosion model with the majority of the ^{56}Ni mixed in the outer layers, as implied by a q = 0.224 is most unlikely for the vast majority of robust explosion models. But this could be the case for a Chandrasekhar mass progenitor that produces a subluminous SN Ia. As mentioned before, in the optically thin limit κ ranges from 0.025 to 0.033 cm^2 g^{-1}. A factor of two (or even three) less of κ = 0.025 cm^2 g^{-1} is unlikely. At most one could conceive of κ to vary by $\sim$ 50 %.

To calculate the amount of intermediate mass elements (IMEs) produced during nuclear burning, we simply subtract the ejected mass from the amount of ^{56}Ni produced. Note this this value also includes the amounts of unburned carbon and oxygen. These values are listed in Table 5.1. Excluding SN 1994D we find that the IMEs range from $\sim$0.11 to $\sim$0.67 $M_\odot$.

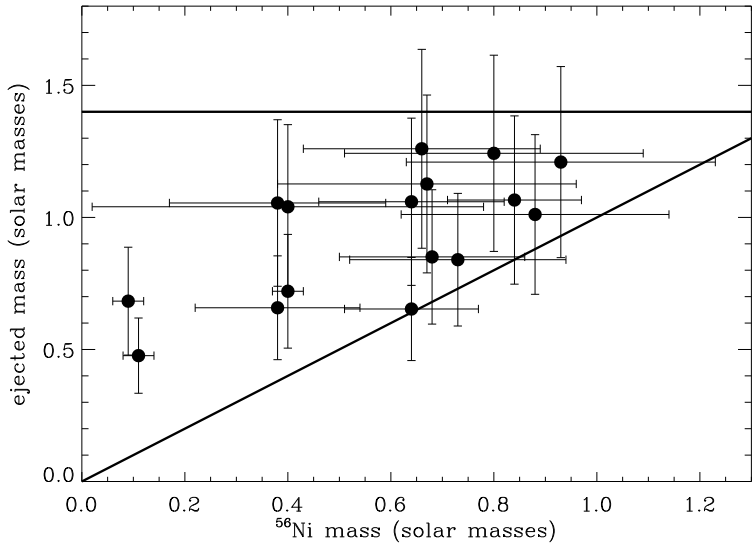

Figure 5.4.: Ejected mass plotted vs. ^{56}Ni mass for 16 SNe Ia. Units are in solar mass. See text for comments concerning the error bars. Solid horizontal line indicates the Chandrasekhar mass. Slanted line has a slope of 1.

In Fig. 5.5 we plot the ejected mass versus $t_\circ$, while holding the other parameters of Eq. (5.11) constant. The solid line (case 1) corresponds to all the fiducial values used to determine the ejected masses in Fig. 5.4. The dashed line (case 2) shows the effect of keeping q and κ fixed at the fiducial values while using v_e = 3625 km s^{-1}. For the dash-dot-dot line (case 3) we used v_e = 3625 km s^{-1}, κ = 0.0084 cm^2 g^{-1} and q = 0.5. Finally the dash-dot line (case 4) corresponds to v_e = 3625 km s^{-1}, q = 1/3, and κ = 0.0084 cm^2 g^{-1}. This figure illustrates the strong dependencies of the ejected masses. Masses much above the Chandrasekhar mass are achieved for only extreme cases. Both case 1 and case 2 provide ejected masses at or near the Chandrasekhar mass for events with large values of $t_\circ$ and substantially less for those events with values of $t_\circ \approx$ 22-26 days.

Another interesting feature displayed in Fig. 5.4 is that there appears to be little or no correlation between the ejected mass and the amount of ^{56}Ni. This is not entirely unexpected because as even with the presumption that all SNe Ia originate from a Chandrasekhar size white dwarf, there still exists a range of ten or more in amount of ^{56}Ni produced. Nevertheless this is additional evidence which suggests that there is a significant variation in the burning of SNe Ia.

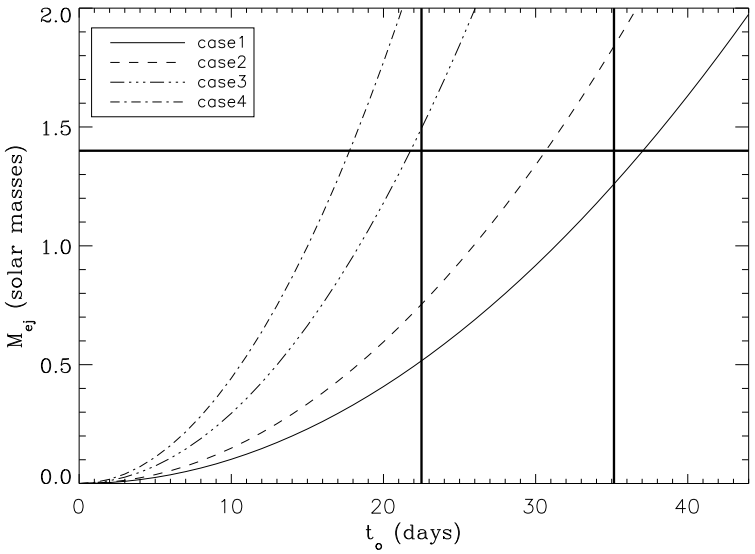

Figure 5.5.: Ejected mass plotted vs. t_o for fixed values of the parameters in Eq (5.11). See Sect. 5.3 and Table 5.2 for a complete description of each curve. Solid vertical lines indicates the minimum and maximum values for t_o in our sample, and the solid horizontal lines indicates the Chandrasekhar mass.

5.4. Discussion

With the stipulation that the UVOIR light curve reasonably traces the true bolometric flux, from within the period of soon after explosion to one hundred days past maximum light, we have been able to derive constraints on the total ejected mass. The appeal of our approach is that, with relative ease and simple assumptions, we have used existing data to gain a deeper understanding on the origins of SNe Ia as well as provide sorely needed constraints on current models.

As previously mentioned, it is commonly believed that SNe Ia are the result of the thermonuclear disruption of a C-O white dwarf. The premise that thermonuclear combustion occurs at the Chandrasekhar limit was invoked to address the issue of homogeneity. However, today it is well established that SNe Ia are not true standard candles as once thought in the past (e.g. Leibundgut 2004).

Table 5.2. Fixed parameters used in Fig. 5.5

case	q	v_e (km s^{-1})	κ (cm^2 g^{-1})
1	0.33	3000	0.0250
2	0.33	3625	0.0250
3	0.50	3625	0.0084
4	0.33	3625	0.0084

Under the main assumption that at times greater than fifty days past maximum light the energy deposition in the ejecta of a SN Ia is solely due to the ^{56}Co→^{56}Fe decay chain, and thus the optical depth has a t^{-2} dependence, we can estimate (from the UVOIR light curve) the epoch when the photosphere transforms from being optically thick to optically thin. With this knowledge we can then use the parameterized SN Ia model of Jeffery (1999) to place constraints on the ejected mass.

The results presented in Fig. 5.4 provide us with evidence that not *all* SNe Ia originate from a Chandrasekhar size white dwarf or other very severe differences in the explosions like the distribution of ^{56}Ni or kinetic energies (expansion velocities) exist. This would then immediately imply that some sort of sub-Chandrasekhar mass model is responsible for at least some SNe Ia. If true, this would be a radical change in thinking from the currently favored paradigm for the progenitor systems of SNe Ia. However, the suggestion that a sub-Chandrasekhar mass model may be a viable candidate for the progenitors of some SNe Ia is certainly not a new concept. Similar to Chandrasekhar mass models, previous attempts to simulate these systems have been plagued with their own problems. We refer the reader to Hillebrandt & Niemeyer (2000) and Livio (2000) for detailed reviews concerning this class of progenitor system; we briefly summarize them here.

As a sub-Chandrasekhar mass white dwarf does not reach the necessary temperatures and densities for thermonuclear combustion to begin, an outside catalyst is required to trigger the thermonuclear runaway. It has been suggested that this agent is associated with detonation(s) located at the base of a helium layer that accretes around the white dwarf (Weaver & Woosley 1980, Nomoto 1980, Woosley et al. 1980, Nomoto 1982, Sutherland & Wheeler 1984, Iben & Tutukov 1984). The helium itself is thought to accrete from the white dwarf's companion star. The detonation(s) result in a compression wave that travels through the white dwarf causing the C-O core to ignite, whereupon a thermonuclear runaway ensues. This mechanism is know by several names which include: an edge lit detonation, a helium ignitor, or an indirect double detonation.

Previous attempts to model sub-Chandrasekhar explosions (Woosley & Weaver 1994a, Livne & Arnett 1995, Höflich & Khokhlov 1996) have met with some success in reproducing the observed light curves. However, these models typically predict a high-velocity layer of ^{56}Ni and helium above the intermediate mass elements, which is not observed in any spectra. It must be noted that relatively little effort has been made to conduct detailed 3-D simulations of *sub*-Chandrasekhar mass models (but, see Benz 1997). With more detailed modeling, this progenitor channel may provide an attractive alternative to the Chandrasekhar mass model. We also note that one appealing advantage offered by this model is the ability to obtain the progenitor statistics predicted by population synthesis calculations (see Livio 2000, and references within).

Previously, Cappellaro et al. (1997) employed a technique that used observations of SNe Ia to determine both the ^{56}Ni mass and the ejected mass. In their method they modeled the *V*-band light curves of a small sample of SNe Ia using a simple Monte Carlo code. We find that our overall results are analogous to what they determined for both the range in the ^{56}Ni mass and the ejected mass. Contrary to their work we employed a different manner to determine these parameters and used UVOIR light curves rather than V-band light curves. By using the UVOIR light curve instead of the *V*-band light curve, we circumvented the crude assumption that the latter is a close surrogate to the former during post maximum times. Indeed, a comparison between our UVOIR light curves to the *V*-band light curves indicates that by fifty days past maximum light, the bolometric correction (m_{bol-m_v}) is $\sim$ 0.2 mag or more. At later times this

difference is amplified, as the near infrared passbands provide an increasing contribution to the bolometric flux (Sollerman et al. 2004).

Although we find that our conclusions are in line with to those presented in Cappellaro et al. (1997), there are subtle differences between the four events that coincide in both studies. The numbers we provide below for our results were obtained using Eq. (5.11) and the fiducial values quoted previously. Also, note that there are slight differences (no larger than $\mu = 0.20$) in the distances used between our work and that of Cappellaro et al.

For SN 1991bg, Cappellaro et al. found a ^{56}Ni mass $M_{Ni} = 0.1\ M_\odot$ and an ejected mass of $M_{ej} = 0.7\ M_\odot$. This is comparable to our findings of $M_{Ni} = 0.11\ M_\odot$ and $M_{ej} = 0.48 \pm 0.14\ M_\odot$. Furthermore, our M_{Ni}/M_{ej} ratio of 0.23 is larger than their 0.14. We found for SN 1992A, $M_{Ni} = 0.40\ M_\odot$ and $M_{ej} = 0.72 \pm 0.27 M_\odot$, as compared to their $M_{Ni} = 0.4\ M_\odot$ and $M_{ej} = 1.0\ M_\odot$. This then gives us a M_{Ni}/M_{ej} ratio of 0.56 compared to their 0.40.

We find that our results for the next two SNe Ia differ more than for the first two stated events. For SN 1994D we calculated $M_{Ni} = 0.64\ M_\odot$ and $M_{ej} = 0.65 \pm 0.25\ M_\odot$, compared to their values of $M_{Ni} = 0.8\ M_\odot$ and $M_{ej} = 1.4\ M_\odot$. Thus we obtain a larger difference in our M_{Ni}/M_{ej} ratio of 0.98 compared to their 0.57. The fact that we have calculated a ^{56}Ni mass that is equal to the ejected mass is questionable. To determine the ^{56}Ni mass of SN 19994D we used a new SBF distance (Ajhar et al. 2001) rather than the SBF distance (Tonry et al. 1997) used by Contardo et al. (2000) who determined a ^{56}Ni mass of 0.40 $M_\odot$. Using the distance modulus adopted by Cappellaro et al. we obtain a ^{56}Ni mass of 0.67 M⊙. Recently Feldmeier et al. (2005) have calculated a planetary nebulae distance to the host galaxy of SN 1994D. In their study they have determined the distance modulus $\mu = 30.66$. This is comparable to the Tonry et al. (1997) distances modulus $\mu = 30.68$. Using the planetary nebulae distance the ^{56}Ni mass would be reduced to $\sim 0.40\ M_\odot$. Nonetheless the ^{56}Ni mass determined by us and Contardo et al. is less than the $0.8\ M_\odot$ calculated by Cappellaro et al. with their method. The discrepancies between these values of the ^{56}Ni mass underscores the effect of the uncertainty in the distances.

Finally, for SN 1991T Cappellaro et al. assumed $M_{ej} = M_{Ni}$ where $M_{Ni} = 1.1\ M_\odot$. We, on the other hand, found $M_{Ni} = 0.93\ M_\odot$ and $M_{ej} = 1.21 \pm 0.36\ M_\odot$. In summary we find the results presented by Cappellaro et al. to be in fair agreement with our calculations, although some discrepancies do exist.

We have presented an investigation of the bolometric behavior of sixteen SNe Ia. In particular we have provided important constraints on the progenitor system(s) of these stellar explosions. Our results suggest that some progenitor system(s) of SN Ia may emanate from the thermonuclear explosion of a sub-Chandrasekhar mass white dwarf. This result may be difficult to reconcile with the current paradigm of the progenitor system of SNe Ia, i.e. a Chandrasekhar mass white dwarf. Moreover, our results suggest that the amount of ^{56}Ni produced during the explosion is most likely not dependent on the mass of the progenitor, but more likely on the manner in which nuclear burning is initiated and the subsequent dynamics of the flame propagation through the white dwarf. The range in synthesized ^{56}Ni possibly indicates that there are two different explosion mechanisms. Further modeling of the explosion mechanism is required in order to investigate how different initial conditions can affect the observed range in luminosity.

In Fig. 5.4 we see –in contrast to current thinking– that the mean ejected mass of many explosions is on the low side. A valid concern is that the parameters used to determine the ejected masses may not exactly represent those of a real SN Ia explosion. One parameter that may be in error, and does have a significant effect on our estimates of the ejected masses is

the adopted value of the e-folding velocity (see Fig 5.5). If we assume slightly larger values of v_e, the mean ejected mass for our sample would be in better agreement with 1.4 M⊙. How this parameter differs in 3-D simulations compared to 1-D simulations is not yet clear. In addition, the simple assumption that any one of the parameters in Eq. (5.11) is unique for all events probably incorrect. This may have a significant effect on the determined ejected mass for each event. However, this does not necessary imply that we would obtain larger ejected masses. It would be helpful if the theorists in the future provided values of v_e and q from their simulations.

An acceptable argument concerning the results presented in this work is the validity of the model used to determine the ejected mass. There may be several assumptions built into the parameterized model of Jeffery (1999) which could be too naïve, and therefore the model may not adequately account for various complicated physical processes that occur within the progenitor of a SN Ia. However, there currently exists no other method to use observed photometry to place constraints on such a parameter.

In principle we would like to compare the UVOIR light curves to detailed NLTE modeled light curves. Unfortunately there has been little success in such an endeavor owing to the complications in performing such time-dependent calculations as well as the limits of atomic line data, however see Kozma et al. (2005). The next step will be to fit UVOIR light curves to a grid of model light curves produced from 3-D radiative transfer calculations, and then place further constraints on the progenitor systems of SNe Ia.

6. Lower limits on the Hubble constant from models of SNe Ia

6.1. Introduction

SNe Ia have become an important distance indicator in modern cosmology. Today, they are utilized to determine the value of the Hubble constant ($H_\circ$) and measure the changes of the past cosmic expansion. For this reason a number of substantial observing campaigns have recently been conducted for SNe Ia at nearby redshifts (see Leibundgut 2000, for a list). As a result there is now a considerable number of events available with superb temporal and photometric coverage. However, there has been little effort made to use these high quality data sets to link observations with the physics of SNe Ia in a systematic way. The purpose of this chapter is to combine results obtained from theoretical models with modern data in order to constrain the value of $H_\circ$.

Prior attempts to couple observations with explosion models of SNe Ia in order to determine the value of $H_\circ$ include the pioneering investigations of Arnett et al. (1985), followed by Branch (1992), Leibundgut & Pinto (1992), Nugent et al. (1995) and Höflich et al. (1996). These works gave promising results, constraining the Hubble constant between $45 \leq H_\circ \leq 105$ km s^{-1} Mpc^{-1}, and revealed that with few assumptions, SNe Ia used in such a manner provide an attractive way to measure $H_\circ$, while circumventing many problems associated with the extragalactic distance ladder (see Böhm-Vitense 1997, Livio et al. 1997).

Here we use bolometric light curves of SNe Ia as a means to link observations with results obtained from models of an exploding C-O white dwarf (see Chapter 2.4 for a summary of the progenitor systems). In particular we utilize a set of well observed SNe Ia to demonstrate, via two methods, (see below Sect. 6.4 and Sect. 6.5) that –under the assumption that SNe Ia are a product of the thermonuclear disruption of a C-O white dwarf– it proves to be rather difficult to obtain a value of $H_\circ < 50$ km s^{-1} Mpc^{-1}. It must be noted that by neglecting the small amount of flux outside the UVOIR wavelength regime we introduce a systematic underestimation on the calculated values of $H_\circ$. However, we address this systematic error when placing constraints on $H_\circ$ (see below). Also, note that the summed UVOIR flux offers the advantage that we do not need to apply any K-corrections[1], which are necessary when just using individual filter passbands of SNe Ia located in the Hubble flow. Essentially, we can reduce the problem to one of energy balances where the energy inputs from the radioactive decays and the losses due to γ ray escape can be compared to the observed wavelength-integrated flux of the SNe Ia.

Our results, along with the recent detection of the integrated Sachs-Wolfe (ISW)[2] effect

[1] K-correction refers to the correction applied to observed photometry that accounts for the effects due to redshift on the spectra energy distribution of distance SN Ia.

[2] The ISW effect is responsible for a portion of the anisotropies that are observed in the cosmic microwave back-

(Boughn & Crittenden 2004a,b) observed in the Wilkinson Microwave Anisotropy Probe data, (Bennett et al. 2003, Spergel et al. 2003) cast doubts on recent discussions in the literature (see Blanchard et al. 2003, Shanks 2005), which suggest "alternatives" to the concordance cosmological model. Spatially flat, matter-dominated Einstein-de Sitter models may produce a temperature power spectrum that can fit CMB observations just as accurately as the best concordance model, which sports a dark energy component. However, Einstein-de Sitter models require very low values of the Hubble constant (e.g. $H_\circ \simeq 46$ km s^{-1} Mpc^{-1}) and are unable to account for the observed ISW effect.

The structure of this chapter is as follows: in Sect. 6.2 we briefly discuss the data used in this chapter. In Sect. 6.3 we discuss different models of SNe Ia and the ^{56}Ni yields we adopt for a typical SN Ia. We then present in Sect. 6.4 a method to derive $H_\circ$ through the combination of observations and the theoretical ^{56}Ni masses calculated in explosion models. Section 6.5 contains a discussion of the classical way to derive $H_\circ$ through the Hubble diagram of SNe Ia. Contrary to previous methods we employ here the bolometric flux. We conclude in Sect. 6.6.

6.2. Observational data

We selected only the SNe Ia listed in Table 3.1 that are located in the Hubble flow (≥ 3000 km s^{-1}). Four of these SNe Ia include *U*-band photometry, and for those events without *U*-filter observations we added a correction as described in Chapter 4.2. At this stage, no corrections were made to account for contributions by *UV*-flux blueward of the atmospheric cutoff and near-infrared *JHK*-band photometry.

Table 6.1 lists all the SNe Ia (and references) considered in this chapter. Also listed are the two observables that are employed to constrain $H_\circ$. This includes the host galaxy recession velocity and the UVOIR bolometric flux at maximum light. Heliocentric velocities obtained from the Nasa/IPAC Extragalactic Database (NED) were converted to the CMB frame. As all SNe Ia listed in Table 6.1 are located in the Hubble flow, we assumed an error of 400 km s^{-1} for all velocities, in order to account for (random) peculiar motions. The uncertainties listed with the bolometric fluxes account for (1) a small measurement error, which is less than 5% and (2) the uncertainties associated with estimates of host galaxy extinction.

6.3. ^{56}Ni yields from explosion models

A key ingredient for the methods presented below (see Sect.6.4 and Sect. 6.5) is the amount of ^{56}Ni produced in a *typical* SN Ia explosion. Both methods depend on the total energy radiated by the SN Ia to establish its distance. Contardo (2001) showed for a small sample of SNe Ia that up to a factor of 10 difference in the yield of ^{56}Ni can exist between individual events. An absolute upper limit for the amount of ^{56}Ni synthesized is the Chandrasekhar mass ($\sim$1.4 $M_\odot$), when the star becomes unstable and either collapses or explodes. However, due to the presence

ground (CMB). These anisotropies are created by CMB photons that transverse evolving gravitational potentials of linear collapsing structures in the nearby universe (i.e. $z < 1$). The detection of the ISW effect implies that the gravitational potentials of linearly collapsing structures are evolving in time, and hence, is the direct consequence of a Λ dominated flat universe.

Table 6.1. Well-observed SNe Ia in the Hubble Flow

SN	Filters	Ref.	$E(B\text{-}V)^{a}_{gal}$	$E(B\text{-}V)_{host}$	v_{CMB} [b] (km s^{-1})	F^{bol}_{max} (erg s^{-1} cm^{-2})
SN1992bc	*BVRI*	1	0.022	0.000	5870	$(1.565\pm0.124)\times10^{-11}$
SN1992bo	*BVRI*	1	0.027	0.000	5151	$(9.106\pm0.967)\times10^{-12}$
SN1993H	*BVRI*	1	0.060	0.050	7112	$(4.640\pm0.613)\times10^{-12}$
SN1995E	*BVRI*	2	0.027	0.740	3478	$(5.726\pm0.622)\times10^{-11}$
SN1995ac	*BVRI*	2	0.042	0.080	14651	$(3.425\pm0.477)\times10^{-12}$
SN1995bd	*BVRI*	2	0.495	0.150	4266	$(2.542\pm0.521)\times10^{-11}$
SN1996bo	*BVRI*	2	0.078	0.280	4857	$(2.382\pm0.237)\times10^{-11}$
SN1999aa	*UBVRI*	3, 4, 5	0.040	0.000	4546	$(2.333\pm0.446)\times10^{-11}$
SN1999aw	*BVRI*	5, 6	0.032	0.000	11754	$(3.525\pm0.700)\times10^{-12}$
SN1999dq	*UBVRI*	3	0.024	0.139	4029	$(3.871\pm0.730)\times10^{-11}$
SN1999ee	*UBVRI*	7	0.020	0.280	3169	$(5.781\pm0.881)\times10^{-11}$
SN1999gp	*UBVRI*	3, 8	0.056	0.070	7783	$(9.270\pm1.082)\times10^{-12}$

[a]Taken from Schlegel et al. (1998) dust maps.

[b]Heliocentric velocities from NED transformed to the cosmic microwave background frame. To account for peculiar velocities we assume throughout this work an error of 400 km s^{-1} for all CMB distances.

References. — (1) - Hamuy et al. 1996, (2) - Riess et al. 1999b, (3) - Jha 2002, (4) - Krisciunas et al. 2000, (5) - Regnault 2000, (6) - Strolger et al. 2002, (7) - Stritzinger et al. 2002, (8) - Krisciunas et al. 2001

of IMEs observed in spectra taken near maximum light, we know that the white dwarf is not completely burned to ^{56}Ni (see also Table 5.1). A lower limit is provided by the subluminous events. Although only a few of these SNe Ia have been observed in detail (due to selection effects) three well observed events indicate ~0.10 $M_\odot$ of ^{56}Ni is synthesized (see Chapter 4.3.1).

To obtain a more quantitative value we turn our attention to recent nucleosynthesis calculations performed at the Max-Planck-Institut für Astrophysik (MPA) (Travaglio et al. 2004), which are based on 3-D Eulerian hydrodynamical simulations (Reinecke et al. 2002a,b) of an exploding white dwarf, that burns via a purely turbulent deflagration flame.[3] Based on their highest resolution simulation (i.e. model b30_3d_768), which consisted of 30 "burning" bubbles and a grid size of 768^3 for 1 octant of a sphere, Travaglio et al. found the total yield of ^{56}Ni to be 0.42 $M_\odot$. However, they found that as the number of ignition spots is increased, more explosion energy is liberated, which may lead to a larger yield of ^{56}Ni. The number of these ignition spots is strictly dependent on the grid resolution of the simulation. This in turn limited by the computational facilities available. One may therefore expect a larger yield of ^{56}Ni as the computational power and hence grid resolution is increased. In addition, more recent calculations that employ ignition conditions representing a foam-like structure, consisting of overlapping and individual bubbles, indicate that it may be possible to liberate a larger fraction of nuclear energy as one employs different ignition conditions (Röpke & Hillebrandt 2005).

We considered a range of results produced by other deflagration models available in the literature, in particular the phenomenological parametrized 1-D model - W7 (Nomoto et al. 1984). Recent nucleosynthesis calculations show that W7 synthesizes 0.59 $M_\odot$ of ^{56}Ni (Iwamoto et al. 1999). It must be noted, however, that 1-D models compared to 3-D calculations are expected to provide a less realistic representation of the physical processes that occur during thermonuclear combustions because they do not properly model the turbulent flame physics. Additionally, multidimensional effects are neglected which do have an important influence on the flame propagation. Nevertheless, W7 is a well established model that can fit the observed spectra rather well (Harkness 1991, Mazzali et al. 1995, Mazzali 2001) and has been used extensively over the last two decades to investigate SNe Ia explosions.

Despite the success of deflagration models, they are currently unable to account for the more luminous SNe Ia, and predict appreciable amounts of unburned carbon, oxygen, and IMEs leftover in the inner ashes of the ejecta, which has not yet been conclusively observed. These shortcomings were the motivation for the delayed detonation models (DDM) (Khokhlov 1991, Woosley 1990, Woosley & Weaver 1994b, Höflich & Khokhlov 1996). In these models the explosions starts as a deflagration flame until a transition occurs, causing the flame to propagate supersonically. At this point the explosion becomes a detonation. Höflich (1995) provided a series of DDMs that range in ^{56}Ni mass between ~0.34 and 0.67 $M_\odot$. His best fit model (M36) for the well observed SN 1994D produces 0.60 $M_\odot$ of ^{56}Ni. The main difference to the pure deflagration models is that DDMs contain an additional free parameter know as the transition density (ρ_{DDT}). This free parameter is not physically understood but is essential to force the transition from deflagration to detonation.

[3] Note that in 3-D deflagration simulations, once the initial conditions are set (i.e. T, ρ, and chemical composition) the only parameter that may be adjusted is the manner in which the flame is ignited. Thus the amount of material burned is determined by the adopted sub-grid model and the fluid motions on the resolved scales (Reinecke et al. 2002a). Unlike 1-D simulations it is impossible to fine tune the amount of material burned at a given density.

Throughout the following analysis we adopt results from the highest resolution MPA simulation and the 1-D model W7. Although these two models are not meant to represent the complete range in observed luminosity for the total population of SNe Ia, they produce results that are illustrative of the majority of observed events. Both of these models are not perfect and, as results shown below indicate, the MPA model may not be representative of the more luminous events. We take the ^{56}Ni masses of these two models to be representative of a fair fraction of observed SNe Ia.

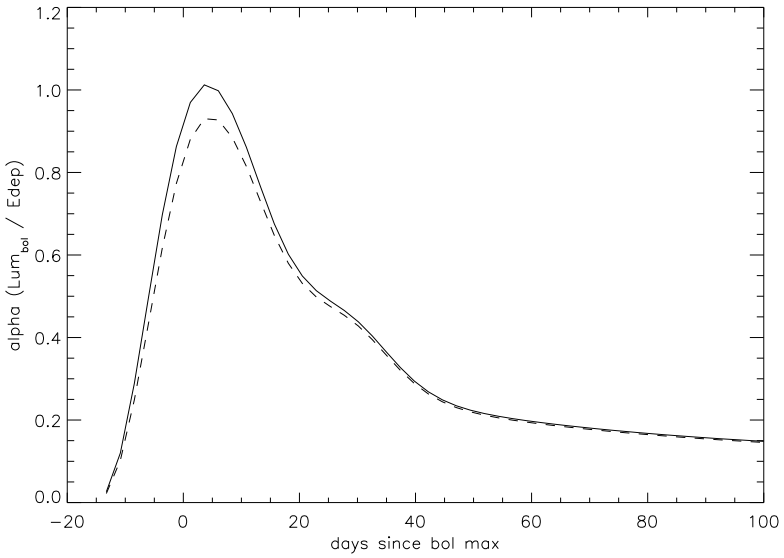

Figure 6.1.: The ratio of bolometric luminosity to energy deposition (i.e. α) for SN 1999ee. We have used a value of 0.74 $M_\odot$ of ^{56}Ni and adopted rise times of 17 days (dashed line) and 19 days (solid line).

As previously noted in Sect. 4.1, just after maximum light the observed luminosity is expected to be larger than the radioactive luminosity, as the ejecta becomes optically thin and allows the release of stored UVOIR photons. At this epoch the photosphere rapidly recedes into the ejecta, revealing deeper layers of the progenitor allowing more spectral lines to radiate. Branch (1992) (see his Table 1) conducted a survey of the best numerical models at the time and found that the models which adequately treat the time dependent nature of the opacity near maximum light predict α (the ratio of energy radiated at the surface to the instantaneous energy production by the radioactive decays) to be slightly larger than unity. He concluded that α=1.2±0.2 was the most applicable value and noted that the value of α appeared to be independent of the rise time.

This parameter is nothing more than a correction factor that is applied to the measured luminosity derived from the model ^{56}Ni masses. In the following, we take α into account in our discussion of the values of $H_\circ$ determined from the models. The ^{56}Ni masses of 0.42 and 0.59 $M_\odot$ correspond to an energy release after 19±3 days (the typical rise time of SNe Ia (Contardo et al. 2000)) of (8.40±1.26)×10^{42} erg s^{-1} and (1.18±0.18)×10^{43} erg s^{-1}, respectively. If we combine the energy production with α=1.2±0.2, the luminosity is increased to (1.01±0.23)×10^{43} erg s^{-1} and (1.42±0.32)×10^{43} erg s^{-1}. We note, however, that radiation transport calculations based on

two MPA 3-D simulations (Blinnikov, private comm.) give the same value of α as calculated by Arnett's more simple analytical models (i.e. α=1).

6.4. $H_\circ$ from model ^{56}Ni masses

In this section we derive a first analytic expression to constrain $H_\circ$ directly from model ^{56}Ni masses. This expression combines the UVOIR peak brightness with the explosion models via Arnett's Rule (Arnett 1982).

6.4.1. Connecting $H_\circ$ and the model luminosities

First, we develop an analytic equation which uses a simple argument that allows one to connect $H_\circ$ with the amount of ^{56}Ni produced in a SN Ia explosion. This relation relies on the fact that $H_\circ$ is defined as the ratio of the local expansion velocity to the luminosity distance, which in turn is obtained from the inverse square law for the ratio of luminosity and the observed brightness. Therefore since the luminosity of a SN Ia depends on the amount of ^{56}Ni, we can use the explosion models as our guide to the absolute luminosity. Combining this with both the measured brightness and recession velocity (or redshift) of any particular event, we can derive a value for $H_\circ$. The first expression to constrain $H_\circ$ therefore combines three elements: (1) Hubble's law of local cosmic expansion, (2) the distance luminosity relation, and (3) Arnett's Rule.

Combining Hubble's law, which is defined by

$$H_\circ = \frac{cz}{D_L} \tag{6.1}$$

with the distance luminosity relation given by

$$D_L = \left(\frac{L}{4\pi F}\right)^{\frac{1}{2}} , \tag{6.2}$$

where F corresponds to the UVOIR flux obtained from the bolometric light curves, L is the luminosity of a *fiducial* SN Ia, and D_L is the luminosity distance, we obtain

$$H_\circ = cz\left(\frac{4\pi F}{L}\right)^{\frac{1}{2}} . \tag{6.3}$$

Substituting Eq. (4.2) into Eq. (4.4) we can relate the luminosity to the mass of ^{56}Ni via $E_{\rm Ni}(t_R)$ (Eq. 4.3), and then if we include the factors that directly equate the luminosity with the ^{56}Ni mass, we obtain our final relation to calculate the Hubble constant

$$H_\circ = cz\left(\frac{4\pi F^{bol}_{max}}{L_{max}}\right)^{\frac{1}{2}} = cz\left(\frac{4\pi F^{bol}_{max}}{\alpha E_{\rm Ni}(t_R)}\right)^{\frac{1}{2}} = cz\left(\frac{4\pi F^{bol}_{max}}{\alpha\epsilon(t_R)M_{\rm Ni}}\right)^{\frac{1}{2}} . \tag{6.4}$$

With Eq. (6.4) only two observables – the bolometric flux ($F^{bol}_{\rm max}$) at maximum and the redshift (z) – are required to determine the value of $H_\circ$.

Uncertainties come from the rise time that determines the peak luminosity, the uncertainty in α, which depends on the radiation escape from the explosion, and of course the amount of ^{56}Ni synthesized in the explosion. Finally we note that our ^{56}Ni mass is "error free" in the sense that the adopted value(s) for this parameter (hence fiducial luminosities) are completely model dependent.

We now have an analytic form for $H_\circ$ that is directly connected to the ^{56}Ni produced in the explosion. The other parameters have to do with the radiation transport: the ratio of energy release to energy input and the time between explosion and maximum luminosity. We stress that this method is completely independent from the extragalactic distance ladder!

6.4.2. Results

In Fig. 6.2 we present results obtained using Eq. (6.4) for all SNe Ia listed in Table 6.1. For each SN Ia we show the derived $H_\circ$, assuming that its observed brightness would correspond to a given nickel mass (in steps of 0.1 $M_\odot$). The inverse square-root dependence of $H_\circ$ on the nickel mass is clearly visible. The '1-σ' error bars that accompany each point account for a recession velocity error of 400 km s^{-1}, an error associated with the reddening correction, a measurement error of the flux ($\leq$ 5%), a 3 day error for the assumed bolometric rise time, and a 2% error for those events that have a *U*-band correction. Note that the most dominant error is the uncertainty associated with the redshift due to peculiar velocities.

It is evident from this figure that for a given mass of ^{56}Ni there exists a range of possible values of $H_\circ$. This is what we expect owing to the fact that there are known intrinsic differences between SNe Ia. Hence, if we (erroneously) assume a single ^{56}Ni mass for all observed SNe Ia, we obtain a range of $H_\circ$ values as in Fig. 6.2.

Two SNe Ia (SN 1992bo and SN 1993H) are clearly situated below the rest of the objects and are both known to be red events with $\Delta m_{15}(B)$ =1.69 (Hamuy et al. 1996). Both also show evidence of weak Ti features in their spectra (Phillips, private comm.). Because the models we have adopted in this work were designed for normal SNe Ia and these two events are subluminous in nature, we exclude them in the following discussion; however, they are included in the Hubble diagram (see Sect. 6.5).[4]

Given the prediction of an explosion model, we can now read off the preferred value of the Hubble constant. Naïvely, one would like to take the mean of the distribution of the SN Ia for a given ^{56}Ni mass and derive a Hubble constant. However, the natural scatter of ^{56}Ni (Contardo et al. 2000, Bowers et al. 1997, Cappellaro et al. 1997) prevents us from doing this because only one value is correct for a given event. The best we can do now is to derive a lower limit for $H_\circ$ by associating the nickel masses with the faintest SNe Ia and hence obtain an underestimate of the Hubble constant.

By choosing a ^{56}Ni mass of 1 $M_\odot$ and associating it with faint SNe Ia we clearly reach a lower limit for $H_\circ$. Note that the highest ^{56}Ni mass derived from a SN Ia with a Cepheid distance is 0.93 $M_\odot$ (see Table 4.1). The solid horizontal line in Fig. 6.2 indicates that evidently more than 1 $M_\odot$ of ^{56}Ni must be produced in a normal SNe Ia explosion in order to obtain $H_\circ < 50$ km s^{-1} Mpc^{-1}. Note that the two dotted vertical lines indicate our adopted ^{56}Ni masses

[4] On a uniform distance scale SN 1992bo and SN 1993H are ~40% less luminous than the other objects and hence produce correspondingly less ^{56}Ni (see Chapter 4.3.1).

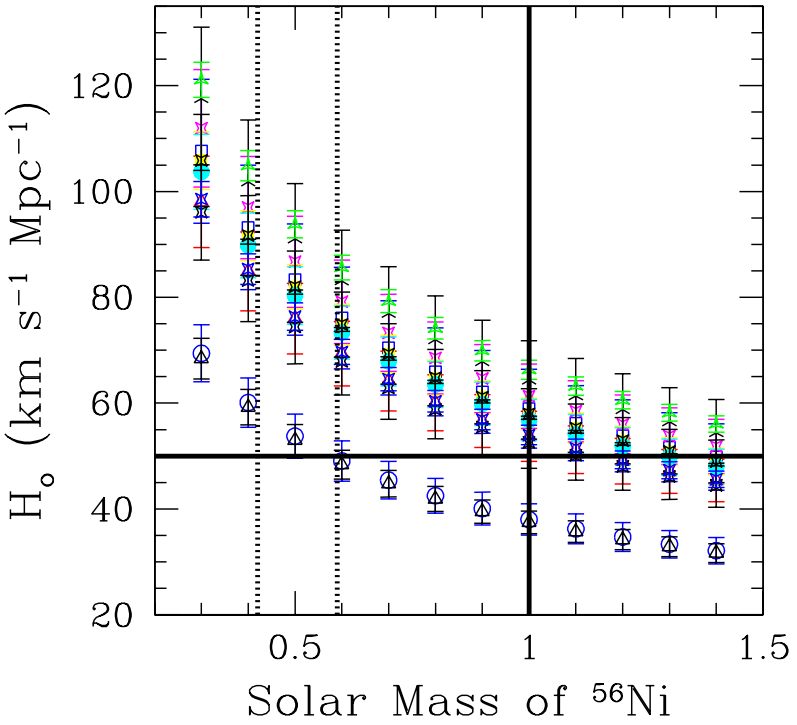

Figure 6.2.: Hubble constant as a function of ^{56}Ni mass for 12 SNe Ia in the Hubble flow for α=1. Error bars represent all uncertainties discussed in section 6.4.1. The dotted lines indicate the two ^{56}Ni masses from our adopted models. The solid vertical line indicates an upper limit on the production of ^{56}Ni expected from the thermonuclear explosion of a C-O white dwarf, and the solid horizontal line corresponds to the lower limit we derive for $H_\circ$.

with α=1.0. For both cases an $H_\circ$ of more than 50 km s^{-1} Mpc^{-1} is favored. Only the two faint SNe Ia fall well below this value.

To obtain an absolute lower limit on $H_\circ$, we present in Fig. 6.3 the least luminous normal event in our sample – SN 1999aa – with 1-σ and 3-σ confidence levels. This SN Ia produces values of $H_\circ$ that are 9% below the mean determined from all 10 normal events. For our adopted ^{56}Ni masses with α=1 we obtain a lower limit on $H_\circ$ with SN 1999aa (3-σ away from the calculated values) to be $\geq$ 40 km s^{-1} Mpc^{-1}. The dashed line in Fig. 6.3 illustrates the effect of increasing α by 20%. We see that this gives us an additional systematic uncertainty that would decrease $H_\circ$ by 9%. The change incurred on the Hubble constant lies directly on top of the quoted lower 1σ confidence level. Finally, we note from Eq. (6.4) that by neglecting ~10% of the flux emitted outside of the optical, we systematically underestimate $H_\circ$ by 5%.

We find that with white dwarfs as progenitors of SNe Ia it is very difficult to obtain a value of $H_\circ$ < 50 km s^{-1} Mpc^{-1}. With 1 $M_\odot$ of ^{56}Ni, one could expect $H_\circ$ ~50 km s^{-1} Mpc^{-1}. Observations and models for the most luminous events indicate that no more than 1 $M_\odot$ of ^{56}Ni is produced. With our adopted ^{56}Ni masses (0.42 $M_\odot$ < ^{56}Ni < 0.59 $M_\odot$) we find from the 1-σ error

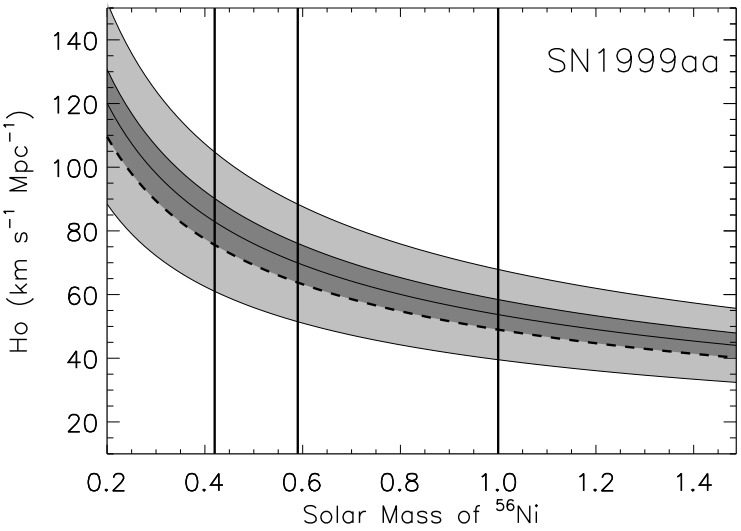

Figure 6.3.: To highlight the absolute lower limit we derive on $H_\circ$ we plot results obtained with SN 1999aa (the least luminous of our 10 normal SNe Ia) with 1-σ (dark shading) and 3-σ (light shading) confi dence levels. Vertical solid lines indicate both the adopted ^{56}Ni masses and the 1 $M_\odot$ upper limit expected from an exploding C-O white dwarf. The dashed line illustrates the effect if α is increased by 20% (i.e. α=1.2).

bars in Fig. 6.3 the Hubble constant to be constrain between $70\pm6 \leq H_\circ \leq 83\pm7$ km s^{-1} Mpc^{-1}.

The problem can, of course, also be inverted to derive a possible range of ^{56}Ni mass given a value of $H_\circ$. This will be interesting to constrain the ^{56}Ni mass for models, should $H_\circ$ be known to high accuracy. For $H_\circ \approx 70$ km s^{-1} Mpc^{-1}we find from Fig. 6.2 a range in the amount of ^{56}Ni produced in a SNe Ia explosion to be 0.5 $M_\odot$ < ^{56}Ni < 1.0 $M_\odot$.

6.5. $H_\circ$ through the Hubble diagram of SNe Ia

With this method we determine $H_\circ$ from the Hubble diagram in a manner similar to what has been previously presented by Tammann & Leibundgut (1990) and Leibundgut (2000) (see also Sandage & Tammann 1993, Hamuy et al. 1995, Phillips et al. 1999, Parodi et al. 2000, for similar applications). We note that this method is similar to the previous method, however, here $H_\circ$ is calculated in a more traditional manner. An analytic expression to constrain $H_\circ$ from our Hubble diagram is trivial to derive from the distance luminosity relation. Solving Eq. (6.2) for F^{bol}_{max} and then taking the logarithm of both sides, we obtain

$$\log(F^{bol}_{max}) = \log\left(\frac{L_{max}}{4\pi D_L^2}\right) . \tag{6.5}$$

Substituting $cz/H_\circ$ for D_L and rewriting the right hand side of Eq. (6.5) we obtain

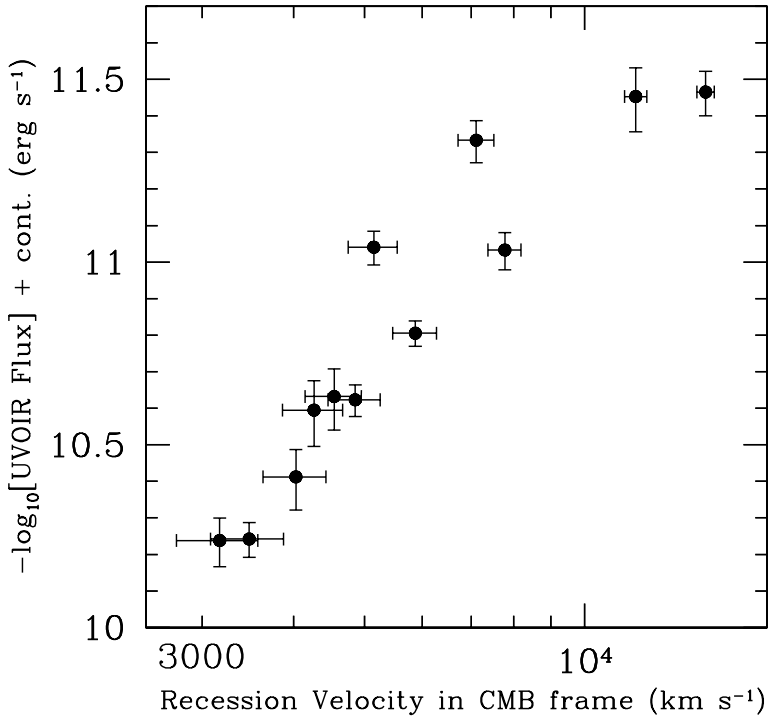

Figure 6.4.: Hubble diagram of 12 SNe Ia in the Hubble flow. The negative logarithm of the UVOIR flux at maximum light is plotted against the logarithm of the recession velocity in the CMB frame. Error bars account for a peculiar velocity of 400 km s^{-1} and uncertainties associated with host galaxy reddening.

$$\log(F_{max}^{bol}) = -2\log(cz) + \log(L_{max}) - \log(4\pi) + 2\log(H_\circ) \; . \tag{6.6}$$

There is a linear relation between $\log(F_{max}^{bol})$ and $\log(cz)$ as can be seen in Fig. 6.4. A linear regression to the data yields a slope of 2.01 ± 0.25, which is fully consistent with the expected slope of 2 for a linear local expansion derived in Eq. (6.6). From Fig. 6.4 it is also obvious that the two faint objects are outliers. If they are ignored, the fit sharpens up to a slope of 1.97 ± 0.10. With a fixed slope to this linear expansion value of 2 we derive the y-intercept, which corresponds to

$$b = -\log(L_{max}) + \log(4\pi) - 2\log(H_\circ) \; . \tag{6.7}$$

Solving Eq. (6.7) for $H_\circ$, we arrive at our final expression for the Hubble constant

$$H_\circ = \left(\frac{4\pi}{10^b L_{max}}\right)^{\frac{1}{2}} \; . \tag{6.8}$$

The Hubble constant is now simply calculated by plugging in the y-intercept, b, derived from the linear regression of the Hubble diagram and a *fiducial* luminosity defined by our adopted models.

6.5.1. Results

In Fig. 6.4 we present our Hubble diagram containing all SNe Ia listed in Table 6.1. Error bars for all events account for both a redshift uncertainty of 400 km s^{-1} and the uncertainties associated with host galaxy reddening. A weighted least-squares fit to the Hubble diagram (for all 12 SNe Ia), with a fixed slope of 2, yields b =3.292±0.047. Plugging this into Eq. (6.8) along with our adopted ^{56}Ni masses of 0.42 $M_\odot$ and 0.59 $M_\odot$ we find $H_\circ$ to be ≥ 85±7 and ≥ 72±6 km s^{-1} Mpc^{-1}(1-σ error) respectively. Accounting for α=1.2±0.2 we obtain lower values of the Hubble constant to be $H_\circ$ ≥ 78±9 and ≥ 66±8 km s^{-1} Mpc^{-1}, respectively.

As an upper limit in the amount of ^{56}Ni synthesized in the most luminous SNe Ia explosion is expected to be ≈ 1 $M_\odot$, we can use the corresponding luminosity as a guide to obtain a lower limit on the Hubble constant through the Hubble diagram. Thus, for 1 $M_\odot$ of ^{56}Ni and α=1 we obtain a value of $H_\circ$ ≥ 55±5 km s^{-1} Mpc^{-1}. As in the previous method, we are underestimating $H_\circ$ by ∼5%, due to flux outside the optical window.

6.6. Discussion

Under the main assumptions: (1) that the progenitors of SNe Ia are C-O white dwarfs, and (2) that the amount of ^{56}Ni synthesized to first order determines the peak luminosity, we are able to use results obtained from state-of-the-art numerical simulations of explosion models to uniquely define the bolometric peak luminosity, and in concert with photometric observations constrain $H_\circ$. The attractiveness of this approach stems from the ability to bypass assumptions that are typically made when one attempts to determine $H_\circ$, i.e. the extragalactic distance ladder and its accumulation of error from rung to rung. We stress that our fitting method does not add any corrections to the data. In other words we *do not* normalize the flux to any decline rate relation (e.g. Δm_{15} (Phillips et al. 1999), MLCS (Riess et al. 1996) or stretch (Perlmutter et al. 1997)).

Uncertainties that marginally affect (in decreasing order of importance) our results include: the abundances of peak Fe group metals – stable and radioactive – produced in the explosion models, the redshift peculiar velocities of each SN Ia, the total absorption, the assumed rise time to bolometric maximum, the exact nature of α, which may slightly vary from SN to SN depending on the exact nature of the opacity and ionization structure of the expanding ejecta, and the amount of flux that we neglect outside of the optical window.

It is still unclear what parameters effect the amount of ^{56}Ni produced in a SN Ia explosion. Obvious candidates are the initial conditions prior to explosion. These include the metallicity of the C-O white dwarf, the central density and the ignition mechanism. If there is a considerable fraction of alpha elements such as ^{22}Ne within the progenitor one would expect more stable isotopes such as ^{58}Ni and ^{54,56}Fe to be produced from burning to NSE, thus reducing the ^{56}Ni yield (e.g. Brachwitz et al. 2000). A higher central density on the other hand would lead to a more robust explosion and hence an increased amount of ^{56}Ni. As discussed earlier the explosion mechanism is still uncertain and different deflagration and detonation scenarios produce

different amounts of peak Fe group elements. Nevertheless with a larger ^{56}Ni mass we obtain smaller values of $H_\circ$. Errors attributed to the adopted recession velocity and reddenings produce scatter in our Hubble diagram but have very little effect on our calculations of $H_\circ$ via Eq. (6.4) or Eq. (6.8). The ±3 day departure from our adopted rise has no more than a 10% effect on our calculations. A change in α by ±20% can affect $H_\circ$ by 9%. Finally, we reiterate from Eq. (6.4) that by neglecting ∼10% of the flux emitted outside of the optical, we are underestimating $H_\circ$ by at least 5% or correspondingly more if more flux is unaccounted in our method.

In Sect. 6.5.1 we determined a rather high value (85 km s^{-1} Mpc^{-1}) for the Hubble constant when using results from the MPA model. This indicates that the amount of ^{56}Ni produced in these 3-D deflagration simulations currently are on the low side. And indeed a large sample of SNe Ia shows that the average distribution of ^{56}Ni mass is slightly higher (~ 0.6 M$_\odot$) (see Chapter 4.3.1). This suggests that their models may need more fine tuning in order to produce a larger amount of ^{56}Ni, and hence match observations more accurately.

There have been many attempts since Kowal (1968) presented his Hubble diagram to exploit SNe Ia to determine $H_\circ$. We refer the reader to Branch (1998) for a detailed review of previous works that attempt to calculate $H_\circ$ based on SNe Ia. He concluded, from methods based on physical considerations similar to the methods presented in this work and methods which utilize SNe Ia that have been independently calibrated by Cepheids, a range in the Hubble constant of $54 \leq H_\circ \leq 67$ km s^{-1} Mpc^{-1}, with a “consensus" on $H_\circ = 60\pm10$ km s^{-1} Mpc^{-1}. More recent investigations of Suntzeff et al. (1999) and Jha (2002) give values of $H_\circ = 64$ km s^{-1} Mpc^{-1}. Finally, (Freedman et al. 2001, Spergel et al. 2003, Altavilla et al. 2004) have all measured slightly larger values of $H_\circ \approx 70$ km s^{-1} Mpc^{-1}with 10% accuracy.

Another method independent of the extragalactic distance ladder that combines X-ray imaging of galactic clusters with the Sunyaev-Zel’dovich effect (SZE) has been recently used to place limits on $H_\circ$ (Myers et al. 1997, Mason et al. 2001, Jones et al. 2001, Reese et al. 2002). These works have provided the detailed study of 41 clusters giving distances which yield an averaged value of $H_\circ \approx 61\pm3$ km s^{-1} Mpc^{-1}(for a review see Reese 2004).

We find from both methods presented here that the Hubble constant must be greater than 50 km s^{-1} Mpc^{-1}in order to be compatible with current SN Ia models. In addition, we stress that this lower limit is based on the assumption that 1 M$_\odot$ is an upper limit on the amount of ^{56}Ni produced in a SN Ia explosion, and not from our adopted models. This result, along with other methods to measure $H_\circ$ using SNe Ia calibrated with Cepheids, SZE/X-ray distances and evidence of the ISW effect, strongly suggest that we do not live in a matter dominated universe without some form of cosmological constant or similar agent.

7. New spectrophotometric standards stars useful for S-corrections

Forward: warning for the non-observer

The subject matter contained in the following chapter consists of considerable technical detail.

7.1. Introduction

From dedicated follow-up observations of SNe it has become clear that systematic magnitude differences can exist between data sets obtained at different telescopes for the same event. These differences can be on the order of several hundredths of a magnitude or more near maximum and potentially larger for late-time photometry when the spectrum enters the nebular phase. This effect is undoubtedly caused by the use of filter sets employed at different telescopes, which do not exactly match each other (Suntzeff et al. 1988, Menzies 1989, Hamuy et al. 1990, Suntzeff 2000), and are magnified when the instrumental filters differ grossly from the standard Johnson/Kron-Cousins passbands. Although the observed photometry is standardized to a common system through the use of color terms, this is not expected to work perfectly. This is because there are radical differences between the normal and continuous spectral energy distributions (SEDs) of the photometric standard stars compared to the SEDs of SNe, which are dominated by strong absorption and emission features.

In Fig 7.1 we compare the photometry for SN 1999ee (Stritzinger et al. 2002) obtained by two different telescopes. The systematic differences between the data obtained with the CTIO 0.9 m and the YALO telescope are clearly visible. Using SNe photometry uncorrected for this effect can lead to incorrect calculations of colors, host galaxy reddening, absolute magnitudes, and can ultimately bias cosmological parameters. However, the photometrist may remedy this by computing spectral corrections or “S-corrections" to correct their photometry to a standard filter transmissivity function. An at least partially successful attempt to reconcile these magnitude differences in the optical for the well observed SN 1999ee was made by Stritzinger et al. (2002). More recently, this photometric technique has been used in the optical and extended to near infrared photometry by Krisciunas et al. (2003), Candia et al. (2003), Krisciunas et al. (2004b), and Pignata et al. (2004) for a number of other well observed SNe.

Spectrophotometric standard stars play a crucial role in determining accurate S-corrections. However, there exists only a small number of moderately faint standard stars –that are of limited color range– useful for spectroscopic calibrations. In this work we construct a large atlas of flux-calibrated spectra in order to enlarge the hitherto available spectrophotometric standards. Our program consists of a large number (~100) of Landolt standard stars, which have well-documented photometric magnitudes and are widely used for photometric calibrations. These

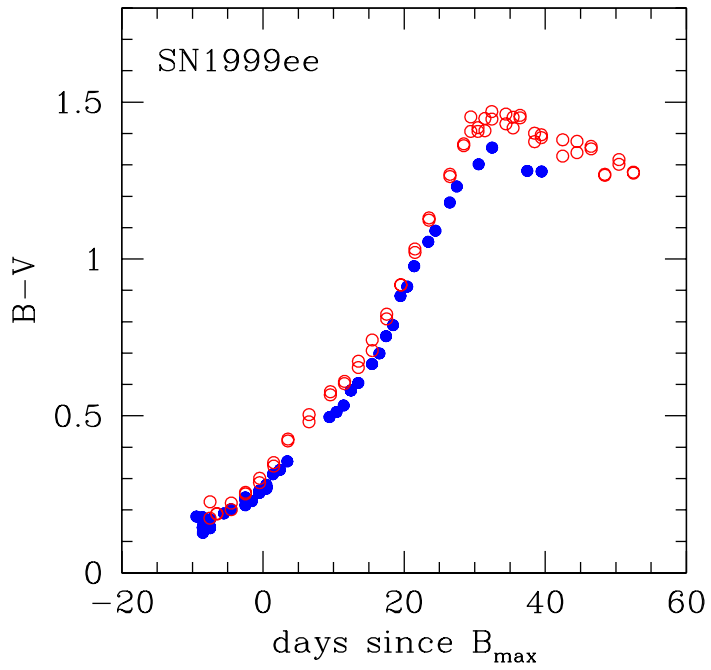

Figure 7.1.: Color evolution (B-V) vs time since maximum *B*-band light for SN 1999ee. Photometry obtained at the CTIO 0.9 m (filled dots) is compared to photometry obtained with the YALO telescope (circles). Note the systematic differences between these two data sets, which increase with time.

standard stars now may be employed to flux-calibrate spectra necessary for determining many physical parameters of stars, (e.g. surface temperatures, radial velocities, abundances, surface gravities, etc.) relate spectral and photometric observations, and to calculate *UBVRIz*-band S-corrections for any celestial object whose SED significantly differs from the standards used to calibrate the observed photometry. These spectra are now available for other researchers, provided in electronic form as FITS files.[1]

The structure of this chapter is as follows. In Sect. 7.2 we briefly discuss the manner in which we compute and employ S-corrections to observed SN photometry. In Sect. 7.3 we present our observations, followed by the spectroscopic reductions in Sect. 7.4. Our results for the program stars are given in Sect. 7.5. Finally, in Sect. 7.5 we also compute synthetic photometry of the Sun, Sirius and Vega and compare these values to magnitudes found in the literature.

7.2. S-corrections

To illustrate the importance of spectrophotometric standards when one attempts to determine S-corrections, we provide a brief description of how to compute the corrections necessary to place

[1] At http://csp1.lco.cl/~mhamuy/SPECSTDS/

observed photometry on a standard transmissivity function. Before one uses spectrophotometry of SNe to compute S-corrections, it is important to characterize how well the modeled passbands employed to determine spectrophotometry match the actual instrumental passbands used at the telescope. This can be checked by computing synthetic magnitudes of spectrophotometric standards using the nominal passbands, and comparing the color terms derived in this way to the color terms derived from broadband photometry. If the instrumental color terms do not match the standardized color terms, it proves necessary to apply wavelength shifts to the nominal passbands such that the color terms agree. [2]

To adjust discordant photometry to the *standard system*, S-corrections are determined using the spectrophotometry of a SN. An S-correction for the V filter is given by the expression

$$\Delta V = V - v - CT_V(b - v) - ZP_V, \tag{7.1}$$

V is the synthetic magnitude of the SN calculated with the standard Bessell passband (see Fig. and b and v correspond to synthetic magnitudes of the SN calculated with the instrumental passbands. CT_V refers to the color term for the corresponding instrumental passband, which should match the color term derived from broadband photometry, and ZP_V is the zero-point obtained from spectrophotometric standard stars. S-corrections can be computed for each night a spectrum of the SNe is obtained.

7.3. Observations

We have adopted six bright ($4.3 < V < 5.7$) secondary standard stars (see Table 7.1) originally published in Hayes (1970), and later re-calibrated by Taylor (1984), Hamuy et al. (1992, 1994) as our defining spectrophotometric system. Note that these stars are secondary standards because they tie the Kitt Peak National Observatory and CTIO spectrophotometric standards (Massey et al. 1988, Hamuy et al. 1992, 1994) to Vega. The program consists of 102 Landolt standard stars located along the celestial equator ranging $7.0 < V < 13.0$. We refer the reader to Landolt (1983, 1992a,b), Hamuy et al. (1992), and references within for spectral classifications, *UBVRI*-band photometry, coordinates, and finding charts. The reference and observed photometry for each star may also be found in the image header of each spectrum.

All observations were obtained with the CTIO 1.5 m, using the R-C spectrograph, during 5-13 February 1999 (UT). Of the eight nights observed, all were photometric except the last night of 12-13 February 1999 (UT). Half of the observations were dedicated to a blue setup while the other half were allocated to a red setup. The blue setup employed a low dispersion grating (300 lines mm^{-1}) with a dispersion of 2.85 Å per pixel blazed at 4000 Å and a 1200×800 LORAL CCD. We observed in first order with a total wavelength coverage of 3300 Å (3100-6400 Å) and a FWHM resolution of 8.6 Å. The red setup consisted of a low dispersion grating (158 lines mm^{-1}) with a dispersion of 5.34 Å per pixel blazed at 8000 Å with the same LORAL CCD.

[2] A different approach was attempted by Jha (2002) where instead of applying wavelength shifts the author changed the shape of his passbands by minimizing the residuals between spectrophotometry of the standards computed using modeled passbands (determined by a cubic spline through an arbitrary number of spline points) and the observed magnitudes. The modeled passbands that produced the smallest residuals can be thought of as the author states, *"typical* realizations of the true response, rather than the exact representation."

We observed in first order with a total wavelength coverage of 4800 Å (5800-10,600 Å) and a FWHM resolution of 16.4 Å. Note that it was necessary to use an OG570 second order blocking filter to suppress any leakage, which would have otherwise contaminated the spectra red-ward of 6000 Å.

Daily observations began with obtaining calibration images. This included bias frames, dome flats with a 2″ and 21″ slit and finally twilight flats through a 21″ slit. Nights in which we observed with the blue set up we took projector flats with a quartz lamp. Note that with the projector flats we used $CuS0_4$ and Corning 9863 filters to prevent saturation of the CCD. The observing procedure consisted of (1) pointing the telescope to the coordinates of the standard star, (2) close the slit to 2″ and then take an exposure with a HeAr lamp, (3) select a random field star for telescope guiding purposes, and (4) take an exposure of the standard star with a slit width of 21″. On the first two nights the secondary standards were each observed at three slit positions and the program stars at two slit positions. By the third night *all* stars were observed with four slit positions.[3]

Each night we typically observed five or six secondary standard stars (see Table 7.1), obtaining between 50 and 70 spectra at a wide range of airmass between z = 1.0 and z = 2.3, in order to solve for the nightly extinction curve. When observing the program stars we restricted the range of airmass to between z = 1.0 and z = 1.3 in order to reduce the differential effects of the Earth's atmosphere such as telluric absorption and atmospheric refraction between the program and spectrophotometric standard stars. Integration times were chosen such that for the majority of 1-D spectra (resulting from adding all the flux in the 2-D image along the spatial direction) the number of counts was between 40,000 and 50,000 ADU per resolution element. Thus, the exposure times for the bright secondary standards ranged between 2 and 7 seconds, while exposure times for the program stars typically ranged between 25 and 400 seconds. Due to the short integration times of the secondary standards it proved necessary to apply a shutter correction to their spectra (see below Sect. 7.4). From multiple exposures taken with 1-s, 2-s , 3-s, 4-s and 6-s exposure times on 6-7 February 1999 (UT) an additive mean shutter error for a one second exposure was determined to be -0.023 seconds ±0.010 (s.d.).

7.4. Spectroscopic reductions

Standard spectroscopic reduction techniques using IRAF[4] were performed to reduce the data. To begin we subtracted the over-scan and bias from all spectra including the HeAr frames. With the blue setup we constructed a flat field image using a combination of dome flats (external illumination), projector flats (internal illumination), and sky flats. The projector flats provide illumination in the ultraviolet end of the CCD ($\lambda < 3800$ Å), the dome flats at redder wavelengths, and the sky flat permitted us to correct the dome and projector flats for uneven illumination along

[3] A preliminary data reduction showed that all of the spectra from 5800 to 7000 Å were choppy at the 2-4% level. Note that this choppiness was similar to broad-scale fringing which is typically seen at wavelengths longward of 8000 Å. To alleviate this problem, the observing procedure was changed to observe all stars at four slit positions at lower flux levels in order to obtain similar total integration times. The co-added frames reduced the level of choppiness by half.

[4] The Image Reduction and Analysis Facility (IRAF) is distributed by the National Optical Astronomy Observatory, which is operated by AURA Inc., under a cooperative agreement with the National Science Foundation.

the slit. With the red setup we only used dome and sky flats. The resulting flats (normalized along the dispersion axis) were divided into all of the observed spectra. Next we extracted 1-D spectra from the 2-D flat fielded images and dispersion-calibrated them to a linear wavelength scale using the HeAr calibrations frames that were taken before each exposure. Shutter corrections were then applied to all the secondary standards by multiplying a factor of

$$\frac{ET}{ET + ST} \tag{7.2}$$

into each spectra, where ET is the requested exposure time in seconds and ST is the mean shutter error given in Sect. 7.3.

If the program stars are to be used as spectrophotometric standards for calculating *U*- and *z*-band spectrophotometry it proved necessary to extend the wavelength range of their spectra beyond the 3300-10,406 Å range of the secondary standards. This was accomplished by fitting synthetic spectra modeled with appropriate physical parameters, to each of our secondary standards, using Robert Kurucz's stellar atmosphere code BILL.f. By extrapolating from the models we obtained six new flux points. These included four flux points blue-ward of 3300 Å at 3250, 3200, 3150 and 3100 Å and two flux points red-ward of 10,406 Å at 10,500 and 10,600 Å. Note that it was necessary to scale the models to the observed blue and red tilt spectra by multiplication of an arbitrary constant. This constant was derived such that the modeled spectrum could reproduce the same values (up to two significant figures) as the flux points given in Table 5 of Hamuy et al. (1992). In addition, because two of the Hamuy et al. (1994) flux points were placed in regions of strong atmospheric absorption, we relocated them from 7782 and 9834 Å to 7845 and 9915 Å, respectively. We also added two additional flux points at 9970 and 10,150 Å. Because there are no flux points from 8376-9834 Å we attempted to add two flux points in this interval at locations free of atmospheric and stellar absorption features, at 8800 and 8920 Å, each with a 10 Å bandwidth. Unfortunately, when deriving the nightly response curve these flux points showed systematic residuals up to ~ 0.10 mag compared to neighboring flux points and were thus omitted.

In Table 7.1 we present re-calibrated monochromatic magnitudes of our spectrophotometric secondary standards from 3100 to 10,600 Å. These values are defined by

$$m_\nu = -2.5\log_{10}[f_\nu] - ZP, \tag{7.3}$$

where f_ν is the monochromatic flux in ergs cm^{-2} s^{-1} Hz^{-1}, and ZP is the zero-point for the magnitude scale. We have chosen the zero-point for the monochromatic magnitude scale to be -48.590 (Massey et al. 1988).

Before we flux calibrate the spectra, it is important to remove as much of the instrumental artifacts (such as fringing) and telluric absorption as possible. The most difficult signature to remove is the flat-fielding error, which introduces very high-order variations in the continuum at the few percent level, due to the continuum fitting algorithms used to take a flat field lamp and "flatten" it with an IRAF task like RESPONSE. Typically we used a polynomial of order 20 to 30 to fit out the flat field response. This will introduce wiggles with a period of roughly 150 Å or so, which are impossible to remove with a polynomial fit to the Hayes flux points, which are often more than 200 Å separated. In the region of 8000-9500 Å the flux points are even more separated, and one cannot fit out these flat-fielding errors.

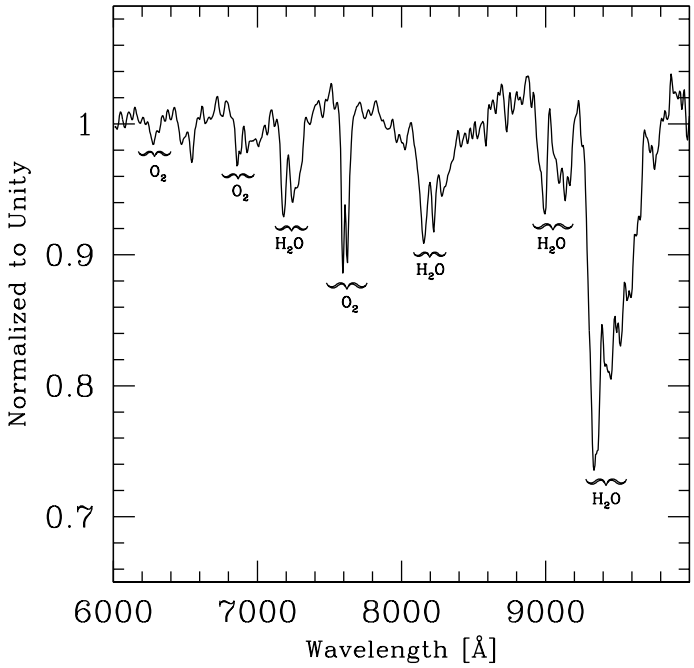

Figure 7.2.: Plot of telluric features removed from all spectra by division of a spectral flat. This figure is the division of a high airmass spectrum by an intermediate airmass spectrum of HR 3454 normalized to unity. The more prominent telluric features are labeled.

However, Bessell (1999) who noticed correlated errors in the Hamuy et al. spectrophotometric standards, has suggested an ingenious way of removing these flat-fielding errors. He proposed that the data be divided by a spectral flat, preferably with a spectrum of an astrophysical source that is close to a black body or otherwise line free. There is no such source, but there are some stars listed in his table such as Feige 110 or VMa2, which are close to being a pure continuum source. Most of these stars were too faint for the 1.5 m so we had to do the next best thing – use the division of an observed spectrum of a hot star with the model of the hot star. We used HR 3454, which was observed every night at an airmass ~1.2. To construct the red spectral flat we first made a theoretical spectrum using the Kurucz code at the same dispersion and wavelength coverage as the observed spectra. Because the Kurucz models are only available for a large grid of physical parameters, it was necessary to interpolate from the models to produce a spectrum that most accurately matched HR 3454.[5] All the red dispersion-calibrated spectra of HR 3454 at an airmass of 1.2 were then averaged and divided by the modeled spectrum. A few of the strongest spectral features, such as Hα, did not cleanly disappear in the spectral flat. Therefore we removed these residuals by interpolation. Next, all of the red dispersion-calibrated data for each night were divided by this spectral flat field. Fig. 7.2 displays the main telluric features red-ward of 6000 Å that were removed from all the red spectra by division of the spectral

[5]This spectrum corresponds to a model produced for physical parameters (T_{eff}, log g, [M/H]) = (18650 K, 3.5, 0).

flat. The most prominent telluric features were those associated with atmospheric H_2O and O_2. We found the O_2 A- and B-bands to be saturated for all observations, whereas the strength of the H_2O features were strongly dependent on both the airmass and the time at which the star was observed.

The blue spectral flat was constructed by averaging all the dispersion-calibrated observations of HR 3454 made at an airmass of 1.2. This was then divided into all of the blue tilt dispersion-calibrated data. Through the use of spectral flat fields we obtained smooth dispersion-calibrated spectra free of large telluric absorption and instrumental features.

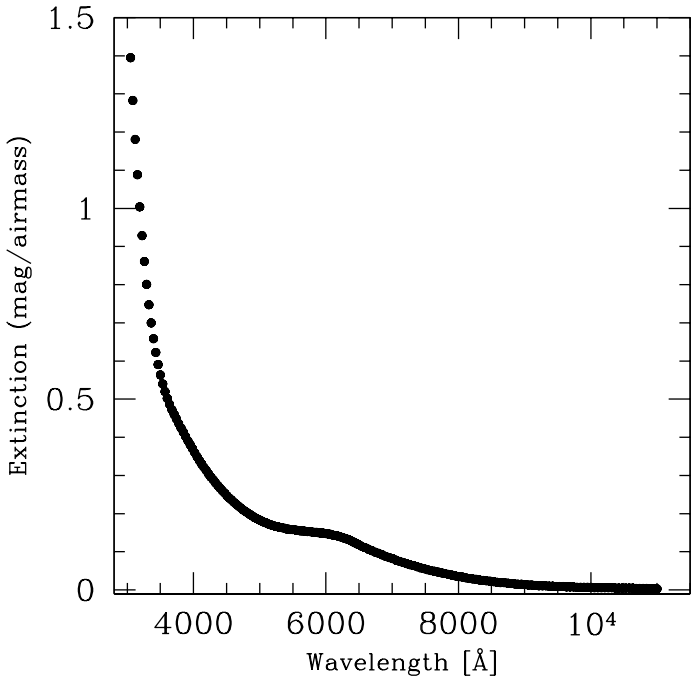

Figure 7.3.: Averaged blue and red atmospheric extinction curves obtained at CTIO on 5-12 February 1999 (UT).

We proceeded to flux-calibrate the data using the newly calibrated spectrophotometric secondary standards. Data from each night was first corrected for atmospheric extinction, via the nightly extinction curves derived from the secondary spectrophotometric standards, which were observed to this end over a range of airmasses. In Fig. 7.3 we present an averaged extinction curve obtained from the seven photometric nights for both the blue and red setups, and in Table 7.2 we list this extinction curve in tabular form. To obtain flux-calibrated spectra, we derived a nightly response curve by fitting a low order cubic spline to the observed flux values obtained from the secondary standards. When deriving nightly response curves we were able to extend the wavelength range past our reddest flux point given in Table 7.1 by 400 Å to 11,000 Å and by 50 Å in the blue to 3050 Å. To calculate spectrophotometry for each star it was necessary to stitch the blue and red spectra together. This was accomplished by first comparing all the blue and red spectra for an individual star at an airmass of 1.5 or less. If there were any spectra that

did not agree with the others they were omitted. We then combined all the spectra by averaging them together (using the IRAF task scombine) to produce a master spectrum for each star. Each master spectrum covers a total wavelength range of 7950 Å (3050-11,000 Å). Note that when considering all individual spectra together the flux offsets were typically extremely small, on the order of ~ 0.001 mag.

An indication that the Bessell method of using spectral flats works well is that the flux calibrations curves were fit with low order polynomials. Without the division of the spectral flats, there were noticeable wiggles in the sensitivity curve that required high order (12 or so) polynomials. With the division of the spectral flats, we could use much lower polynomial fits. This gives us confidence that the fits into the red regions where there are fewer flux points will introduce smaller systematic effects in the flux scale.

7.5. Results

7.5.1. Program stars

In this section we want to assess the spectrophotometric properties of our spectra by comparing broad-band synthetic magnitudes to those measured by Landolt. As all objects were measured

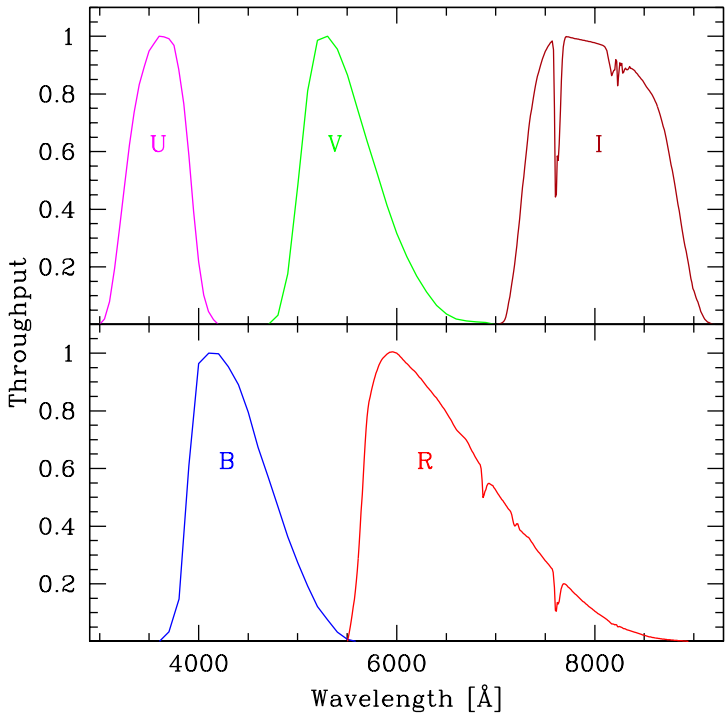

Figure 7.4.: Johnson/Kron-Cousins *UBVRI* standard passbands from Bessell (1990). The Bessell transmission functions have been divided by λ for integrations with photon flux, and multiplied by an atmospheric line opacity spectrum, because they are used with spectra that have had telluric features removed.

with a photon detector, a synthetic magnitude on the natural system must be calculated as the convolution of a star's photon flux (N_λ) with the filter instrumental passband (S(λ)), i.e.

$$\text{mag} = -2.5 \log_{10} \int N_\lambda \, S(\lambda) \, d\lambda \; + \; ZP, \tag{7.4}$$

where ZP is the zero-point for the magnitude scale. As a minimum, S(λ) should include the transparency of the Earth's atmosphere, the filter transmission, the quantum efficiency (QE) of the detector, and mirror reflectivities.

Note that there is often confusion about the form of S(λ). Some references use a function of the form R(λ)=λ*S(λ) and integrate R(λ)*F(λ), where F(λ) is in units of ergs s^{-1} cm^{-2} $Å^{-1}$. In equation 7.4 we are specifying the photon flux in units of photons s^{-1} cm^{-2} $Å^{-1}$. With this definition, the meaning of S(λ) is very easy to understand – it is just the fraction of photons (or energy) that is detected with respect to the incident flux outside the earth's atmosphere. S(λ) accounts for all the flux lost due to the flux passing though the atmosphere, telescope, and instrument.

To construct the standard passbands we adopted the Johnson/Kron-Cousins *UBVRI* transmission functions given in Bessell (1990) (see Fig. 7.4). Note, however, that the Bessell transmission functions are intended for use with energy rather then photon distributions (see Appendix in Bessell 1983). Thus, it was necessary to divide these functions by λ before employing them in Eq. (7.4) (Suntzeff et al. 1999, Hamuy et al. 2001). Because telluric absorption features were removed from the spectra, an atmospheric opacity spectrum was included in the construction of the standard passbands.

Armed with the standard passbands we proceeded to calculate synthetic magnitudes for our spectra using zero-points determined from secondary spectrophotometric standards (Landolt 1992b, Hamuy et al. 1994, Landolot 1999) rather than Vega, which has uncertain *UBVRI*-band optical photometry. When calculating zero-points we did not include telluric absorption in the passbands because Hamuy et al. did not removed these features from their spectra. Table 7.3 lists the resulting zero-points. In Table 7.4 we list synthetic magnitudes for all standard stars computed with Eq. (7.4) and the standard passbands, as well as the difference between observed and synthetic magnitudes. Note that the optical photometry for the secondary standards was taken from Hamuy et al. (1992). Sufficient wavelength coverage was obtained for 98 of the 108 standard stars listed in Table 7.4 to calculate *UBVRI* magnitudes. The remaining ten stars were observed in either the blue or red tilt except HD57884 and HD60826 whose spectra were cut off blue-ward of 4000 Å. In Table 7.4 we also identify stars that are known or thought to be variable stars.

In Fig. 7.5 we present, for all standards observed, the difference between observed and synthetic magnitudes computed with the standard passbands, as a function of observed color. Overall there is a high internal accuracy between the observed and synthetic magnitudes as seen in Table 7.5, which lists the mean difference and associated standard deviation for each band. We find that the mean difference between the observed photometry and our *UBVRI*-band synthetic magnitudes is 1% or less. However, it is evident from Fig. 7.5 that slight color terms do exist, most notably in the *U*- *B*- and *R*-bands. This color dependence reflects a small mismatch between the Bessell functions and the standards Johnson/Kron-Cousins system and/or a possible error in the fundamental spectrophotometric calibration. To remedy this problem our approach consisted of applying wavelength shifts to the Bessell functions until we obtained a zero color

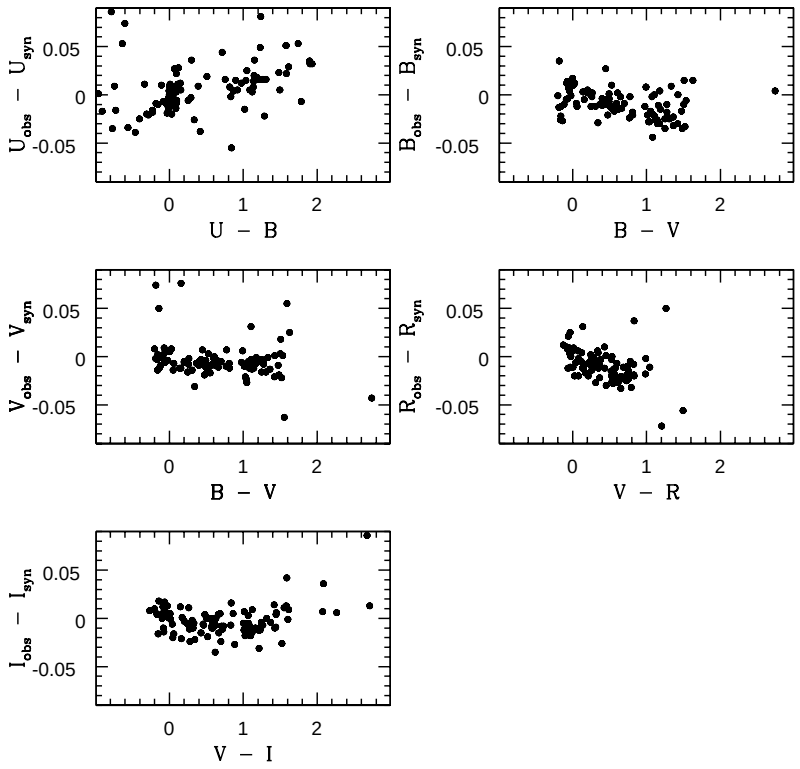

Figure 7.5.: The difference between observed and synthetic magnitudes derived using the Bessell passbands (see Fig. 7.4) as a function of color. Significant outliers are variable stars, identified in Table 7.4.

dependence. Table 7.6 lists the resulting shifts. Although small compared to the Bessell bandwidths ($\sim$ 1000 Å), they have a non-negligible effect on the synthetic magnitudes and the shifted standard passbands can be considered the best models for the Johnson/Kron-Cousins system. In Table 7.7 we provide our new modeled standard passbands. Note, however, that we did not include an atmospheric line opacity spectrum in the *R*- and *I*-bands listed in Table 7.7. Users who wish to compute spectrophotometry with spectra that have had telluric absorption features removed must include these features in both of these passbands. Due to limited space we have not included them in this thesis. But one may retrieve these two passbands that include the atmospheric spectrum in Stritzinger et al. (2005).

In Fig. 7.6 we present the comparison of Bessell's standard passbands (dotted lines) to our new modeled passbands (dashed lines). In addition, to complement the shifted passbands we provide a convenient list of wavelength shifts (see Table 7.8) one would apply to the standard passbands in order to increase the color term by 0.01 mag mag^{-1}. Note in Table 7.8 the color term (for example the *B*-band) is in the form of $B = zpt + b_{nat} + \dot{K}(B-V)$. Also listed is the color used in each color term.

With the *V*-band spectrophotometry and dispersion-calibrated spectra we investigated the LORAL CCD's response for all the nights on which observations were conducted. In Fig. 7.7

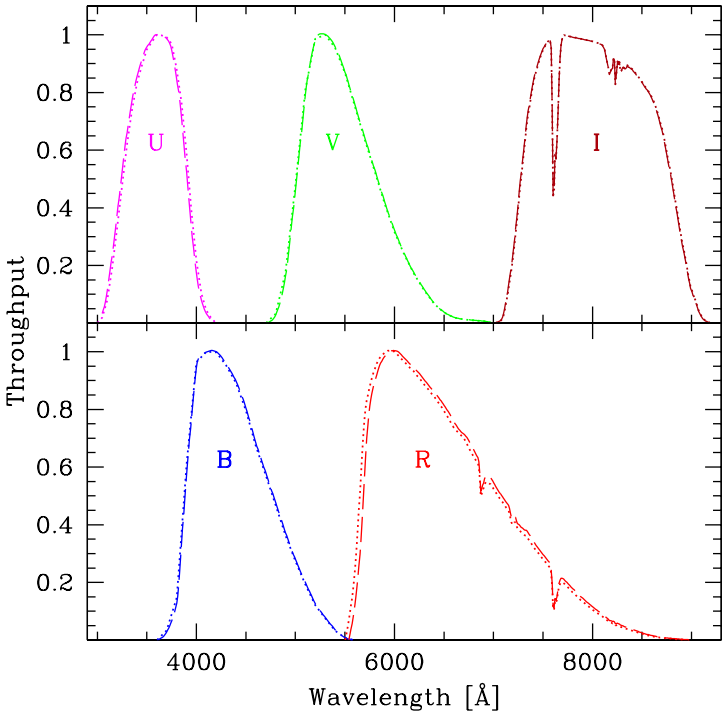

Figure 7.6.: Comparison of the Bessell Johnson/Kron-Cousins passbands (dotted lines) to our new modeled passbands (dashed lines) that include the shifts listed in Table 7.6.

we present the difference between standard and synthetic *V*-band magnitudes as a function of counts in the extracted 1-D spectra at the effective *V*-band wavelength for all observations. We conclude from Fig. 7.7 that the response function of the LORAL CCD was linear to within 2%.

7.5.2. The Sun, Sirius and Vega

In addition to the selected Landolt standard stars in this work, we have calculated spectrophotometry for the Sun, Sirius and Vega. As there are no spectrophotometric standards in the infrared comparable to that in the optical, these objects can be useful to characterize accurately the modeled passbands when computing *JHK*-band S-corrections (see Krisciunas et al. (2004b)). Spectra for these objects have been constructed using a combination of empirical and modeled data. The reader is referred to Appendix A in Krisciunas et al. (2003) for a more detailed description of the construction of these spectra; below we provide a brief summary for each of these stars.

Our solar spectrum combines empirical data from Livingston & Wallace (1991) scaled to a solar model from the Kurucz Web site (Kurucz et al. 1984) with physical parameters (T_{eff}, log g, v_{micro}, mixing length/scale height) = 5777 K, 4.438, 1.5 km s^{-1}, 1.25. For Vega we have adopted observational data from Hayes et al. (1985). His data were combined with the Kurucz spectrum vega090250000p.asc5 with physical parameters (T_{eff}, log g, v_{micro}, mixing length/scale height) = 9550 K, 3.950, -0.5, 2 km s^{-1}, 0. The Kurucz model was then scaled to match the flux points

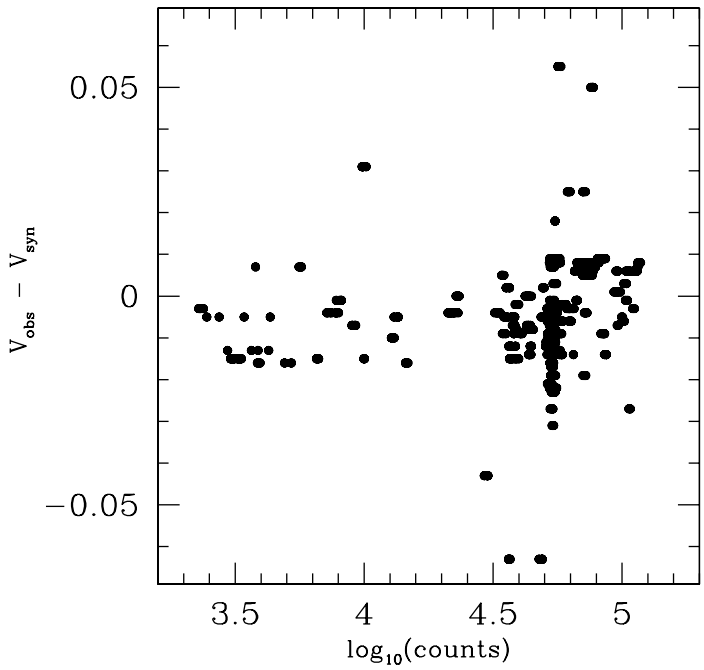

Figure 7.7.: *V*-band observed minus synthetic magnitudes, verses photon counts detected by the LORAL CCD, at the *V*-band's effective wavelength.

of Hayes et al. (1985). The Sirius spectrum was constructed using the Kurucz model sir.ascsq5 scaled to force the synthetic V magnitude to equal the observed value of -1.430 (Bessell et al. 1998). Note that each of these spectra were convolved to 2 Å and re-sampled to 1 Å per pixel.

To compute *UBVRI* synthetic photometry we employed our new modeled passbands (shown in Fig. 7.6) and the zero-points listed in Table 7.3. To calculate *JHK*-band synthetic magnitudes we constructed instrumental passbands, (see Fig. 7.8), which included information associated with the Las Campanas Observatory's 1 m Henrietta Swope telescope where the Persson et al. (1998) infrared system was established. This includes Persson et al. J_S, H, and K_S filter transmissivities, a Rockwell NICMOS2 QE response function, two aluminum reflections, a Dewar window transmissivity, multiple reflections associated with optical elements within the C40IRC camera, and an atmospheric line opacity spectrum. Zero-points were calculated by forcing the synthetic magnitudes of Vega to equal that of the Elias et al. (1982) CIT photometric system, i.e. $(J, H, K) = (0, 0, 0)$. The resulting *JHK*-band zero-points were -11.954, -11.895, and -12.063, respectively.

Table 7.9 lists the published photometry (from multiple sources), our synthetic photometry and the difference between the two in the sense of observed minus synthetic. The difference between Vega's *V*-band observed and synthetic magnitudes shows that our zero-points, calculated using the secondary standards from Hamuy et al. (1994), have an associated error ~ 0.01 mag. The large differences in the *UB*-bands may be due to the difficulty in obtaining accurate measurements of a star as bright as Vega. We find poor agreement for the Sun between *UJHK*

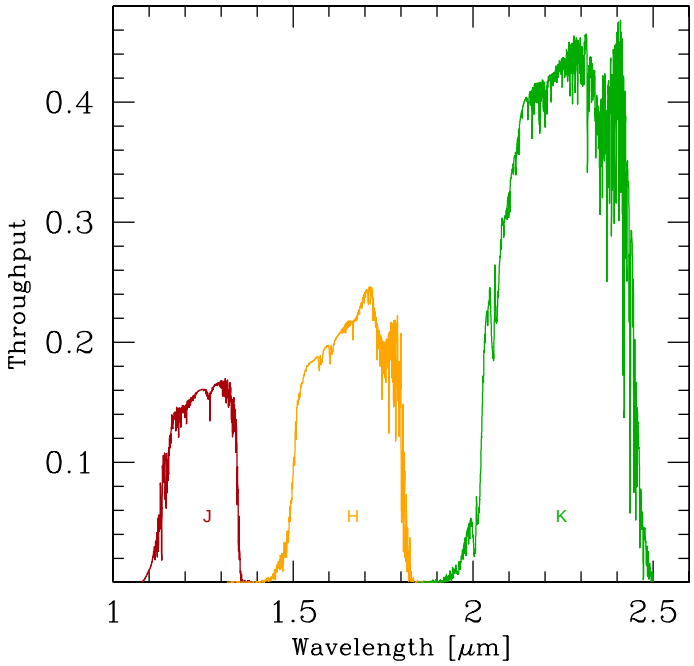

Figure 7.8.: Infrared passbands corresponding to Persson et al. (1998) J_S, H, and K_S transmission functions, a NICMOS2 QE, multiple mirror reflections, a Dewar window transmissivity, and an atmospheric line opacity spectrum.

observed and synthetic magnitudes. This as well is not surprising considering the difficulty in obtaining precise photometry of a source as bright and extended as the Sun. Some of the large U-band difference may be a result of the large variability of both the Sun's flux in the ultraviolet and Earth's atmospheric transmissivity. The differences in the infrared may be attributed to telluric absorption features that were not sufficiently accounted for in our manufactured instrumental passbands. The near infrared spectrophotometry of Sirius matches well with observed photometry to within 1% or less, while in the optical the difference is on the order of 4% or less.

Table 7.1. Spectrophotometric Secondary Standards

λ [Å]	$\Delta\lambda$	HR 718	HR 1544	HR 3454	HR 4468	HR 4963	HR 5501
3100	45	5.265	5.634	4.080	5.581	5.669	6.737
3150	45	5.256	5.611	4.099	5.576	5.653	6.731
3200	45	5.243	5.589	4.109	5.567	5.637	6.726
3250	45	5.230	5.566	4.125	5.557	5.618	6.717
3300	25	5.218	5.542	4.135	5.552	5.601	6.712
3390	45	5.188	5.519	4.145	5.530	5.563	6.675
3448	45	5.185	5.498	4.168	5.519	5.544	6.667
3509	45	5.175	5.485	4.185	5.517	5.519	6.654
3571	45	5.155	5.466	4.203	5.502	5.499	6.639
3636	45	5.117	5.422	4.197	5.474	5.451	6.608
4036	45	3.930	4.065	3.822	4.337	4.084	5.373
4167	45	3.983	4.110	3.892	4.383	4.123	5.410
4255	45	4.006	4.123	3.916	4.409	4.144	5.427
4464	45	···	4.160	3.983	4.461	4.181	5.476
4566	45	4.091	4.194	4.034	4.502	4.224	5.510
4785	45	4.134	4.222	4.104	4.545	4.247	5.551
5000	45	4.182	4.274	4.175	4.592	4.290	5.587
5264	45	4.235	4.322	4.239	4.653	4.339	5.638
5556	45	4.291	4.363	4.318	4.713	4.376	5.689
5840	45	4.336	4.403	4.388	4.770	4.422	5.738
6058	45	4.393	4.452	4.460	4.822	4.474	5.791
6440	45	4.465	4.516	4.544	4.902	4.543	5.846
6792	45	4.532	4.562	4.623	4.961	4.590	5.889
7102	45	4.593	4.616	4.709	5.019	4.646	5.952
7554	45	4.678	4.693	4.797	5.104	4.718	6.031
7845	45	4.740	4.745	4.861	5.168	4.779	6.065
8092	45	4.766	4.763	4.912	5.194	4.796	6.099
8376	45	4.829	4.825	4.986	5.253	4.847	6.147
8800	10	4.824	4.850	5.039	5.287	4.843	6.177
8920	10	4.827	4.854	5.058	5.298	4.847	6.185
9915	45	4.862	4.867	5.193	5.354	4.888	6.225
9970	45	4.867	4.871	5.202	5.358	4.893	6.231
10150	45	4.891	4.882	5.234	5.378	4.919	6.251
10256	45	4.944	4.898	5.261	5.378	4.926	6.240
10406	45	4.968	4.914	5.296	5.414	4.960	6.271
10500	45	4.986	4.944	5.319	5.443	5.004	6.333
10600	45	5.022	4.965	5.351	5.469	5.041	6.366

Note. —All values are in monochromatic magnitudes $m_\nu = -2.5 \log_{10}(f_\nu) - 48.590$.

Table 7.2. Averaged Extinction Curve for CTIO

λ	Extinction [mag/airmass]
3050.00	1.395
3084.65	1.283
3119.31	1.181
3153.96	1.088
3188.61	1.004
3223.27	0.929
3257.92	0.861
3292.57	0.801
3327.23	0.748
3361.88	0.700
3396.54	0.659
3431.19	0.623
3465.84	0.591
3500.50	0.564
3535.15	0.540
3569.80	0.520
3604.46	0.502
3639.11	0.487
3673.76	0.473
3708.42	0.460
3743.07	0.448
3777.72	0.436
3812.38	0.425
3847.03	0.414
3881.69	0.402
3916.34	0.391
3950.99	0.381
3985.65	0.370
4020.30	0.360
4054.95	0.349
4089.61	0.339
4124.26	0.330
4158.91	0.321
4193.57	0.313
4228.22	0.304
4262.87	0.296
4297.53	0.289
4332.18	0.281
4366.83	0.274
4401.49	0.267
4436.14	0.260
4470.79	0.254
4505.45	0.247
4540.10	0.241
4574.76	0.236

Table 7.2 (cont'd)

λ	Extinction [mag/airmass]
4609.41	0.230
4644.06	0.225
4678.72	0.220
4713.37	0.215
4748.02	0.210
4782.68	0.206
4817.33	0.202
4851.98	0.198
4886.64	0.194
4921.29	0.190
4955.94	0.187
4990.60	0.184
5025.25	0.181
5059.91	0.178
5094.56	0.176
5129.21	0.173
5163.87	0.171
5198.52	0.169
5233.17	0.167
5267.83	0.166
5302.48	0.164
5337.13	0.163
5371.79	0.162
5406.44	0.160
5441.09	0.159
5475.75	0.158
5510.40	0.158
5545.05	0.157
5579.71	0.156
5614.36	0.155
5649.02	0.155
5683.67	0.154
5718.32	0.153
5752.98	0.153
5787.63	0.152
5822.28	0.151
5856.94	0.151
5891.59	0.150
5926.24	0.149
5960.90	0.149
5995.55	0.148
6030.20	0.147
6064.86	0.146
6099.51	0.144
6134.17	0.143

Table 7.2 (cont'd)

λ	Extinction [mag/airmass]
6168.82	0.142
6203.47	0.140
6238.13	0.138
6272.78	0.136
6307.43	0.134
6342.09	0.132
6376.74	0.129
6411.39	0.126
6446.05	0.123
6480.70	0.120
6482.85	0.120
6535.38	0.115
6587.91	0.111
6640.44	0.107
6692.96	0.103
6745.49	0.099
6798.02	0.096
6850.55	0.092
6903.07	0.088
6955.60	0.085
7008.13	0.082
7060.65	0.078
7113.18	0.075
7165.71	0.072
7218.24	0.069
7270.76	0.066
7323.29	0.064
7375.82	0.061
7428.35	0.058
7480.87	0.056
7533.40	0.053
7585.93	0.051
7638.45	0.049
7690.98	0.047
7743.51	0.045
7796.04	0.043
7848.56	0.041
7901.09	0.039
7953.62	0.037
8006.15	0.035
8058.67	0.034
8111.20	0.032
8163.73	0.030
8216.25	0.029
8268.78	0.028

Table 7.2 (cont'd)

λ	Extinction [mag/airmass]
8321.31	0.026
8373.84	0.025
8426.36	0.024
8478.89	0.023
8531.42	0.022
8583.95	0.020
8636.47	0.019
8689.00	0.019
8741.53	0.018
8794.05	0.017
8846.58	0.016
8899.11	0.015
8951.64	0.015
9004.16	0.014
9056.69	0.013
9109.22	0.013
9161.75	0.012
9214.27	0.011
9266.80	0.011
9319.33	0.011
9371.85	0.010
9424.38	0.010
9476.91	0.009
9529.44	0.009
9581.96	0.009
9634.49	0.008
9687.02	0.008
9739.55	0.008
9792.07	0.007
9844.60	0.007
9897.13	0.007
9949.65	0.007
10002.2	0.007
10054.7	0.006
10107.2	0.006
10159.8	0.006
10212.3	0.006
10264.8	0.006
10317.3	0.006
10369.9	0.005
10422.4	0.005
10474.9	0.005
10527.5	0.005
10580.0	0.005
10632.5	0.005

Table 7.2 (cont'd)

λ	Extinction [mag/airmass]
10685.0	0.004
10737.6	0.004
10790.1	0.004
10842.6	0.004
10895.1	0.003
10947.7	0.003
11000.2	0.003

Table 7.3. Zero-points employed in Eq. 7.4 with standard passbands

Filter	Zero-point
U	14.244
B	15.279
V	14.850
R	15.053
I	14.556

Table 7.4. Synthetic Magnitudes for All Stars[†]

Star	U_{syn}	U_{obs}-U_{syn}	B_{syn}	B_{obs}-B_{syn}	V_{syn}	V_{obs}-V_{syn}	R_{syn}	R_{obs}-R_{syn}	I_{syn}	I_{obs}-I_{syn}
bd−0°454	11.849	+0.051	10.321	0	8.894	+0.001	8.152	−0.015	7.446	+0.004
bd+1°2447	12.318	+0.081	11.146	+0.015	9.634	+0.018	8.619	−0.011	7.380	+0.006
bd+5°1668[c]	12.597	+0.016	11.460	−0.060	9.906	−0.063	8.709	−0.072	7.116	+0.013
bd+5°2468	8.706	−0.034	9.242	−0.010	9.357	−0.009	9.383	+0.003	9.435	+0.005
bd+5°2529	12.001	+0.018	10.866	−0.035	9.584	−0.003	8.805	−0.005	8.125	+0.006
cd−32°9927	...	...	...	...	...	...	...	...	10.112	−0.005
eg21	...	...	...	...	...	...	...	...	11.526	+0.004
g162-66	11.861	−0.010	12.873	−0.026	13.015	−0.003	13.126	+0.012	13.270	+0.008
hd118246[a]	7.259	+0.053	7.895	+0.053	8.039	+0.050	8.098	+0.025	8.180	−0.010
hd12021	8.413	−0.025	8.780	+0.012	8.872	+0.002	8.907	+0.009	8.972	0
hd11983	...	...	...	...	...	...	...	...	6.627	+0.011
hd121968	9.177	−0.017	10.081	−0.013	10.256	−0.002	10.319	+0.008	10.421	+0.005
hd129975	11.741	+0.035	9.887	−0.010	8.370	+0.003	7.563	−0.019	6.769	−0.001
hd16581	7.853	−0.020	8.131	+0.007	8.201	−0.006	8.220	0	8.254	+0.004
hd21197	10.143	+0.014	9.046	−0.030	7.869	−0.003	7.191	−0.011	6.624	−0.004
hd36395	10.616	+0.049	9.451	−0.017	7.969	−0.009	6.993	−0.018	5.877	+0.007
hd47761[b]	8.207	+0.074	8.798	+0.085	8.648	+0.076	8.555	+0.031	8.469	−0.024
hd50167	11.087	+0.053	9.402	−0.006	7.860	+0.001	7.043	−0.008	6.265	+0.013
hd52533	6.655	+0.001	7.619	−0.005	7.702	0	7.706	+0.007	7.734	+0.006
hd57884[b]	...	...	...	...	9.028	+0.107	7.821	+0.050	6.726	+0.122
hd60826[b]	...	...	...	...	9.026	−0.043	7.544	−0.056	6.220	+0.086
hd65079[c]	6.778	+0.086	7.615	+0.035	7.758	+0.074	7.763	+0.124	7.782	+0.180
hd72055	7.555	−0.039	8.003	−0.027	8.125	−0.012	8.142	+0.002	8.187	+0.012
hd76082	10.612	+0.005	9.553	−0.026	8.422	−0.013	7.851	−0.027	7.326	−0.018
hd79097[a]	11.130	+0.032	9.214	+0.015	7.576	+0.025	6.613	−0.002	5.478	+0.036
hd84971	7.742	−0.035	8.499	−0.022	8.650	−0.014	8.711	−0.012	8.804	−0.016
hd97503	10.998	+0.003	9.910	−0.030	8.703	−0.001	7.993	−0.011	7.385	0
hr0718	4.106	+0.010	4.209	+0.014	4.272	+0.007	4.294	+0.008	4.331	+0.011
hr1544	4.372	−0.008	4.355	+0.010	4.349	+0.006	4.332	+0.009	4.322	−0.006
hr3454	3.343	+0.009	4.096	−0.001	4.287	+0.008	4.368	+0.010	4.485	+0.010
hr4468	4.459	−0.009	4.616	+0.014	4.691	+0.009	4.718	+0.005	4.746	+0.017

Table 7.4 (cont'd)

Star	U_{syn}	U_{obs}-U_{syn}	B_{syn}	B_{obs}-B_{syn}	V_{syn}	V_{obs}-V_{syn}	R_{syn}	R_{obs}-R_{syn}	I_{syn}	I_{obs}-I_{syn}
hr4963	4.379	−0.014	4.358	+0.017	4.370	+0.005	4.364	+0.008	4.360	+0.005
hr5501	5.585	−0.007	5.659	−0.001	5.685	−0.004	5.688	−0.011	5.694	+0.013
ltt1788	13.349	−0.021	13.618	−0.007	...	...	...	...	...	...
ltt2415	12.388	−0.016	12.604	−0.004	...	...	...	...	...	...
ltt3218	...	...	...	...	...	...	...	...	11.646	−0.003
ltt4364	...	...	...	...	...	...	...	...	11.189	−0.002
sa94-305	11.876	+0.022	10.342	−0.030	8.910	−0.021	8.155	−0.023	7.455	−0.009
sa94-308	9.229	+0.004	9.241	−0.004	8.754	−0.011	8.459	−0.006	8.177	−0.010
sa94-342	10.706	+0.044	10.026	+0.008	9.035	+0.006	8.517	−0.003	8.019	+0.007
sa95-52	10.145	+0.027	10.093	+0.010	9.571	+0.003	9.273	−0.006	8.971	−0.008
sa95-96	10.234	−0.005	10.154	+0.003	10.022	−0.012	9.933	−0.002	9.835	+0.001
sa95-132	12.776	+0.036	12.485	+0.027	12.057	+0.007	11.805	0	11.519	0
sa95-206	9.259	−0.005	9.251	−0.012	8.748	−0.011	8.449	−0.002	8.162	0
sa96-36	10.946	+0.010	10.836	+0.002	10.598	−0.007	10.469	−0.012	10.331	−0.010
sa96-180[c]	10.875	−0.055	10.027	−0.048	8.957	−0.027	8.410	−0.028	7.892	−0.013
sa96-235	13.097	+0.015	12.216	−0.002	11.145	−0.005	10.594	−0.013	10.069	+0.003
sa96-393	10.283	+0.007	10.261	−0.013	9.659	−0.007	9.303	+0.004	8.960	+0.005
sa96-406	9.656	+0.012	9.518	+0.002	9.306	−0.006	9.189	−0.005	9.068	−0.005
sa96-737	14.191	+0.019	13.041	+0.009	11.717	−0.001	11.002	−0.019	10.298	−0.010
sa97-249	12.487	−0.003	12.383	+0.003	11.737	−0.002	11.373	−0.004	11.021	−0.005
sa97-346	9.957	+0.011	9.863	−0.009	9.261	−0.001	8.916	+0.006	8.594	+0.004
sa97-351	10.057	+0.022	9.978	+0.005	9.786	−0.005	9.653	+0.004	9.506	+0.011
sa98-193	12.326	+0.036	11.206	+0.004	10.033	−0.003	9.442	−0.027	8.889	−0.012
sa98-320	11.451	+0.008	10.349	−0.026	9.192	−0.012	8.605	−0.021	8.079	−0.015
sa98-653	...	...	...	...	...	...	...	...	9.523	−0.001
sa98-667	8.059	+0.011	8.394	+0.012	8.370	+0.008	8.301	+0.006	8.217	+0.012
sa98-978	11.284	−0.009	11.179	+0.002	10.572	0	10.235	−0.012	9.916	−0.015
sa99-6	3.612	−0.022	12.328	−0.025	11.070	−0.016	10.435	−0.033	9.837	−0.012
sa99-185	10.388	+0.012	9.445	−0.020	8.354	−0.010	7.799	−0.018	7.278	−0.005
sa99-296	10.890	+0.016	9.656	−0.015	8.460	−0.006	7.861	−0.007	7.322	+0.009
sa99-358	10.871	+0.019	10.383	−0.002	9.598	+0.007	9.163	+0.010	8.751	+0.016

Table 7.4 (cont'd)

Star	U_{syn}	U_{obs}-U_{syn}	B_{syn}	B_{obs}-B_{syn}	V_{syn}	V_{obs}-V_{syn}	R_{syn}	R_{obs}-R_{syn}	I_{syn}	I_{obs}-I_{syn}
sa99-408	10.257	0	10.223	−0.009	9.812	−0.005	9.553	+0.001	9.306	+0.002
sa99-418	9.289	−0.010	9.429	+0.004	9.469	+0.005	9.471	+0.006	9.489	+0.001
sa99-438	8.534	−0.016	9.255	−0.012	9.396	+0.002	9.436	+0.021	9.521	+0.018
sa99-447	9.143	−0.018	9.354	−0.004	9.422	−0.005	9.460	−0.011	9.505	−0.014
sa100-95	10.111	+0.009	9.750	−0.021	8.927	−0.012	8.492	−0.030	8.058	−0.027
sa100-162	11.918	+0.005	10.444	−0.018	9.158	−0.008	8.522	−0.021	7.959	−0.012
sa100-241	10.403	−0.006	10.301	−0.005	10.151	−0.012	10.081	−0.020	9.997	−0.021
sa100-280	12.291	0	12.292	+0.001	11.803	−0.004	11.510	−0.006	11.221	−0.010
sa100-606	8.790	+0.028	8.702	−0.009	8.655	−0.014	8.635	−0.020	8.613	−0.020
sa101-24	10.127	+0.015	9.127	−0.022	8.000	−0.003	7.434	−0.012	6.914	−0.008
sa101-281	12.844	−0.038	12.405	−0.018	11.582	−0.007	11.122	+0.001	10.706	+0.005
sa101-282	10.430	+0.011	10.436	−0.005	10.005	−0.003	9.756	−0.014	9.501	−0.019
sa101-311	8.492	+0.009	8.496	+0.002	8.235	−0.002	8.082	−0.008	7.921	−0.010
sa101-324	12.031	+0.020	10.914	−0.011	9.750	−0.008	9.174	−0.023	8.643	−0.011
sa101-333	11.114	−0.007	9.355	−0.035	7.854	−0.019	7.072	−0.032	6.337	−0.026
sa101-363	10.255	+0.009	10.137	−0.002	9.882	−0.008	9.740	−0.012	9.587	−0.010
sa101-389	10.397	−0.009	10.399	−0.010	9.967	−0.005	9.707	−0.001	9.459	0
sa102-58	9.470	−0.009	9.452	−0.012	9.387	−0.007	9.342	−0.006	9.336	−0.016
sa102-276	10.389	−0.011	10.409	−0.007	9.915	−0.005	9.625	−0.006	9.343	−0.008
sa102-381	8.315	+0.005	8.237	−0.012	7.930	−0.014	7.760	−0.017	7.592	−0.022
sa102-466	11.218	+0.005	10.319	−0.017	9.255	−0.009	8.701	−0.018	8.184	−0.007
sa102-472	10.579	+0.008	9.789	−0.021	8.764	−0.010	8.246	−0.020	7.755	−0.012
sa102-620	12.187	−0.015	11.196	−0.044	10.081	−0.012	9.450	−0.023	8.912	−0.010
sa102-625	9.477	0	9.454	−0.012	8.907	−0.017	8.605	−0.027	8.304	−0.035
sa102-1081	10.828	−0.006	10.581	−0.014	9.914	−0.011	9.559	−0.022	9.229	−0.024
sa103-302	10.181	−0.008	10.239	−0.010	9.868	−0.007	9.639	−0.006	9.403	−0.007
sa103-462	10.778	−0.014	10.692	−0.017	10.120	−0.009	9.794	−0.007	9.481	0
sa103-483	8.870	+0.003	8.785	−0.005	8.359	−0.006	8.106	+0.002	7.869	+0.004
sa104-306[b]	12.447	+0.181	10.876	+0.086	9.315	+0.055	8.501	+0.037	7.737	+0.042
sa104-337	12.337	−0.026	11.999	−0.024	11.217	−0.010	10.785	−0.012	10.382	−0.007
sa104-461	10.170	−0.019	10.202	−0.021	9.724	−0.019	9.427	−0.011	9.128	−0.003

Table 7.4 (cont'd)

Star	U_{syn}	U_{obs}-U_{syn}	B_{syn}	B_{obs}-B_{syn}	V_{syn}	V_{obs}-V_{syn}	R_{syn}	R_{obs}-R_{syn}	I_{syn}	I_{obs}-I_{syn}
sa104-598	13.610	+0.025	12.585	0	11.448	+0.031	10.832	−0.023	10.295	−0.031
sa105-28	10.250	+0.004	9.412	−0.028	8.368	−0.023	7.833	−0.021	7.332	−0.005
sa105-66	9.155	−0.020	9.131	−0.029	8.791	−0.031	8.569	−0.020	8.346	−0.015
sa105-205	11.748	+0.029	10.193	−0.032	8.811	−0.013	8.064	−0.010	7.365	+0.014
sa105-214	7.583	−0.003	7.604	−0.014	7.077	−0.015	6.759	−0.010	6.445	−0.007
sa105-405	11.703	+0.032	9.863	−0.033	8.331	−0.022	7.497	−0.020	6.683	+0.009
sa105-448	9.457	+0.005	9.437	−0.012	9.192	−0.016	9.035	−0.008	8.869	−0.004
sa105-663	11.143	+0.016	10.415	−0.012	9.432	−0.006	8.919	−0.015	8.428	−0.005
sa106-575	12.109	+0.023	10.674	−0.025	9.357	−0.016	8.691	−0.022	8.083	−0.007
sa106-700	12.678	+0.051	11.170	−0.023	9.798	−0.013	9.082	−0.025	8.419	−0.004
sa106-834	10.084	−0.003	9.798	−0.009	9.093	−0.005	8.712	−0.003	8.360	−0.008
sa106-1250	9.986	−0.002	9.180	−0.028	8.144	−0.021	7.617	−0.026	7.115	−0.018
sa107-35	10.347	+0.016	9.064	−0.010	7.786	−0.007	7.137	−0.021	6.537	−0.007
sa107-544	9.589	+0.005	9.449	−0.011	9.046	−0.009	8.812	−0.008	8.586	−0.006
sa107-684	9.136	−0.012	9.067	−0.015	8.442	−0.009	8.085	−0.008	7.733	−0.008

[†]Observed magnitudes taken from Landolt (1983), Landolt (1992a), Landolt (1992b), Hamuy et al. (1992) & Landolot (1999).

[a]Landolt (1983) lists as possible variable.

[b]Landolt (1983) lists as variable.

[c]Possible variable star.

Table 7.5. Mean differences and standard deviations between observed and synthetic magnitudes

Filter	Mean Difference	s. d.
U	+0.007	0.023
B	−0.010	0.011
V	−0.006	0.006
R	−0.008	0.010
I	−0.003	0.007

Note. — Mean values were determined utilizing an outlier resistance algorithm. Standard deviations were determined using a robust sigma algorithm.

Table 7.6. Wavelength shifts applied to Bessell passbands

Passband	Shift [Å]	
U	16	blue
B	8.5	red
V	6	red
R	38	red
I	5	blue

Table 7.7. Normalized Standard Passbands

λ	U	λ	B	λ	V	λ	R	λ	I
3000	0.000	3600	0.000	4700	0.000	5500	0.000	7000	0.000
3050	0.034	3700	0.028	4800	0.027	5600	0.121	7100	0.030
3100	0.113	3800	0.126	4900	0.160	5700	0.576	7200	0.261
3150	0.236	3900	0.569	5000	0.462	5800	0.895	7300	0.603
3200	0.376	4000	0.945	5100	0.790	5900	0.983	7400	0.834
3250	0.525	4100	0.998	5200	0.979	6000	1.000	7500	0.950
3300	0.662	4200	1.000	5300	1.000	6100	0.978	7600	0.994
3350	0.770	4300	0.958	5400	0.960	6200	0.943	7700	1.000
3400	0.855	4400	0.898	5500	0.873	6300	0.903	7800	0.992
3450	0.913	4500	0.806	5600	0.759	6400	0.861	7900	0.985
3500	0.958	4600	0.685	5700	0.645	6500	0.815	8000	0.977
3550	0.983	4700	0.581	5800	0.533	6600	0.759	8100	0.964
3600	1.000	4800	0.478	5900	0.422	6700	0.714	8200	0.943
3650	0.997	4900	0.373	6000	0.324	6800	0.660	8300	0.922
3700	0.987	5000	0.280	6100	0.241	6900	0.604	8400	0.883
3750	0.947	5100	0.200	6200	0.173	7000	0.547	8500	0.836
3800	0.851	5200	0.127	6300	0.118	7100	0.493	8600	0.780
3850	0.713	5300	0.079	6400	0.070	7200	0.444	8700	0.670
3900	0.526	5400	0.037	6500	0.039	7300	0.397	8800	0.492
3950	0.334	5500	0.009	6600	0.021	7400	0.345	8900	0.285
4000	0.175	5600	0.000	6700	0.013	7500	0.297	9000	0.127
4050	0.080	···	···	6800	0.010	8000	0.116	9100	0.024
4100	0.035	···	···	6900	0.007	8500	0.025	9200	0.000
4150	0.010	···	···	7000	0.000	9000	0.000	···	···
4200	0.000	···	···	···	···	···	···	···	···

Note. — Note that the *R* and *I*-bands must be mulitplied by an atmospheric line opacity spectrum before being used to calculate synthetic magnitudes with the standard stars presented in this paper.

Table 7.8. Filter Shifts

Passband	Shift [Å]	Color Term
U	12	$(U - B)$
B	7.4	$(B - V)$
V	15.2	$(B - V)$
R	12.4	$(V - R)$
I	40.5	$(V - I)$

Note. — All shifts to the red.

Table 7.9. Spectrophotometry of the Sun, Sirius & Vega

passband	*U*	*B*	*V*	*R*	*I*	*J*	*H*	*K*	ref.
Sun									
m_{obs}	−25.947	−26.104	−26.755	−27.118	−27.464	−27.885	−28.219	−28.261	1
m_{syn}	−25.968	−26.105	−26.764	−27.121	−27.456	−27.939	−28.260	−28.307	
m_{obs} - m_{syn}	+0.021	+0.001	+0.009	+0.003	−0.008	+0.054	+0.041	+0.046	
Sirius									
m_{obs}	−1.480	−1.435	−1.430	−1.419	−1.412	−1.385	−1.382	−1.367	2
m_{syn}	−1.438	−1.435	−1.423	−1.390	−1.374	−1.392	−1.381	−1.377	
m_{obs} - m_{syn}	−0.042	0	−0.007	−0.029	−0.038	+0.007	−0.001	+0.010	
Vega									
m_{obs}	+0.025	+0.025	+0.030	+0.039	+0.035	−0.001	0	−0.001	3
m_{syn}	+0.088	+0.003	+0.026	+0.052	+0.045	0	0	0	
m_{obs} - m_{syn}	−0.063	+0.022	+0.004	−0.013	−0.010	−0.001	0	−0.001	

References. — (1) Averaged values from Table A3 of Bessell et al. (1998) referenced from Stebbins & Kron (1957), Colina et al. (1996) & Cayrel et al. (1996); (2) Table A2 Bessell et al. (1998) & references within, *UBRI* averaged values, *JHK* Table A1 Cohen et al. (1999); (3) Table A2 Bessell et al. (1998), *B* averaged value, *JHK* Table A2 Cohen et al. (1999).

8. Conclusion

To conclude we summarize the highlights of this thesis.

- We found that the range in the amount of synthesized ^{56}Ni indicates a significant variation in the burning mechanism. In order to explain a factor of ten range in the observed bolometric luminosity more detailed modeling of the explosion mechanism is required.

- With the UVOIR light curve we calculated, for the first time, the γ-ray escape fraction for a large number of events. This quantity is a powerful diagnostic to measure the energy release and can be compared to complicated multi-group calculations.

- By fitting a radioactive decay energy deposition function to the quasi-exponential phase, it was found that the ejected mass varies by at least a factor of two. This result suggests that a sub-Chandrasekhar mass model could be responsible for the progenitor system of some SNe Ia.

- Through coupling observations of SNe Ia with results obtained from the best available numerical models we constrained the Hubble constant, independently of any external calibrators. We found an absolute lower limit of $H_\circ > 50$ km s^{-1} Mpc^{-1}. In addition, we construct a Hubble diagram with UVOIR light curves of 12 type Ia supernovae located in the Hubble flow, and when adopting the most likely values (obtained from 1-D and 3-D deflagration simulations) of the amount of ^{56}Ni produced in a *typical* event, we found values of $H_\circ \geq 66\pm8$ and $\geq 78\pm9$ km s^{-1} Mpc^{-1}, respectively.

- Thirty-eight UVOIR light curves are presented in the Appendix for other researchers. This catalog will be an invaluable tool for comparing light curves computed from models to real observations.

- We presented CCD observations of 102 Landolt standard stars obtained with the R-C spectrograph on the CTIO 1.5 m telescope. Observers in both hemispheres will find these spectra useful for flux-calibrating spectra and through the use of accurately constructed instrumental passbands be able to compute accurate corrections to bring instrumental magnitudes to any desired standard photometric system (S-corrections).

- *UBVRI* Johnson/Kron-Cousins passbands were re-calibrated using our set of new spectrophotometric standards stars.

A. An Atlas of *UVOIR* light curves

The thirty-eight UVOIR light curves presented in this Appendix can be a powerful tool for future studies of SNe Ia. In case improved distances become available each light curve is given in units of flux (ergs s^{-1} cm^{-2}). For SN 1992bo and SN 1990N we were unable to accurately fit the secondary maximum. However times of maximum and the late time declines are accurately fitted.

Table A.1. SN 1989B

JD +2447000	*UVOIR* Flux	Flux error	JD +2447000	*UVOIR* Flux	Flux error
558.643	5.26140×10^{-10}	2.61640×10^{-11}	587.789	2.14630×10^{-10}	9.91010×10^{-12}
559.372	5.61640×10^{-10}	2.73730×10^{-11}	588.518	2.07530×10^{-10}	9.62650×10^{-12}
560.101	6.22270×10^{-10}	2.88300×10^{-11}	589.246	2.01220×10^{-10}	9.37110×10^{-12}
560.829	6.83860×10^{-10}	3.06450×10^{-11}	589.975	1.95520×10^{-10}	9.13590×10^{-12}
561.558	7.30030×10^{-10}	3.23060×10^{-11}	590.703	1.89970×10^{-10}	8.89830×10^{-12}
562.286	7.60670×10^{-10}	3.35430×10^{-11}	591.432	1.83870×10^{-10}	8.62530×10^{-12}
563.015	7.79750×10^{-10}	3.43720×10^{-11}	592.161	1.76790×10^{-10}	8.29540×10^{-12}
563.744	7.90460×10^{-10}	3.48730×10^{-11}	592.889	1.68940×10^{-10}	7.91970×10^{-12}
564.472	7.94690×10^{-10}	3.51030×10^{-11}	593.618	1.60930×10^{-10}	7.53230×10^{-12}
565.201	7.93500×10^{-10}	3.50960×10^{-11}	594.347	1.53400×10^{-10}	7.16450×10^{-12}
565.930	7.87560×10^{-10}	3.48740×10^{-11}	595.075	1.46590×10^{-10}	6.82970×10^{-12}
566.658	7.77330×10^{-10}	3.44550×10^{-11}	595.804	1.40500×10^{-10}	6.52720×10^{-12}
567.387	7.63250×10^{-10}	3.38560×10^{-11}	596.533	1.34970×10^{-10}	6.25140×10^{-12}
568.116	7.45750×10^{-10}	3.30950×10^{-11}	597.261	1.29870×10^{-10}	5.99720×10^{-12}
568.844	7.25290×10^{-10}	3.21930×10^{-11}	597.990	1.25140×10^{-10}	5.76150×10^{-12}
569.573	7.02340×10^{-10}	3.11740×10^{-11}	598.719	1.20730×10^{-10}	5.54300×10^{-12}
570.302	6.77410×10^{-10}	3.00590×10^{-11}	599.447	1.16630×10^{-10}	5.34070×10^{-12}
571.030	6.50970×10^{-10}	2.88740×10^{-11}	600.176	1.12820×10^{-10}	5.15370×10^{-12}
571.759	6.23490×10^{-10}	2.76400×10^{-11}	600.905	1.09270×10^{-10}	4.98110×10^{-12}
572.487	5.95420×10^{-10}	2.63790×10^{-11}	601.633	1.05980×10^{-10}	4.82150×10^{-12}
573.216	5.67170×10^{-10}	2.51110×10^{-11}	602.362	1.02910×10^{-10}	4.67400×10^{-12}
573.945	5.39100×10^{-10}	2.38520×10^{-11}	603.090	1.00050×10^{-10}	4.53710×10^{-12}
574.673	5.11530×10^{-10}	2.26180×10^{-11}	603.819	9.73710×10^{-11}	4.40990×10^{-12}
575.402	4.84720×10^{-10}	2.14220×10^{-11}	604.548	9.48620×10^{-11}	4.29110×10^{-12}
576.131	4.58890×10^{-10}	2.02730×10^{-11}	605.276	9.25020×10^{-11}	4.17990×10^{-12}
576.859	4.34210×10^{-10}	1.91800×10^{-11}	606.005	9.02720×10^{-11}	4.07530×10^{-12}
577.588	4.10800×10^{-10}	1.81470×10^{-11}	606.734	8.81590×10^{-11}	3.97660×10^{-12}
578.317	3.88740×10^{-10}	1.71790×10^{-11}	607.462	8.61490×10^{-11}	3.88300×10^{-12}
579.045	3.68090×10^{-10}	1.62780×10^{-11}	608.191	8.42310×10^{-11}	3.79400×10^{-12}
579.774	3.48850×10^{-10}	1.54440×10^{-11}	608.920	8.23950×10^{-11}	3.70900×10^{-12}
580.503	3.31030×10^{-10}	1.46780×10^{-11}	609.648	8.06340×10^{-11}	3.62760×10^{-12}
581.231	3.14560×10^{-10}	1.39760×10^{-11}	610.377	7.89390×10^{-11}	3.54960×10^{-12}
581.960	2.99410×10^{-10}	1.33370×10^{-11}	611.106	7.73060×10^{-11}	3.47450×10^{-12}
582.688	2.85490×10^{-10}	1.27570×10^{-11}	611.834	7.57290×10^{-11}	3.40210×10^{-12}
583.417	2.72720×10^{-10}	1.22310×10^{-11}	612.563	7.42030×10^{-11}	3.33230×10^{-12}
584.146	2.60990×10^{-10}	1.17540×10^{-11}	613.291	7.27260×10^{-11}	3.26470×10^{-12}
584.874	2.50200×10^{-10}	1.13200×10^{-11}	614.020	7.12940×10^{-11}	3.19940×10^{-12}
585.603	2.40250×10^{-10}	1.09240×10^{-11}	614.749	6.99050×10^{-11}	3.13600×10^{-12}
586.332	2.31020×10^{-10}	1.05590×10^{-11}	615.477	6.85560×10^{-11}	3.07470×10^{-12}
587.060	2.22480×10^{-10}	1.02210×10^{-11}	616.206	6.72450×10^{-11}	3.01510×10^{-12}

Table A.1 (cont'd)

JD +2447000	*UVOIR* Flux	Flux error	JD +2447000	*UVOIR* Flux	Flux error
616.935	6.59710×10^{-11}	2.95730×10^{-12}	646.080	3.35220×10^{-11}	1.50340×10^{-12}
617.663	6.47310×10^{-11}	2.90110×10^{-12}	646.809	3.30060×10^{-11}	1.48060×10^{-12}
618.392	6.35240×10^{-11}	2.84650×10^{-12}	647.538	3.24990×10^{-11}	1.45820×10^{-12}
619.121	6.23500×10^{-11}	2.79340×10^{-12}	648.266	3.20020×10^{-11}	1.43620×10^{-12}
619.849	6.12060×10^{-11}	2.74170×10^{-12}	648.995	3.15130×10^{-11}	1.41460×10^{-12}
620.578	6.00910×10^{-11}	2.69140×10^{-12}	649.724	3.10330×10^{-11}	1.39350×10^{-12}
621.307	5.90040×10^{-11}	2.64250×10^{-12}	650.452	3.05620×10^{-11}	1.37270×10^{-12}
622.035	5.79440×10^{-11}	2.59480×10^{-12}	651.181	3.00990×10^{-11}	1.35230×10^{-12}
622.764	5.69110×10^{-11}	2.54830×10^{-12}	651.910	2.96440×10^{-11}	1.33230×10^{-12}
623.492	5.59030×10^{-11}	2.50290×10^{-12}	652.638	2.91970×10^{-11}	1.31270×10^{-12}
624.221	5.49180×10^{-11}	2.45870×10^{-12}	653.367	2.87570×10^{-11}	1.29340×10^{-12}
624.950	5.39580×10^{-11}	2.41560×10^{-12}	654.095	2.83260×10^{-11}	1.27450×10^{-12}
625.678	5.30190×10^{-11}	2.37350×10^{-12}	654.824	2.79020×10^{-11}	1.25590×10^{-12}
626.407	5.21030×10^{-11}	2.33240×10^{-12}	655.553	2.74850×10^{-11}	1.23770×10^{-12}
627.136	5.12080×10^{-11}	2.29230×10^{-12}	656.281	2.70750×10^{-11}	1.21980×10^{-12}
627.864	5.03320×10^{-11}	2.25310×10^{-12}	657.010	2.66730×10^{-11}	1.20220×10^{-12}
628.593	4.94770×10^{-11}	2.21470×10^{-12}	657.739	2.62770×10^{-11}	1.18500×10^{-12}
629.322	4.86410×10^{-11}	2.17730×10^{-12}	658.467	2.58880×10^{-11}	1.16800×10^{-12}
630.050	4.78230×10^{-11}	2.14070×10^{-12}	659.196	2.55060×10^{-11}	1.15140×10^{-12}
630.779	4.70230×10^{-11}	2.10490×10^{-12}	659.925	2.51300×10^{-11}	1.13500×10^{-12}
631.508	4.62400×10^{-11}	2.06990×10^{-12}	660.653	2.47600×10^{-11}	1.11900×10^{-12}
632.236	4.54740×10^{-11}	2.03560×10^{-12}	661.382	2.43970×10^{-11}	1.10320×10^{-12}
632.965	4.47240×10^{-11}	2.00210×10^{-12}	662.111	2.40390×10^{-11}	1.08770×10^{-12}
633.693	4.39900×10^{-11}	1.96930×10^{-12}	662.839	2.36880×10^{-11}	1.07250×10^{-12}
634.422	4.32710×10^{-11}	1.93720×10^{-12}	663.568	2.33430×10^{-11}	1.05760×10^{-12}
635.151	4.25660×10^{-11}	1.90570×10^{-12}	664.297	2.30030×10^{-11}	1.04290×10^{-12}
635.879	4.18770×10^{-11}	1.87490×10^{-12}	665.025	2.26690×10^{-11}	1.02850×10^{-12}
636.608	4.12010×10^{-11}	1.84480×10^{-12}	665.754	2.23400×10^{-11}	1.01430×10^{-12}
637.337	4.05380×10^{-11}	1.81520×10^{-12}	666.482	2.20170×10^{-11}	1.00040×10^{-12}
638.065	3.98890×10^{-11}	1.78630×10^{-12}	667.211	2.17000×10^{-11}	9.86750×10^{-13}
638.794	3.92530×10^{-11}	1.75790×10^{-12}	667.940	2.13870×10^{-11}	9.73310×10^{-13}
639.523	3.86290×10^{-11}	1.73020×10^{-12}	668.668	2.10800×10^{-11}	9.60110×10^{-13}
640.251	3.80170×10^{-11}	1.70290×10^{-12}	669.397	2.07770×10^{-11}	9.47140×10^{-13}
640.980	3.74170×10^{-11}	1.67620×10^{-12}	670.126	2.04800×10^{-11}	9.34390×10^{-13}
641.709	3.68290×10^{-11}	1.65010×10^{-12}	670.854	2.01870×10^{-11}	9.21860×10^{-13}
642.437	3.62510×10^{-11}	1.62440×10^{-12}	671.583	1.98990×10^{-11}	9.09540×10^{-13}
643.166	3.56850×10^{-11}	1.59930×10^{-12}	672.312	1.96160×10^{-11}	8.97440×10^{-13}
643.894	3.51290×10^{-11}	1.57460×10^{-12}	673.040	1.93380×10^{-11}	8.85540×10^{-13}
644.623	3.45830×10^{-11}	1.55040×10^{-12}	673.769	1.90640×10^{-11}	8.73840×10^{-13}
645.352	3.40480×10^{-11}	1.52670×10^{-12}	674.497	1.87940×10^{-11}	8.62350×10^{-13}

Table A.1 (cont'd)

JD +2447000	*UVOIR* Flux	Flux error	JD +2447000	*UVOIR* Flux	Flux error
675.226	1.85290×10^{-11}	8.51050×10^{-13}	687.613	1.46160×10^{-11}	6.85260×10^{-13}
675.955	1.82680×10^{-11}	8.39940×10^{-13}	688.342	1.44170×10^{-11}	6.76880×10^{-13}
676.683	1.80110×10^{-11}	8.29010×10^{-13}	689.070	1.42220×10^{-11}	6.68630×10^{-13}
677.412	1.77590×10^{-11}	8.18270×10^{-13}	689.799	1.40290×10^{-11}	6.60510×10^{-13}
678.141	1.75100×10^{-11}	8.07710×10^{-13}	690.528	1.38390×10^{-11}	6.52520×10^{-13}
678.869	1.72650×10^{-11}	7.97330×10^{-13}	691.256	1.36530×10^{-11}	6.44650×10^{-13}
679.598	1.70250×10^{-11}	7.87120×10^{-13}	691.985	1.34690×10^{-11}	6.36910×10^{-13}
680.327	1.67880×10^{-11}	7.77070×10^{-13}	692.714	1.32880×10^{-11}	6.29290×10^{-13}
681.055	1.65550×10^{-11}	7.67200×10^{-13}	693.442	1.31100×10^{-11}	6.21790×10^{-13}
681.784	1.63250×10^{-11}	7.57480×10^{-13}	694.171	1.29340×10^{-11}	6.14400×10^{-13}
682.513	1.61000×10^{-11}	7.47930×10^{-13}	694.899	1.27610×10^{-11}	6.07130×10^{-13}
683.241	1.58780×10^{-11}	7.38530×10^{-13}	695.628	1.25910×10^{-11}	5.99970×10^{-13}
683.970	1.56590×10^{-11}	7.29290×10^{-13}	696.357	1.24240×10^{-11}	5.92930×10^{-13}
684.698	1.54440×10^{-11}	7.20190×10^{-13}	697.085	1.22590×10^{-11}	5.85980×10^{-13}
685.427	1.52320×10^{-11}	7.11250×10^{-13}	697.814	1.20960×10^{-11}	5.79150×10^{-13}
686.156	1.50230×10^{-11}	7.02450×10^{-13}	698.543	1.19360×10^{-11}	5.72420×10^{-13}
686.884	1.48180×10^{-11}	6.93790×10^{-13}	699.271	1.17790×10^{-11}	5.65790×10^{-13}

Table A.2. SN 1990N

JD +2440000	*UVOIR* Flux	Flux error	JD +2440000	*UVOIR* Flux	Flux error
8072.65	9.17640×10^{11}	4.03710×10^{12}	8118.55	4.83040×10^{11}	2.52720×10^{12}
8073.80	1.14850×10^{10}	5.06090×10^{12}	8119.70	4.39550×10^{11}	2.26910×10^{12}
8074.94	1.36150×10^{10}	6.01380×10^{12}	8120.85	3.93190×10^{11}	1.98980×10^{12}
8076.09	1.55270×10^{10}	6.87590×10^{12}	8122.00	3.47220×10^{11}	1.71420×10^{12}
8077.24	1.71910×10^{10}	7.63130×10^{12}	8123.14	3.04280×10^{11}	1.46240×10^{12}
8078.39	1.85800×10^{10}	8.26590×10^{12}	8124.29	2.66110×10^{11}	1.24640×10^{12}
8079.53	1.96710×10^{10}	8.76790×10^{12}	8125.44	2.33430×10^{11}	1.07070×10^{12}
8080.68	2.04520×10^{10}	9.12950×10^{12}	8126.58	2.06240×10^{11}	9.33440×10^{13}
8081.83	2.09180×10^{10}	9.34790×10^{12}	8127.73	1.84040×10^{11}	8.29000×10^{13}
8082.98	2.10750×10^{10}	9.42530×10^{12}	8128.88	1.66110×10^{11}	7.50420×10^{13}
8084.12	2.09410×10^{10}	9.36920×10^{12}	8130.03	1.51680×10^{11}	6.91070×10^{13}
8085.27	2.05420×10^{10}	9.19120×10^{12}	8131.17	1.40040×10^{11}	6.45480×10^{13}
8086.42	1.99110×10^{10}	8.90660×10^{12}	8132.32	1.30590×10^{11}	6.09570×10^{13}
8087.57	1.90910×10^{10}	8.53360×10^{12}	8133.47	1.22850×10^{11}	5.80440×10^{13}
8088.71	1.81220×10^{10}	8.09190×10^{12}	8134.62	1.16420×10^{11}	5.56140×10^{13}
8089.86	1.70510×10^{10}	7.60200×10^{12}	8135.77	1.11020×10^{11}	5.35330×10^{13}
8091.01	1.59180×10^{10}	7.08370×10^{12}	8136.91	1.06420×10^{11}	5.17120×10^{13}
8092.16	1.47630×10^{10}	6.55540×10^{12}	8138.06	1.02450×10^{11}	5.00910×10^{13}
8093.31	1.36200×10^{10}	6.03300×10^{12}	8139.21	9.89710×10^{12}	4.86260×10^{13}
8094.45	1.25160×10^{10}	5.52990×10^{12}	8140.36	9.58880×10^{12}	4.72880×10^{13}
8095.60	1.14730×10^{10}	5.05610×10^{12}	8141.50	9.31230×10^{12}	4.60530×10^{13}
8096.75	1.05070×10^{10}	4.61920×10^{12}	8142.65	9.06140×10^{12}	4.49060×10^{13}
8097.90	9.62890×10^{11}	4.22380×10^{12}	8143.80	8.83160×10^{12}	4.38330×10^{13}
8099.04	8.84420×10^{11}	3.87230×10^{12}	8144.95	8.61910×10^{12}	4.28240×10^{13}
8100.19	8.15550×10^{11}	3.56600×10^{12}	8146.09	8.42100×10^{12}	4.18700×10^{13}
8101.34	7.56260×10^{11}	3.30490×10^{12}	8147.24	8.23500×10^{12}	4.09660×10^{13}
8102.49	7.06360×10^{11}	3.08860×10^{12}	8148.39	8.05940×10^{12}	4.01060×10^{13}
8103.63	6.65560×10^{11}	2.91680×10^{12}	8149.54	7.89270×10^{12}	3.92840×10^{13}
8104.78	6.33450×10^{11}	2.78950×10^{12}	8150.68	7.73380×10^{12}	3.84980×10^{13}
8105.93	6.09580×10^{11}	2.70660×10^{12}	8151.83	7.58180×10^{12}	3.77440×10^{13}
8107.08	5.93320×10^{11}	2.66750×10^{12}	8152.98	7.43600×10^{12}	3.70200×10^{13}
8108.22	5.83850×10^{11}	2.67020×10^{12}	8154.13	7.29560×10^{12}	3.63220×10^{13}
8109.37	5.79980×10^{11}	2.70960×10^{12}	8155.27	7.16030×10^{12}	3.56490×10^{13}
8110.52	5.80030×10^{11}	2.77630×10^{12}	8156.42	7.02960×10^{12}	3.49990×10^{13}
8111.67	5.81760×10^{11}	2.85560×10^{12}	8157.57	6.90320×10^{12}	3.43700×10^{13}
8112.81	5.82410×10^{11}	2.92790×10^{12}	8158.72	6.78070×10^{12}	3.37610×10^{13}
8113.96	5.78960×10^{11}	2.97050×10^{12}	8159.87	6.66180×10^{12}	3.31710×10^{13}
8115.11	5.68570×10^{11}	2.96190×10^{12}	8161.01	6.54640×10^{12}	3.25980×10^{13}
8116.26	5.49260×10^{11}	2.88650×10^{12}	8162.16	6.43420×10^{12}	3.20410×10^{13}
8117.40	5.20410×10^{11}	2.73910×10^{12}	8163.31	6.32500×10^{12}	3.15000×10^{13}

Table A.2 (cont'd)

JD +2440000	*UVOIR* Flux	Flux error	JD +2440000	*UVOIR* Flux	Flux error
8164.46	6.21870×10^{12}	3.09730×10^{13}	8210.36	3.33620×10^{12}	1.67130×10^{13}
8165.60	6.11510×10^{12}	3.04590×10^{13}	8211.51	3.28620×10^{12}	1.64650×10^{13}
8166.75	6.01400×10^{12}	2.99590×10^{13}	8212.65	3.23710×10^{12}	1.62220×10^{13}
8167.90	5.91530×10^{12}	2.94700×10^{13}	8213.80	3.18860×10^{12}	1.59820×10^{13}
8169.04	5.81900×10^{12}	2.89930×10^{13}	8214.95	3.14090×10^{12}	1.57450×10^{13}
8170.19	5.72480×10^{12}	2.85270×10^{13}	8216.10	3.09400×10^{12}	1.55130×10^{13}
8171.34	5.63270×10^{12}	2.80720×10^{13}	8217.24	3.04770×10^{12}	1.52840×10^{13}
8172.49	5.54260×10^{12}	2.76260×10^{13}	8218.39	3.00210×10^{12}	1.50580×10^{13}
8173.64	5.45440×10^{12}	2.71900×10^{13}	8219.54	2.95730×10^{12}	1.48350×10^{13}
8174.78	5.36810×10^{12}	2.67630×10^{13}	8220.69	2.91310×10^{12}	1.46160×10^{13}
8175.93	5.28350×10^{12}	2.63450×10^{13}	8221.83	2.86960×10^{12}	1.44010×10^{13}
8177.08	5.20060×10^{12}	2.59350×10^{13}	8222.98	2.82670×10^{12}	1.41880×10^{13}
8178.23	5.11930×10^{12}	2.55330×10^{13}	8224.13	2.78450×10^{12}	1.39790×10^{13}
8179.37	5.03960×10^{12}	2.51390×10^{13}	8225.28	2.74300×10^{12}	1.37730×10^{13}
8180.52	4.96130×10^{12}	2.47520×10^{13}	8226.42	2.70200×10^{12}	1.35700×10^{13}
8181.67	4.88460×10^{12}	2.43730×10^{13}	8227.57	2.66170×10^{12}	1.33700×10^{13}
8182.82	4.80920×10^{12}	2.40000×10^{13}	8228.72	2.62200×10^{12}	1.31730×10^{13}
8183.96	4.73520×10^{12}	2.36340×10^{13}	8229.87	2.58280×10^{12}	1.29790×10^{13}
8185.11	4.66260×10^{12}	2.32750×10^{13}	8231.01	2.54430×10^{12}	1.27880×10^{13}
8186.26	4.59120×10^{12}	2.29220×10^{13}	8232.16	2.50640×10^{12}	1.25990×10^{13}
8187.41	4.52100×10^{12}	2.25750×10^{13}	8233.31	2.46900×10^{12}	1.24140×10^{13}
8188.56	4.45210×10^{12}	2.22350×10^{13}	8234.46	2.43220×10^{12}	1.22310×10^{13}
8189.70	4.38430×10^{12}	2.18990×10^{13}	8235.61	2.39590×10^{12}	1.20510×10^{13}
8190.85	4.31770×10^{12}	2.15700×10^{13}	8236.75	2.36020×10^{12}	1.18740×10^{13}
8192.00	4.25220×10^{12}	2.12460×10^{13}	8237.90	2.32500×10^{12}	1.16990×10^{13}
8193.14	4.18780×10^{12}	2.09270×10^{13}	8239.05	2.29030×10^{12}	1.15270×10^{13}
8194.29	4.12440×10^{12}	2.06140×10^{13}	8240.20	2.25620×10^{12}	1.13580×10^{13}
8195.44	4.06210×10^{12}	2.03060×10^{13}	8241.34	2.22260×10^{12}	1.11910×10^{13}
8196.59	4.00070×10^{12}	2.00020×10^{13}	8242.49	2.18940×10^{12}	1.10260×10^{13}
8197.74	3.94040×10^{12}	1.97040×10^{13}	8243.64	2.15680×10^{12}	1.08640×10^{13}
8198.88	3.88100×10^{12}	1.94100×10^{13}	8244.79	2.12470×10^{12}	1.07040×10^{13}
8200.03	3.82260×10^{12}	1.91210×10^{13}	8245.93	2.09300×10^{12}	1.05470×10^{13}
8201.18	3.76510×10^{12}	1.88360×10^{13}	8247.08	2.06190×10^{12}	1.03920×10^{13}
8202.33	3.70850×10^{12}	1.85560×10^{13}	8248.23	2.03120×10^{12}	1.02400×10^{13}
8203.47	3.65280×10^{12}	1.82800×10^{13}	8249.38	2.00090×10^{12}	1.00890×10^{13}
8204.62	3.59790×10^{12}	1.80090×10^{13}	8250.52	1.97110×10^{12}	9.94120×10^{14}
8205.77	3.54390×10^{12}	1.77410×10^{13}	8251.67	1.94180×10^{12}	9.79530×10^{14}
8206.92	3.49080×10^{12}	1.74780×10^{13}	8252.82	1.91290×10^{12}	9.65160×10^{14}
8208.06	3.43850×10^{12}	1.72190×10^{13}	8253.97	1.88440×10^{12}	9.51000×10^{14}
8209.21	3.38690×10^{12}	1.69640×10^{13}	8255.11	1.85630×10^{12}	9.37050×10^{14}

Table A.2 (cont'd)

JD +2440000	*UVOIR* Flux	Flux error	JD +2440000	*UVOIR* Flux	Flux error
8256.26	1.82870×10^{12}	9.23310×10^{14}	8279.21	1.35530×10^{12}	6.87460×10^{14}
8257.41	1.80150×10^{12}	9.09770×10^{14}	8280.36	1.33520×10^{12}	6.77410×10^{14}
8258.56	1.77470×10^{12}	8.96430×10^{14}	8281.51	1.31540×10^{12}	6.67510×10^{14}
8259.71	1.74830×10^{12}	8.83290×10^{14}	8282.66	1.29580×10^{12}	6.57760×10^{14}
8260.85	1.72230×10^{12}	8.70340×10^{14}	8283.80	1.27660×10^{12}	6.48150×10^{14}
8262.00	1.69670×10^{12}	8.57590×10^{14}	8284.95	1.25760×10^{12}	6.38690×10^{14}
8263.15	1.67140×10^{12}	8.45030×10^{14}	8286.10	1.23900×10^{12}	6.29360×10^{14}
8264.29	1.64660×10^{12}	8.32650×10^{14}	8287.25	1.22060×10^{12}	6.20170×10^{14}
8265.44	1.62210×10^{12}	8.20450×10^{14}	8288.39	1.20250×10^{12}	6.11120×10^{14}
8266.59	1.59800×10^{12}	8.08440×10^{14}	8289.54	1.18460×10^{12}	6.02200×10^{14}
8267.74	1.57420×10^{12}	7.96600×10^{14}	8290.69	1.16700×10^{12}	5.93410×10^{14}
8268.89	1.55080×10^{12}	7.84940×10^{14}	8291.84	1.14970×10^{12}	5.84760×10^{14}
8270.03	1.52780×10^{12}	7.73450×10^{14}	8292.98	1.13270×10^{12}	5.76230×10^{14}
8271.18	1.50500×10^{12}	7.62130×10^{14}	8294.13	1.11590×10^{12}	5.67820×10^{14}
8272.33	1.48270×10^{12}	7.50980×10^{14}	8295.28	1.09930×10^{12}	5.59540×10^{14}
8273.48	1.46060×10^{12}	7.40000×10^{14}	8296.43	1.08300×10^{12}	5.51380×10^{14}
8274.62	1.43890×10^{12}	7.29170×10^{14}	8297.58	1.06690×10^{12}	5.43340×10^{14}
8275.77	1.41760×10^{12}	7.18510×10^{14}	8298.72	1.05110×10^{12}	5.35420×10^{14}
8276.92	1.39650×10^{12}	7.08010×10^{14}	8299.87	1.03550×10^{12}	5.27620×10^{14}
8278.07	1.37580×10^{12}	6.97660×10^{14}	...	...	...

Table A.3. SN 1991T

JD +2440000	*UVOIR* Flux	Flux error	JD +2440000	*UVOIR* Flux	Flux error
8360.45	7.26560×10^{-11}	3.71530×10^{-12}	8378.54	7.07260×10^{-10}	3.12020×10^{-11}
8360.90	9.13940×10^{-11}	4.31140×10^{-12}	8379.00	7.01520×10^{-10}	3.09360×10^{-11}
8361.36	1.13630×10^{-10}	5.14760×10^{-12}	8379.45	6.94190×10^{-10}	3.05990×10^{-11}
8361.81	1.38370×10^{-10}	6.18900×10^{-12}	8379.90	6.85300×10^{-10}	3.01920×10^{-11}
8362.26	1.64600×10^{-10}	7.36710×10^{-12}	8380.35	6.74960×10^{-10}	2.97210×10^{-11}
8362.71	1.91510×10^{-10}	8.61440×10^{-12}	8380.80	6.63250×10^{-10}	2.91890×10^{-11}
8363.17	2.18470×10^{-10}	9.87940×10^{-12}	8381.26	6.50300×10^{-10}	2.86030×10^{-11}
8363.62	2.45090×10^{-10}	1.11280×10^{-11}	8381.71	6.36260×10^{-10}	2.79690×10^{-11}
8364.07	2.71100×10^{-10}	1.23410×10^{-11}	8382.16	6.21280×10^{-10}	2.72940×10^{-11}
8364.52	2.96390×10^{-10}	1.35090×10^{-11}	8382.61	6.05520×10^{-10}	2.65860×10^{-11}
8364.97	3.20900×10^{-10}	1.46280×10^{-11}	8383.07	5.89170×10^{-10}	2.58520×10^{-11}
8365.43	3.44640×10^{-10}	1.56990×10^{-11}	8383.52	5.72380×10^{-10}	2.51000×10^{-11}
8365.88	3.67630×10^{-10}	1.67240×10^{-11}	8383.97	5.55320×10^{-10}	2.43370×10^{-11}
8366.33	3.89930×10^{-10}	1.77080×10^{-11}	8384.42	5.38140×10^{-10}	2.35690×10^{-11}
8366.78	4.11590×10^{-10}	1.86530×10^{-11}	8384.87	5.20980×10^{-10}	2.28030×10^{-11}
8367.24	4.32640×10^{-10}	1.95630×10^{-11}	8385.33	5.03970×10^{-10}	2.20450×10^{-11}
8367.69	4.53140×10^{-10}	2.04430×10^{-11}	8385.78	4.87200×10^{-10}	2.12990×10^{-11}
8368.14	4.73120×10^{-10}	2.12940×10^{-11}	8386.23	4.70780×10^{-10}	2.05690×10^{-11}
8368.59	4.92590×10^{-10}	2.21190×10^{-11}	8386.68	4.54780×10^{-10}	1.98590×10^{-11}
8369.04	5.11570×10^{-10}	2.29200×10^{-11}	8387.14	4.39250×10^{-10}	1.91700×10^{-11}
8369.50	5.30040×10^{-10}	2.36980×10^{-11}	8387.59	4.24230×10^{-10}	1.85060×10^{-11}
8369.95	5.47980×10^{-10}	2.44530×10^{-11}	8388.04	4.09770×10^{-10}	1.78680×10^{-11}
8370.40	5.65380×10^{-10}	2.51850×10^{-11}	8388.49	3.95880×10^{-10}	1.72560×10^{-11}
8370.85	5.82170×10^{-10}	2.58930×10^{-11}	8388.94	3.82570×10^{-10}	1.66710×10^{-11}
8371.31	5.98310×10^{-10}	2.65750×10^{-11}	8389.40	3.69850×10^{-10}	1.61140×10^{-11}
8371.76	6.13740×10^{-10}	2.72290×10^{-11}	8389.85	3.57710×10^{-10}	1.55840×10^{-11}
8372.21	6.28370×10^{-10}	2.78520×10^{-11}	8390.30	3.46140×10^{-10}	1.50820×10^{-11}
8372.66	6.42140×10^{-10}	2.84410×10^{-11}	8390.75	3.35150×10^{-10}	1.46060×10^{-11}
8373.12	6.54970×10^{-10}	2.89910×10^{-11}	8391.21	3.24700×10^{-10}	1.41560×10^{-11}
8373.57	6.66760×10^{-10}	2.95000×10^{-11}	8391.66	3.14780×10^{-10}	1.37320×10^{-11}
8374.02	6.77450×10^{-10}	2.99620×10^{-11}	8392.11	3.05380×10^{-10}	1.33310×10^{-11}
8374.47	6.86930×10^{-10}	3.03730×10^{-11}	8392.56	2.96480×10^{-10}	1.29540×10^{-11}
8374.92	6.95140×10^{-10}	3.07290×10^{-11}	8393.01	2.88050×10^{-10}	1.25990×10^{-11}
8375.38	7.02000×10^{-10}	3.10270×10^{-11}	8393.47	2.80070×10^{-10}	1.22650×10^{-11}
8375.83	7.07430×10^{-10}	3.12620×10^{-11}	8393.92	2.72520×10^{-10}	1.19500×10^{-11}
8376.28	7.11380×10^{-10}	3.14300×10^{-11}	8394.37	2.65380×10^{-10}	1.16550×10^{-11}
8376.73	7.13790×10^{-10}	3.15300×10^{-11}	8394.82	2.58620×10^{-10}	1.13770×10^{-11}
8377.19	7.14610×10^{-10}	3.15580×10^{-11}	8395.28	2.52230×10^{-10}	1.11150×10^{-11}
8377.64	7.13810×10^{-10}	3.15140×10^{-11}	8395.73	2.46190×10^{-10}	1.08690×10^{-11}
8378.09	7.11360×10^{-10}	3.13950×10^{-11}	8396.18	2.40460×10^{-10}	1.06370×10^{-11}

Table A.3 (cont'd)

JD +2440000	*UVOIR* Flux	Flux error	JD +2440000	*UVOIR* Flux	Flux error
8396.63	2.35040×10^{-10}	1.04180×10^{-11}	8414.72	1.11760×10^{-10}	5.02620×10^{-12}
8397.08	2.29890×10^{-10}	1.02100×10^{-11}	8415.18	1.09640×10^{-10}	4.92640×10^{-12}
8397.54	2.25010×10^{-10}	1.00140×10^{-11}	8415.63	1.07580×10^{-10}	4.82950×10^{-12}
8397.99	2.20360×10^{-10}	9.82760×10^{-12}	8416.08	1.05570×10^{-10}	4.73530×10^{-12}
8398.44	2.15940×10^{-10}	9.64990×10^{-12}	8416.53	1.03620×10^{-10}	4.64400×10^{-12}
8398.89	2.11720×10^{-10}	9.48030×10^{-12}	8416.99	1.01730×10^{-10}	4.55550×10^{-12}
8399.35	2.07680×10^{-10}	9.31760×10^{-12}	8417.44	9.98960×10^{-11}	4.46980×10^{-12}
8399.80	2.03820×10^{-10}	9.16120×10^{-12}	8417.89	9.81170×10^{-11}	4.38690×10^{-12}
8400.25	2.00100×10^{-10}	9.01020×10^{-12}	8418.34	9.63930×10^{-11}	4.30680×10^{-12}
8400.70	1.96520×10^{-10}	8.86380×10^{-12}	8418.79	9.47240×10^{-11}	4.22930×10^{-12}
8401.16	1.93070×10^{-10}	8.72140×10^{-12}	8419.25	9.31080×10^{-11}	4.15450×10^{-12}
8401.61	1.89720×10^{-10}	8.58240×10^{-12}	8419.70	9.15440×10^{-11}	4.08220×10^{-12}
8402.06	1.86460×10^{-10}	8.44620×10^{-12}	8420.15	9.00310×10^{-11}	4.01230×10^{-12}
8402.51	1.83290×10^{-10}	8.31230×10^{-12}	8420.60	8.85650×10^{-11}	3.94470×10^{-12}
8402.96	1.80200×10^{-10}	8.18020×10^{-12}	8421.06	8.71470×10^{-11}	3.87940×10^{-12}
8403.42	1.77160×10^{-10}	8.04960×10^{-12}	8421.51	8.57740×10^{-11}	3.81630×10^{-12}
8403.87	1.74180×10^{-10}	7.92020×10^{-12}	8421.96	8.44440×10^{-11}	3.75520×10^{-12}
8404.32	1.71250×10^{-10}	7.79150×10^{-12}	8422.41	8.31550×10^{-11}	3.69600×10^{-12}
8404.77	1.68360×10^{-10}	7.66350×10^{-12}	8422.86	8.19050×10^{-11}	3.63870×10^{-12}
8405.23	1.65500×10^{-10}	7.53590×10^{-12}	8423.32	8.06930×10^{-11}	3.58320×10^{-12}
8405.68	1.62670×10^{-10}	7.40860×10^{-12}	8423.77	7.95150×10^{-11}	3.52930×10^{-12}
8406.13	1.59870×10^{-10}	7.28160×10^{-12}	8424.22	7.83720×10^{-11}	3.47700×10^{-12}
8406.58	1.57090×10^{-10}	7.15470×10^{-12}	8424.67	7.72600×10^{-11}	3.42620×10^{-12}
8407.04	1.54340×10^{-10}	7.02810×10^{-12}	8425.13	7.61780×10^{-11}	3.37680×10^{-12}
8407.49	1.51600×10^{-10}	6.90170×10^{-12}	8425.58	7.51240×10^{-11}	3.32870×10^{-12}
8407.94	1.48880×10^{-10}	6.77570×10^{-12}	8426.03	7.40970×10^{-11}	3.28190×10^{-12}
8408.39	1.46190×10^{-10}	6.65000×10^{-12}	8426.48	7.30960×10^{-11}	3.23620×10^{-12}
8408.84	1.43510×10^{-10}	6.52490×10^{-12}	8426.93	7.21180×10^{-11}	3.19170×10^{-12}
8409.30	1.40860×10^{-10}	6.40050×10^{-12}	8427.39	7.11630×10^{-11}	3.14820×10^{-12}
8409.75	1.38230×10^{-10}	6.27690×10^{-12}	8427.84	7.02280×10^{-11}	3.10570×10^{-12}
8410.20	1.35640×10^{-10}	6.15440×10^{-12}	8428.29	6.93150×10^{-11}	3.06410×10^{-12}
8410.65	1.33070×10^{-10}	6.03310×10^{-12}	8428.74	6.84200×10^{-11}	3.02340×10^{-12}
8411.11	1.30530×10^{-10}	5.91320×10^{-12}	8429.20	6.75430×10^{-11}	2.98360×10^{-12}
8411.56	1.28030×10^{-10}	5.79500×10^{-12}	8429.65	6.66830×10^{-11}	2.94450×10^{-12}
8412.01	1.25570×10^{-10}	5.67850×10^{-12}	8430.10	6.58390×10^{-11}	2.90630×10^{-12}
8412.46	1.23150×10^{-10}	5.56400×10^{-12}	8430.55	6.50110×10^{-11}	2.86870×10^{-12}
8412.92	1.20770×10^{-10}	5.45160×10^{-12}	8431.00	6.41970×10^{-11}	2.83180×10^{-12}
8413.37	1.18440×10^{-10}	5.34150×10^{-12}	8431.46	6.33970×10^{-11}	2.79560×10^{-12}
8413.82	1.16170×10^{-10}	5.23380×10^{-12}	8431.91	6.26110×10^{-11}	2.76010×10^{-12}
8414.27	1.13940×10^{-10}	5.12870×10^{-12}	8432.36	6.18370×10^{-11}	2.72510×10^{-12}

Table A.3 (cont'd)

JD +2440000	*UVOIR* Flux	Flux error	JD +2440000	*UVOIR* Flux	Flux error
8432.81	6.10760×10^{-11}	2.69080×10^{-12}	8441.41	4.85110×10^{-11}	2.12930×10^{-12}
8433.27	6.03270×10^{-11}	2.65700×10^{-12}	8441.86	4.79350×10^{-11}	2.10390×10^{-12}
8433.72	5.95890×10^{-11}	2.62370×10^{-12}	8442.31	4.73660×10^{-11}	2.07880×10^{-12}
8434.17	5.88620×10^{-11}	2.59100×10^{-12}	8442.76	4.68040×10^{-11}	2.05400×10^{-12}
8434.62	5.81450×10^{-11}	2.55880×10^{-12}	8443.22	4.62500×10^{-11}	2.02960×10^{-12}
8435.08	5.74390×10^{-11}	2.52710×10^{-12}	8443.67	4.57030×10^{-11}	2.00560×10^{-12}
8435.53	5.67440×10^{-11}	2.49590×10^{-12}	8444.12	4.51620×10^{-11}	1.98180×10^{-12}
8435.98	5.60570×10^{-11}	2.46510×10^{-12}	8444.57	4.46290×10^{-11}	1.95840×10^{-12}
8436.43	5.53810×10^{-11}	2.43480×10^{-12}	8445.03	4.41030×10^{-11}	1.93540×10^{-12}
8436.88	5.47130×10^{-11}	2.40500×10^{-12}	8445.48	4.35830×10^{-11}	1.91260×10^{-12}
8437.34	5.40550×10^{-11}	2.37560×10^{-12}	8445.93	4.30700×10^{-11}	1.89020×10^{-12}
8437.79	5.34060×10^{-11}	2.34660×10^{-12}	8446.38	4.25640×10^{-11}	1.86800×10^{-12}
8438.24	5.27650×10^{-11}	2.31810×10^{-12}	8446.83	4.20640×10^{-11}	1.84620×10^{-12}
8438.69	5.21330×10^{-11}	2.28990×10^{-12}	8447.29	4.15710×10^{-11}	1.82470×10^{-12}
8439.15	5.15090×10^{-11}	2.26220×10^{-12}	8447.74	4.10830×10^{-11}	1.80350×10^{-12}
8439.60	5.08940×10^{-11}	2.23480×10^{-12}	8448.19	4.06030×10^{-11}	1.78250×10^{-12}
8440.05	5.02860×10^{-11}	2.20790×10^{-12}	8448.64	4.01280×10^{-11}	1.76190×10^{-12}
8440.50	4.96870×10^{-11}	2.18130×10^{-12}	8449.10	3.96590×10^{-11}	1.74150×10^{-12}
8440.96	4.90950×10^{-11}	2.15510×10^{-12}	8449.55	3.91960×10^{-11}	1.72150×10^{-12}

Table A.4. SN 1991bg

JD +2440000	*UVOIR* Flux	Flux error	JD +2440000	*UVOIR* Flux	Flux error
8597.24	6.04489×10^{-12}	4.06955×10^{-13}	8629.40	8.06552×10^{-12}	3.92406×10^{-13}
8598.04	8.58875×10^{-12}	5.69347×10^{-13}	8630.20	7.75283×10^{-12}	3.76328×10^{-13}
8598.84	1.16934×10^{-11}	7.45954×10^{-13}	8631.00	7.46225×10^{-12}	3.61441×10^{-13}
8599.65	1.60459×10^{-11}	9.45688×10^{-13}	8631.81	7.19102×10^{-12}	3.47614×10^{-13}
8600.45	2.19513×10^{-11}	1.18490×10^{-12}	8632.61	6.93704×10^{-12}	3.34721×10^{-13}
8601.26	2.89890×10^{-11}	1.46381×10^{-12}	8633.42	6.69828×10^{-12}	3.22650×10^{-13}
8602.06	3.59931×10^{-11}	1.75160×10^{-12}	8634.22	6.47301×10^{-12}	3.11305×10^{-13}
8602.86	4.19199×10^{-11}	2.00542×10^{-12}	8635.03	6.25969×10^{-12}	3.00615×10^{-13}
8603.67	4.62487×10^{-11}	2.19707×10^{-12}	8635.83	6.05724×10^{-12}	2.90489×10^{-13}
8604.47	4.89088×10^{-11}	2.31951×10^{-12}	8636.63	5.86450×10^{-12}	2.80886×10^{-13}
8605.28	5.00719×10^{-11}	2.37817×10^{-12}	8637.44	5.68041×10^{-12}	2.71733×10^{-13}
8606.08	5.00015×10^{-11}	2.38348×10^{-12}	8638.24	5.50430×10^{-12}	2.63001×10^{-13}
8606.88	4.89708×10^{-11}	2.34627×10^{-12}	8639.04	5.33547×10^{-12}	2.54644×10^{-13}
8607.69	4.72245×10^{-11}	2.27599×10^{-12}	8639.85	5.17331×10^{-12}	2.46628×10^{-13}
8608.49	4.49763×10^{-11}	2.18133×10^{-12}	8640.65	5.01730×10^{-12}	2.38922×10^{-13}
8609.30	4.24046×10^{-11}	2.06924×10^{-12}	8641.46	4.86691×10^{-12}	2.31503×10^{-13}
8610.10	3.96557×10^{-11}	1.94643×10^{-12}	8642.26	4.72207×10^{-12}	2.24353×10^{-13}
8610.91	3.68495×10^{-11}	1.81849×10^{-12}	8643.07	4.58220×10^{-12}	2.17464×10^{-13}
8611.71	3.40799×10^{-11}	1.68970×10^{-12}	8643.87	4.44727×10^{-12}	2.10807×10^{-13}
8612.51	3.14121×10^{-11}	1.56390×10^{-12}	8644.67	4.31680×10^{-12}	2.04376×10^{-13}
8613.32	2.88960×10^{-11}	1.44361×10^{-12}	8645.48	4.19091×10^{-12}	1.98163×10^{-13}
8614.12	2.65576×10^{-11}	1.33065×10^{-12}	8646.28	4.06922×10^{-12}	1.92163×10^{-13}
8614.92	2.44108×10^{-11}	1.22580×10^{-12}	8647.08	3.95174×10^{-12}	1.86368×10^{-13}
8615.73	2.24585×10^{-11}	1.12951×10^{-12}	8647.89	3.83822×10^{-12}	1.80783×10^{-13}
8616.53	2.06945×10^{-11}	1.04179×10^{-12}	8648.69	3.72863×10^{-12}	1.75380×10^{-13}
8617.34	1.91099×10^{-11}	9.62313×10^{-13}	8649.50	3.62295×10^{-12}	1.70183×10^{-13}
8618.14	1.76917×10^{-11}	8.90578×10^{-13}	8650.30	3.52090×10^{-12}	1.65163×10^{-13}
8618.95	1.64234×10^{-11}	8.26021×10^{-13}	8651.11	3.42244×10^{-12}	1.60334×10^{-13}
8619.75	1.52912×10^{-11}	7.68014×10^{-13}	8651.91	3.32763×10^{-12}	1.55677×10^{-13}
8620.55	1.42809×10^{-11}	7.15949×10^{-13}	8652.71	3.23617×10^{-12}	1.51204×10^{-13}
8621.36	1.33789×10^{-11}	6.69219×10^{-13}	8653.52	3.14811×10^{-12}	1.46906×10^{-13}
8622.16	1.25715×10^{-11}	6.27263×10^{-13}	8654.32	3.06325×10^{-12}	1.42763×10^{-13}
8622.96	1.18488×10^{-11}	5.89560×10^{-13}	8655.13	2.98150×10^{-12}	1.38797×10^{-13}
8623.77	1.11989×10^{-11}	5.55637×10^{-13}	8655.93	2.90276×10^{-12}	1.34975×10^{-13}
8624.57	1.06140×10^{-11}	5.25046×10^{-13}	8656.73	2.82693×10^{-12}	1.31310×10^{-13}
8625.38	1.00853×10^{-11}	4.97412×10^{-13}	8657.54	2.75390×10^{-12}	1.27779×10^{-13}
8626.18	9.60571×10^{-12}	4.72363×10^{-13}	8658.34	2.68344×10^{-12}	1.24404×10^{-13}
8626.99	9.16900×10^{-12}	4.49595×10^{-13}	8659.15	2.61567×10^{-12}	1.21152×10^{-13}
8627.79	8.76980×10^{-12}	4.28841×10^{-13}	8659.95	2.55023×10^{-12}	1.18022×10^{-13}
8628.59	8.40328×10^{-12}	4.09856×10^{-13}	8660.75	2.48713×10^{-12}	1.15015×10^{-13}

Table A.4 (cont'd)

JD +2440000	*UVOIR* Flux	Flux error	JD +2440000	*UVOIR* Flux	Flux error
8661.56	2.42635×10^{-12}	1.12128×10^{-13}	8693.72	1.02165×10^{-12}	4.72220×10^{-14}
8662.36	2.36754×10^{-12}	1.09340×10^{-13}	8694.52	1.00120×10^{-12}	4.62907×10^{-14}
8663.17	2.31081×10^{-12}	1.06663×10^{-13}	8695.33	9.81168×10^{-13}	4.53793×10^{-14}
8663.97	2.25593×10^{-12}	1.04080×10^{-13}	8696.13	9.61577×10^{-13}	4.44859×10^{-14}
8664.77	2.20288×10^{-12}	1.01588×10^{-13}	8696.93	9.42397×10^{-13}	4.36130×10^{-14}
8665.58	2.15154×10^{-12}	9.91815×10^{-14}	8697.74	9.23646×10^{-13}	4.27588×10^{-14}
8666.38	2.10181×10^{-12}	9.68573×10^{-14}	8698.54	9.05296×10^{-13}	4.19234×10^{-14}
8667.19	2.05367×10^{-12}	9.46099×10^{-14}	8699.35	8.87358×10^{-13}	4.11057×10^{-14}
8667.99	2.00691×10^{-12}	9.24369×10^{-14}	8700.15	8.69822×10^{-13}	4.03069×10^{-14}
8668.79	1.96164×10^{-12}	9.03318×10^{-14}	8700.96	8.52659×10^{-13}	3.95256×10^{-14}
8669.60	1.91774×10^{-12}	8.82934×10^{-14}	8701.76	8.35863×10^{-13}	3.87615×10^{-14}
8670.40	1.87500×10^{-12}	8.63166×10^{-14}	8702.56	8.19421×10^{-13}	3.80118×10^{-14}
8671.21	1.83354×10^{-12}	8.44004×10^{-14}	8703.37	8.03310×10^{-13}	3.72781×10^{-14}
8672.01	1.79325×10^{-12}	8.25408×10^{-14}	8704.17	7.87491×10^{-13}	3.65575×10^{-14}
8672.81	1.75414×10^{-12}	8.07347×10^{-14}	8704.97	7.71962×10^{-13}	3.58493×10^{-14}
8673.62	1.71610×10^{-12}	7.89815×10^{-14}	8705.78	7.56692×10^{-13}	3.51542×10^{-14}
8674.42	1.67905×10^{-12}	7.72781×10^{-14}	8706.58	7.41690×10^{-13}	3.44700×10^{-14}
8675.23	1.64297×10^{-12}	7.56218×10^{-14}	8707.39	7.26951×10^{-13}	3.37985×10^{-14}
8676.03	1.60800×10^{-12}	7.40127×10^{-14}	8708.19	7.12511×10^{-13}	3.31392×10^{-14}
8676.83	1.57380×10^{-12}	7.24467×10^{-14}	8709.00	6.98442×10^{-13}	3.24976×10^{-14}
8677.64	1.54060×10^{-12}	7.09243×10^{-14}	...	...	...
8678.44	1.50830×10^{-12}	6.94422×10^{-14}	...	...	...
8679.25	1.47679×10^{-12}	6.80005×10^{-14}	...	...	...
8680.05	1.44618×10^{-12}	6.65961×10^{-14}	...	...	...
8680.85	1.41625×10^{-12}	6.52278×10^{-14}	...	...	...
8681.66	1.38711×10^{-12}	6.38946×10^{-14}	...	...	...
8682.46	1.35865×10^{-12}	6.25939×10^{-14}	...	...	...
8683.27	1.33086×10^{-12}	6.13269×10^{-14}	...	...	...
8684.07	1.30385×10^{-12}	6.00899×10^{-14}	...	...	...
8684.87	1.27739×10^{-12}	5.88816×10^{-14}	...	...	...
8685.68	1.25148×10^{-12}	5.77018×10^{-14}	...	...	...
8686.48	1.22622×10^{-12}	5.65491×10^{-14}	...	...	...
8687.29	1.20149×10^{-12}	5.54221×10^{-14}	...	...	...
8688.09	1.17741×10^{-12}	5.43197×10^{-14}	...	...	...
8688.89	1.15374×10^{-12}	5.32404×10^{-14}	...	...	...
8689.70	1.13049×10^{-12}	5.21842×10^{-14}	...	...	...
8690.50	1.10788×10^{-12}	5.11509×10^{-14}	...	...	...
8691.31	1.08568×10^{-12}	5.01375×10^{-14}	...	...	...
8692.11	1.06386×10^{-12}	4.91451×10^{-14}	...	...	...

Table A.5. SN 1992A

JD +2440000	*UVOIR* Flux	Flux error	JD +2440000	*UVOIR* Flux	Flux error
8630.58	4.98150×10^{-11}	2.95530×10^{-12}	8653.69	7.28810×10^{-11}	3.18870×10^{-12}
8631.16	5.86700×10^{-11}	3.12760×10^{-12}	8654.27	6.99580×10^{-11}	3.06360×10^{-12}
8631.73	6.96520×10^{-11}	3.38830×10^{-12}	8654.85	6.73420×10^{-11}	2.95360×10^{-12}
8632.31	8.18400×10^{-11}	3.74260×10^{-12}	8655.43	6.50000×10^{-11}	2.85720×10^{-12}
8632.89	9.41530×10^{-11}	4.16510×10^{-12}	8656.00	6.28960×10^{-11}	2.77260×10^{-12}
8633.47	1.05860×10^{-10}	4.61610×10^{-12}	8656.58	6.09920×10^{-11}	2.69780×10^{-12}
8634.04	1.16630×10^{-10}	5.06360×10^{-12}	8657.16	5.92500×10^{-11}	2.63070×10^{-12}
8634.62	1.26370×10^{-10}	5.48830×10^{-12}	8657.74	5.76310×10^{-11}	2.56910×10^{-12}
8635.20	1.35080×10^{-10}	5.88050×10^{-12}	8658.32	5.60970×10^{-11}	2.51100×10^{-12}
8635.78	1.42830×10^{-10}	6.23600×10^{-12}	8658.89	5.46140×10^{-11}	2.45440×10^{-12}
8636.36	1.49700×10^{-10}	6.55330×10^{-12}	8659.47	5.31520×10^{-11}	2.39760×10^{-12}
8636.93	1.55710×10^{-10}	6.83200×10^{-12}	8660.05	5.16880×10^{-11}	2.33940×10^{-12}
8637.51	1.60910×10^{-10}	7.07200×10^{-12}	8660.63	5.02030×10^{-11}	2.27870×10^{-12}
8638.09	1.65300×10^{-10}	7.27320×10^{-12}	8661.21	4.86870×10^{-11}	2.21510×10^{-12}
8638.67	1.68870×10^{-10}	7.43550×10^{-12}	8661.78	4.71340×10^{-11}	2.14850×10^{-12}
8639.25	1.71620×10^{-10}	7.55840×10^{-12}	8662.36	4.55470×10^{-11}	2.07900×10^{-12}
8639.82	1.73510×10^{-10}	7.64190×10^{-12}	8662.94	4.39320×10^{-11}	2.00700×10^{-12}
8640.40	1.74540×10^{-10}	7.68560×10^{-12}	8663.52	4.22990×10^{-11}	1.93340×10^{-12}
8640.98	1.74690×10^{-10}	7.68950×10^{-12}	8664.09	4.06620×10^{-11}	1.85870×10^{-12}
8641.56	1.73950×10^{-10}	7.65390×10^{-12}	8664.67	3.90340×10^{-11}	1.78390×10^{-12}
8642.14	1.72320×10^{-10}	7.57950×10^{-12}	8665.25	3.74310×10^{-11}	1.70980×10^{-12}
8642.71	1.69830×10^{-10}	7.46760×10^{-12}	8665.83	3.58670×10^{-11}	1.63700×10^{-12}
8643.29	1.66520×10^{-10}	7.32030×10^{-12}	8666.41	3.43530×10^{-11}	1.56640×10^{-12}
8643.87	1.62470×10^{-10}	7.14060×10^{-12}	8666.99	3.29020×10^{-11}	1.49850×10^{-12}
8644.45	1.57740×10^{-10}	6.93190×10^{-12}	8667.56	3.15210×10^{-11}	1.43370×10^{-12}
8645.03	1.52440×10^{-10}	6.69860×10^{-12}	8668.14	3.02160×10^{-11}	1.37250×10^{-12}
8645.60	1.46690×10^{-10}	6.44560×10^{-12}	8668.72	2.89910×10^{-11}	1.31510×10^{-12}
8646.18	1.40610×10^{-10}	6.17810×10^{-12}	8669.30	2.78480×10^{-11}	1.26160×10^{-12}
8646.76	1.34320×10^{-10}	5.90120×10^{-12}	8669.87	2.67870×10^{-11}	1.21200×10^{-12}
8647.34	1.27940×10^{-10}	5.62010×10^{-12}	8670.45	2.58050×10^{-11}	1.16640×10^{-12}
8647.92	1.21570×10^{-10}	5.33950×10^{-12}	8671.03	2.49000×10^{-11}	1.12440×10^{-12}
8648.49	1.15320×10^{-10}	5.06350×10^{-12}	8671.61	2.40660×10^{-11}	1.08590×10^{-12}
8649.07	1.09270×10^{-10}	4.79570×10^{-12}	8672.19	2.33000×10^{-11}	1.05070×10^{-12}
8649.65	1.03470×10^{-10}	4.53920×10^{-12}	8672.76	2.25950×10^{-11}	1.01850×10^{-12}
8650.23	9.79980×10^{-11}	4.29630×10^{-12}	8673.34	2.19460×10^{-11}	9.88980×10^{-13}
8650.80	9.28700×10^{-11}	4.06870×10^{-12}	8673.92	2.13490×10^{-11}	9.61860×10^{-13}
8651.38	8.81150×10^{-11}	3.85780×10^{-12}	8674.50	2.07960×10^{-11}	9.36860×10^{-13}
8651.96	8.37430×10^{-11}	3.66420×10^{-12}	8675.08	2.02840×10^{-11}	9.13720×10^{-13}
8652.54	7.97540×10^{-11}	3.48830×10^{-12}	8675.65	1.98070×10^{-11}	8.92210×10^{-13}
8653.12	7.61390×10^{-11}	3.32990×10^{-12}	8676.23	1.93620×10^{-11}	8.72110×10^{-13}

Table A.5 (cont'd)

JD +2440000	*UVOIR* Flux	Flux error	JD +2440000	*UVOIR* Flux	Flux error
8676.81	1.89440×10^{-11}	8.53240×10^{-13}	8699.92	9.71900×10^{-12}	4.30480×10^{-13}
8677.39	1.85500×10^{-11}	8.35420×10^{-13}	8700.50	9.57030×10^{-12}	4.23890×10^{-13}
8677.96	1.81780×10^{-11}	8.18510×10^{-13}	8701.08	9.42430×10^{-12}	4.17430×10^{-13}
8678.54	1.78240×10^{-11}	8.02400×10^{-13}	8701.66	9.28080×10^{-12}	4.11090×10^{-13}
8679.12	1.74870×10^{-11}	7.86990×10^{-13}	8702.24	9.13970×10^{-12}	4.04880×10^{-13}
8679.70	1.71640×10^{-11}	7.72180×10^{-13}	8702.81	9.00120×10^{-12}	3.98800×10^{-13}
8680.28	1.68530×10^{-11}	7.57910×10^{-13}	8703.39	8.86510×10^{-12}	3.92830×10^{-13}
8680.85	1.65540×10^{-11}	7.44120×10^{-13}	8703.97	8.73130×10^{-12}	3.86980×10^{-13}
8681.43	1.62640×10^{-11}	7.30750×10^{-13}	8704.55	8.59980×10^{-12}	3.81240×10^{-13}
8682.01	1.59840×10^{-11}	7.17780×10^{-13}	8705.13	8.47070×10^{-12}	3.75620×10^{-13}
8682.59	1.57120×10^{-11}	7.05160×10^{-13}	8705.70	8.34380×10^{-12}	3.70110×10^{-13}
8683.17	1.54470×10^{-11}	6.92870×10^{-13}	8706.28	8.21910×10^{-12}	3.64700×10^{-13}
8683.74	1.51890×10^{-11}	6.80880×10^{-13}	8706.86	8.09650×10^{-12}	3.59400×10^{-13}
8684.32	1.49380×10^{-11}	6.69180×10^{-13}	8707.44	7.97610×10^{-12}	3.54210×10^{-13}
8684.90	1.46920×10^{-11}	6.57750×10^{-13}	8708.01	7.85780×10^{-12}	3.49120×10^{-13}
8685.48	1.44510×10^{-11}	6.46570×10^{-13}	8708.59	7.74150×10^{-12}	3.44130×10^{-13}
8686.05	1.42160×10^{-11}	6.35640×10^{-13}	8709.17	7.62730×10^{-12}	3.39230×10^{-13}
8686.63	1.39860×10^{-11}	6.24940×10^{-13}	8709.75	7.51500×10^{-12}	3.34430×10^{-13}
8687.21	1.37600×10^{-11}	6.14460×10^{-13}	8710.33	7.40460×10^{-12}	3.29730×10^{-13}
8687.79	1.35390×10^{-11}	6.04210×10^{-13}	8710.91	7.29620×10^{-12}	3.25110×10^{-13}
8688.37	1.33220×10^{-11}	5.94160×10^{-13}	8711.48	7.18960×10^{-12}	3.20590×10^{-13}
8688.95	1.31090×10^{-11}	5.84320×10^{-13}	8712.06	7.08490×10^{-12}	3.16150×10^{-13}
8689.52	1.29000×10^{-11}	5.74680×10^{-13}	8712.64	6.98200×10^{-12}	3.11800×10^{-13}
8690.10	1.26950×10^{-11}	5.65230×10^{-13}	8713.22	6.88090×10^{-12}	3.07540×10^{-13}
8690.68	1.24930×10^{-11}	5.55970×10^{-13}	8713.79	6.78150×10^{-12}	3.03360×10^{-13}
8691.26	1.22960×10^{-11}	5.46890×10^{-13}	8714.37	6.68380×10^{-12}	2.99250×10^{-13}
8691.83	1.21010×10^{-11}	5.38000×10^{-13}	8714.95	6.58780×10^{-12}	2.95230×10^{-13}
8692.41	1.19110×10^{-11}	5.29280×10^{-13}	8715.53	6.49340×10^{-12}	2.91290×10^{-13}
8692.99	1.17240×10^{-11}	5.20740×10^{-13}	8716.11	6.40070×10^{-12}	2.87420×10^{-13}
8693.57	1.15400×10^{-11}	5.12370×10^{-13}	8716.68	6.30950×10^{-12}	2.83620×10^{-13}
8694.15	1.13590×10^{-11}	5.04160×10^{-13}	8717.26	6.21990×10^{-12}	2.79900×10^{-13}
8694.72	1.11820×10^{-11}	4.96110×10^{-13}	8717.84	6.13190×10^{-12}	2.76250×10^{-13}
8695.30	1.10070×10^{-11}	4.88220×10^{-13}	8718.42	6.04530×10^{-12}	2.72670×10^{-13}
8695.88	1.08360×10^{-11}	4.80490×10^{-13}	8719.00	5.96020×10^{-12}	2.69160×10^{-13}
8696.46	1.06680×10^{-11}	4.72910×10^{-13}	8719.57	5.87660×10^{-12}	2.65710×10^{-13}
8697.04	1.05030×10^{-11}	4.65490×10^{-13}	8720.15	5.79430×10^{-12}	2.62330×10^{-13}
8697.61	1.03400×10^{-11}	4.58200×10^{-13}	8720.73	5.71350×10^{-12}	2.59020×10^{-13}
8698.19	1.01810×10^{-11}	4.51070×10^{-13}	8721.31	5.63410×10^{-12}	2.55770×10^{-13}
8698.77	1.00240×10^{-11}	4.44070×10^{-13}	8721.88	5.55590×10^{-12}	2.52570×10^{-13}
8699.35	9.87030×10^{-12}	4.37210×10^{-13}	8722.46	5.47910×10^{-12}	2.49440×10^{-13}

Table A.5 (cont'd)

JD +2440000	*UVOIR* Flux	Flux error	JD +2440000	*UVOIR* Flux	Flux error
8723.04	5.40370×10^{-12}	2.46370×10^{-13}	8734.02	4.18610×10^{-12}	1.97610×10^{-13}
8723.62	5.32940×10^{-12}	2.43350×10^{-13}	8734.60	4.13200×10^{-12}	1.95480×10^{-13}
8724.20	5.25640×10^{-12}	2.40390×10^{-13}	8735.18	4.07880×10^{-12}	1.93390×10^{-13}
8724.77	5.18470×10^{-12}	2.37490×10^{-13}	8735.75	4.02650×10^{-12}	1.91330×10^{-13}
8725.35	5.11410×10^{-12}	2.34640×10^{-13}	8736.33	3.97500×10^{-12}	1.89310×10^{-13}
8725.93	5.04480×10^{-12}	2.31840×10^{-13}	8736.91	3.92440×10^{-12}	1.87320×10^{-13}
8726.51	4.97660×10^{-12}	2.29100×10^{-13}	8737.49	3.87450×10^{-12}	1.85360×10^{-13}
8727.08	4.90950×10^{-12}	2.26400×10^{-13}	8738.07	3.82550×10^{-12}	1.83440×10^{-13}
8727.66	4.84350×10^{-12}	2.23750×10^{-13}	8738.64	3.77720×10^{-12}	1.81560×10^{-13}
8728.24	4.77870×10^{-12}	2.21160×10^{-13}	8739.22	3.72980×10^{-12}	1.79700×10^{-13}
8728.82	4.71490×10^{-12}	2.18610×10^{-13}	8739.80	3.68300×10^{-12}	1.77870×10^{-13}
8729.40	4.65220×10^{-12}	2.16100×10^{-13}	8740.38	3.63710×10^{-12}	1.76080×10^{-13}
8729.97	4.59050×10^{-12}	2.13640×10^{-13}	8740.96	3.59180×10^{-12}	1.74310×10^{-13}
8730.55	4.52980×10^{-12}	2.11230×10^{-13}	8741.53	3.54730×10^{-12}	1.72580×10^{-13}
8731.13	4.47010×10^{-12}	2.08850×10^{-13}	8742.11	3.50340×10^{-12}	1.70870×10^{-13}
8731.71	4.41140×10^{-12}	2.06520×10^{-13}	8742.69	3.46030×10^{-12}	1.69190×10^{-13}
8732.29	4.35370×10^{-12}	2.04240×10^{-13}	8743.27	3.41790×10^{-12}	1.67540×10^{-13}
8732.86	4.29690×10^{-12}	2.01990×10^{-13}	8743.84	3.37610×10^{-12}	1.65910×10^{-13}
8733.44	4.24100×10^{-12}	1.99780×10^{-13}	8744.42	3.33490×10^{-12}	1.64320×10^{-13}

Table A.6. SN 1992bc

JD +2440000	*UVOIR* Flux	Flux error	JD +2440000	*UVOIR* Flux	Flux error
8904.22	1.03848e-11	5.25416e-13	8929.33	6.16858e-12	3.05166e-13
8904.85	1.11822e-11	5.66077e-13	8929.95	5.90047e-12	2.90844e-13
8905.48	1.19030e-11	6.02574e-13	8930.58	5.65147e-12	2.77564e-13
8906.10	1.25519e-11	6.35280e-13	8931.21	5.42086e-12	2.65287e-13
8906.73	1.31332e-11	6.64548e-13	8931.84	5.20804e-12	2.53995e-13
8907.36	1.36510e-11	6.90613e-13	8932.46	5.01231e-12	2.43643e-13
8907.99	1.41076e-11	7.13651e-13	8933.09	4.83281e-12	2.34200e-13
8908.61	1.45031e-11	7.33768e-13	8933.72	4.66881e-12	2.25615e-13
8909.24	1.48383e-11	7.51002e-13	8934.35	4.51923e-12	2.17852e-13
8909.87	1.51137e-11	7.65355e-13	8934.97	4.38335e-12	2.10852e-13
8910.50	1.53295e-11	7.76811e-13	8935.60	4.25995e-12	2.04569e-13
8911.12	1.54851e-11	7.85326e-13	8936.23	4.14805e-12	1.98918e-13
8911.75	1.55798e-11	7.90883e-13	8936.86	4.04648e-12	1.93866e-13
8912.38	1.56158e-11	7.93462e-13	8937.49	3.95398e-12	1.89319e-13
8913.01	1.55918e-11	7.93077e-13	8938.11	3.86922e-12	1.85216e-13
8913.63	1.55109e-11	7.89764e-13	8938.74	3.79097e-12	1.81464e-13
8914.26	1.53738e-11	7.83581e-13	8939.37	3.71771e-12	1.78004e-13
8914.89	1.51842e-11	7.74627e-13	8940.00	3.64815e-12	1.74754e-13
8915.52	1.49437e-11	7.63069e-13	8940.62	3.58099e-12	1.71634e-13
8916.15	1.46590e-11	7.49054e-13	8941.25	3.51516e-12	1.68587e-13
8916.77	1.43322e-11	7.32806e-13	8941.88	3.44950e-12	1.65553e-13
8917.40	1.39679e-11	7.14554e-13	8942.51	3.38328e-12	1.62486e-13
8918.03	1.35724e-11	6.94553e-13	8943.13	3.31587e-12	1.59360e-13
8918.66	1.31515e-11	6.73076e-13	8943.76	3.24710e-12	1.56151e-13
8919.28	1.27103e-11	6.50413e-13	8944.39	3.17681e-12	1.52856e-13
8919.91	1.22525e-11	6.26828e-13	8945.02	3.10495e-12	1.49471e-13
8920.54	1.17858e-11	6.02607e-13	8945.64	3.03202e-12	1.46018e-13
8921.17	1.13136e-11	5.78015e-13	8946.27	2.95799e-12	1.42506e-13
8921.79	1.08409e-11	5.53300e-13	8946.90	2.88351e-12	1.38955e-13
8922.42	1.03721e-11	5.28694e-13	8947.53	2.80877e-12	1.35376e-13
8923.05	9.91048e-12	5.04381e-13	8948.16	2.73433e-12	1.31780e-13
8923.68	9.45935e-12	4.80551e-13	8948.78	2.66031e-12	1.28200e-13
8924.30	9.02157e-12	4.57359e-13	8949.41	2.58704e-12	1.24637e-13
8924.93	8.59912e-12	4.34928e-13	8950.04	2.51487e-12	1.21101e-13
8925.56	8.19377e-12	4.13353e-13	8950.67	2.44382e-12	1.17617e-13
8926.19	7.80683e-12	3.92731e-13	8951.29	2.37436e-12	1.14196e-13
8926.82	7.43934e-12	3.73102e-13	8951.92	2.30639e-12	1.10840e-13
8927.44	7.09147e-12	3.54524e-13	8952.55	2.24016e-12	1.07564e-13
8928.07	6.76373e-12	3.36992e-13	8953.18	2.17571e-12	1.04377e-13
8928.70	6.45621e-12	3.20552e-13	8953.80	2.11327e-12	1.01287e-13

Table A.6 (cont'd)

JD +2440000	*UVOIR* Flux	Flux error	JD +2440000	*UVOIR* Flux	Flux error
8954.43	2.05287e-12	9.83007e-14	8979.54	9.33258e-13	4.45649e-14
8955.06	1.99454e-12	9.54251e-14	8980.17	9.19956e-13	4.39306e-14
8955.69	1.93840e-12	9.26638e-14	8980.79	9.06869e-13	4.33082e-14
8956.31	1.88447e-12	9.00189e-14	8981.42	8.94020e-13	4.26966e-14
8956.94	1.83289e-12	8.74934e-14	8982.05	8.81378e-13	4.20959e-14
8957.57	1.78345e-12	8.50870e-14	8982.68	8.68945e-13	4.15061e-14
8958.20	1.73626e-12	8.27981e-14	8983.30	8.56724e-13	4.09264e-14
8958.83	1.69136e-12	8.06253e-14	8983.93	8.44702e-13	4.03567e-14
8959.45	1.64852e-12	7.85655e-14	8984.56	8.32873e-13	3.97971e-14
8960.08	1.60786e-12	7.66139e-14	8985.19	8.21248e-13	3.92477e-14
8960.71	1.56929e-12	7.47653e-14	8985.81	8.09817e-13	3.87074e-14
8961.34	1.53258e-12	7.30165e-14	8986.44	7.98569e-13	3.81763e-14
8961.96	1.49775e-12	7.13602e-14	8987.07	7.87503e-13	3.76553e-14
8962.59	1.46468e-12	6.97911e-14	8987.70	7.76622e-13	3.71424e-14
8963.22	1.43338e-12	6.83037e-14	8988.32	7.65911e-13	3.66387e-14
8963.85	1.40352e-12	6.68926e-14	8988.95	7.55383e-13	3.61440e-14
8964.47	1.37509e-12	6.55523e-14	8989.58	7.45015e-13	3.56573e-14
8965.10	1.34811e-12	6.42752e-14	8990.21	7.34806e-13	3.51785e-14
8965.73	1.32234e-12	6.30589e-14	8990.83	7.24764e-13	3.47075e-14
8966.36	1.29769e-12	6.18970e-14	8991.46	7.14877e-13	3.42443e-14
8966.98	1.27424e-12	6.07847e-14	8992.09	7.05135e-13	3.37888e-14
8967.61	1.25168e-12	5.97178e-14	8992.72	6.95544e-13	3.33409e-14
8968.24	1.23000e-12	5.86938e-14	8993.35	6.86094e-13	3.28995e-14
8968.87	1.20920e-12	5.77071e-14	8993.97	6.76783e-13	3.24656e-14
8969.50	1.18906e-12	5.67554e-14	8994.60	6.67609e-13	3.20380e-14
8970.12	1.16968e-12	5.58365e-14	8995.23	6.58560e-13	3.16166e-14
8970.75	1.15095e-12	5.49458e-14	8995.86	6.49647e-13	3.12016e-14
8971.38	1.13276e-12	5.40821e-14	8996.48	6.40847e-13	3.07927e-14
8972.01	1.11522e-12	5.32431e-14	8997.11	6.32182e-13	3.03900e-14
8972.63	1.09799e-12	5.24255e-14	8997.74	6.23628e-13	2.99935e-14
8973.26	1.08134e-12	5.16302e-14	8998.37	6.15200e-13	2.96021e-14
8973.89	1.06506e-12	5.08539e-14	8998.99	6.06895e-13	2.92169e-14
8974.52	1.04917e-12	5.00956e-14	8999.62	5.98694e-13	2.88369e-14
8975.14	1.03363e-12	4.93530e-14	9000.25	5.90610e-13	2.84634e-14
8975.77	1.01844e-12	4.86283e-14	9000.88	5.82643e-13	2.80951e-14
8976.40	1.00354e-12	4.79172e-14	9001.50	5.74796e-13	2.77322e-14
8977.03	9.88954e-13	4.72206e-14	9002.13	5.67060e-13	2.73749e-14
8977.65	9.74638e-13	4.65378e-14	9002.76	5.59448e-13	2.70232e-14
8978.28	9.60595e-13	4.58674e-14	9003.39	5.51938e-13	2.66761e-14
8978.91	9.46804e-13	4.52098e-14	9004.02	5.44546e-13	2.63359e-14

Table A.6 (cont'd)

JD +2440000	*UVOIR* Flux	Flux error	JD +2440000	*UVOIR* Flux	Flux error
9004.64	5.37282e-13	2.60005e-14	9011.55	4.64335e-13	2.26499e-14
9005.27	5.30117e-13	2.56711e-14	9012.17	4.58236e-13	2.23699e-14
9005.90	5.23081e-13	2.53465e-14	9012.80	4.52206e-13	2.20933e-14
9006.53	5.16144e-13	2.50279e-14	9013.43	4.46245e-13	2.18202e-14
9007.15	5.09326e-13	2.47141e-14	9014.06	4.40348e-13	2.15509e-14
9007.78	5.02615e-13	2.44062e-14	9014.69	4.34544e-13	2.12845e-14
9008.41	4.96008e-13	2.41030e-14	9015.31	4.28816e-13	2.10220e-14
9009.04	4.89492e-13	2.38032e-14	9015.94	4.23212e-13	2.07656e-14
9009.66	4.83075e-13	2.35089e-14	9016.57	4.17755e-13	2.05169e-14
9010.29	4.76751e-13	2.32187e-14	9017.20	4.12506e-13	2.02765e-14

Table A.7. SN 1992bo

JD +2440000	*UVOIR* Flux	Flux error	JD +2440000	*UVOIR* Flux	Flux error
8977.41	1.77461e-12	8.91035e-14	9001.53	3.02574e-12	1.45220e-13
8978.01	2.87895e-12	1.40104e-13	9002.14	2.95620e-12	1.42471e-13
8978.62	4.05216e-12	1.97118e-13	9002.74	2.93660e-12	1.42393e-13
8979.22	5.08604e-12	2.48674e-13	9003.34	2.98869e-12	1.46504e-13
8979.82	5.91990e-12	2.90466e-13	9003.94	3.14042e-12	1.57422e-13
8980.43	6.57671e-12	3.23197e-13	9004.55	3.41314e-12	1.78263e-13
8981.03	7.10047e-12	3.49169e-13	9005.15	3.77970e-12	2.08605e-13
8981.63	7.52887e-12	3.70508e-13	9005.75	4.10424e-12	2.37718e-13
8982.24	7.88761e-12	3.88619e-13	9006.36	4.16871e-12	2.46235e-13
8982.84	8.19196e-12	4.04296e-13	9006.96	3.86593e-12	2.24302e-13
8983.44	8.44967e-12	4.17907e-13	9007.56	3.33270e-12	1.84198e-13
8984.04	8.66379e-12	4.29524e-13	9008.17	2.79715e-12	1.46093e-13
8984.65	8.83428e-12	4.39038e-13	9008.77	2.38337e-12	1.19596e-13
8985.25	8.95993e-12	4.46319e-13	9009.37	2.09869e-12	1.03497e-13
8985.85	9.03836e-12	4.51156e-13	9009.97	1.90724e-12	9.36406e-14
8986.46	9.06778e-12	4.53395e-13	9010.58	1.77389e-12	8.70296e-14
8987.06	9.04642e-12	4.52894e-13	9011.18	1.67461e-12	8.20936e-14
8987.66	8.97388e-12	4.49588e-13	9011.78	1.59489e-12	7.80696e-14
8988.27	8.85027e-12	4.43492e-13	9012.39	1.52668e-12	7.45917e-14
8988.87	8.67769e-12	4.34706e-13	9012.99	1.46586e-12	7.14807e-14
8989.47	8.45936e-12	4.23398e-13	9013.59	1.41035e-12	6.86512e-14
8990.08	8.19998e-12	4.09840e-13	9014.20	1.35915e-12	6.60616e-14
8990.68	7.90519e-12	3.94357e-13	9014.80	1.31203e-12	6.36894e-14
8991.28	7.58208e-12	3.77349e-13	9015.40	1.26841e-12	6.15137e-14
8991.88	7.23785e-12	3.59216e-13	9016.00	1.22806e-12	5.95179e-14
8992.49	6.88021e-12	3.40386e-13	9016.61	1.19087e-12	5.76840e-14
8993.09	6.51627e-12	3.21271e-13	9017.21	1.15639e-12	5.59954e-14
8993.69	6.15309e-12	3.02247e-13	9017.81	1.12440e-12	5.44358e-14
8994.30	5.79660e-12	2.83634e-13	9018.42	1.09457e-12	5.29876e-14
8994.90	5.45208e-12	2.65718e-13	9019.02	1.06677e-12	5.16378e-14
8995.50	5.12333e-12	2.48716e-13	9019.62	1.04070e-12	5.03733e-14
8996.11	4.81376e-12	2.32803e-13	9020.23	1.01618e-12	4.91814e-14
8996.71	4.52517e-12	2.18066e-13	9020.83	9.93027e-13	4.80554e-14
8997.31	4.25891e-12	2.04581e-13	9021.43	9.71080e-13	4.69838e-14
8997.92	4.01538e-12	1.92354e-13	9022.04	9.50207e-13	4.59623e-14
8998.52	3.79453e-12	1.81401e-13	9022.64	9.30264e-13	4.49826e-14
8999.12	3.59595e-12	1.71695e-13	9023.24	9.11167e-13	4.40414e-14
8999.72	3.41889e-12	1.63179e-13	9023.84	8.92807e-13	4.31340e-14
9000.33	3.26347e-12	1.55872e-13	9024.45	8.75109e-13	4.22560e-14
9000.93	3.13100e-12	1.49828e-13	9025.05	8.58009e-13	4.14058e-14

Table A.7 (cont'd)

JD +2440000	*UVOIR* Flux	Flux error	JD +2440000	*UVOIR* Flux	Flux error
9025.65	8.41445e-13	4.05815e-14	9049.77	4.07401e-13	1.93021e-14
9026.26	8.25371e-13	3.97801e-14	9050.38	4.00293e-13	1.89648e-14
9026.86	8.09729e-13	3.89988e-14	9050.98	3.93312e-13	1.86349e-14
9027.46	7.94505e-13	3.82390e-14	9051.58	3.86459e-13	1.83114e-14
9028.07	7.79649e-13	3.74966e-14	9052.19	3.79732e-13	1.79943e-14
9028.67	7.65148e-13	3.67720e-14	9052.79	3.73124e-13	1.76825e-14
9029.27	7.50986e-13	3.60655e-14	9053.39	3.66633e-13	1.73772e-14
9029.87	7.37136e-13	3.53741e-14	9054.00	3.60272e-13	1.70784e-14
9030.48	7.23582e-13	3.46992e-14	9054.60	3.54020e-13	1.67838e-14
9031.08	7.10318e-13	3.40389e-14	9055.20	3.47877e-13	1.64970e-14
9031.68	6.97326e-13	3.33933e-14	9055.80	3.41854e-13	1.62145e-14
9032.29	6.84601e-13	3.27615e-14	9056.41	3.35942e-13	1.59375e-14
9032.89	6.72146e-13	3.21438e-14	9057.01	3.30141e-13	1.56661e-14
9033.49	6.59942e-13	3.15392e-14	9057.61	3.24451e-13	1.54003e-14
9034.10	6.47991e-13	3.09490e-14	9058.22	3.18873e-13	1.51400e-14
9034.70	6.36273e-13	3.03709e-14	9058.82	3.13385e-13	1.48842e-14
9035.30	6.24791e-13	2.98062e-14	9059.42	3.08010e-13	1.46340e-14
9035.90	6.13546e-13	2.92528e-14	9060.03	3.02736e-13	1.43884e-14
9036.51	6.02527e-13	2.87118e-14	9060.63	2.97563e-13	1.41483e-14
9037.11	5.91735e-13	2.81832e-14	9061.23	2.92481e-13	1.39128e-14
9037.71	5.81147e-13	2.76648e-14	9061.83	2.87501e-13	1.36807e-14
9038.32	5.70775e-13	2.71588e-14	9062.44	2.82621e-13	1.34542e-14
9038.92	5.60607e-13	2.66630e-14	9063.04	2.77820e-13	1.32321e-14
9039.52	5.50643e-13	2.61785e-14	9063.64	2.73119e-13	1.30145e-14
9040.13	5.40870e-13	2.57040e-14	9064.25	2.68496e-13	1.28003e-14
9040.73	5.31289e-13	2.52385e-14	9064.85	2.63962e-13	1.25915e-14
9041.33	5.21896e-13	2.47842e-14	9065.45	2.59515e-13	1.23850e-14
9041.93	5.12681e-13	2.43387e-14	9066.06	2.55145e-13	1.21839e-14
9042.54	5.03642e-13	2.39031e-14	9066.66	2.50851e-13	1.19850e-14
9043.14	4.94779e-13	2.34751e-14	9067.26	2.46643e-13	1.17915e-14
9043.74	4.86079e-13	2.30570e-14	9067.86	2.42500e-13	1.16001e-14
9044.35	4.77540e-13	2.26464e-14	9068.47	2.38442e-13	1.14130e-14
9044.95	4.69164e-13	2.22445e-14	9069.07	2.34447e-13	1.12291e-14
9045.55	4.60937e-13	2.18511e-14	9069.67	2.30516e-13	1.10483e-14
9046.16	4.52870e-13	2.14652e-14	9070.28	2.26659e-13	1.08707e-14
9046.76	4.44940e-13	2.10867e-14	9070.88	2.22876e-13	1.06964e-14
9047.36	4.37159e-13	2.07157e-14	9071.48	2.19156e-13	1.05252e-14
9047.96	4.29514e-13	2.03520e-14	9072.08	2.15489e-13	1.03570e-14
9048.57	4.22006e-13	1.99946e-14	9072.69	2.11897e-13	1.01916e-14
9049.17	4.14635e-13	1.96447e-14	9073.29	2.08369e-13	1.00293e-14

Table A.7 (cont'd)

JD +2440000	*UVOIR* Flux	Flux error	JD +2440000	*UVOIR* Flux	Flux error
9073.89	2.04894e-13	9.86982e-15	9082.94	1.59793e-13	7.79952e-15
9074.50	2.01484e-13	9.71318e-15	9083.54	1.57209e-13	7.68070e-15
9075.10	1.98130e-13	9.55929e-15	9084.15	1.54666e-13	7.56385e-15
9075.70	1.94841e-13	9.40827e-15	9084.75	1.52164e-13	7.44880e-15
9076.31	1.91609e-13	9.25993e-15	9085.35	1.49690e-13	7.33560e-15
9076.91	1.88444e-13	9.11442e-15	9085.96	1.47266e-13	7.22400e-15
9077.51	1.85325e-13	8.97153e-15	9086.56	1.44879e-13	7.11399e-15
9078.12	1.82275e-13	8.83131e-15	9087.16	1.42521e-13	7.00562e-15
9078.72	1.79283e-13	8.69375e-15	9087.76	1.40204e-13	6.89895e-15
9079.32	1.76338e-13	8.55875e-15	9088.37	1.37931e-13	6.79404e-15
9079.92	1.73451e-13	8.42632e-15	9088.97	1.35696e-13	6.69127e-15
9080.53	1.70621e-13	8.29633e-15	9089.57	1.33519e-13	6.59069e-15
9081.13	1.67838e-13	8.16866e-15	9090.18	1.31398e-13	6.49318e-15
9081.73	1.65112e-13	8.04338e-15	9090.78	1.29350e-13	6.39914e-15
9082.34	1.62430e-13	7.92046e-15	...	...	...

Table A.8. SN 1993H

JD +2440000	*UVOIR* Flux	Flux error	JD +2440000	*UVOIR* Flux	Flux error
9065.55	2.76228×10^{-12}	1.30527×10^{-13}	9087.66	1.27827×10^{-12}	6.18287×10^{-14}
9066.11	3.17508×10^{-12}	1.49533×10^{-13}	9088.22	1.23033×10^{-12}	5.95592×10^{-14}
9066.66	3.55205×10^{-12}	1.67909×10^{-13}	9088.77	1.18400×10^{-12}	5.73606×10^{-14}
9067.21	3.87787×10^{-12}	1.84393×10^{-13}	9089.32	1.13904×10^{-12}	5.52243×10^{-14}
9067.76	4.14535×10^{-12}	1.98271×10^{-13}	9089.87	1.09536×10^{-12}	5.31451×10^{-14}
9068.32	4.35269×10^{-12}	2.09265×10^{-13}	9090.43	1.05298×10^{-12}	5.11253×10^{-14}
9068.87	4.50124×10^{-12}	2.17305×10^{-13}	9090.98	1.01204×10^{-12}	4.91678×10^{-14}
9069.42	4.59461×10^{-12}	2.22509×10^{-13}	9091.53	9.72629×10^{-13}	4.72808×10^{-14}
9069.97	4.63739×10^{-12}	2.25058×10^{-13}	9092.08	9.34911×10^{-13}	4.54715×10^{-14}
9070.53	4.63514×10^{-12}	2.25238×10^{-13}	9092.64	8.99001×10^{-13}	4.37442×10^{-14}
9071.08	4.59379×10^{-12}	2.23345×10^{-13}	9093.19	8.65020×10^{-13}	4.21066×10^{-14}
9071.63	4.51928×10^{-12}	2.19695×10^{-13}	9093.74	8.33006×10^{-13}	4.05606×10^{-14}
9072.19	4.41769×10^{-12}	2.14606×10^{-13}	9094.30	8.03011×10^{-13}	3.91079×10^{-14}
9072.74	4.29457×10^{-12}	2.08400×10^{-13}	9094.85	7.74981×10^{-13}	3.77467×10^{-14}
9073.29	4.15493×10^{-12}	2.01369×10^{-13}	9095.40	7.48864×10^{-13}	3.64737×10^{-14}
9073.84	4.00361×10^{-12}	1.93764×10^{-13}	9095.96	7.24572×10^{-13}	3.52864×10^{-14}
9074.40	3.84443×10^{-12}	1.85805×10^{-13}	9096.51	7.01987×10^{-13}	3.41784×10^{-14}
9074.95	3.68109×10^{-12}	1.77676×10^{-13}	9097.06	6.80994×10^{-13}	3.31447×10^{-14}
9075.50	3.51639×10^{-12}	1.69535×10^{-13}	9097.61	6.61447×10^{-13}	3.21789×10^{-14}
9076.06	3.35272×10^{-12}	1.61502×10^{-13}	9098.17	6.43238×10^{-13}	3.12751×10^{-14}
9076.61	3.19213×10^{-12}	1.53647×10^{-13}	9098.72	6.26237×10^{-13}	3.04285×10^{-14}
9077.16	3.03578×10^{-12}	1.46057×10^{-13}	9099.27	6.10326×10^{-13}	2.96331×10^{-14}
9077.71	2.88504×10^{-12}	1.38764×10^{-13}	9099.82	5.95402×10^{-13}	2.88854×10^{-14}
9078.27	2.74069×10^{-12}	1.31808×10^{-13}	9100.38	5.81361×10^{-13}	2.81786×10^{-14}
9078.82	2.60330×10^{-12}	1.25203×10^{-13}	9100.93	5.68110×10^{-13}	2.75092×10^{-14}
9079.37	2.47319×10^{-12}	1.18959×10^{-13}	9101.48	5.55559×10^{-13}	2.68758×10^{-14}
9079.92	2.35040×10^{-12}	1.13069×10^{-13}	9102.04	5.43652×10^{-13}	2.62720×10^{-14}
9080.48	2.23514×10^{-12}	1.07543×10^{-13}	9102.59	5.32320×10^{-13}	2.56974×10^{-14}
9081.03	2.12717×10^{-12}	1.02369×10^{-13}	9103.14	5.21487×10^{-13}	2.51478×10^{-14}
9081.58	2.02639×10^{-12}	9.75383×10^{-14}	9103.69	5.11118×10^{-13}	2.46209×10^{-14}
9082.14	1.93242×10^{-12}	9.30375×10^{-14}	9104.25	5.01160×10^{-13}	2.41156×10^{-14}
9082.69	1.84511×10^{-12}	8.88518×10^{-14}	9104.80	4.91579×10^{-13}	2.36287×10^{-14}
9083.24	1.76400×10^{-12}	8.49629×10^{-14}	9105.35	4.82333×10^{-13}	2.31602×10^{-14}
9083.79	1.68859×10^{-12}	8.13534×10^{-14}	9105.90	4.73391×10^{-13}	2.27069×10^{-14}
9084.35	1.61836×10^{-12}	7.79994×10^{-14}	9106.46	4.64721×10^{-13}	2.22690×10^{-14}
9084.90	1.55302×10^{-12}	7.48783×10^{-14}	9107.01	4.56303×10^{-13}	2.18442×10^{-14}
9085.45	1.49183×10^{-12}	7.19620×10^{-14}	9107.56	4.48129×10^{-13}	2.14328×10^{-14}
9086.00	1.43416×10^{-12}	6.92248×10^{-14}	9108.12	4.40168×10^{-13}	2.10337×10^{-14}
9086.56	1.37975×10^{-12}	6.66408×10^{-14}	9108.67	4.32411×10^{-13}	2.06450×10^{-14}
9087.11	1.32788×10^{-12}	6.41835×10^{-14}	9109.22	4.24840×10^{-13}	2.02666×10^{-14}

Table A.8 (cont'd)

JD +2440000	*UVOIR* Flux	Flux error	JD +2440000	*UVOIR* Flux	Flux error
9109.77	4.17457×10^{-13}	1.98977×10^{-14}	9131.88	2.14318×10^{-13}	1.01280×10^{-14}
9110.33	4.10232×10^{-13}	1.95384×10^{-14}	9132.44	2.10844×10^{-13}	9.96560×10^{-15}
9110.88	4.03168×10^{-13}	1.91877×10^{-14}	9132.99	2.07422×10^{-13}	9.80587×10^{-15}
9111.43	3.96245×10^{-13}	1.88458×10^{-14}	9133.54	2.04063×10^{-13}	9.64877×10^{-15}
9111.99	3.89478×10^{-13}	1.85117×10^{-14}	9134.10	2.00757×10^{-13}	9.49419×10^{-15}
9112.54	3.82847×10^{-13}	1.81856×10^{-14}	9134.65	1.97504×10^{-13}	9.34224×10^{-15}
9113.09	3.76354×10^{-13}	1.78664×10^{-14}	9135.20	1.94304×10^{-13}	9.19284×10^{-15}
9113.64	3.69981×10^{-13}	1.75553×10^{-14}	9135.75	1.91145×10^{-13}	9.04576×10^{-15}
9114.20	3.63739×10^{-13}	1.72504×10^{-14}	9136.31	1.88051×10^{-13}	8.90125×10^{-15}
9114.75	3.57621×10^{-13}	1.69516×10^{-14}	9136.86	1.85000×10^{-13}	8.75909×10^{-15}
9115.30	3.51617×10^{-13}	1.66602×10^{-14}	9137.41	1.81991×10^{-13}	8.61939×10^{-15}
9115.85	3.45729×10^{-13}	1.63740×10^{-14}	9137.96	1.79047×10^{-13}	8.48185×10^{-15}
9116.41	3.39958×10^{-13}	1.60943×10^{-14}	9138.52	1.76147×10^{-13}	8.34670×10^{-15}
9116.96	3.34285×10^{-13}	1.58200×10^{-14}	9139.07	1.73291×10^{-13}	8.21384×10^{-15}
9117.51	3.28720×10^{-13}	1.55522×10^{-14}	9139.62	1.70478×10^{-13}	8.08328×10^{-15}
9118.07	3.23266×10^{-13}	1.52900×10^{-14}	9140.18	1.67720×10^{-13}	7.95492×10^{-15}
9118.62	3.17912×10^{-13}	1.50322×10^{-14}	9140.73	1.65006×10^{-13}	7.82866×10^{-15}
9119.17	3.12658×10^{-13}	1.47799×10^{-14}	9141.28	1.62337×10^{-13}	7.70464×10^{-15}
9119.72	3.07494×10^{-13}	1.45333×10^{-14}	9141.83	1.59713×10^{-13}	7.58272×10^{-15}
9120.28	3.02432×10^{-13}	1.42911×10^{-14}	9142.39	1.57133×10^{-13}	7.46283×10^{-15}
9120.83	2.97461×10^{-13}	1.40535×10^{-14}	9142.94	1.54599×10^{-13}	7.34518×10^{-15}
9121.38	2.92569×10^{-13}	1.38205×10^{-14}	9143.49	1.52109×10^{-13}	7.22945×10^{-15}
9121.93	2.87780×10^{-13}	1.35919×10^{-14}	9144.04	1.49654×10^{-13}	7.11574×10^{-15}
9122.49	2.83070×10^{-13}	1.33679×10^{-14}	9144.60	1.47254×10^{-13}	7.00396×10^{-15}
9123.04	2.78440×10^{-13}	1.31484×10^{-14}	9145.15	1.44889×10^{-13}	6.89420×10^{-15}
9123.59	2.73900×10^{-13}	1.29334×10^{-14}	9145.70	1.42557×10^{-13}	6.78625×10^{-15}
9124.15	2.69439×10^{-13}	1.27218×10^{-14}	9146.26	1.40270×10^{-13}	6.68021×10^{-15}
9124.70	2.65056×10^{-13}	1.25136×10^{-14}	9146.81	1.38028×10^{-13}	6.57597×10^{-15}
9125.25	2.60741×10^{-13}	1.23109×10^{-14}	9147.36	1.35820×10^{-13}	6.47352×10^{-15}
9125.80	2.56503×10^{-13}	1.21105×10^{-14}	9147.92	1.33645×10^{-13}	6.37274×10^{-15}
9126.36	2.52343×10^{-13}	1.19145×10^{-14}	9148.47	1.31515×10^{-13}	6.27384×10^{-15}
9126.91	2.48249×10^{-13}	1.17206×10^{-14}	9149.02	1.29407×10^{-13}	6.17649×10^{-15}
9127.46	2.44220×10^{-13}	1.15312×10^{-14}	9149.57	1.27342×10^{-13}	6.08079×10^{-15}
9128.01	2.40267×10^{-13}	1.13450×10^{-14}	9150.13	1.25321×10^{-13}	5.98661×10^{-15}
9128.57	2.36368×10^{-13}	1.11620×10^{-14}	9150.68	1.23322×10^{-13}	5.89406×10^{-15}
9129.12	2.32545×10^{-13}	1.09822×10^{-14}	9151.23	1.21356×10^{-13}	5.80303×10^{-15}
9129.67	2.28774×10^{-13}	1.08057×10^{-14}	9151.78	1.19421×10^{-13}	5.71350×10^{-15}
9130.23	2.25079×10^{-13}	1.06320×10^{-14}	9152.34	1.17519×10^{-13}	5.62535×10^{-15}
9130.78	2.21425×10^{-13}	1.04611×10^{-14}	9152.89	1.15649×10^{-13}	5.53870×10^{-15}
9131.33	2.17845×10^{-13}	1.02932×10^{-14}	9153.44	1.13810×10^{-13}	5.45343×10^{-15}

Table A.8 (cont'd)

JD +2440000	*UVOIR* Flux	Flux error	JD +2440000	*UVOIR* Flux	Flux error
9154.00	1.12003×10^{-13}	5.36942×10^{-15}	9164.50	8.26843×10^{-14}	4.00892×10^{-15}
9154.55	1.10218×10^{-13}	5.28689×10^{-15}	9165.05	8.13882×10^{-14}	3.94866×10^{-15}
9155.10	1.08464×10^{-13}	5.20552×10^{-15}	9165.60	8.01137×10^{-14}	3.88955×10^{-15}
9155.65	1.06743×10^{-13}	5.12552×10^{-15}	9166.16	7.88617×10^{-14}	3.83123×10^{-15}
9156.21	1.05045×10^{-13}	5.04679×10^{-15}	9166.71	7.76297×10^{-14}	3.77401×10^{-15}
9156.76	1.03374×10^{-13}	4.96934×10^{-15}	9167.26	7.64182×10^{-14}	3.71766×10^{-15}
9157.31	1.01729×10^{-13}	4.89306×10^{-15}	9167.81	7.52258×10^{-14}	3.66215×10^{-15}
9157.86	1.00112×10^{-13}	4.81808×10^{-15}	9168.37	7.40520×10^{-14}	3.60747×10^{-15}
9158.42	9.85201×10^{-14}	4.74418×10^{-15}	9168.92	7.28952×10^{-14}	3.55358×10^{-15}
9158.97	9.69549×10^{-14}	4.67159×10^{-15}	9169.47	7.17552×10^{-14}	3.50048×10^{-15}
9159.52	9.54162×10^{-14}	4.60021×10^{-15}	9170.03	7.06317×10^{-14}	3.44816×10^{-15}
9160.08	9.39019×10^{-14}	4.52995×10^{-15}	9170.58	6.95235×10^{-14}	3.39659×10^{-15}
9160.63	9.24136×10^{-14}	4.46082×10^{-15}	9171.13	6.84319×10^{-14}	3.34559×10^{-15}
9161.18	9.09501×10^{-14}	4.39292×10^{-15}	9171.68	6.73565×10^{-14}	3.29540×10^{-15}
9161.73	8.95118×10^{-14}	4.32607×10^{-15}	9172.24	6.62984×10^{-14}	3.24607×10^{-15}
9162.29	8.80988×10^{-14}	4.26048×10^{-15}	9172.79	6.52581×10^{-14}	3.19747×10^{-15}
9162.84	8.67090×10^{-14}	4.19593×10^{-15}	9173.34	6.42393×10^{-14}	3.14994×10^{-15}
9163.39	8.53435×10^{-14}	4.13254×10^{-15}	9173.89	6.32432×10^{-14}	3.10342×10^{-15}
9163.94	8.40023×10^{-14}	4.07021×10^{-15}	9174.45	6.22756×10^{-14}	3.05827×10^{-15}

Table A.9. SN 1994D

JD +2449000	*UVOIR* Flux	Flux error	JD +2449000	*UVOIR* Flux	Flux error
421.106	4.82680×10^{-11}	2.09960×10^{-12}	451.256	9.64910×10^{-11}	4.25320×10^{-12}
421.859	7.30770×10^{-11}	3.15350×10^{-12}	452.010	9.27700×10^{-11}	4.11200×10^{-12}
422.613	1.01270×10^{-10}	4.37390×10^{-12}	452.764	8.91620×10^{-11}	3.97360×10^{-12}
423.367	1.31160×10^{-10}	5.67590×10^{-12}	453.518	8.55960×10^{-11}	3.83380×10^{-12}
424.121	1.61500×10^{-10}	6.99920×10^{-12}	454.271	8.20320×10^{-11}	3.69010×10^{-12}
424.874	1.91430×10^{-10}	8.30470×10^{-12}	455.025	7.84630×10^{-11}	3.54190×10^{-12}
425.628	2.20270×10^{-10}	9.56580×10^{-12}	455.779	7.49020×10^{-11}	3.38970×10^{-12}
426.382	2.47490×10^{-10}	1.07620×10^{-11}	456.533	7.13760×10^{-11}	3.23500×10^{-12}
427.136	2.72610×10^{-10}	1.18740×10^{-11}	457.286	6.79180×10^{-11}	3.07980×10^{-12}
427.889	2.95230×10^{-10}	1.28840×10^{-11}	458.040	6.45630×10^{-11}	2.92640×10^{-12}
428.643	3.14980×10^{-10}	1.37770×10^{-11}	458.794	6.13400×10^{-11}	2.77700×10^{-12}
429.397	3.31530×10^{-10}	1.45370×10^{-11}	459.548	5.82770×10^{-11}	2.63370×10^{-12}
430.151	3.44630×10^{-10}	1.51490×10^{-11}	460.302	5.53940×10^{-11}	2.49810×10^{-12}
430.905	3.54090×10^{-10}	1.56040×10^{-11}	461.055	5.27050×10^{-11}	2.37140×10^{-12}
431.658	3.59810×10^{-10}	1.58920×10^{-11}	461.809	5.02150×10^{-11}	2.25420×10^{-12}
432.412	3.61800×10^{-10}	1.60120×10^{-11}	462.563	4.79270×10^{-11}	2.14700×10^{-12}
433.166	3.60170×10^{-10}	1.59660×10^{-11}	463.317	4.58360×10^{-11}	2.04940×10^{-12}
433.920	3.55130×10^{-10}	1.57620×10^{-11}	464.070	4.39330×10^{-11}	1.96120×10^{-12}
434.673	3.47010×10^{-10}	1.54130×10^{-11}	464.824	4.22060×10^{-11}	1.88160×10^{-12}
435.427	3.36190×10^{-10}	1.49360×10^{-11}	465.578	4.06400×10^{-11}	1.80990×10^{-12}
436.181	3.23150×10^{-10}	1.43530×10^{-11}	466.332	3.92210×10^{-11}	1.74530×10^{-12}
436.935	3.08370×10^{-10}	1.36870×10^{-11}	467.085	3.79310×10^{-11}	1.68690×10^{-12}
437.688	2.92360×10^{-10}	1.29610×10^{-11}	467.839	3.67560×10^{-11}	1.63390×10^{-12}
438.442	2.75610×10^{-10}	1.22000×10^{-11}	468.593	3.56800×10^{-11}	1.58550×10^{-12}
439.196	2.58570×10^{-10}	1.14230×10^{-11}	469.347	3.46910×10^{-11}	1.54100×10^{-12}
439.950	2.41620×10^{-10}	1.06510×10^{-11}	470.100	3.37750×10^{-11}	1.49990×10^{-12}
440.704	2.25110×10^{-10}	9.89880×10^{-12}	470.854	3.29220×10^{-11}	1.46160×10^{-12}
441.457	2.09290×10^{-10}	9.17880×10^{-12}	471.608	3.21240×10^{-11}	1.42560×10^{-12}
442.211	1.94370×10^{-10}	8.50080×10^{-12}	472.362	3.13710×10^{-11}	1.39170×10^{-12}
442.965	1.80490×10^{-10}	7.87160×10^{-12}	473.116	3.06580×10^{-11}	1.35950×10^{-12}
443.719	1.67730×10^{-10}	7.29550×10^{-12}	473.869	2.99790×10^{-11}	1.32880×10^{-12}
444.472	1.56140×10^{-10}	6.77500×10^{-12}	474.623	2.93300×10^{-11}	1.29940×10^{-12}
445.226	1.45730×10^{-10}	6.31070×10^{-12}	475.377	2.87060×10^{-11}	1.27110×10^{-12}
445.980	1.36480×10^{-10}	5.90180×10^{-12}	476.131	2.81050×10^{-11}	1.24380×10^{-12}
446.734	1.28320×10^{-10}	5.54630×10^{-12}	476.884	2.75250×10^{-11}	1.21750×10^{-12}
447.487	1.21170×10^{-10}	5.24070×10^{-12}	477.638	2.69620×10^{-11}	1.19200×10^{-12}
448.241	1.14950×10^{-10}	4.98010×10^{-12}	478.392	2.64170×10^{-11}	1.16720×10^{-12}
448.995	1.09510×10^{-10}	4.75860×10^{-12}	479.146	2.58870×10^{-11}	1.14320×10^{-12}
449.749	1.04720×10^{-10}	4.56890×10^{-12}	479.900	2.53710×10^{-11}	1.11980×10^{-12}
450.503	1.00430×10^{-10}	4.40310×10^{-12}	480.653	2.48680×10^{-11}	1.09700×10^{-12}

Table A.9 (cont'd)

JD +2449000	*UVOIR* Flux	Flux error	JD +2449000	*UVOIR* Flux	Flux error
481.407	2.43780×10^{-11}	1.07490×10^{-12}	511.558	1.14570×10^{-11}	5.05550×10^{-13}
482.161	2.39000×10^{-11}	1.05330×10^{-12}	512.312	1.12520×10^{-11}	4.96760×10^{-13}
482.915	2.34330×10^{-11}	1.03220×10^{-12}	513.065	1.10500×10^{-11}	4.88160×10^{-13}
483.668	2.29770×10^{-11}	1.01170×10^{-12}	513.819	1.08530×10^{-11}	4.79730×10^{-13}
484.422	2.25310×10^{-11}	9.91630×10^{-13}	514.573	1.06590×10^{-11}	4.71490×10^{-13}
485.176	2.20960×10^{-11}	9.72080×10^{-13}	515.327	1.04700×10^{-11}	4.63410×10^{-13}
485.930	2.16700×10^{-11}	9.52990×10^{-13}	516.080	1.02840×10^{-11}	4.55500×10^{-13}
486.683	2.12530×10^{-11}	9.34350×10^{-13}	516.834	1.01010×10^{-11}	4.47750×10^{-13}
487.437	2.08460×10^{-11}	9.16150×10^{-13}	517.588	9.92270×10^{-12}	4.40160×10^{-13}
488.191	2.04470×10^{-11}	8.98370×10^{-13}	518.342	9.74750×10^{-12}	4.32720×10^{-13}
488.945	2.00570×10^{-11}	8.80990×10^{-13}	519.095	9.57580×10^{-12}	4.25440×10^{-13}
489.698	1.96750×10^{-11}	8.64020×10^{-13}	519.849	9.40740×10^{-12}	4.18300×10^{-13}
490.452	1.93020×10^{-11}	8.47430×10^{-13}	520.603	9.24240×10^{-12}	4.11310×10^{-13}
491.206	1.89360×10^{-11}	8.31220×10^{-13}	521.357	9.08050×10^{-12}	4.04470×10^{-13}
491.960	1.85780×10^{-11}	8.15370×10^{-13}	522.111	8.92180×10^{-12}	3.97760×10^{-13}
492.714	1.82270×10^{-11}	7.99880×10^{-13}	522.864	8.76620×10^{-12}	3.91180×10^{-13}
493.467	1.78840×10^{-11}	7.84730×10^{-13}	523.618	8.61360×10^{-12}	3.84740×10^{-13}
494.221	1.75480×10^{-11}	7.69920×10^{-13}	524.372	8.46400×10^{-12}	3.78420×10^{-13}
494.975	1.72190×10^{-11}	7.55440×10^{-13}	525.126	8.31720×10^{-12}	3.72230×10^{-13}
495.729	1.68960×10^{-11}	7.41280×10^{-13}	525.879	8.17330×10^{-12}	3.66170×10^{-13}
496.482	1.65800×10^{-11}	7.27430×10^{-13}	526.633	8.03220×10^{-12}	3.60220×10^{-13}
497.236	1.62710×10^{-11}	7.13890×10^{-13}	527.387	7.89380×10^{-12}	3.54400×10^{-13}
497.990	1.59680×10^{-11}	7.00640×10^{-13}	528.141	7.75800×10^{-12}	3.48680×10^{-13}
498.744	1.56720×10^{-11}	6.87680×10^{-13}	528.894	7.62480×10^{-12}	3.43080×10^{-13}
499.497	1.53810×10^{-11}	6.75010×10^{-13}	529.648	7.49420×10^{-12}	3.37590×10^{-13}
500.251	1.50960×10^{-11}	6.62610×10^{-13}	530.402	7.36610×10^{-12}	3.32210×10^{-13}
501.005	1.48180×10^{-11}	6.50470×10^{-13}	531.156	7.24040×10^{-12}	3.26930×10^{-13}
501.759	1.45440×10^{-11}	6.38610×10^{-13}	531.910	7.11710×10^{-12}	3.21750×10^{-13}
502.513	1.42770×10^{-11}	6.26990×10^{-13}	532.663	6.99620×10^{-12}	3.16680×10^{-13}
503.266	1.40150×10^{-11}	6.15630×10^{-13}	533.417	6.87750×10^{-12}	3.11700×10^{-13}
504.020	1.37580×10^{-11}	6.04510×10^{-13}	534.171	6.76110×10^{-12}	3.06820×10^{-13}
504.774	1.35060×10^{-11}	5.93630×10^{-13}	534.925	6.64690×10^{-12}	3.02030×10^{-13}
505.528	1.32590×10^{-11}	5.82990×10^{-13}	535.678	6.53480×10^{-12}	2.97330×10^{-13}
506.281	1.30180×10^{-11}	5.72570×10^{-13}	536.432	6.42480×10^{-12}	2.92720×10^{-13}
507.035	1.27810×10^{-11}	5.62370×10^{-13}	537.186	6.31690×10^{-12}	2.88200×10^{-13}
507.789	1.25490×10^{-11}	5.52390×10^{-13}	537.940	6.21110×10^{-12}	2.83760×10^{-13}
508.543	1.23220×10^{-11}	5.42620×10^{-13}	538.693	6.10720×10^{-12}	2.79410×10^{-13}
509.296	1.20990×10^{-11}	5.33050×10^{-13}	539.447	6.00520×10^{-12}	2.75140×10^{-13}
510.050	1.18810×10^{-11}	5.23690×10^{-13}	540.201	5.90520×10^{-12}	2.70950×10^{-13}
510.804	1.16670×10^{-11}	5.14520×10^{-13}	540.955	5.80700×10^{-12}	2.66840×10^{-13}

Table A.9 (cont'd)

JD +2449000	*UVOIR* Flux	Flux error	JD +2449000	*UVOIR* Flux	Flux error
541.709	5.71060×10^{-12}	2.62800×10^{-13}	546.231	5.16860×10^{-12}	2.40090×10^{-13}
542.462	5.61600×10^{-12}	2.58840×10^{-13}	546.985	5.08400×10^{-12}	2.36550×10^{-13}
543.216	5.52320×10^{-12}	2.54950×10^{-13}	547.739	5.00090×10^{-12}	2.33070×10^{-13}
543.970	5.43200×10^{-12}	2.51130×10^{-13}	548.492	4.91940×10^{-12}	2.29650×10^{-13}
544.724	5.34260×10^{-12}	2.47380×10^{-13}	549.246	4.83930×10^{-12}	2.26290×10^{-13}
545.477	5.25480×10^{-12}	2.43710×10^{-13}	550.000	4.76070×10^{-12}	2.22990×10^{-13}

Table A.10. SN 1994ae

JD +2440000	*UVOIR* Flux	Flux error	JD +2440000	*UVOIR* Flux	Flux error
9676.42	9.20586×10^{-11}	4.62496×10^{-12}	9704.96	5.02137×10^{-11}	2.42383×10^{-12}
9677.13	1.01243×10^{-10}	5.08641×10^{-12}	9705.67	4.84329×10^{-11}	2.33397×10^{-12}
9677.84	1.09745×10^{-10}	5.51386×10^{-12}	9706.39	4.68329×10^{-11}	2.25429×10^{-12}
9678.56	1.17557×10^{-10}	5.90765×10^{-12}	9707.10	4.53888×10^{-11}	2.18349×10^{-12}
9679.27	1.24679×10^{-10}	6.26827×10^{-12}	9707.81	4.40789×10^{-11}	2.12043×10^{-12}
9679.99	1.31104×10^{-10}	6.59565×10^{-12}	9708.53	4.28794×10^{-11}	2.06354×10^{-12}
9680.70	1.36808×10^{-10}	6.88915×10^{-12}	9709.24	4.17691×10^{-11}	2.01151×10^{-12}
9681.41	1.41792×10^{-10}	7.14740×10^{-12}	9709.96	4.07260×10^{-11}	1.96313×10^{-12}
9682.13	1.46020×10^{-10}	7.36911×10^{-12}	9710.67	3.97293×10^{-11}	1.91722×10^{-12}
9682.84	1.49451×10^{-10}	7.55249×10^{-12}	9711.38	3.87619×10^{-11}	1.87270×10^{-12}
9683.55	1.52093×10^{-10}	7.69588×10^{-12}	9712.10	3.78074×10^{-11}	1.82871×10^{-12}
9684.27	1.53894×10^{-10}	7.79776×10^{-12}	9712.81	3.68554×10^{-11}	1.78463×10^{-12}
9684.98	1.54854×10^{-10}	7.85711×10^{-12}	9713.52	3.58954×10^{-11}	1.73983×10^{-12}
9685.69	1.54980×10^{-10}	7.87301×10^{-12}	9714.24	3.49204×10^{-11}	1.69401×10^{-12}
9686.41	1.54272×10^{-10}	7.84588×10^{-12}	9714.95	3.39289×10^{-11}	1.64689×10^{-12}
9687.12	1.52750×10^{-10}	7.77622×10^{-12}	9715.66	3.29195×10^{-11}	1.59872×10^{-12}
9687.83	1.50451×10^{-10}	7.66587×10^{-12}	9716.38	3.18945×10^{-11}	1.54945×10^{-12}
9688.55	1.47445×10^{-10}	7.51733×10^{-12}	9717.09	3.08595×10^{-11}	1.49937×10^{-12}
9689.26	1.43780×10^{-10}	7.33404×10^{-12}	9717.80	2.98192×10^{-11}	1.44875×10^{-12}
9689.97	1.39559×10^{-10}	7.11994×10^{-12}	9718.52	2.87818×10^{-11}	1.39813×10^{-12}
9690.69	1.34861×10^{-10}	6.87972×10^{-12}	9719.23	2.77549×10^{-11}	1.34771×10^{-12}
9691.40	1.29800×10^{-10}	6.61837×10^{-12}	9719.94	2.67447×10^{-11}	1.29813×10^{-12}
9692.12	1.24446×10^{-10}	6.34111×10^{-12}	9720.66	2.57591×10^{-11}	1.24962×10^{-12}
9692.83	1.18916×10^{-10}	6.05313×10^{-12}	9721.37	2.48047×10^{-11}	1.20263×10^{-12}
9693.54	1.13301×10^{-10}	5.75940×10^{-12}	9722.08	2.38873×10^{-11}	1.15738×10^{-12}
9694.26	1.07684×10^{-10}	5.46441×10^{-12}	9722.80	2.30095×10^{-11}	1.11422×10^{-12}
9694.97	1.02139×10^{-10}	5.17214×10^{-12}	9723.51	2.21748×10^{-11}	1.07327×10^{-12}
9695.68	9.67299×10^{-11}	4.88623×10^{-12}	9724.23	2.13849×10^{-11}	1.03456×10^{-12}
9696.40	9.15096×10^{-11}	4.60954×10^{-12}	9724.94	2.06412×10^{-11}	9.98191×10^{-13}
9697.11	8.65198×10^{-11}	4.34443×10^{-12}	9725.65	1.99442×10^{-11}	9.64125×10^{-13}
9697.82	8.17893×10^{-11}	4.09257×10^{-12}	9726.37	1.92909×10^{-11}	9.32314×10^{-13}
9698.54	7.73394×10^{-11}	3.85547×10^{-12}	9727.08	1.86806×10^{-11}	9.02658×10^{-13}
9699.25	7.31842×10^{-11}	3.63395×10^{-12}	9727.79	1.81104×10^{-11}	8.75038×10^{-13}
9699.96	6.93295×10^{-11}	3.42846×10^{-12}	9728.51	1.75794×10^{-11}	8.49318×10^{-13}
9700.68	6.57746×10^{-11}	3.23926×10^{-12}	9729.22	1.70847×10^{-11}	8.25358×10^{-13}
9701.39	6.25148×10^{-11}	3.06623×10^{-12}	9729.93	1.66221×10^{-11}	8.03014×10^{-13}
9702.11	5.95409×10^{-11}	2.90888×10^{-12}	9730.65	1.61907×10^{-11}	7.82144×10^{-13}
9702.82	5.68394×10^{-11}	2.76683×10^{-12}	9731.36	1.57874×10^{-11}	7.62603×10^{-13}
9703.53	5.43961×10^{-11}	2.63922×10^{-12}	9732.08	1.54090×10^{-11}	7.44268×10^{-13}
9704.25	5.21936×10^{-11}	2.52516×10^{-12}	9732.79	1.50536×10^{-11}	7.27012×10^{-13}

Table A.10 (cont'd)

JD +2440000	*UVOIR* Flux	Flux error	JD +2440000	*UVOIR* Flux	Flux error
9733.50	1.47179×10^{-11}	7.10732×10^{-13}	9762.04	7.39610×10^{-12}	3.53907×10^{-13}
9734.22	1.44009×10^{-11}	6.95322×10^{-13}	9762.76	7.28008×10^{-12}	3.48385×10^{-13}
9734.93	1.41005×10^{-11}	6.80684×10^{-13}	9763.47	7.16619×10^{-12}	3.42975×10^{-13}
9735.64	1.38155×10^{-11}	6.66758×10^{-13}	9764.19	7.05420×10^{-12}	3.37655×10^{-13}
9736.36	1.35429×10^{-11}	6.53443×10^{-13}	9764.90	6.94419×10^{-12}	3.32444×10^{-13}
9737.07	1.32836×10^{-11}	6.40687×10^{-13}	9765.61	6.83614×10^{-12}	3.27331×10^{-13}
9737.78	1.30333×10^{-11}	6.28446×10^{-13}	9766.33	6.72981×10^{-12}	3.22304×10^{-13}
9738.50	1.27930×10^{-11}	6.16641×10^{-13}	9767.04	6.62539×10^{-12}	3.17372×10^{-13}
9739.21	1.25617×10^{-11}	6.05261×10^{-13}	9767.75	6.52254×10^{-12}	3.12525×10^{-13}
9739.92	1.23371×10^{-11}	5.94238×10^{-13}	9768.47	6.42136×10^{-12}	3.07762×10^{-13}
9740.64	1.21203×10^{-11}	5.83559×10^{-13}	9769.18	6.32195×10^{-12}	3.03081×10^{-13}
9741.35	1.19101×10^{-11}	5.73191×10^{-13}	9769.89	6.22397×10^{-12}	2.98472×10^{-13}
9742.07	1.17043×10^{-11}	5.63108×10^{-13}	9770.61	6.12764×10^{-12}	2.93946×10^{-13}
9742.78	1.15050×10^{-11}	5.53288×10^{-13}	9771.32	6.03287×10^{-12}	2.89503×10^{-13}
9743.49	1.13101×10^{-11}	5.43716×10^{-13}	9772.04	5.93954×10^{-12}	2.85132×10^{-13}
9744.21	1.11206×10^{-11}	5.34371×10^{-13}	9772.75	5.84768×10^{-12}	2.80835×10^{-13}
9744.92	1.09343×10^{-11}	5.25239×10^{-13}	9773.46	5.75732×10^{-12}	2.76613×10^{-13}
9745.63	1.07524×10^{-11}	5.16307×10^{-13}	9774.18	5.66859×10^{-12}	2.72467×10^{-13}
9746.35	1.05742×10^{-11}	5.07576×10^{-13}	9774.89	5.58119×10^{-12}	2.68387×10^{-13}
9747.06	1.03997×10^{-11}	4.99034×10^{-13}	9775.60	5.49536×10^{-12}	2.64385×10^{-13}
9747.77	1.02285×10^{-11}	4.90657×10^{-13}	9776.32	5.41103×10^{-12}	2.60464×10^{-13}
9748.49	1.00607×10^{-11}	4.82458×10^{-13}	9777.03	5.32822×10^{-12}	2.56613×10^{-13}
9749.20	9.89594×10^{-12}	4.74425×10^{-13}	9777.74	5.24684×10^{-12}	2.52833×10^{-13}
9749.92	9.73432×10^{-12}	4.66548×10^{-13}	9778.46	5.16702×10^{-12}	2.49125×10^{-13}
9750.63	9.57561×10^{-12}	4.58817×10^{-13}	9779.17	5.08853×10^{-12}	2.45489×10^{-13}
9751.34	9.41983×10^{-12}	4.51243×10^{-13}	9779.88	5.01159×10^{-12}	2.41914×10^{-13}
9752.06	9.26678×10^{-12}	4.43817×10^{-13}	9780.60	4.93596×10^{-12}	2.38420×10^{-13}
9752.77	9.11661×10^{-12}	4.36541×10^{-13}	9781.31	4.86171×10^{-12}	2.34985×10^{-13}
9753.48	8.96910×10^{-12}	4.29403×10^{-13}	9782.03	4.78870×10^{-12}	2.31605×10^{-13}
9754.20	8.82431×10^{-12}	4.22396×10^{-13}	9782.74	4.71685×10^{-12}	2.28289×10^{-13}
9754.91	8.68202×10^{-12}	4.15530×10^{-13}	9783.45	4.64601×10^{-12}	2.25024×10^{-13}
9755.62	8.54250×10^{-12}	4.08808×10^{-13}	9784.17	4.57633×10^{-12}	2.21806×10^{-13}
9756.34	8.40542×10^{-12}	4.02208×10^{-13}	9784.88	4.50753×10^{-12}	2.18643×10^{-13}
9757.05	8.27094×10^{-12}	3.95743×10^{-13}	9785.59	4.43960×10^{-12}	2.15513×10^{-13}
9757.76	8.13883×10^{-12}	3.89402×10^{-13}	9786.31	4.37254×10^{-12}	2.12427×10^{-13}
9758.48	8.00922×10^{-12}	3.83186×10^{-13}	9787.02	4.30643×10^{-12}	2.09388×10^{-13}
9759.19	7.88202×10^{-12}	3.77096×10^{-13}	9787.73	4.24145×10^{-12}	2.06394×10^{-13}
9759.90	7.75722×10^{-12}	3.71119×10^{-13}	9788.45	4.17785×10^{-12}	2.03469×10^{-13}
9760.62	7.63460×10^{-12}	3.65268×10^{-13}	9789.16	4.11590×10^{-12}	2.00636×10^{-13}
9761.33	7.51426×10^{-12}	3.59531×10^{-13}	9789.87	4.05648×10^{-12}	1.97917×10^{-13}

Table A.10 (cont'd)

JD +2440000	*UVOIR* Flux	Flux error	JD +2440000	*UVOIR* Flux	Flux error
9776.32	5.41103×10^{-12}	2.60464×10^{-13}	9783.45	4.64601×10^{-12}	2.25024×10^{-13}
9777.03	5.32822×10^{-12}	2.56613×10^{-13}	9784.17	4.57633×10^{-12}	2.21806×10^{-13}
9777.74	5.24684×10^{-12}	2.52833×10^{-13}	9784.88	4.50753×10^{-12}	2.18643×10^{-13}
9778.46	5.16702×10^{-12}	2.49125×10^{-13}	9785.59	4.43960×10^{-12}	2.15513×10^{-13}
9779.17	5.08853×10^{-12}	2.45489×10^{-13}	9786.31	4.37254×10^{-12}	2.12427×10^{-13}
9779.88	5.01159×10^{-12}	2.41914×10^{-13}	9787.02	4.30643×10^{-12}	2.09388×10^{-13}
9780.60	4.93596×10^{-12}	2.38420×10^{-13}	9787.73	4.24145×10^{-12}	2.06394×10^{-13}
9781.31	4.86171×10^{-12}	2.34985×10^{-13}	9788.45	4.17785×10^{-12}	2.03469×10^{-13}
9782.03	4.78870×10^{-12}	2.31605×10^{-13}	9789.16	4.11590×10^{-12}	2.00636×10^{-13}
9782.74	4.71685×10^{-12}	2.28289×10^{-13}	9789.87	4.05648×10^{-12}	1.97917×10^{-13}

Table A.11. SN 1995D

JD +2440000	*UVOIR* Flux	Flux error	JD +2440000	*UVOIR* Flux	Flux error
9761.63	5.63524×10^{-11}	2.70235×10^{-12}	9785.75	3.82632×10^{-11}	1.85194×10^{-12}
9762.24	6.61886×10^{-11}	3.18890×10^{-12}	9786.36	3.68517×10^{-11}	1.77772×10^{-12}
9762.84	7.45678×10^{-11}	3.64968×10^{-12}	9786.96	3.55571×10^{-11}	1.71022×10^{-12}
9763.44	8.12647×10^{-11}	4.03491×10^{-12}	9787.56	3.43758×10^{-11}	1.64903×10^{-12}
9764.04	8.64687×10^{-11}	4.33856×10^{-12}	9788.17	3.32996×10^{-11}	1.59388×10^{-12}
9764.65	9.04755×10^{-11}	4.57199×10^{-12}	9788.77	3.23193×10^{-11}	1.54436×10^{-12}
9765.25	9.35551×10^{-11}	4.74986×10^{-12}	9789.37	3.14298×10^{-11}	1.49995×10^{-12}
9765.85	9.59097×10^{-11}	4.88450×10^{-12}	9789.97	3.06218×10^{-11}	1.46012×10^{-12}
9766.46	9.76786×10^{-11}	4.98493×10^{-12}	9790.58	2.98873×10^{-11}	1.42470×10^{-12}
9767.06	9.89542×10^{-11}	5.05715×10^{-12}	9791.18	2.92176×10^{-11}	1.39297×10^{-12}
9767.66	9.97925×10^{-11}	5.10486×10^{-12}	9791.78	2.86059×10^{-11}	1.36444×10^{-12}
9768.27	1.00229e-10	5.13058×10^{-12}	9792.39	2.80425×10^{-11}	1.33873×10^{-12}
9768.87	1.00285e-10	5.13566×10^{-12}	9792.99	2.75199×10^{-11}	1.31526×10^{-12}
9769.47	9.99745×10^{-11}	5.12093×10^{-12}	9793.59	2.70297×10^{-11}	1.29367×10^{-12}
9770.08	9.93121×10^{-11}	5.08758×10^{-12}	9794.20	2.65634×10^{-11}	1.27337×10^{-12}
9770.68	9.83095×10^{-11}	5.03587×10^{-12}	9794.80	2.61149×10^{-11}	1.25390×10^{-12}
9771.28	9.69813×10^{-11}	4.96699×10^{-12}	9795.40	2.56769×10^{-11}	1.23501×10^{-12}
9771.88	9.53462×10^{-11}	4.88174×10^{-12}	9796.00	2.52422×10^{-11}	1.21612×10^{-12}
9772.49	9.34272×10^{-11}	4.78123×10^{-12}	9796.61	2.48059×10^{-11}	1.19699×10^{-12}
9773.09	9.12488×10^{-11}	4.66702×10^{-12}	9797.21	2.43640×10^{-11}	1.17727×10^{-12}
9773.69	8.88426×10^{-11}	4.54070×10^{-12}	9797.81	2.39116×10^{-11}	1.15691×10^{-12}
9774.30	8.62390×10^{-11}	4.40362×10^{-12}	9798.42	2.34461×10^{-11}	1.13558×10^{-12}
9774.90	8.34751×10^{-11}	4.25803×10^{-12}	9799.02	2.29669×10^{-11}	1.11335×10^{-12}
9775.50	8.05846×10^{-11}	4.10538×10^{-12}	9799.62	2.24724×10^{-11}	1.09009×10^{-12}
9776.11	7.76074×10^{-11}	3.94800×10^{-12}	9800.23	2.19635×10^{-11}	1.06587×10^{-12}
9776.71	7.45769×10^{-11}	3.78750×10^{-12}	9800.83	2.14419×10^{-11}	1.04075×10^{-12}
9777.31	7.15270×10^{-11}	3.62584×10^{-12}	9801.43	2.09085×10^{-11}	1.01487×10^{-12}
9777.92	6.84901×10^{-11}	3.46453×10^{-12}	9802.04	2.03664×10^{-11}	9.88379×10^{-13}
9778.52	6.54955×10^{-11}	3.30515×10^{-12}	9802.64	1.98198×10^{-11}	9.61475×10^{-13}
9779.12	6.25663×10^{-11}	3.14906×10^{-12}	9803.24	1.92708×10^{-11}	9.34345×10^{-13}
9779.72	5.97230×10^{-11}	2.99737×10^{-12}	9803.84	1.87227×10^{-11}	9.07198×10^{-13}
9780.33	5.69851×10^{-11}	2.85108×10^{-12}	9804.45	1.81789×10^{-11}	8.80223×10^{-13}
9780.93	5.43627×10^{-11}	2.71084×10^{-12}	9805.05	1.76437×10^{-11}	8.53618×10^{-13}
9781.53	5.18697×10^{-11}	2.57752×10^{-12}	9805.65	1.71195×10^{-11}	8.27541×10^{-13}
9782.14	4.95106×10^{-11}	2.45116×10^{-12}	9806.26	1.66086×10^{-11}	8.02143×10^{-13}
9782.74	4.72901×10^{-11}	2.33242×10^{-12}	9806.86	1.61144×10^{-11}	7.77562×10^{-13}
9783.34	4.52098×10^{-11}	2.22110×10^{-12}	9807.46	1.56360×10^{-11}	7.53882×10^{-13}
9783.94	4.32701×10^{-11}	2.11759×10^{-12}	9808.07	1.51780×10^{-11}	7.31200×10^{-13}
9784.55	4.14681×10^{-11}	2.02156×10^{-12}	9808.67	1.47394×10^{-11}	7.09546×10^{-13}
9785.15	3.98015×10^{-11}	1.93315×10^{-12}	9809.27	1.43215×10^{-11}	6.88960×10^{-13}

Table A.11 (cont'd)

JD +2440000	*UVOIR* Flux	Flux error	JD +2440000	*UVOIR* Flux	Flux error
9809.87	1.39244×10^{-11}	6.69452×10^{-13}	9834.00	6.96156×10^{-12}	3.30886×10^{-13}
9810.48	1.35473×10^{-11}	6.51006×10^{-13}	9834.60	6.86765×10^{-12}	3.26312×10^{-13}
9811.08	1.31912×10^{-11}	6.33606×10^{-13}	9835.20	6.77520×10^{-12}	3.21812×10^{-13}
9811.68	1.28543×10^{-11}	6.17217×10^{-13}	9835.80	6.68391×10^{-12}	3.17386×10^{-13}
9812.29	1.25365×10^{-11}	6.01799×10^{-13}	9836.41	6.59401×10^{-12}	3.13025×10^{-13}
9812.89	1.22370×10^{-11}	5.87291×10^{-13}	9837.01	6.50552×10^{-12}	3.08739×10^{-13}
9813.49	1.19546×10^{-11}	5.73634×10^{-13}	9837.61	6.41822×10^{-12}	3.04518×10^{-13}
9814.10	1.16874×10^{-11}	5.60786×10^{-13}	9838.22	6.33212×10^{-12}	3.00363×10^{-13}
9814.70	1.14364×10^{-11}	5.48665×10^{-13}	9838.82	6.24746×10^{-12}	2.96285×10^{-13}
9815.30	1.11984×10^{-11}	5.37228×10^{-13}	9839.42	6.16392×10^{-12}	2.92264×10^{-13}
9815.90	1.09736×10^{-11}	5.26414×10^{-13}	9840.03	6.08162×10^{-12}	2.88320×10^{-13}
9816.51	1.07599×10^{-11}	5.16157×10^{-13}	9840.63	6.00056×10^{-12}	2.84433×10^{-13}
9817.11	1.05574×10^{-11}	5.06428×10^{-13}	9841.23	5.92075×10^{-12}	2.80613×10^{-13}
9817.71	1.03649×10^{-11}	4.97152×10^{-13}	9841.83	5.84220×10^{-12}	2.76851×10^{-13}
9818.32	1.01813×10^{-11}	4.88306×10^{-13}	9842.44	5.76469×10^{-12}	2.73157×10^{-13}
9818.92	1.00060×10^{-11}	4.79849×10^{-13}	9843.04	5.68844×10^{-12}	2.69521×10^{-13}
9819.52	9.83801×10^{-12}	4.71725×10^{-13}	9843.64	5.61333×10^{-12}	2.65952×10^{-13}
9820.13	9.67674×10^{-12}	4.63913×10^{-13}	9844.25	5.53937×10^{-12}	2.62430×10^{-13}
9820.73	9.52181×10^{-12}	4.56391×10^{-13}	9844.85	5.46644×10^{-12}	2.58976×10^{-13}
9821.33	9.37236×10^{-12}	4.49116×10^{-13}	9845.45	5.39465×10^{-12}	2.55578×10^{-13}
9821.93	9.22794×10^{-12}	4.42086×10^{-13}	9846.06	5.32388×10^{-12}	2.52237×10^{-13}
9822.54	9.08819×10^{-12}	4.35257×10^{-13}	9846.66	5.25424×10^{-12}	2.48951×10^{-13}
9823.14	8.95279×10^{-12}	4.28628×10^{-13}	9847.26	5.18548×10^{-12}	2.45710×10^{-13}
9823.74	8.82105×10^{-12}	4.22177×10^{-13}	9847.86	5.11782×10^{-12}	2.42524×10^{-13}
9824.35	8.69296×10^{-12}	4.15893×10^{-13}	9848.47	5.05115×10^{-12}	2.39393×10^{-13}
9824.95	8.56806×10^{-12}	4.09751×10^{-13}	9849.07	4.98534×10^{-12}	2.36305×10^{-13}
9825.55	8.44612×10^{-12}	4.03763×10^{-13}	9849.67	4.92050×10^{-12}	2.33270×10^{-13}
9826.16	8.32691×10^{-12}	3.97895×10^{-13}	9850.28	4.85649×10^{-12}	2.30278×10^{-13}
9826.76	8.21028×10^{-12}	3.92156×10^{-13}	9850.88	4.79344×10^{-12}	2.27338×10^{-13}
9827.36	8.09602×10^{-12}	3.86525×10^{-13}	9851.48	4.73122×10^{-12}	2.24441×10^{-13}
9827.96	7.98400×10^{-12}	3.81011×10^{-13}	9852.08	4.66983×10^{-12}	2.21574×10^{-13}
9828.57	7.87399×10^{-12}	3.75603×10^{-13}	9852.69	4.60926×10^{-12}	2.18759×10^{-13}
9829.17	7.76597×10^{-12}	3.70290×10^{-13}	9853.29	4.54940×10^{-12}	2.15996×10^{-13}
9829.77	7.65973×10^{-12}	3.65060×10^{-13}	9853.89	4.49047×10^{-12}	2.13263×10^{-13}
9830.38	7.55525×10^{-12}	3.59935×10^{-13}	9854.50	4.43227×10^{-12}	2.10561×10^{-13}
9830.98	7.45254×10^{-12}	3.54892×10^{-13}	9855.10	4.37490×10^{-12}	2.07912×10^{-13}
9831.58	7.35137×10^{-12}	3.49933×10^{-13}	9855.70	4.31827×10^{-12}	2.05305×10^{-13}
9832.19	7.25164×10^{-12}	3.45057×10^{-13}	9856.31	4.26248×10^{-12}	2.02729×10^{-13}
9832.79	7.15357×10^{-12}	3.40253×10^{-13}	9856.91	4.20733×10^{-12}	2.00197×10^{-13}
9833.39	7.05684×10^{-12}	3.35533×10^{-13}	9857.51	4.15306×10^{-12}	1.97697×10^{-13}

Table A.11 (cont'd)

JD +2440000	*UVOIR* Flux	Flux error	JD +2440000	*UVOIR* Flux	Flux error
9858.12	4.09957×10^{-12}	1.95241×10^{-13}	9865.96	3.47261×10^{-12}	1.66751×10^{-13}
9858.72	4.04676×10^{-12}	1.92830×10^{-13}	9866.56	3.42913×10^{-12}	1.64789×10^{-13}
9859.32	3.99475×10^{-12}	1.90454×10^{-13}	9867.16	3.38613×10^{-12}	1.62856×10^{-13}
9859.92	3.94355×10^{-12}	1.88113×10^{-13}	9867.76	3.34367×10^{-12}	1.60950×10^{-13}
9860.53	3.89318×10^{-12}	1.85807×10^{-13}	9868.37	3.30176×10^{-12}	1.59061×10^{-13}
9861.13	3.84353×10^{-12}	1.83548×10^{-13}	9868.97	3.26027×10^{-12}	1.57198×10^{-13}
9861.73	3.79461×10^{-12}	1.81326×10^{-13}	9869.57	3.21921×10^{-12}	1.55363×10^{-13}
9862.34	3.74653×10^{-12}	1.79139×10^{-13}	9870.18	3.17864×10^{-12}	1.53546×10^{-13}
9862.94	3.69916×10^{-12}	1.76988×10^{-13}	9870.78	3.13861×10^{-12}	1.51763×10^{-13}
9863.54	3.65251×10^{-12}	1.74873×10^{-13}	9871.38	3.09937×10^{-12}	1.50006×10^{-13}
9864.15	3.60657×10^{-12}	1.72793×10^{-13}	9871.99	3.06086×10^{-12}	1.48287×10^{-13}
9864.75	3.56130×10^{-12}	1.70746×10^{-13}	9872.59	3.02347×10^{-12}	1.46627×10^{-13}
9865.35	3.51658×10^{-12}	1.68733×10^{-13}	9873.19	2.98754×10^{-12}	1.45023×10^{-13}

Table A.12. SN 1995E

JD +2440000	*UVOIR* Flux	Flux error	JD +2440000	*UVOIR* Flux	Flux error
9768.56	3.82126×10^{-11}	2.27945×10^{-12}	9791.08	2.20542×10^{-11}	1.07054×10^{-12}
9769.13	4.07230×10^{-11}	2.33595×10^{-12}	9791.64	2.12074×10^{-11}	1.02732×10^{-12}
9769.69	4.39979×10^{-11}	2.41385×10^{-12}	9792.20	2.04255×10^{-11}	9.87686×10^{-13}
9770.25	4.72538×10^{-11}	2.50955×10^{-12}	9792.76	1.97060×10^{-11}	9.51393×10^{-13}
9770.81	5.00278×10^{-11}	2.60690×10^{-12}	9793.33	1.90435×10^{-11}	9.18270×10^{-13}
9771.38	5.22102×10^{-11}	2.69303×10^{-12}	9793.89	1.84357×10^{-11}	8.88109×10^{-13}
9771.94	5.38623×10^{-11}	2.76346×10^{-12}	9794.45	1.78776×10^{-11}	8.60712×10^{-13}
9772.50	5.50864×10^{-11}	2.81859×10^{-12}	9795.01	1.73671×10^{-11}	8.35863×10^{-13}
9773.07	5.59769×10^{-11}	2.85996×10^{-12}	9795.58	1.69001×10^{-11}	8.13372×10^{-13}
9773.63	5.65943×10^{-11}	2.88956×10^{-12}	9796.14	1.64727×10^{-11}	7.93050×10^{-13}
9774.19	5.69819×10^{-11}	2.90817×10^{-12}	9796.70	1.60842×10^{-11}	7.74702×10^{-13}
9774.75	5.71624×10^{-11}	2.91673×10^{-12}	9797.27	1.57306×10^{-11}	7.58146×10^{-13}
9775.32	5.71505×10^{-11}	2.91548×10^{-12}	9797.83	1.54092×10^{-11}	7.43162×10^{-13}
9775.88	5.69510×10^{-11}	2.90452×10^{-12}	9798.39	1.51142×10^{-11}	7.29478×10^{-13}
9776.44	5.65697×10^{-11}	2.88396×10^{-12}	9798.96	1.48419×10^{-11}	7.16782×10^{-13}
9777.00	5.60097×10^{-11}	2.85415×10^{-12}	9799.52	1.45822×10^{-11}	7.04668×10^{-13}
9777.57	5.52771×10^{-11}	2.81514×10^{-12}	9800.08	1.43283×10^{-11}	6.92667×10^{-13}
9778.13	5.43798×10^{-11}	2.76722×10^{-12}	9800.64	1.40679×10^{-11}	6.80280×10^{-13}
9778.69	5.33251×10^{-11}	2.71118×10^{-12}	9801.21	1.37933×10^{-11}	6.67015×10^{-13}
9779.26	5.21283×10^{-11}	2.64750×10^{-12}	9801.77	1.34954×10^{-11}	6.52520×10^{-13}
9779.82	5.08017×10^{-11}	2.57710×10^{-12}	9802.33	1.31706×10^{-11}	6.36616×10^{-13}
9780.38	4.93634×10^{-11}	2.50078×10^{-12}	9802.89	1.28206×10^{-11}	6.19366×10^{-13}
9780.94	4.78321×10^{-11}	2.41960×10^{-12}	9803.46	1.24505×10^{-11}	6.01073×10^{-13}
9781.51	4.62260×10^{-11}	2.33465×10^{-12}	9804.02	1.20674×10^{-11}	5.82175×10^{-13}
9782.07	4.45671×10^{-11}	2.24692×10^{-12}	9804.58	1.16806×10^{-11}	5.63124×10^{-13}
9782.63	4.28740×10^{-11}	2.15748×10^{-12}	9805.15	1.12997×10^{-11}	5.44346×10^{-13}
9783.20	4.11645×10^{-11}	2.06732×10^{-12}	9805.71	1.09288×10^{-11}	5.26143×10^{-13}
9783.76	3.94574×10^{-11}	1.97739×10^{-12}	9806.27	1.05734×10^{-11}	5.08725×10^{-13}
9784.32	3.77681×10^{-11}	1.88852×10^{-12}	9806.83	1.02357×10^{-11}	4.92179×10^{-13}
9784.88	3.61099×10^{-11}	1.80155×10^{-12}	9807.40	9.91583×10^{-12}	4.76543×10^{-13}
9785.45	3.44956×10^{-11}	1.71694×10^{-12}	9807.96	9.61366×10^{-12}	4.61788×10^{-13}
9786.01	3.29353×10^{-11}	1.63524×10^{-12}	9808.52	9.32807×10^{-12}	4.47891×10^{-13}
9786.57	3.14363×10^{-11}	1.55682×10^{-12}	9809.08	9.05814×10^{-12}	4.34778×10^{-13}
9787.14	3.00042×10^{-11}	1.48213×10^{-12}	9809.65	8.80285×10^{-12}	4.22432×10^{-13}
9787.70	2.86445×10^{-11}	1.41125×10^{-12}	9810.21	8.56135×10^{-12}	4.10798×10^{-13}
9788.26	2.73590×10^{-11}	1.34446×10^{-12}	9810.77	8.33302×10^{-12}	3.99836×10^{-13}
9788.82	2.61480×10^{-11}	1.28163×10^{-12}	9811.34	8.11722×10^{-12}	3.89519×10^{-13}
9789.39	2.50140×10^{-11}	1.22289×10^{-12}	9811.90	7.91341×10^{-12}	3.79802×10^{-13}
9789.95	2.39550×10^{-11}	1.16819×10^{-12}	9812.46	7.72113×10^{-12}	3.70659×10^{-13}
9790.51	2.29688×10^{-11}	1.11747×10^{-12}	9813.03	7.53958×10^{-12}	3.62037×10^{-13}

Table A.12 (cont'd)

JD +2440000	*UVOIR* Flux	Flux error	JD +2440000	*UVOIR* Flux	Flux error
9813.59	7.36827×10^{-12}	3.53917×10^{-13}	9836.10	3.85642×10^{-12}	1.85968×10^{-13}
9814.15	7.20649×10^{-12}	3.46259×10^{-13}	9836.66	3.80049×10^{-12}	1.83314×10^{-13}
9814.71	7.05357×10^{-12}	3.39023×10^{-13}	9837.23	3.74552×10^{-12}	1.80691×10^{-13}
9815.28	6.90877×10^{-12}	3.32167×10^{-13}	9837.79	3.69126×10^{-12}	1.78109×10^{-13}
9815.84	6.77151×10^{-12}	3.25662×10^{-13}	9838.35	3.63784×10^{-12}	1.75569×10^{-13}
9816.40	6.64107×10^{-12}	3.19476×10^{-13}	9838.92	3.58515×10^{-12}	1.73071×10^{-13}
9816.96	6.51674×10^{-12}	3.13569×10^{-13}	9839.48	3.53318×10^{-12}	1.70604×10^{-13}
9817.53	6.39815×10^{-12}	3.07934×10^{-13}	9840.04	3.48195×10^{-12}	1.68168×10^{-13}
9818.09	6.28454×10^{-12}	3.02515×10^{-13}	9840.60	3.43155×10^{-12}	1.65775×10^{-13}
9818.65	6.17545×10^{-12}	2.97317×10^{-13}	9841.17	3.38179×10^{-12}	1.63413×10^{-13}
9819.22	6.07056×10^{-12}	2.92297×10^{-13}	9841.73	3.33289×10^{-12}	1.61093×10^{-13}
9819.78	5.96937×10^{-12}	2.87456×10^{-13}	9842.29	3.28462×10^{-12}	1.58806×10^{-13}
9820.34	5.87158×10^{-12}	2.82764×10^{-13}	9842.85	3.23710×10^{-12}	1.56551×10^{-13}
9820.90	5.77690×10^{-12}	2.78211×10^{-13}	9843.42	3.19024×10^{-12}	1.54339×10^{-13}
9821.47	5.68491×10^{-12}	2.73787×10^{-13}	9843.98	3.14402×10^{-12}	1.52148×10^{-13}
9822.03	5.59542×10^{-12}	2.69482×10^{-13}	9844.54	3.09858×10^{-12}	1.50002×10^{-13}
9822.59	5.50834×10^{-12}	2.65277×10^{-13}	9845.11	3.05391×10^{-12}	1.47878×10^{-13}
9823.16	5.42335×10^{-12}	2.61181×10^{-13}	9845.67	3.00979×10^{-12}	1.45798×10^{-13}
9823.72	5.34036×10^{-12}	2.57185×10^{-13}	9846.23	2.96634×10^{-12}	1.43741×10^{-13}
9824.28	5.25917×10^{-12}	2.53268×10^{-13}	9846.79	2.92368×10^{-12}	1.41717×10^{-13}
9824.84	5.17977×10^{-12}	2.49441×10^{-13}	9847.36	2.88159×10^{-12}	1.39727×10^{-13}
9825.41	5.10197×10^{-12}	2.45693×10^{-13}	9847.92	2.84017×10^{-12}	1.37771×10^{-13}
9825.97	5.02563×10^{-12}	2.42014×10^{-13}	9848.48	2.79943×10^{-12}	1.35849×10^{-13}
9826.53	4.95089×10^{-12}	2.38413×10^{-13}	9849.04	2.75927×10^{-12}	1.33950×10^{-13}
9827.10	4.87753×10^{-12}	2.34871×10^{-13}	9849.61	2.71978×10^{-12}	1.32085×10^{-13}
9827.66	4.80541×10^{-12}	2.31407×10^{-13}	9850.17	2.68086×10^{-12}	1.30243×10^{-13}
9828.22	4.73466×10^{-12}	2.28001×10^{-13}	9850.73	2.64252×10^{-12}	1.28434×10^{-13}
9828.78	4.66516×10^{-12}	2.24662×10^{-13}	9851.30	2.60485×10^{-12}	1.26660×10^{-13}
9829.35	4.59679×10^{-12}	2.21380×10^{-13}	9851.86	2.56774×10^{-12}	1.24908×10^{-13}
9829.91	4.52955×10^{-12}	2.18154×10^{-13}	9852.42	2.53120×10^{-12}	1.23179×10^{-13}
9830.47	4.46342×10^{-12}	2.14984×10^{-13}	9852.99	2.49532×10^{-12}	1.21483×10^{-13}
9831.04	4.39840×10^{-12}	2.11858×10^{-13}	9853.55	2.45989×10^{-12}	1.19810×10^{-13}
9831.60	4.33438×10^{-12}	2.08798×10^{-13}	9854.11	2.42501×10^{-12}	1.18158×10^{-13}
9832.16	4.27134×10^{-12}	2.05782×10^{-13}	9854.67	2.39057×10^{-12}	1.16540×10^{-13}
9832.72	4.20938×10^{-12}	2.02821×10^{-13}	9855.24	2.35678×10^{-12}	1.14943×10^{-13}
9833.29	4.14829×10^{-12}	1.99891×10^{-13}	9855.80	2.32343×10^{-12}	1.13368×10^{-13}
9833.85	4.08816×10^{-12}	1.97027×10^{-13}	9856.36	2.29061×10^{-12}	1.11814×10^{-13}
9834.41	4.02888×10^{-12}	1.94193×10^{-13}	9856.92	2.25821×10^{-12}	1.10292×10^{-13}
9834.97	3.97056×10^{-12}	1.91413×10^{-13}	9857.49	2.22624×10^{-12}	1.08780×10^{-13}
9835.54	3.91307×10^{-12}	1.88675×10^{-13}	9858.05	2.19479×10^{-12}	1.07296×10^{-13}

Table A.12 (cont'd)

JD +2440000	*UVOIR* Flux	Flux error	JD +2440000	*UVOIR* Flux	Flux error
9858.61	2.16387×10^{-12}	1.05832×10^{-13}	9869.31	1.65380×10^{-12}	8.17091×10^{-14}
9859.18	2.13326×10^{-12}	1.04388×10^{-13}	9869.87	1.63086×10^{-12}	8.06234×10^{-14}
9859.74	2.10318×10^{-12}	1.02966×10^{-13}	9870.43	1.60836×10^{-12}	7.95539×10^{-14}
9860.30	2.07352×10^{-12}	1.01563×10^{-13}	9871.00	1.58610×10^{-12}	7.85003×10^{-14}
9860.86	2.04416×10^{-12}	1.00181×10^{-13}	9871.56	1.56428×10^{-12}	7.74622×10^{-14}
9861.43	2.01534×10^{-12}	9.88166×10^{-14}	9872.12	1.54267×10^{-12}	7.64393×10^{-14}
9861.99	1.98694×10^{-12}	9.74729×10^{-14}	9872.68	1.52138×10^{-12}	7.54297×10^{-14}
9862.55	1.95885×10^{-12}	9.61471×10^{-14}	9873.25	1.50039×10^{-12}	7.44344×10^{-14}
9863.12	1.93131×10^{-12}	9.48419×10^{-14}	9873.81	1.47970×10^{-12}	7.34505×10^{-14}
9863.68	1.90410×10^{-12}	9.35551×10^{-14}	9874.37	1.45929×10^{-12}	7.24799×10^{-14}
9864.24	1.87722×10^{-12}	9.22872×10^{-14}	9874.93	1.43906×10^{-12}	7.15190×10^{-14}
9864.80	1.85089×10^{-12}	9.10371×10^{-14}	9875.50	1.41911×10^{-12}	7.05711×10^{-14}
9865.37	1.82479×10^{-12}	8.98073×10^{-14}	9876.06	1.39945×10^{-12}	6.96333×10^{-14}
9865.93	1.79926×10^{-12}	8.85959×10^{-14}	9876.62	1.37998×10^{-12}	6.87085×10^{-14}
9866.49	1.77397×10^{-12}	8.74019×10^{-14}	9877.19	1.36084×10^{-12}	6.77958×10^{-14}
9867.06	1.74924×10^{-12}	8.62276×10^{-14}	9877.75	1.34197×10^{-12}	6.68985×10^{-14}
9867.62	1.72477×10^{-12}	8.50711×10^{-14}	9878.31	1.32353×10^{-12}	6.60195×10^{-14}
9868.18	1.70076×10^{-12}	8.39323×10^{-14}	9878.87	1.30550×10^{-12}	6.51609×10^{-14}
9868.74	1.67710×10^{-12}	8.28124×10^{-14}	9879.44	1.28809×10^{-12}	6.43305×10^{-14}

Table A.13. SN 1995ac

JD +2440000	*UVOIR* Flux	Flux error	JD +2440000	*UVOIR* Flux	Flux error
9984.22	2.38857×10^{-12}	1.29759×10^{-13}	10008.3	1.59105×10^{-12}	7.64925×10^{-14}
9984.82	2.57037×10^{-12}	1.35717×10^{-13}	10008.9	1.52767×10^{-12}	7.32494×10^{-14}
9985.43	2.72882×10^{-12}	1.41716×10^{-13}	10009.5	1.46814×10^{-12}	7.02193×10^{-14}
9986.03	2.86012×10^{-12}	1.47245×10^{-13}	10010.2	1.41253×10^{-12}	6.74064×10^{-14}
9986.63	2.96768×10^{-12}	1.52111×10^{-13}	10010.8	1.36072×10^{-12}	6.48067×10^{-14}
9987.24	3.05609×10^{-12}	1.56344×10^{-13}	10011.4	1.31289×10^{-12}	6.24217×10^{-14}
9987.84	3.13028×10^{-12}	1.60026×10^{-13}	10012.0	1.26892×10^{-12}	6.02511×10^{-14}
9988.44	3.19332×10^{-12}	1.63241×10^{-13}	10012.6	1.22875×10^{-12}	5.82931×10^{-14}
9989.04	3.24757×10^{-12}	1.66045×10^{-13}	10013.2	1.19229×10^{-12}	5.65451×10^{-14}
9989.65	3.29410×10^{-12}	1.68452×10^{-13}	10013.8	1.15948×10^{-12}	5.50020×10^{-14}
9990.25	3.33356×10^{-12}	1.70475×10^{-13}	10014.4	1.12994×10^{-12}	5.36572×10^{-14}
9990.85	3.36587×10^{-12}	1.72104×10^{-13}	10015.0	1.10371×10^{-12}	5.25013×10^{-14}
9991.46	3.39085×10^{-12}	1.73304×10^{-13}	10015.6	1.08021×10^{-12}	5.15223×10^{-14}
9992.06	3.40814×10^{-12}	1.74056×10^{-13}	10016.2	1.05927×10^{-12}	5.07039×10^{-14}
9992.66	3.41705×10^{-12}	1.74346×10^{-13}	10016.8	1.04039×10^{-12}	5.00284×10^{-14}
9993.27	3.41706×10^{-12}	1.74147×10^{-13}	10017.4	1.02316×10^{-12}	4.94747×10^{-14}
9993.87	3.40765×10^{-12}	1.73427×10^{-13}	10018.0	1.00715×10^{-12}	4.90167×10^{-14}
9994.47	3.38856×10^{-12}	1.72191×10^{-13}	10018.6	9.91906×10^{-13}	4.86222×10^{-14}
9995.08	3.35954×10^{-12}	1.70442×10^{-13}	10019.2	9.76922×10^{-13}	4.82534×10^{-14}
9995.68	3.32033×10^{-12}	1.68165×10^{-13}	10019.8	9.61658×10^{-13}	4.78641×10^{-14}
9996.28	3.27147×10^{-12}	1.65382×10^{-13}	10020.4	9.45624×10^{-13}	4.74070×10^{-14}
9996.88	3.21303×10^{-12}	1.62122×10^{-13}	10021.0	9.28319×10^{-13}	4.68334×10^{-14}
9997.49	3.14602×10^{-12}	1.58436×10^{-13}	10021.6	9.09361×10^{-13}	4.61065×10^{-14}
9998.09	3.07107×10^{-12}	1.54355×10^{-13}	10022.2	8.88518×10^{-13}	4.51988×10^{-14}
9998.69	2.98951×10^{-12}	1.49947×10^{-13}	10022.8	8.65751×10^{-13}	4.41065×10^{-14}
9999.30	2.90221×10^{-12}	1.45267×10^{-13}	10023.4	8.41231×10^{-13}	4.28432×10^{-14}
9999.90	2.81050×10^{-12}	1.40370×10^{-13}	10024.0	8.15315×10^{-13}	4.14401×10^{-14}
10000.5	2.71572×10^{-12}	1.35334×10^{-13}	10024.6	7.88480×10^{-13}	3.99410×10^{-14}
10001.1	2.61902×10^{-12}	1.30201×10^{-13}	10025.2	7.61280×10^{-13}	3.83941×10^{-14}
10001.7	2.52145×10^{-12}	1.25057×10^{-13}	10025.8	7.34255×10^{-13}	3.68452×10^{-14}
10002.3	2.42418×10^{-12}	1.19926×10^{-13}	10026.4	7.07884×10^{-13}	3.53357×10^{-14}
10002.9	2.32780×10^{-12}	1.14855×10^{-13}	10027.0	6.82530×10^{-13}	3.38935×10^{-14}
10003.5	2.23334×10^{-12}	1.09893×10^{-13}	10027.6	6.58463×10^{-13}	3.25396×10^{-14}
10004.1	2.14135×10^{-12}	1.05067×10^{-13}	10028.2	6.35835×10^{-13}	3.12830×10^{-14}
10004.7	2.05204×10^{-12}	1.00398×10^{-13}	10028.8	6.14699×10^{-13}	3.01274×10^{-14}
10005.3	1.96608×10^{-12}	9.59080×10^{-14}	10029.4	5.95039×10^{-13}	2.90701×10^{-14}
10005.9	1.88350×10^{-12}	9.16087×10^{-14}	10030.0	5.76775×10^{-13}	2.81026×10^{-14}
10006.5	1.80469×10^{-12}	8.75140×10^{-14}	10030.7	5.59817×10^{-13}	2.72178×10^{-14}
10007.1	1.72966×10^{-12}	8.36270×10^{-14}	10031.3	5.44042×10^{-13}	2.64063×10^{-14}
10007.7	1.65841×10^{-12}	7.99530×10^{-14}	10031.9	5.29312×10^{-13}	2.56575×10^{-14}

Table A.13 (cont'd)

JD +2440000	*UVOIR* Flux	Flux error	JD +2440000	*UVOIR* Flux	Flux error
10032.5	5.15504×10^{-13}	2.49631×10^{-14}	10056.6	2.49897×10^{-13}	1.16834×10^{-14}
10033.1	5.02515×10^{-13}	2.43156×10^{-14}	10057.2	2.46421×10^{-13}	1.15135×10^{-14}
10033.7	4.90230×10^{-13}	2.37077×10^{-14}	10057.8	2.43018×10^{-13}	1.13478×10^{-14}
10034.3	4.78589×10^{-13}	2.31343×10^{-14}	10058.4	2.39678×10^{-13}	1.11863×10^{-14}
10034.9	4.67499×10^{-13}	2.25889×10^{-14}	10059.0	2.36401×10^{-13}	1.10291×10^{-14}
10035.5	4.56909×10^{-13}	2.20697×10^{-14}	10059.6	2.33187×10^{-13}	1.08752×10^{-14}
10036.1	4.46780×10^{-13}	2.15736×10^{-14}	10060.2	2.30038×10^{-13}	1.07253×10^{-14}
10036.7	4.37071×10^{-13}	2.10964×10^{-14}	10060.8	2.26953×10^{-13}	1.05790×10^{-14}
10037.3	4.27754×10^{-13}	2.06382×10^{-14}	10061.4	2.23912×10^{-13}	1.04363×10^{-14}
10037.9	4.18788×10^{-13}	2.01960×10^{-14}	10062.0	2.20946×10^{-13}	1.02972×10^{-14}
10038.5	4.10176×10^{-13}	1.97709×10^{-14}	10062.6	2.18024×10^{-13}	1.01614×10^{-14}
10039.1	4.01898×10^{-13}	1.93598×10^{-14}	10063.2	2.15157×10^{-13}	1.00292×10^{-14}
10039.7	3.93914×10^{-13}	1.89629×10^{-14}	10063.8	2.12346×10^{-13}	9.90020×10^{-15}
10040.3	3.86234×10^{-13}	1.85790×10^{-14}	10064.4	2.09591×10^{-13}	9.77451×10^{-15}
10040.9	3.78840×10^{-13}	1.82083×10^{-14}	10065.0	2.06891×10^{-13}	9.65205×10^{-15}
10041.5	3.71700×10^{-13}	1.78497×10^{-14}	10065.6	2.04237×10^{-13}	9.53272×10^{-15}
10042.1	3.64825×10^{-13}	1.75033×10^{-14}	10066.2	2.01639×10^{-13}	9.41640×10^{-15}
10042.7	3.58194×10^{-13}	1.71680×10^{-14}	10066.8	1.99087×10^{-13}	9.30313×10^{-15}
10043.3	3.51786×10^{-13}	1.68439×10^{-14}	10067.4	1.96591×10^{-13}	9.19266×10^{-15}
10043.9	3.45602×10^{-13}	1.65298×10^{-14}	10068.0	1.94130×10^{-13}	9.08512×10^{-15}
10044.5	3.39629×10^{-13}	1.62258×10^{-14}	10068.6	1.91725×10^{-13}	8.98039×10^{-15}
10045.1	3.33847×10^{-13}	1.59307×10^{-14}	10069.2	1.89355×10^{-13}	8.87824×10^{-15}
10045.7	3.28254×10^{-13}	1.56457×10^{-14}	10069.8	1.87040×10^{-13}	8.77888×10^{-15}
10046.3	3.22829×10^{-13}	1.53685×10^{-14}	10070.5	1.84760×10^{-13}	8.68198×10^{-15}
10046.9	3.17571×10^{-13}	1.50990×10^{-14}	10071.1	1.82524×10^{-13}	8.58751×10^{-15}
10047.5	3.12469×10^{-13}	1.48385×10^{-14}	10071.7	1.80333×10^{-13}	8.49547×10^{-15}
10048.1	3.07522×10^{-13}	1.45857×10^{-14}	10072.3	1.78185×10^{-13}	8.40584×10^{-15}
10048.7	3.02708×10^{-13}	1.43396×10^{-14}	10072.9	1.76071×10^{-13}	8.31838×10^{-15}
10049.3	2.98026×10^{-13}	1.41011×10^{-14}	10073.5	1.73988×10^{-13}	8.23308×10^{-15}
10050.0	2.93464×10^{-13}	1.38681×10^{-14}	10074.1	1.71949×10^{-13}	8.14993×10^{-15}
10050.6	2.89032×10^{-13}	1.36427×10^{-14}	10074.7	1.69941×10^{-13}	8.06879×10^{-15}
10051.2	2.84698×10^{-13}	1.34227×10^{-14}	10075.3	1.67964×10^{-13}	7.98965×10^{-15}
10051.8	2.80472×10^{-13}	1.32092×10^{-14}	10075.9	1.66030×10^{-13}	7.91251×10^{-15}
10052.4	2.76353×10^{-13}	1.30000×10^{-14}	10076.5	1.64126×10^{-13}	7.83703×10^{-15}
10053.0	2.72319×10^{-13}	1.27972×10^{-14}	10077.1	1.62243×10^{-13}	7.76352×10^{-15}
10053.6	2.68381×10^{-13}	1.25997×10^{-14}	10077.7	1.60401×10^{-13}	7.69167×10^{-15}
10054.2	2.64526×10^{-13}	1.24076×10^{-14}	10078.3	1.58591×10^{-13}	7.62146×10^{-15}
10054.8	2.60757×10^{-13}	1.22197×10^{-14}	10078.9	1.56800×10^{-13}	7.55301×10^{-15}
10055.4	2.57060×10^{-13}	1.20360×10^{-14}	10079.5	1.55052×10^{-13}	7.48612×10^{-15}
10056.0	2.53437×10^{-13}	1.18576×10^{-14}	10080.1	1.53324×10^{-13}	7.42079×10^{-15}

Table A.13 (cont'd)

JD +2440000	*UVOIR* Flux	Flux error	JD +2440000	*UVOIR* Flux	Flux error
10080.7	1.51628×10^{-13}	7.35705×10^{-15}	10089.1	1.30805×10^{-13}	6.61544×10^{-15}
10081.3	1.49964×10^{-13}	7.29478×10^{-15}	10089.7	1.29510×10^{-13}	6.57203×10^{-15}
10081.9	1.48322×10^{-13}	7.23404×10^{-15}	10090.4	1.28247×10^{-13}	6.52956×10^{-15}
10082.5	1.46712×10^{-13}	7.17482×10^{-15}	10091.0	1.26993×10^{-13}	6.48797×10^{-15}
10083.1	1.45126×10^{-13}	7.11715×10^{-15}	10091.6	1.25758×10^{-13}	6.44730×10^{-15}
10083.7	1.43573×10^{-13}	7.06084×10^{-15}	10092.2	1.24530×10^{-13}	6.40731×10^{-15}
10084.3	1.42044×10^{-13}	7.00592×10^{-15}	10092.8	1.23330×10^{-13}	6.36794×10^{-15}
10084.9	1.40549×10^{-13}	6.95249×10^{-15}	10093.4	1.22147×10^{-13}	6.32930×10^{-15}
10085.5	1.39079×10^{-13}	6.90038×10^{-15}	10094.0	1.20971×10^{-13}	6.29118×10^{-15}
10086.1	1.37633×10^{-13}	6.84978×10^{-15}	10094.6	1.19814×10^{-13}	6.25378×10^{-15}
10086.7	1.36222×10^{-13}	6.80040×10^{-15}	10095.2	1.18678×10^{-13}	6.21722×10^{-15}
10087.3	1.34824×10^{-13}	6.75233×10^{-15}	10095.8	1.17569×10^{-13}	6.18154×10^{-15}
10087.9	1.33461×10^{-13}	6.70555×10^{-15}	10096.4	1.16482×10^{-13}	6.14732×10^{-15}
10088.5	1.32122×10^{-13}	6.65992×10^{-15}	10097.0	1.15428×10^{-13}	6.11498×10^{-15}

Table A.14. SN 1995al

JD +2440000	*UVOIR* Flux	Flux error	JD +2440000	*UVOIR* Flux	Flux error
10021.0	8.88365×10^{-11}	4.83706×10^{-12}	10051.2	4.43640×10^{-11}	2.12627×10^{-12}
10021.8	9.73662×10^{-11}	5.14907×10^{-12}	10051.9	4.33360×10^{-11}	2.07877×10^{-12}
10022.5	1.05212×10^{-10}	5.46811×10^{-12}	10052.7	4.20385×10^{-11}	2.01673×10^{-12}
10023.3	1.12150×10^{-10}	5.77135×10^{-12}	10053.4	4.05242×10^{-11}	1.94366×10^{-12}
10024.0	1.18162×10^{-10}	6.04717×10^{-12}	10054.2	3.89936×10^{-11}	1.87102×10^{-12}
10024.8	1.23314×10^{-10}	6.29186×10^{-12}	10055.0	3.76099×10^{-11}	1.80708×10^{-12}
10025.6	1.27671×10^{-10}	6.50474×10^{-12}	10055.7	3.64116×10^{-11}	1.75268×10^{-12}
10026.3	1.31271×10^{-10}	6.68504×10^{-12}	10056.5	3.53549×10^{-11}	1.70480×10^{-12}
10027.1	1.34125×10^{-10}	6.83198×10^{-12}	10057.2	3.43680×10^{-11}	1.65951×10^{-12}
10027.8	1.36250×10^{-10}	6.94388×10^{-12}	10058.0	3.34000×10^{-11}	1.61447×10^{-12}
10028.6	1.37627×10^{-10}	7.01914×10^{-12}	10058.7	3.24265×10^{-11}	1.56818×10^{-12}
10029.3	1.38242×10^{-10}	7.05602×10^{-12}	10059.5	3.14351×10^{-11}	1.52036×10^{-12}
10030.1	1.38088×10^{-10}	7.05351×10^{-12}	10060.2	3.04277×10^{-11}	1.47126×10^{-12}
10030.8	1.37177×10^{-10}	7.01143×10^{-12}	10061.0	2.94106×10^{-11}	1.42104×10^{-12}
10031.6	1.35528×10^{-10}	6.93035×10^{-12}	10061.7	2.83887×10^{-11}	1.37041×10^{-12}
10032.3	1.33192×10^{-10}	6.81172×10^{-12}	10062.5	2.73741×10^{-11}	1.31988×10^{-12}
10033.1	1.30200×10^{-10}	6.65827×10^{-12}	10063.2	2.63731×10^{-11}	1.26998×10^{-12}
10033.8	1.26641×10^{-10}	6.47356×10^{-12}	10064.0	2.53952×10^{-11}	1.22135×10^{-12}
10034.6	1.22589×10^{-10}	6.26157×10^{-12}	10064.7	2.44492×10^{-11}	1.17432×10^{-12}
10035.4	1.18133×10^{-10}	6.02711×10^{-12}	10065.5	2.35408×10^{-11}	1.12934×10^{-12}
10036.1	1.13370×10^{-10}	5.77541×10^{-12}	10066.3	2.26746×10^{-11}	1.08660×10^{-12}
10036.9	1.08393×10^{-10}	5.51149×10^{-12}	10067.0	2.18542×10^{-11}	1.04633×10^{-12}
10037.6	1.03294×10^{-10}	5.24029×10^{-12}	10067.8	2.10813×10^{-11}	1.00858×10^{-12}
10038.4	9.81599×10^{-11}	4.96656×10^{-12}	10068.5	2.03561×10^{-11}	9.73358×10^{-13}
10039.1	9.30684×10^{-11}	4.69466×10^{-12}	10069.3	1.96781×10^{-11}	9.40595×10^{-13}
10039.9	8.80852×10^{-11}	4.42817×10^{-12}	10070.0	1.90466×10^{-11}	9.10162×10^{-13}
10040.6	8.32665×10^{-11}	4.17022×10^{-12}	10070.8	1.84577×10^{-11}	8.81928×10^{-13}
10041.4	7.86573×10^{-11}	3.92340×10^{-12}	10071.5	1.79106×10^{-11}	8.55725×10^{-13}
10042.1	7.42889×10^{-11}	3.68956×10^{-12}	10072.3	1.74003×10^{-11}	8.31372×10^{-13}
10042.9	7.01872×10^{-11}	3.47017×10^{-12}	10073.0	1.69248×10^{-11}	8.08687×10^{-13}
10043.6	6.63645×10^{-11}	3.26604×10^{-12}	10073.8	1.64801×10^{-11}	7.87500×10^{-13}
10044.4	6.28301×10^{-11}	3.07780×10^{-12}	10074.5	1.60631×10^{-11}	7.67646×10^{-13}
10045.2	5.95841×10^{-11}	2.90532×10^{-12}	10075.3	1.56719×10^{-11}	7.48984×10^{-13}
10045.9	5.66220×10^{-11}	2.74876×10^{-12}	10076.1	1.53044×10^{-11}	7.31380×10^{-13}
10046.7	5.39423×10^{-11}	2.60789×10^{-12}	10076.8	1.49565×10^{-11}	7.14699×10^{-13}
10047.4	5.15489×10^{-11}	2.48309×10^{-12}	10077.6	1.46261×10^{-11}	6.98850×10^{-13}
10048.2	4.94634×10^{-11}	2.37550×10^{-12}	10078.3	1.43123×10^{-11}	6.83737×10^{-13}
10048.9	4.77233×10^{-11}	2.28694×10^{-12}	10079.1	1.40127×10^{-11}	6.69279×10^{-13}
10049.7	4.63467×10^{-11}	2.21876×10^{-12}	10079.8	1.37255×10^{-11}	6.55411×10^{-13}
10050.4	4.52853×10^{-11}	2.16832×10^{-12}	10080.6	1.34505×10^{-11}	6.42070×10^{-13}

Table A.14 (cont'd)

JD +2440000	*UVOIR* Flux	Flux error	JD +2440000	*UVOIR* Flux	Flux error
10081.3	1.31857×10^{-11}	6.29211×10^{-13}	10111.5	6.46535×10^{-12}	3.08281×10^{-13}
10082.1	1.29299×10^{-11}	6.16803×10^{-13}	10112.2	6.35617×10^{-12}	3.03247×10^{-13}
10082.8	1.26830×10^{-11}	6.04778×10^{-13}	10113.0	6.24908×10^{-12}	2.98308×10^{-13}
10083.6	1.24430×10^{-11}	5.93135×10^{-13}	10113.7	6.14376×10^{-12}	2.93462×10^{-13}
10084.3	1.22107×10^{-11}	5.81818×10^{-13}	10114.5	6.04030×10^{-12}	2.88699×10^{-13}
10085.1	1.19852×10^{-11}	5.70835×10^{-13}	10115.3	5.93859×10^{-12}	2.84028×10^{-13}
10085.9	1.17652×10^{-11}	5.60140×10^{-13}	10116.0	5.83864×10^{-12}	2.79441×10^{-13}
10086.6	1.15507×10^{-11}	5.49720×10^{-13}	10116.8	5.74048×10^{-12}	2.74937×10^{-13}
10087.4	1.13417×10^{-11}	5.39562×10^{-13}	10117.5	5.64401×10^{-12}	2.70518×10^{-13}
10088.1	1.11369×10^{-11}	5.29652×10^{-13}	10118.3	5.54927×10^{-12}	2.66175×10^{-13}
10088.9	1.09365×10^{-11}	5.19979×10^{-13}	10119.0	5.45618×10^{-12}	2.61929×10^{-13}
10089.6	1.07414×10^{-11}	5.10528×10^{-13}	10119.8	5.36487×10^{-12}	2.57752×10^{-13}
10090.4	1.05500×10^{-11}	5.01288×10^{-13}	10120.5	5.27528×10^{-12}	2.53665×10^{-13}
10091.1	1.03624×10^{-11}	4.92247×10^{-13}	10121.3	5.18743×10^{-12}	2.49659×10^{-13}
10091.9	1.01787×10^{-11}	4.83404×10^{-13}	10122.0	5.10135×10^{-12}	2.45736×10^{-13}
10092.6	9.99855×10^{-12}	4.74749×10^{-13}	10122.8	5.01683×10^{-12}	2.41896×10^{-13}
10093.4	9.82185×10^{-12}	4.66281×10^{-13}	10123.5	4.93409×10^{-12}	2.38129×10^{-13}
10094.1	9.64855×10^{-12}	4.57979×10^{-13}	10124.3	4.85292×10^{-12}	2.34444×10^{-13}
10094.9	9.47860×10^{-12}	4.49855×10^{-13}	10125.0	4.77328×10^{-12}	2.30831×10^{-13}
10095.7	9.31188×10^{-12}	4.41899×10^{-13}	10125.8	4.69524×10^{-12}	2.27298×10^{-13}
10096.4	9.14821×10^{-12}	4.34112×10^{-13}	10126.6	4.61864×10^{-12}	2.23820×10^{-13}
10097.2	8.98774×10^{-12}	4.26484×10^{-13}	10127.3	4.54331×10^{-12}	2.20405×10^{-13}
10097.9	8.83036×10^{-12}	4.19007×10^{-13}	10128.1	4.46928×10^{-12}	2.17061×10^{-13}
10098.7	8.67592×10^{-12}	4.11692×10^{-13}	10128.8	4.39628×10^{-12}	2.13753×10^{-13}
10099.4	8.52454×10^{-12}	4.04519×10^{-13}	10129.6	4.32446×10^{-12}	2.10508×10^{-13}
10100.2	8.37603×10^{-12}	3.97512×10^{-13}	10130.3	4.25360×10^{-12}	2.07307×10^{-13}
10100.9	8.23042×10^{-12}	3.90639×10^{-13}	10131.1	4.18384×10^{-12}	2.04150×10^{-13}
10101.7	8.08764×10^{-12}	3.83911×10^{-13}	10131.8	4.11521×10^{-12}	2.01044×10^{-13}
10102.4	7.94758×10^{-12}	3.77331×10^{-13}	10132.6	4.04798×10^{-12}	1.98012×10^{-13}
10103.2	7.81036×10^{-12}	3.70898×10^{-13}	10133.3	3.98258×10^{-12}	1.95055×10^{-13}
10103.9	7.67588×10^{-12}	3.64591×10^{-13}	10134.1	3.91960×10^{-12}	1.92229×10^{-13}
10104.7	7.54403×10^{-12}	3.58420×10^{-13}	...	...	...
10105.5	7.41471×10^{-12}	3.52375×10^{-13}	...	...	...
10106.2	7.28788×10^{-12}	3.46455×10^{-13}	...	...	...
10107.0	7.16355×10^{-12}	3.40670×10^{-13}	...	...	...
10107.7	7.04170×10^{-12}	3.34997×10^{-13}	...	...	...
10108.5	6.92207×10^{-12}	3.29436×10^{-13}	...	...	...
10109.2	6.80465×10^{-12}	3.23985×10^{-13}	...	...	...
10110.0	6.68951×10^{-12}	3.18654×10^{-13}	...	...	...

Table A.15. SN 1995bd

JD +2440000	*UVOIR* Flux	Flux error	JD +2440000	*UVOIR* Flux	Flux error
10078.2	1.59127×10^{-11}	7.92966×10^{-13}	10103.3	1.00339×10^{-11}	4.88171×10^{-13}
10078.8	1.73555×10^{-11}	8.66358×10^{-13}	10103.9	9.66720×10^{-12}	4.69360×10^{-13}
10079.4	1.86746×10^{-11}	9.33769×10^{-13}	10104.5	9.33129×10^{-12}	4.52137×10^{-13}
10080.0	1.98677×10^{-11}	9.95060×10^{-13}	10105.2	9.02443×10^{-12}	4.36413×10^{-13}
10080.7	2.09383×10^{-11}	1.05015×10^{-12}	10105.8	8.74486×10^{-12}	4.22136×10^{-13}
10081.3	2.18878×10^{-11}	1.09903×10^{-12}	10106.4	8.49102×10^{-12}	4.09221×10^{-13}
10081.9	2.27184×10^{-11}	1.14167×10^{-12}	10107.1	8.26125×10^{-12}	3.97613×10^{-13}
10082.6	2.34327×10^{-11}	1.17810×10^{-12}	10107.7	8.05378×10^{-12}	3.87221×10^{-13}
10083.2	2.40317×10^{-11}	1.20837×10^{-12}	10108.3	7.86696×10^{-12}	3.77979×10^{-13}
10083.8	2.45174×10^{-11}	1.23257×10^{-12}	10108.9	7.69899×10^{-12}	3.69803×10^{-13}
10084.4	2.48929×10^{-11}	1.25086×10^{-12}	10109.6	7.54810×10^{-12}	3.62608×10^{-13}
10085.1	2.51598×10^{-11}	1.26338×10^{-12}	10110.2	7.41248×10^{-12}	3.56307×10^{-13}
10085.7	2.53215×10^{-11}	1.27027×10^{-12}	10110.8	7.29010×10^{-12}	3.50785×10^{-13}
10086.3	2.53778×10^{-11}	1.27195×10^{-12}	10111.5	7.17895×10^{-12}	3.45945×10^{-13}
10087.0	2.53345×10^{-11}	1.26835×10^{-12}	10112.1	7.07686×10^{-12}	3.41657×10^{-13}
10087.6	2.51914×10^{-11}	1.26001×10^{-12}	10112.7	6.98177×10^{-12}	3.37782×10^{-13}
10088.2	2.49555×10^{-11}	1.24690×10^{-12}	10113.3	6.89151×10^{-12}	3.34190×10^{-13}
10088.8	2.46290×10^{-11}	1.22948×10^{-12}	10114.0	6.80372×10^{-12}	3.30755×10^{-13}
10089.5	2.42161×10^{-11}	1.20789×10^{-12}	10114.6	6.71638×10^{-12}	3.27316×10^{-13}
10090.1	2.37231×10^{-11}	1.18247×10^{-12}	10115.2	6.62760×10^{-12}	3.23768×10^{-13}
10090.7	2.31575×10^{-11}	1.15354×10^{-12}	10115.9	6.53544×10^{-12}	3.19973×10^{-13}
10091.4	2.25286×10^{-11}	1.12149×10^{-12}	10116.5	6.43835×10^{-12}	3.15836×10^{-13}
10092.0	2.18440×10^{-11}	1.08675×10^{-12}	10117.1	6.33532×10^{-12}	3.11286×10^{-13}
10092.6	2.11138×10^{-11}	1.04980×10^{-12}	10117.7	6.22545×10^{-12}	3.06259×10^{-13}
10093.2	2.03506×10^{-11}	1.01120×10^{-12}	10118.4	6.10828×10^{-12}	3.00740×10^{-13}
10093.9	1.95637×10^{-11}	9.71460×10^{-13}	10119.0	5.98381×10^{-12}	2.94722×10^{-13}
10094.5	1.87669×10^{-11}	9.31151×10^{-13}	10119.6	5.85249×10^{-12}	2.88243×10^{-13}
10095.1	1.79675×10^{-11}	8.90779×10^{-13}	10120.3	5.71481×10^{-12}	2.81354×10^{-13}
10095.8	1.71766×10^{-11}	8.50818×10^{-13}	10120.9	5.57180×10^{-12}	2.74118×10^{-13}
10096.4	1.64010×10^{-11}	8.11681×10^{-13}	10121.5	5.42473×10^{-12}	2.66608×10^{-13}
10097.0	1.56494×10^{-11}	7.73685×10^{-13}	10122.1	5.27491×10^{-12}	2.58933×10^{-13}
10097.6	1.49257×10^{-11}	7.37107×10^{-13}	10122.8	5.12353×10^{-12}	2.51160×10^{-13}
10098.3	1.42359×10^{-11}	7.02144×10^{-13}	10123.4	4.97214×10^{-12}	2.43397×10^{-13}
10098.9	1.35800×10^{-11}	6.68946×10^{-13}	10124.0	4.82200×10^{-12}	2.35712×10^{-13}
10099.5	1.29624×10^{-11}	6.37585×10^{-13}	10124.6	4.67431×10^{-12}	2.28172×10^{-13}
10100.2	1.23813×10^{-11}	6.08087×10^{-13}	10125.3	4.53003×10^{-12}	2.20847×10^{-13}
10100.8	1.18396×10^{-11}	5.80463×10^{-13}	10125.9	4.38995×10^{-12}	2.13792×10^{-13}
10101.4	1.13347×10^{-11}	5.54715×10^{-13}	10126.5	4.25491×10^{-12}	2.07032×10^{-13}
10102.0	1.08659×10^{-11}	5.30786×10^{-13}	10127.2	4.12550×10^{-12}	2.00582×10^{-13}
10102.7	1.04330×10^{-11}	5.08620×10^{-13}	10127.8	4.00177×10^{-12}	1.94487×10^{-13}

Table A.15 (cont'd)

JD +2440000	*UVOIR* Flux	Flux error	JD +2440000	*UVOIR* Flux	Flux error
10128.4	3.88420×10^{-12}	1.88728×10^{-13}	10153.5	1.89037×10^{-12}	9.16482×10^{-14}
10129.0	3.77274×10^{-12}	1.83308×10^{-13}	10154.2	1.86524×10^{-12}	9.03564×10^{-14}
10129.7	3.66732×10^{-12}	1.78216×10^{-13}	10154.8	1.84054×10^{-12}	8.90870×10^{-14}
10130.3	3.56787×10^{-12}	1.73457×10^{-13}	10155.4	1.81616×10^{-12}	8.78394×10^{-14}
10130.9	3.47419×10^{-12}	1.68986×10^{-13}	10156.1	1.79211×10^{-12}	8.66124×10^{-14}
10131.6	3.38590×10^{-12}	1.64806×10^{-13}	10156.7	1.76861×10^{-12}	8.54075×10^{-14}
10132.2	3.30289×10^{-12}	1.60885×10^{-13}	10157.3	1.74534×10^{-12}	8.42226×10^{-14}
10132.8	3.22477×10^{-12}	1.57203×10^{-13}	10157.9	1.72251×10^{-12}	8.30579×10^{-14}
10133.4	3.15121×10^{-12}	1.53749×10^{-13}	10158.6	1.70002×10^{-12}	8.19144×10^{-14}
10134.1	3.08180×10^{-12}	1.50492×10^{-13}	10159.2	1.67787×10^{-12}	8.07902×10^{-14}
10134.7	3.01623×10^{-12}	1.47410×10^{-13}	10159.8	1.65607×10^{-12}	7.96853×10^{-14}
10135.3	2.95439×10^{-12}	1.44504×10^{-13}	10160.5	1.63472×10^{-12}	7.85999×10^{-14}
10136.0	2.89563×10^{-12}	1.41730×10^{-13}	10161.1	1.61360×10^{-12}	7.75327×10^{-14}
10136.6	2.83997×10^{-12}	1.39100×10^{-13}	10161.7	1.59283×10^{-12}	7.64850×10^{-14}
10137.2	2.78708×10^{-12}	1.36580×10^{-13}	10162.3	1.57241×10^{-12}	7.54544×10^{-14}
10137.8	2.73662×10^{-12}	1.34172×10^{-13}	10163.0	1.55222×10^{-12}	7.44419×10^{-14}
10138.5	2.68839×10^{-12}	1.31854×10^{-13}	10163.6	1.53248×10^{-12}	7.34466×10^{-14}
10139.1	2.64228×10^{-12}	1.29624×10^{-13}	10164.2	1.51296×10^{-12}	7.24681×10^{-14}
10139.7	2.59805×10^{-12}	1.27484×10^{-13}	10164.8	1.49368×10^{-12}	7.15063×10^{-14}
10140.4	2.55560×10^{-12}	1.25400×10^{-13}	10165.5	1.47472×10^{-12}	7.05602×10^{-14}
10141.0	2.51460×10^{-12}	1.23393×10^{-13}	10166.1	1.45610×10^{-12}	6.96294×10^{-14}
10141.6	2.47515×10^{-12}	1.21431×10^{-13}	10166.7	1.43769×10^{-12}	6.87138×10^{-14}
10142.2	2.43691×10^{-12}	1.19536×10^{-13}	10167.4	1.41961×10^{-12}	6.78134×10^{-14}
10142.9	2.40000×10^{-12}	1.17685×10^{-13}	10168.0	1.40163×10^{-12}	6.69268×10^{-14}
10143.5	2.36407×10^{-12}	1.15888×10^{-13}	10168.6	1.38408×10^{-12}	6.60539×10^{-14}
10144.1	2.32923×10^{-12}	1.14124×10^{-13}	10169.2	1.36662×10^{-12}	6.51935×10^{-14}
10144.7	2.29536×10^{-12}	1.12415×10^{-13}	10169.9	1.34948×10^{-12}	6.43478×10^{-14}
10145.4	2.26225×10^{-12}	1.10727×10^{-13}	10170.5	1.33254×10^{-12}	6.35143×10^{-14}
10146.0	2.23000×10^{-12}	1.09092×10^{-13}	10171.1	1.31580×10^{-12}	6.26933×10^{-14}
10146.6	2.19849×10^{-12}	1.07479×10^{-13}	10171.8	1.29927×10^{-12}	6.18846×10^{-14}
10147.3	2.16772×10^{-12}	1.05901×10^{-13}	10172.4	1.28305×10^{-12}	6.10883×10^{-14}
10147.9	2.13758×10^{-12}	1.04355×10^{-13}	10173.0	1.26692×10^{-12}	6.03044×10^{-14}
10148.5	2.10807×10^{-12}	1.02839×10^{-13}	10173.6	1.25111×10^{-12}	5.95320×10^{-14}
10149.1	2.07908×10^{-12}	1.01350×10^{-13}	10174.3	1.23540×10^{-12}	5.87713×10^{-14}
10149.8	2.05071×10^{-12}	9.98898×10^{-14}	10174.9	1.22002×10^{-12}	5.80222×10^{-14}
10150.4	2.02275×10^{-12}	9.84551×10^{-14}	10175.5	1.20474×10^{-12}	5.72852×10^{-14}
10151.0	1.99542×10^{-12}	9.70454×10^{-14}	10176.2	1.18968×10^{-12}	5.65592×10^{-14}
10151.7	1.96851×10^{-12}	9.56606×10^{-14}	10176.8	1.17496×10^{-12}	5.58455×10^{-14}
10152.3	1.94201×10^{-12}	9.43000×10^{-14}	10177.4	1.16036×10^{-12}	5.51434×10^{-14}
10152.9	1.91603×10^{-12}	9.29625×10^{-14}	10178.0	1.14600×10^{-12}	5.44529×10^{-14}

Table A.15 (cont'd)

JD +2440000	*UVOIR* Flux	Flux error	JD +2440000	*UVOIR* Flux	Flux error
10178.7	1.13176×10^{-12}	5.37741×10^{-14}	10185.6	9.89106×10^{-13}	4.70117×10^{-14}
10179.3	1.11787×10^{-12}	5.31062×10^{-14}	10186.2	9.77112×10^{-13}	4.64499×10^{-14}
10179.9	1.10411×10^{-12}	5.24503×10^{-14}	10186.8	9.65242×10^{-13}	4.58949×10^{-14}
10180.6	1.09059×10^{-12}	5.18063×10^{-14}	10187.5	9.53486×10^{-13}	4.53468×10^{-14}
10181.2	1.07727×10^{-12}	5.11731×10^{-14}	10188.1	9.41857×10^{-13}	4.48050×10^{-14}
10181.8	1.06415×10^{-12}	5.05506×10^{-14}	10188.7	9.30384×10^{-13}	4.42716×10^{-14}
10182.4	1.05123×10^{-12}	4.99374×10^{-14}	10189.3	9.19082×10^{-13}	4.37472×10^{-14}
10183.1	1.03848×10^{-12}	4.93354×10^{-14}	10190.0	9.08018×10^{-13}	4.32344×10^{-14}
10183.7	1.02591×10^{-12}	4.87420×10^{-14}	10190.6	8.97272×10^{-13}	4.27383×10^{-14}
10184.3	1.01350×10^{-12}	4.81569×10^{-14}	10191.2	8.86945×10^{-13}	4.22619×10^{-14}

Table A.16. SN 1996X

JD +2440000	*UVOIR* Flux	Flux error	JD +2440000	*UVOIR* Flux	Flux error
50170.6	2.67550×10^{-11}	2.44650×10^{-12}	50194.7	1.08250e-10	4.82300×10^{-12}
50171.2	2.67410×10^{-11}	2.40590×10^{-12}	50195.3	1.04770e-10	4.67100×10^{-12}
50171.8	2.67910×10^{-11}	2.36680×10^{-12}	50195.9	1.01080e-10	4.50940×10^{-12}
50172.4	2.69130×10^{-11}	2.32960×10^{-12}	50196.5	9.72280×10^{-11}	4.34030×10^{-12}
50173.0	2.66190×10^{-11}	2.29460×10^{-12}	50197.1	9.32720×10^{-11}	4.16570×10^{-12}
50173.6	2.69200×10^{-11}	2.26220×10^{-12}	50197.7	8.92570×10^{-11}	3.98780×10^{-12}
50174.2	2.73260×10^{-11}	2.23290×10^{-12}	50198.3	8.52280×10^{-11}	3.80840×10^{-12}
50174.8	2.78520×10^{-11}	2.20700×10^{-12}	50198.9	8.12260×10^{-11}	3.62950×10^{-12}
50175.4	2.85170×10^{-11}	2.18510×10^{-12}	50199.5	7.72890×10^{-11}	3.45290×10^{-12}
50176.0	2.93430×10^{-11}	2.16800×10^{-12}	50200.2	7.34480×10^{-11}	3.28010×10^{-12}
50176.6	3.03540×10^{-11}	2.15670×10^{-12}	50200.8	6.97330×10^{-11}	3.11240×10^{-12}
50177.2	3.15750×10^{-11}	2.15250×10^{-12}	50201.4	6.61650×10^{-11}	2.95090×10^{-12}
50177.8	3.30340×10^{-11}	2.15710×10^{-12}	50202.0	6.27610×10^{-11}	2.79660×10^{-12}
50178.4	3.47690×10^{-11}	2.17260×10^{-12}	50202.6	5.95360×10^{-11}	2.65010×10^{-12}
50179.0	3.67800×10^{-11}	2.20130×10^{-12}	50203.2	5.64970×10^{-11}	2.51190×10^{-12}
50179.6	3.91130×10^{-11}	2.24570×10^{-12}	50203.8	5.36500×10^{-11}	2.38240×10^{-12}
50180.2	4.18590×10^{-11}	2.30800×10^{-12}	50204.4	5.09960×10^{-11}	2.26170×10^{-12}
50180.9	4.51820×10^{-11}	2.39050×10^{-12}	50205.0	4.85360×10^{-11}	2.14990×10^{-12}
50181.5	4.92740×10^{-11}	2.49630×10^{-12}	50205.6	4.62670×10^{-11}	2.04710×10^{-12}
50182.1	5.42610×10^{-11}	2.63070×10^{-12}	50206.2	4.41850×10^{-11}	1.95310×10^{-12}
50182.7	6.01460×10^{-11}	2.80100×10^{-12}	50206.8	4.22840×10^{-11}	1.86780×10^{-12}
50183.3	6.67930×10^{-11}	3.01320×10^{-12}	50207.4	4.05590×10^{-11}	1.79100×10^{-12}
50183.9	7.39570×10^{-11}	3.26680×10^{-12}	50208.0	3.90000×10^{-11}	1.72240×10^{-12}
50184.5	8.13370×10^{-11}	3.55330×10^{-12}	50208.6	3.75990×10^{-11}	1.66160×10^{-12}
50185.1	8.86220×10^{-11}	3.85770×10^{-12}	50209.2	3.63460×10^{-11}	1.60820×10^{-12}
50185.7	9.55340×10^{-11}	4.16230×10^{-12}	50209.8	3.52270×10^{-11}	1.56160×10^{-12}
50186.3	1.01850e-10	4.45090×10^{-12}	50210.4	3.42300×10^{-11}	1.52110×10^{-12}
50186.9	1.07390e-10	4.71070×10^{-12}	50211.0	3.33380×10^{-11}	1.48580×10^{-12}
50187.5	1.12070e-10	4.93290×10^{-12}	50211.6	3.25340×10^{-11}	1.45480×10^{-12}
50188.1	1.15830e-10	5.11300×10^{-12}	50212.2	3.17990×10^{-11}	1.42700×10^{-12}
50188.7	1.18670e-10	5.24960×10^{-12}	50212.8	3.11130×10^{-11}	1.40130×10^{-12}
50189.3	1.20620e-10	5.34380×10^{-12}	50213.4	3.04570×10^{-11}	1.37670×10^{-12}
50189.9	1.21720e-10	5.39810×10^{-12}	50214.0	2.98120×10^{-11}	1.35200×10^{-12}
50190.5	1.22030e-10	5.41610×10^{-12}	50214.6	2.91580×10^{-11}	1.32640×10^{-12}
50191.1	1.21640e-10	5.40150×10^{-12}	50215.2	2.84830×10^{-11}	1.29910×10^{-12}
50191.7	1.20610e-10	5.35820×10^{-12}	50215.8	2.77740×10^{-11}	1.26960×10^{-12}
50192.3	1.19010e-10	5.28960×10^{-12}	50216.4	2.70270×10^{-11}	1.23750×10^{-12}
50192.9	1.16920e-10	5.19900×10^{-12}	50217.0	2.62380×10^{-11}	1.20280×10^{-12}
50193.5	1.14380e-10	5.08930×10^{-12}	50217.6	2.54110×10^{-11}	1.16580×10^{-12}
50194.1	1.11480e-10	4.96320×10^{-12}	50218.2	2.45540×10^{-11}	1.12680×10^{-12}

Table A.16 (cont'd)

JD +2440000	*UVOIR* Flux	Flux error	JD +2440000	*UVOIR* Flux	Flux error
50218.8	2.36760×10^{-11}	1.08650×10^{-12}	50243.0	8.78420×10^{-12}	3.93030×10^{-13}
50219.4	2.27890×10^{-11}	1.04540×10^{-12}	50243.6	8.64880×10^{-12}	3.86740×10^{-13}
50220.1	2.19060×10^{-11}	1.00420×10^{-12}	50244.2	8.51590×10^{-12}	3.80580×10^{-13}
50220.7	2.10380×10^{-11}	9.63510×10^{-13}	50244.8	8.38560×10^{-12}	3.74540×10^{-13}
50221.3	2.01970×10^{-11}	9.23980×10^{-13}	50245.4	8.25770×10^{-12}	3.68620×10^{-13}
50221.9	1.93920×10^{-11}	8.86050×10^{-13}	50246.0	8.13220×10^{-12}	3.62810×10^{-13}
50222.5	1.86280×10^{-11}	8.50100×10^{-13}	50246.6	8.00890×10^{-12}	3.57120×10^{-13}
50223.1	1.79120×10^{-11}	8.16360×10^{-13}	50247.2	7.88790×10^{-12}	3.51550×10^{-13}
50223.7	1.72440×10^{-11}	7.84980×10^{-13}	50247.8	7.76910×10^{-12}	3.46080×10^{-13}
50224.3	1.66250×10^{-11}	7.55990×10^{-13}	50248.4	7.65240×10^{-12}	3.40710×10^{-13}
50224.9	1.60560×10^{-11}	7.29350×10^{-13}	50249.0	7.53770×10^{-12}	3.35450×10^{-13}
50225.5	1.55320×10^{-11}	7.04950×10^{-13}	50249.6	7.42510×10^{-12}	3.30290×10^{-13}
50226.1	1.50510×10^{-11}	6.82650×10^{-13}	50250.2	7.31440×10^{-12}	3.25230×10^{-13}
50226.7	1.46110×10^{-11}	6.62250×10^{-13}	50250.8	7.20560×10^{-12}	3.20260×10^{-13}
50227.3	1.42060×10^{-11}	6.43590×10^{-13}	50251.4	7.09870×10^{-12}	3.15390×10^{-13}
50227.9	1.38340×10^{-11}	6.26460×10^{-13}	50252.0	6.99370×10^{-12}	3.10610×10^{-13}
50228.5	1.34910×10^{-11}	6.10690×10^{-13}	50252.6	6.89040×10^{-12}	3.05920×10^{-13}
50229.1	1.31730×10^{-11}	5.96100×10^{-13}	50253.2	6.78890×10^{-12}	3.01320×10^{-13}
50229.7	1.28770×10^{-11}	5.82540×10^{-13}	50253.8	6.68910×10^{-12}	2.96810×10^{-13}
50230.3	1.26010×10^{-11}	5.69870×10^{-13}	50254.4	6.59100×10^{-12}	2.92380×10^{-13}
50230.9	1.23410×10^{-11}	5.57960×10^{-13}	50255.0	6.49450×10^{-12}	2.88030×10^{-13}
50231.5	1.20960×10^{-11}	5.46710×10^{-13}	50255.6	6.39960×10^{-12}	2.83760×10^{-13}
50232.1	1.18640×10^{-11}	5.36030×10^{-13}	50256.2	6.30630×10^{-12}	2.79570×10^{-13}
50232.7	1.16430×10^{-11}	5.25830×10^{-13}	50256.8	6.21460×10^{-12}	2.75460×10^{-13}
50233.3	1.14310×10^{-11}	5.16070×10^{-13}	50257.4	6.12440×10^{-12}	2.71430×10^{-13}
50233.9	1.12280×10^{-11}	5.06670×10^{-13}	50258.0	6.03580×10^{-12}	2.67470×10^{-13}
50234.5	1.10320×10^{-11}	4.97610×10^{-13}	50258.6	5.94850×10^{-12}	2.63580×10^{-13}
50235.1	1.08430×10^{-11}	4.88830×10^{-13}	50259.2	5.86270×10^{-12}	2.59760×10^{-13}
50235.7	1.06590×10^{-11}	4.80320×10^{-13}	50259.8	5.77840×10^{-12}	2.56020×10^{-13}
50236.3	1.04810×10^{-11}	4.72040×10^{-13}	50260.5	5.69540×10^{-12}	2.52340×10^{-13}
50236.9	1.03080×10^{-11}	4.63990×10^{-13}	50261.1	5.61380×10^{-12}	2.48730×10^{-13}
50237.5	1.01390×10^{-11}	4.56140×10^{-13}	50261.7	5.53350×10^{-12}	2.45180×10^{-13}
50238.1	9.97480×10^{-12}	4.48480×10^{-13}	50262.3	5.45460×10^{-12}	2.41700×10^{-13}
50238.7	9.81430×10^{-12}	4.41000×10^{-13}	50262.9	5.37690×10^{-12}	2.38290×10^{-13}
50239.3	9.65750×10^{-12}	4.33690×10^{-13}	50263.5	5.30050×10^{-12}	2.34930×10^{-13}
50239.9	9.50410×10^{-12}	4.26540×10^{-13}	50264.1	5.22540×10^{-12}	2.31640×10^{-13}
50240.6	9.35400×10^{-12}	4.19550×10^{-13}	50264.7	5.15140×10^{-12}	2.28400×10^{-13}
50241.2	9.20720×10^{-12}	4.12710×10^{-13}	50265.3	5.07870×10^{-12}	2.25230×10^{-13}
50241.8	9.06330×10^{-12}	4.06010×10^{-13}	50265.9	5.00720×10^{-12}	2.22110×10^{-13}
50242.4	8.92240×10^{-12}	3.99450×10^{-13}	50266.5	4.93680×10^{-12}	2.19050×10^{-13}

Table A.16 (cont'd)

JD +2440000	*UVOIR* Flux	Flux error	JD +2440000	*UVOIR* Flux	Flux error
50267.1	4.86760×10^{-12}	2.16040×10^{-13}	50278.5	3.74440×10^{-12}	1.68040×10^{-13}
50267.7	4.79950×10^{-12}	2.13090×10^{-13}	50279.1	3.69420×10^{-12}	1.65930×10^{-13}
50268.3	4.73240×10^{-12}	2.10190×10^{-13}	50279.8	3.64490×10^{-12}	1.63860×10^{-13}
50268.9	4.66650×10^{-12}	2.07340×10^{-13}	50280.4	3.59630×10^{-12}	1.61820×10^{-13}
50269.5	4.60170×10^{-12}	2.04540×10^{-13}	50281.0	3.54840×10^{-12}	1.59820×10^{-13}
50270.1	4.53780×10^{-12}	2.01790×10^{-13}	50281.6	3.50130×10^{-12}	1.57850×10^{-13}
50270.7	4.47500×10^{-12}	1.99090×10^{-13}	50282.2	3.45500×10^{-12}	1.55910×10^{-13}
50271.3	4.41330×10^{-12}	1.96440×10^{-13}	50282.8	3.40930×10^{-12}	1.54010×10^{-13}
50271.9	4.35250×10^{-12}	1.93840×10^{-13}	50283.4	3.36440×10^{-12}	1.52140×10^{-13}
50272.5	4.29260×10^{-12}	1.91280×10^{-13}	50284.0	3.32020×10^{-12}	1.50300×10^{-13}
50273.1	4.23380×10^{-12}	1.88770×10^{-13}	50284.6	3.27660×10^{-12}	1.48500×10^{-13}
50273.7	4.17590×10^{-12}	1.86300×10^{-13}	50285.2	3.23380×10^{-12}	1.46720×10^{-13}
50274.3	4.11890×10^{-12}	1.83870×10^{-13}	50285.8	3.19160×10^{-12}	1.44970×10^{-13}
50274.9	4.06280×10^{-12}	1.81490×10^{-13}	50286.4	3.15000×10^{-12}	1.43250×10^{-13}
50275.5	4.00760×10^{-12}	1.79150×10^{-13}	50287.0	3.10910×10^{-12}	1.41560×10^{-13}
50276.1	3.95320×10^{-12}	1.76850×10^{-13}	50287.6	3.06880×10^{-12}	1.39900×10^{-13}
50276.7	3.89980×10^{-12}	1.74590×10^{-13}	50288.2	3.02910×10^{-12}	1.38270×10^{-13}
50277.3	3.84720×10^{-12}	1.72370×10^{-13}	50288.8	2.99010×10^{-12}	1.36660×10^{-13}
50277.9	3.79540×10^{-12}	1.70180×10^{-13}	50289.4	2.95160×10^{-12}	1.35080×10^{-13}

Table A.17. SN 1996bo

JD +2440000	*UVOIR* Flux	Flux error	JD +2440000	*UVOIR* Flux	Flux error
10378.3	6.86009×10^{-12}	3.80356×10^{-13}	10404.4	8.20690×10^{-12}	3.95651×10^{-13}
10378.9	9.52537×10^{-12}	5.04411×10^{-13}	10405.1	7.97835×10^{-12}	3.84494×10^{-13}
10379.6	1.22293×10^{-11}	6.28587×10^{-13}	10405.7	7.78609×10^{-12}	3.75138×10^{-13}
10380.3	1.46909×10^{-11}	7.44295×10^{-13}	10406.4	7.62434×10^{-12}	3.67322×10^{-13}
10380.9	1.67762×10^{-11}	8.45028×10^{-13}	10407.0	7.48638×10^{-12}	3.60741×10^{-13}
10381.6	1.84751×10^{-11}	9.28735×10^{-13}	10407.7	7.36439×10^{-12}	3.55011×10^{-13}
10382.2	1.98315×10^{-11}	9.96609×10^{-13}	10408.3	7.24992×10^{-12}	3.49752×10^{-13}
10382.9	2.09089×10^{-11}	1.05117×10^{-12}	10409.0	7.13413×10^{-12}	3.44565×10^{-13}
10383.5	2.17634×10^{-11}	1.09488×10^{-12}	10409.6	7.00874×10^{-12}	3.39032×10^{-13}
10384.2	2.24375×10^{-11}	1.12966×10^{-12}	10410.3	6.86674×10^{-12}	3.32818×10^{-13}
10384.8	2.29597×10^{-11}	1.15681×10^{-12}	10411.0	6.70315×10^{-12}	3.25664×10^{-13}
10385.5	2.33470×10^{-11}	1.17705×10^{-12}	10411.6	6.51592×10^{-12}	3.17438×10^{-13}
10386.1	2.36091×10^{-11}	1.19074×10^{-12}	10412.3	6.30598×10^{-12}	3.08167×10^{-13}
10386.8	2.37495×10^{-11}	1.19800×10^{-12}	10412.9	6.07692×10^{-12}	2.97981×10^{-13}
10387.4	2.37712×10^{-11}	1.19887×10^{-12}	10413.6	5.83424×10^{-12}	2.87088×10^{-13}
10388.1	2.36741×10^{-11}	1.19337×10^{-12}	10414.2	5.58428×10^{-12}	2.75773×10^{-13}
10388.7	2.34589×10^{-11}	1.18155×10^{-12}	10414.9	5.33366×10^{-12}	2.64299×10^{-13}
10389.4	2.31270×10^{-11}	1.16361×10^{-12}	10415.5	5.08805×10^{-12}	2.52912×10^{-13}
10390.0	2.26854×10^{-11}	1.13983×10^{-12}	10416.2	4.85222×10^{-12}	2.41827×10^{-13}
10390.7	2.21392×10^{-11}	1.11067×10^{-12}	10416.8	4.62966×10^{-12}	2.31188×10^{-13}
10391.4	2.15004×10^{-11}	1.07669×10^{-12}	10417.5	4.42247×10^{-12}	2.21118×10^{-13}
10392.0	2.07796×10^{-11}	1.03860×10^{-12}	10418.1	4.23189×10^{-12}	2.11692×10^{-13}
10392.7	1.99943×10^{-11}	9.97219×10^{-13}	10418.8	4.05823×10^{-12}	2.02949×10^{-13}
10393.3	1.91578×10^{-11}	9.53386×10^{-13}	10419.4	3.90116×10^{-12}	1.94912×10^{-13}
10394.0	1.82880×10^{-11}	9.07962×10^{-13}	10420.1	3.75964×10^{-12}	1.87571×10^{-13}
10394.6	1.74007×10^{-11}	8.61829×10^{-13}	10420.8	3.63272×10^{-12}	1.80894×10^{-13}
10395.3	1.65106×10^{-11}	8.15772×10^{-13}	10421.4	3.51893×10^{-12}	1.74840×10^{-13}
10395.9	1.56332×10^{-11}	7.70479×10^{-13}	10422.1	3.41699×10^{-12}	1.69368×10^{-13}
10396.6	1.47782×10^{-11}	7.26556×10^{-13}	10422.7	3.32533×10^{-12}	1.64414×10^{-13}
10397.2	1.39577×10^{-11}	6.84502×10^{-13}	10423.4	3.24267×10^{-12}	1.59927×10^{-13}
10397.9	1.31775×10^{-11}	6.44689×10^{-13}	10424.0	3.16776×10^{-12}	1.55853×10^{-13}
10398.5	1.24438×10^{-11}	6.07387×10^{-13}	10424.7	3.09942×10^{-12}	1.52129×10^{-13}
10399.2	1.17604×10^{-11}	5.72796×10^{-13}	10425.3	3.03682×10^{-12}	1.48715×10^{-13}
10399.8	1.11302×10^{-11}	5.41026×10^{-13}	10426.0	2.97891×10^{-12}	1.45567×10^{-13}
10400.5	1.05547×10^{-11}	5.12114×10^{-13}	10426.6	2.92495×10^{-12}	1.42634×10^{-13}
10401.2	1.00341×10^{-11}	4.86077×10^{-13}	10427.3	2.87444×10^{-12}	1.39895×10^{-13}
10401.8	9.56759×10^{-12}	4.62832×10^{-13}	10427.9	2.82675×10^{-12}	1.37318×10^{-13}
10402.5	9.15386×10^{-12}	4.42299×10^{-13}	10428.6	2.78137×10^{-12}	1.34874×10^{-13}
10403.1	8.79103×10^{-12}	4.24375×10^{-13}	10429.2	2.73821×10^{-12}	1.32552×10^{-13}
10403.8	8.47640×10^{-12}	4.08881×10^{-13}	10429.9	2.69675×10^{-12}	1.30332×10^{-13}

Table A.17 (cont'd)

JD +2440000	*UVOIR* Flux	Flux error	JD +2440000	*UVOIR* Flux	Flux error
10430.6	2.65681×10^{-12}	1.28193×10^{-13}	10456.7	1.62237×10^{-12}	7.63155×10^{-14}
10431.2	2.61819×10^{-12}	1.26136×10^{-13}	10457.3	1.60432×10^{-12}	7.55003×10^{-14}
10431.9	2.58091×10^{-12}	1.24153×10^{-13}	10458.0	1.58661×10^{-12}	7.47005×10^{-14}
10432.5	2.54456×10^{-12}	1.22232×10^{-13}	10458.6	1.56924×10^{-12}	7.39153×10^{-14}
10433.2	2.50937×10^{-12}	1.20364×10^{-13}	10459.3	1.55199×10^{-12}	7.31449×10^{-14}
10433.8	2.47504×10^{-12}	1.18550×10^{-13}	10460.0	1.53508×10^{-12}	7.23892×10^{-14}
10434.5	2.44158×10^{-12}	1.16791×10^{-13}	10460.6	1.51840×10^{-12}	7.16485×10^{-14}
10435.1	2.40889×10^{-12}	1.15075×10^{-13}	10461.3	1.50207×10^{-12}	7.09205×10^{-14}
10435.8	2.37708×10^{-12}	1.13404×10^{-13}	10461.9	1.48586×10^{-12}	7.02064×10^{-14}
10436.4	2.34596×10^{-12}	1.11777×10^{-13}	10462.6	1.47000×10^{-12}	6.95061×10^{-14}
10437.1	2.31552×10^{-12}	1.10196×10^{-13}	10463.2	1.45436×10^{-12}	6.88185×10^{-14}
10437.7	2.28577×10^{-12}	1.08660×10^{-13}	10463.9	1.43897×10^{-12}	6.81425×10^{-14}
10438.4	2.25671×10^{-12}	1.07157×10^{-13}	10464.5	1.42380×10^{-12}	6.74801×10^{-14}
10439.0	2.22823×10^{-12}	1.05693×10^{-13}	10465.2	1.40875×10^{-12}	6.68278×10^{-14}
10439.7	2.20034×10^{-12}	1.04266×10^{-13}	10465.8	1.39403×10^{-12}	6.61878×10^{-14}
10440.4	2.17302×10^{-12}	1.02873×10^{-13}	10466.5	1.37953×10^{-12}	6.55578×10^{-14}
10441.0	2.14627×10^{-12}	1.01514×10^{-13}	10467.1	1.36514×10^{-12}	6.49386×10^{-14}
10441.7	2.11999×10^{-12}	1.00187×10^{-13}	10467.8	1.35097×10^{-12}	6.43301×10^{-14}
10442.3	2.09427×10^{-12}	9.88916×10^{-14}	10468.4	1.33711×10^{-12}	6.37300×10^{-14}
10443.0	2.06900×10^{-12}	9.76260×10^{-14}	10469.1	1.32325×10^{-12}	6.31391×10^{-14}
10443.6	2.04418×10^{-12}	9.63892×10^{-14}	10469.7	1.30970×10^{-12}	6.25575×10^{-14}
10444.3	2.01980×10^{-12}	9.51799×10^{-14}	10470.4	1.29624×10^{-12}	6.19837×10^{-14}
10444.9	1.99585×10^{-12}	9.39976×10^{-14}	10471.1	1.28298×10^{-12}	6.14180×10^{-14}
10445.6	1.97233×10^{-12}	9.28401×10^{-14}	10471.7	1.26993×10^{-12}	6.08611×10^{-14}
10446.2	1.94913×10^{-12}	9.17072×10^{-14}	10472.4	1.25696×10^{-12}	6.03111×10^{-14}
10446.9	1.92634×10^{-12}	9.05974×10^{-14}	10473.0	1.24420×10^{-12}	5.97689×10^{-14}
10447.5	1.90387×10^{-12}	8.95106×10^{-14}	10473.7	1.23164×10^{-12}	5.92336×10^{-14}
10448.2	1.88180×10^{-12}	8.84457×10^{-14}	10474.3	1.21918×10^{-12}	5.87054×10^{-14}
10448.8	1.86004×10^{-12}	8.74015×10^{-14}	10475.0	1.20682×10^{-12}	5.81842×10^{-14}
10449.5	1.83858×10^{-12}	8.63777×10^{-14}	10475.6	1.19467×10^{-12}	5.76716×10^{-14}
10450.2	1.81753×10^{-12}	8.53746×10^{-14}	10476.3	1.18263×10^{-12}	5.71654×10^{-14}
10450.8	1.79667×10^{-12}	8.43898×10^{-14}	10476.9	1.17081×10^{-12}	5.66659×10^{-14}
10451.5	1.77622×10^{-12}	8.34234×10^{-14}	10477.6	1.15922×10^{-12}	5.61745×10^{-14}
10452.1	1.75596×10^{-12}	8.24756×10^{-14}	10478.2	1.14765×10^{-12}	5.56902×10^{-14}
10452.8	1.73601×10^{-12}	8.15453×10^{-14}	10478.9	1.13630×10^{-12}	5.52132×10^{-14}
10453.4	1.71637×10^{-12}	8.06315×10^{-14}	10479.5	1.12509×10^{-12}	5.47438×10^{-14}
10454.1	1.69704×10^{-12}	7.97355×10^{-14}	10480.2	1.11412×10^{-12}	5.42820×10^{-14}
10454.7	1.67792×10^{-12}	7.88564×10^{-14}	10480.9	1.10328×10^{-12}	5.38279×10^{-14}
10455.4	1.65911×10^{-12}	7.79933×10^{-14}	10481.5	1.09258×10^{-12}	5.33803×10^{-14}
10456.0	1.64063×10^{-12}	7.71463×10^{-14}	10482.2	1.08211×10^{-12}	5.29391×10^{-14}

Table A.17 (cont'd)

JD +2440000	*UVOIR* Flux	Flux error	JD +2440000	*UVOIR* Flux	Flux error
10482.8	1.07170×10^{-12}	5.25052×10^{-14}	10486.7	1.01195×10^{-12}	5.00050×10^{-14}
10483.5	1.06146×10^{-12}	5.20771×10^{-14}	10487.4	1.00230×10^{-12}	4.95997×10^{-14}
10484.1	1.05135×10^{-12}	5.16544×10^{-14}	10488.0	9.92740×10^{-13}	4.91978×10^{-14}
10484.8	1.04136×10^{-12}	5.12365×10^{-14}	10488.7	9.83248×10^{-13}	4.87987×10^{-14}
10485.4	1.03147×10^{-12}	5.08220×10^{-14}	10489.3	9.73872×10^{-13}	4.84048×10^{-14}
10486.1	1.02167×10^{-12}	5.04123×10^{-14}	10490.0	9.64660×10^{-13}	4.80164×10^{-14}

Table A.18. SN 1997bp

JD +2450000	*UVOIR* Flux	Flux error	JD +2450000	*UVOIR* Flux	Flux error
545.553	6.84350×10^{-11}	3.05150×10^{-12}	567.663	2.81600×10^{-11}	1.25200×10^{-12}
546.106	7.03540×10^{-11}	3.14190×10^{-12}	568.216	2.74550×10^{-11}	1.22360×10^{-12}
546.658	7.19970×10^{-11}	3.21910×10^{-12}	568.769	2.68180×10^{-11}	1.19850×10^{-12}
547.211	7.33560×10^{-11}	3.28270×10^{-12}	569.322	2.62430×10^{-11}	1.17650×10^{-12}
547.764	7.44250×10^{-11}	3.33230×10^{-12}	569.874	2.57270×10^{-11}	1.15730×10^{-12}
548.317	7.52030×10^{-11}	3.36800×10^{-12}	570.427	2.52650×10^{-11}	1.14080×10^{-12}
548.869	7.56910×10^{-11}	3.38980×10^{-12}	570.980	2.48490×10^{-11}	1.12660×10^{-12}
549.422	7.58940×10^{-11}	3.39810×10^{-12}	571.533	2.44750×10^{-11}	1.11430×10^{-12}
549.975	7.58180×10^{-11}	3.39340×10^{-12}	572.085	2.41330×10^{-11}	1.10370×10^{-12}
550.528	7.54730×10^{-11}	3.37630×10^{-12}	572.638	2.38170×10^{-11}	1.09430×10^{-12}
551.080	7.48710×10^{-11}	3.34750×10^{-12}	573.191	2.35150×10^{-11}	1.08540×10^{-12}
551.633	7.40260×10^{-11}	3.30760×10^{-12}	573.744	2.32200×10^{-11}	1.07670×10^{-12}
552.186	7.29540×10^{-11}	3.25760×10^{-12}	574.297	2.29200×10^{-11}	1.06740×10^{-12}
552.739	7.16730×10^{-11}	3.19820×10^{-12}	574.849	2.26070×10^{-11}	1.05700×10^{-12}
553.291	7.02050×10^{-11}	3.13050×10^{-12}	575.402	2.22720×10^{-11}	1.04510×10^{-12}
553.844	6.85710×10^{-11}	3.05550×10^{-12}	575.955	2.19080×10^{-11}	1.03110×10^{-12}
554.397	6.67960×10^{-11}	2.97430×10^{-12}	576.508	2.15110×10^{-11}	1.01480×10^{-12}
554.950	6.49040×10^{-11}	2.88790×10^{-12}	577.060	2.10770×10^{-11}	9.96010×10^{-13}
555.503	6.29200×10^{-11}	2.79750×10^{-12}	577.613	2.06070×10^{-11}	9.74770×10^{-13}
556.055	6.08700×10^{-11}	2.70420×10^{-12}	578.166	2.01030×10^{-11}	9.51270×10^{-13}
556.608	5.87780×10^{-11}	2.60920×10^{-12}	578.719	1.95700×10^{-11}	9.25820×10^{-13}
557.161	5.66680×10^{-11}	2.51340×10^{-12}	579.271	1.90140×10^{-11}	8.98870×10^{-13}
557.714	5.45590×10^{-11}	2.41780×10^{-12}	579.824	1.84430×10^{-11}	8.70880×10^{-13}
558.266	5.24710×10^{-11}	2.32330×10^{-12}	580.377	1.78650×10^{-11}	8.42380×10^{-13}
558.819	5.04210×10^{-11}	2.23070×10^{-12}	580.930	1.72870×10^{-11}	8.13820×10^{-13}
559.372	4.84230×10^{-11}	2.14060×10^{-12}	581.482	1.67170×10^{-11}	7.85670×10^{-13}
559.925	4.64880×10^{-11}	2.05350×10^{-12}	582.035	1.61610×10^{-11}	7.58270×10^{-13}
560.477	4.46240×10^{-11}	1.96980×10^{-12}	582.588	1.56240×10^{-11}	7.31930×10^{-13}
561.030	4.28400×10^{-11}	1.88990×10^{-12}	583.141	1.51100×10^{-11}	7.06860×10^{-13}
561.583	4.11400×10^{-11}	1.81400×10^{-12}	583.693	1.46220×10^{-11}	6.83200×10^{-13}
562.136	3.95270×10^{-11}	1.74230×10^{-12}	584.246	1.41620×10^{-11}	6.61020×10^{-13}
562.688	3.80040×10^{-11}	1.67480×10^{-12}	584.799	1.37300×10^{-11}	6.40350×10^{-13}
563.241	3.65690×10^{-11}	1.61160×10^{-12}	585.352	1.33260×10^{-11}	6.21150×10^{-13}
563.794	3.52240×10^{-11}	1.55260×10^{-12}	585.905	1.29490×10^{-11}	6.03360×10^{-13}
564.347	3.39680×10^{-11}	1.49780×10^{-12}	586.457	1.25990×10^{-11}	5.86910×10^{-13}
564.899	3.27970×10^{-11}	1.44720×10^{-12}	587.010	1.22730×10^{-11}	5.71680×10^{-13}
565.452	3.17110×10^{-11}	1.40050×10^{-12}	587.563	1.19700×10^{-11}	5.57570×10^{-13}
566.005	3.07070×10^{-11}	1.35780×10^{-12}	588.116	1.16880×10^{-11}	5.44470×10^{-13}
566.558	2.97820×10^{-11}	1.31890×10^{-12}	588.668	1.14260×10^{-11}	5.32260×10^{-13}
567.111	2.89340×10^{-11}	1.28370×10^{-12}	589.221	1.11800×10^{-11}	5.20850×10^{-13}

Table A.18 (cont'd)

JD +2450000	*UVOIR* Flux	Flux error	JD +2450000	*UVOIR* Flux	Flux error
589.774	1.09510×10^{-11}	5.10150×10^{-13}	611.884	6.14930×10^{-12}	2.76850×10^{-13}
590.327	1.07350×10^{-11}	5.00060×10^{-13}	612.437	6.07270×10^{-12}	2.73230×10^{-13}
590.879	1.05320×10^{-11}	4.90510×10^{-13}	612.990	5.99750×10^{-12}	2.69680×10^{-13}
591.432	1.03400×10^{-11}	4.81440×10^{-13}	613.543	5.92350×10^{-12}	2.66200×10^{-13}
591.985	1.01570×10^{-11}	4.72780×10^{-13}	614.095	5.85060×10^{-12}	2.62790×10^{-13}
592.538	9.98390×10^{-12}	4.64500×10^{-13}	614.648	5.77900×10^{-12}	2.59440×10^{-13}
593.090	9.81820×10^{-12}	4.56540×10^{-13}	615.201	5.70860×10^{-12}	2.56160×10^{-13}
593.643	9.65950×10^{-12}	4.48880×10^{-13}	615.754	5.63920×10^{-12}	2.52940×10^{-13}
594.196	9.50690×10^{-12}	4.41480×10^{-13}	616.307	5.57100×10^{-12}	2.49790×10^{-13}
594.749	9.35990×10^{-12}	4.34310×10^{-13}	616.859	5.50390×10^{-12}	2.46700×10^{-13}
595.302	9.21790×10^{-12}	4.27350×10^{-13}	617.412	5.43790×10^{-12}	2.43670×10^{-13}
595.854	9.08030×10^{-12}	4.20590×10^{-13}	617.965	5.37300×10^{-12}	2.40690×10^{-13}
596.407	8.94680×10^{-12}	4.14010×10^{-13}	618.518	5.30900×10^{-12}	2.37780×10^{-13}
596.960	8.81690×10^{-12}	4.07600×10^{-13}	619.070	5.24610×10^{-12}	2.34920×10^{-13}
597.513	8.69050×10^{-12}	4.01340×10^{-13}	619.623	5.18420×10^{-12}	2.32110×10^{-13}
598.065	8.56710×10^{-12}	3.95230×10^{-13}	620.176	5.12330×10^{-12}	2.29360×10^{-13}
598.618	8.44660×10^{-12}	3.89250×10^{-13}	620.729	5.06340×10^{-12}	2.26660×10^{-13}
599.171	8.32870×10^{-12}	3.83400×10^{-13}	621.281	5.00440×10^{-12}	2.24020×10^{-13}
599.724	8.21340×10^{-12}	3.77670×10^{-13}	621.834	4.94640×10^{-12}	2.21420×10^{-13}
600.276	8.10050×10^{-12}	3.72070×10^{-13}	622.387	4.88920×10^{-12}	2.18880×10^{-13}
600.829	7.98980×10^{-12}	3.66570×10^{-13}	622.940	4.83300×10^{-12}	2.16380×10^{-13}
601.382	7.88130×10^{-12}	3.61190×10^{-13}	623.492	4.77770×10^{-12}	2.13930×10^{-13}
601.935	7.77480×10^{-12}	3.55920×10^{-13}	624.045	4.72320×10^{-12}	2.11520×10^{-13}
602.487	7.67030×10^{-12}	3.50750×10^{-13}	624.598	4.66950×10^{-12}	2.09160×10^{-13}
603.040	7.56780×10^{-12}	3.45680×10^{-13}	625.151	4.61680×10^{-12}	2.06850×10^{-13}
603.593	7.46700×10^{-12}	3.40720×10^{-13}	625.703	4.56480×10^{-12}	2.04580×10^{-13}
604.146	7.36810×10^{-12}	3.35840×10^{-13}	626.256	4.51360×10^{-12}	2.02350×10^{-13}
604.698	7.27090×10^{-12}	3.31070×10^{-13}	626.809	4.46330×10^{-12}	2.00160×10^{-13}
605.251	7.17550×10^{-12}	3.26390×10^{-13}	627.362	4.41370×10^{-12}	1.98010×10^{-13}
605.804	7.08170×10^{-12}	3.21800×10^{-13}	627.915	4.36490×10^{-12}	1.95910×10^{-13}
606.357	6.98950×10^{-12}	3.17290×10^{-13}	628.467	4.31690×10^{-12}	1.93840×10^{-13}
606.910	6.89890×10^{-12}	3.12880×10^{-13}	629.020	4.26960×10^{-12}	1.91810×10^{-13}
607.462	6.80980×10^{-12}	3.08550×10^{-13}	629.573	4.22300×10^{-12}	1.89810×10^{-13}
608.015	6.72230×10^{-12}	3.04310×10^{-13}	630.126	4.17710×10^{-12}	1.87850×10^{-13}
608.568	6.63620×10^{-12}	3.00150×10^{-13}	630.678	4.13200×10^{-12}	1.85930×10^{-13}
609.121	6.55160×10^{-12}	2.96070×10^{-13}	631.231	4.08750×10^{-12}	1.84040×10^{-13}
609.673	6.46840×10^{-12}	2.92080×10^{-13}	631.784	4.04370×10^{-12}	1.82190×10^{-13}
610.226	6.38660×10^{-12}	2.88160×10^{-13}	632.337	4.00060×10^{-12}	1.80370×10^{-13}
610.779	6.30620×10^{-12}	2.84310×10^{-13}	632.889	3.95820×10^{-12}	1.78580×10^{-13}
611.332	6.22710×10^{-12}	2.80550×10^{-13}	633.442	3.91640×10^{-12}	1.76820×10^{-13}

Table A.18 (cont'd)

JD +2450000	*UVOIR* Flux	Flux error	JD +2450000	*UVOIR* Flux	Flux error
633.995	3.87520×10^{-12}	1.75100×10^{-13}	644.497	3.20040×10^{-12}	1.47370×10^{-13}
634.548	3.83470×10^{-12}	1.73400×10^{-13}	645.050	3.16990×10^{-12}	1.46140×10^{-13}
635.101	3.79470×10^{-12}	1.71740×10^{-13}	645.603	3.13990×10^{-12}	1.44920×10^{-13}
635.653	3.75540×10^{-12}	1.70100×10^{-13}	646.156	3.11030×10^{-12}	1.43730×10^{-13}
636.206	3.71670×10^{-12}	1.68490×10^{-13}	646.709	3.08110×10^{-12}	1.42560×10^{-13}
636.759	3.67850×10^{-12}	1.66910×10^{-13}	647.261	3.05230×10^{-12}	1.41400×10^{-13}
637.312	3.64100×10^{-12}	1.65350×10^{-13}	647.814	3.02390×10^{-12}	1.40270×10^{-13}
637.864	3.60390×10^{-12}	1.63830×10^{-13}	648.367	2.99600×10^{-12}	1.39150×10^{-13}
638.417	3.56750×10^{-12}	1.62320×10^{-13}	648.920	2.96840×10^{-12}	1.38040×10^{-13}
638.970	3.53160×10^{-12}	1.60850×10^{-13}	649.472	2.94130×10^{-12}	1.36960×10^{-13}
639.523	3.49620×10^{-12}	1.59400×10^{-13}	650.025	2.91450×10^{-12}	1.35890×10^{-13}
640.075	3.46130×10^{-12}	1.57970×10^{-13}	650.578	2.88810×10^{-12}	1.34840×10^{-13}
640.628	3.42700×10^{-12}	1.56570×10^{-13}	651.131	2.86210×10^{-12}	1.33800×10^{-13}
641.181	3.39320×10^{-12}	1.55190×10^{-13}	651.683	2.83650×10^{-12}	1.32780×10^{-13}
641.734	3.35990×10^{-12}	1.53830×10^{-13}	652.236	2.81120×10^{-12}	1.31770×10^{-13}
642.286	3.32700×10^{-12}	1.52490×10^{-13}	652.789	2.78630×10^{-12}	1.30780×10^{-13}
642.839	3.29470×10^{-12}	1.51180×10^{-13}	653.342	2.76170×10^{-12}	1.29800×10^{-13}
643.392	3.26280×10^{-12}	1.49890×10^{-13}	653.894	2.73750×10^{-12}	1.28840×10^{-13}
643.945	3.23140×10^{-12}	1.48620×10^{-13}	654.447	2.71360×10^{-12}	1.27890×10^{-13}

Table A.19. SN 1997bq

JD +2450000	*UVOIR* Flux	Flux error	JD +2450000	*UVOIR* Flux	Flux error
547.593	1.79290×10^{-11}	8.40180×10^{-13}	571.312	3.16520×10^{-11}	1.44130×10^{-12}
548.186	2.27530×10^{-11}	1.03040×10^{-12}	571.905	3.03150×10^{-11}	1.37700×10^{-12}
548.779	2.73950×10^{-11}	1.23290×10^{-12}	572.497	2.90620×10^{-11}	1.31670×10^{-12}
549.372	3.15920×10^{-11}	1.42290×10^{-12}	573.090	2.78920×10^{-11}	1.26030×10^{-12}
549.965	3.53560×10^{-11}	1.59430×10^{-12}	573.683	2.68010×10^{-11}	1.20770×10^{-12}
550.558	3.87760×10^{-11}	1.74930×10^{-12}	574.276	2.57840×10^{-11}	1.15880×10^{-12}
551.151	4.19340×10^{-11}	1.89180×10^{-12}	574.869	2.48390×10^{-11}	1.11360×10^{-12}
551.744	4.48810×10^{-11}	2.02440×10^{-12}	575.462	2.39590×10^{-11}	1.07180×10^{-12}
552.337	4.76430×10^{-11}	2.14850×10^{-12}	576.055	2.31400×10^{-11}	1.03320×10^{-12}
552.930	5.02270×10^{-11}	2.26460×10^{-12}	576.648	2.23770×10^{-11}	9.97640×10^{-13}
553.523	5.26240×10^{-11}	2.37240×10^{-12}	577.241	2.16640×10^{-11}	9.64790×10^{-13}
554.116	5.48220×10^{-11}	2.47130×10^{-12}	577.834	2.09950×10^{-11}	9.34420×10^{-13}
554.709	5.68020×10^{-11}	2.56060×10^{-12}	578.427	2.03670×10^{-11}	9.06260×10^{-13}
555.302	5.85460×10^{-11}	2.63930×10^{-12}	579.020	1.97730×10^{-11}	8.80040×10^{-13}
555.894	6.00340×10^{-11}	2.70680×10^{-12}	579.613	1.92090×10^{-11}	8.55500×10^{-13}
556.487	6.12510×10^{-11}	2.76230×10^{-12}	580.206	1.86710×10^{-11}	8.32380×10^{-13}
557.080	6.21830×10^{-11}	2.80530×10^{-12}	580.799	1.81550×10^{-11}	8.10450×10^{-13}
557.673	6.28220×10^{-11}	2.83540×10^{-12}	581.392	1.76570×10^{-11}	7.89490×10^{-13}
558.266	6.31640×10^{-11}	2.85260×10^{-12}	581.985	1.71750×10^{-11}	7.69290×10^{-13}
558.859	6.32090×10^{-11}	2.85670×10^{-12}	582.578	1.67060×10^{-11}	7.49690×10^{-13}
559.452	6.29640×10^{-11}	2.84820×10^{-12}	583.171	1.62470×10^{-11}	7.30540×10^{-13}
560.045	6.24410×10^{-11}	2.82750×10^{-12}	583.764	1.57960×10^{-11}	7.11720×10^{-13}
560.638	6.16580×10^{-11}	2.79530×10^{-12}	584.357	1.53540×10^{-11}	6.93120×10^{-13}
561.231	6.06340×10^{-11}	2.75240×10^{-12}	584.950	1.49180×10^{-11}	6.74690×10^{-13}
561.824	5.93950×10^{-11}	2.69990×10^{-12}	585.543	1.44880×10^{-11}	6.56380×10^{-13}
562.417	5.79690×10^{-11}	2.63880×10^{-12}	586.136	1.40640×10^{-11}	6.38170×10^{-13}
563.010	5.63840×10^{-11}	2.57040×10^{-12}	586.729	1.36460×10^{-11}	6.20040×10^{-13}
563.603	5.46710×10^{-11}	2.49580×10^{-12}	587.322	1.32340×10^{-11}	6.02020×10^{-13}
564.196	5.28600×10^{-11}	2.41640×10^{-12}	587.915	1.28290×10^{-11}	5.84130×10^{-13}
564.789	5.09790×10^{-11}	2.33330×10^{-12}	588.508	1.24320×10^{-11}	5.66410×10^{-13}
565.382	4.90560×10^{-11}	2.24770×10^{-12}	589.101	1.20430×10^{-11}	5.48900×10^{-13}
565.975	4.71170×10^{-11}	2.16070×10^{-12}	589.693	1.16630×10^{-11}	5.31660×10^{-13}
566.568	4.51830×10^{-11}	2.07320×10^{-12}	590.286	1.12920×10^{-11}	5.14740×10^{-13}
567.161	4.32740×10^{-11}	1.98620×10^{-12}	590.879	1.09330×10^{-11}	4.98190×10^{-13}
567.754	4.14060×10^{-11}	1.90040×10^{-12}	591.472	1.05850×10^{-11}	4.82070×10^{-13}
568.347	3.95940×10^{-11}	1.81650×10^{-12}	592.065	1.02480×10^{-11}	4.66410×10^{-13}
568.940	3.78480×10^{-11}	1.73500×10^{-12}	592.658	9.92470×10^{-12}	4.51270×10^{-13}
569.533	3.61750×10^{-11}	1.65650×10^{-12}	593.251	9.61390×10^{-12}	4.36680×10^{-13}
570.126	3.45830×10^{-11}	1.58110×10^{-12}	593.844	9.31630×10^{-12}	4.22670×10^{-13}
570.719	3.30750×10^{-11}	1.50930×10^{-12}	594.437	9.03220×10^{-12}	4.09250×10^{-13}

Table A.19 (cont'd)

JD +2450000	*UVOIR* Flux	Flux error	JD +2450000	*UVOIR* Flux	Flux error
595.030	8.76160×10^{-12}	3.96460×10^{-13}	618.749	4.83720×10^{-12}	2.13210×10^{-13}
595.623	8.50460×10^{-12}	3.84280×10^{-13}	619.342	4.81090×10^{-12}	2.12020×10^{-13}
596.216	8.26080×10^{-12}	3.72730×10^{-13}	619.935	4.78540×10^{-12}	2.10870×10^{-13}
596.809	8.03030×10^{-12}	3.61810×10^{-13}	620.528	4.76050×10^{-12}	2.09740×10^{-13}
597.402	7.81270×10^{-12}	3.51500×10^{-13}	621.121	4.73620×10^{-12}	2.08650×10^{-13}
597.995	7.60760×10^{-12}	3.41790×10^{-13}	621.714	4.71240×10^{-12}	2.07580×10^{-13}
598.588	7.41460×10^{-12}	3.32660×10^{-13}	622.307	4.68910×10^{-12}	2.06540×10^{-13}
599.181	7.23330×10^{-12}	3.24100×10^{-13}	622.899	4.66630×10^{-12}	2.05520×10^{-13}
599.774	7.06310×10^{-12}	3.16080×10^{-13}	623.492	4.64390×10^{-12}	2.04510×10^{-13}
600.367	6.90370×10^{-12}	3.08580×10^{-13}	624.085	4.62190×10^{-12}	2.03530×10^{-13}
600.960	6.75440×10^{-12}	3.01570×10^{-13}	624.678	4.60020×10^{-12}	2.02560×10^{-13}
601.553	6.61470×10^{-12}	2.95020×10^{-13}	625.271	4.57880×10^{-12}	2.01610×10^{-13}
602.146	6.48410×10^{-12}	2.88920×10^{-13}	625.864	4.55770×10^{-12}	2.00670×10^{-13}
602.739	6.36210×10^{-12}	2.83230×10^{-13}	626.457	4.53680×10^{-12}	1.99750×10^{-13}
603.332	6.24800×10^{-12}	2.77920×10^{-13}	627.050	4.51620×10^{-12}	1.98840×10^{-13}
603.925	6.14160×10^{-12}	2.72970×10^{-13}	627.643	4.49590×10^{-12}	1.97940×10^{-13}
604.518	6.04210×10^{-12}	2.68370×10^{-13}	628.236	4.47570×10^{-12}	1.97050×10^{-13}
605.111	5.94920×10^{-12}	2.64070×10^{-13}	628.829	4.45580×10^{-12}	1.96170×10^{-13}
605.703	5.86240×10^{-12}	2.60060×10^{-13}	629.422	4.43600×10^{-12}	1.95300×10^{-13}
606.297	5.78130×10^{-12}	2.56330×10^{-13}	630.015	4.41640×10^{-12}	1.94440×10^{-13}
606.889	5.70550×10^{-12}	2.52840×10^{-13}	630.608	4.39690×10^{-12}	1.93590×10^{-13}
607.482	5.63450×10^{-12}	2.49580×10^{-13}	631.201	4.37760×10^{-12}	1.92750×10^{-13}
608.075	5.56800×10^{-12}	2.46530×10^{-13}	631.794	4.35850×10^{-12}	1.91910×10^{-13}
608.668	5.50570×10^{-12}	2.43670×10^{-13}	632.387	4.33950×10^{-12}	1.91090×10^{-13}
609.261	5.44720×10^{-12}	2.40990×10^{-13}	632.980	4.32070×10^{-12}	1.90260×10^{-13}
609.854	5.39220×10^{-12}	2.38480×10^{-13}	633.573	4.30200×10^{-12}	1.89450×10^{-13}
610.447	5.34040×10^{-12}	2.36110×10^{-13}	634.166	4.28340×10^{-12}	1.88650×10^{-13}
611.040	5.29170×10^{-12}	2.33890×10^{-13}	634.759	4.26490×10^{-12}	1.87850×10^{-13}
611.633	5.24560×10^{-12}	2.31780×10^{-13}	635.352	4.24660×10^{-12}	1.87050×10^{-13}
612.226	5.20210×10^{-12}	2.29800×10^{-13}	635.945	4.22840×10^{-12}	1.86270×10^{-13}
612.819	5.16080×10^{-12}	2.27920×10^{-13}	636.538	4.21030×10^{-12}	1.85490×10^{-13}
613.412	5.12170×10^{-12}	2.26130×10^{-13}	637.131	4.19230×10^{-12}	1.84710×10^{-13}
614.005	5.08440×10^{-12}	2.24430×10^{-13}	637.724	4.17440×10^{-12}	1.83940×10^{-13}
614.598	5.04890×10^{-12}	2.22820×10^{-13}	638.317	4.15670×10^{-12}	1.83180×10^{-13}
615.191	5.01490×10^{-12}	2.21270×10^{-13}	638.910	4.13900×10^{-12}	1.82420×10^{-13}
615.784	4.98240×10^{-12}	2.19790×10^{-13}	639.503	4.12150×10^{-12}	1.81670×10^{-13}
616.377	4.95120×10^{-12}	2.18380×10^{-13}	640.095	4.10410×10^{-12}	1.80930×10^{-13}
616.970	4.92120×10^{-12}	2.17010×10^{-13}	640.688	4.08670×10^{-12}	1.80190×10^{-13}
617.563	4.89220×10^{-12}	2.15700×10^{-13}	641.281	4.06950×10^{-12}	1.79450×10^{-13}
618.156	4.86430×10^{-12}	2.14430×10^{-13}	641.874	4.05240×10^{-12}	1.78720×10^{-13}

Table A.19 (cont'd)

JD +2450000	*UVOIR* Flux	Flux error	JD +2450000	*UVOIR* Flux	Flux error
642.467	4.03540×10^{-12}	1.78000×10^{-13}	654.327	3.71530×10^{-12}	1.64540×10^{-13}
643.060	4.01850×10^{-12}	1.77280×10^{-13}	654.920	3.70030×10^{-12}	1.63920×10^{-13}
643.653	4.00170×10^{-12}	1.76570×10^{-13}	655.513	3.68530×10^{-12}	1.63290×10^{-13}
644.246	3.98500×10^{-12}	1.75860×10^{-13}	656.106	3.67040×10^{-12}	1.62680×10^{-13}
644.839	3.96830×10^{-12}	1.75160×10^{-13}	656.698	3.65560×10^{-12}	1.62060×10^{-13}
645.432	3.95180×10^{-12}	1.74460×10^{-13}	657.291	3.64090×10^{-12}	1.61450×10^{-13}
646.025	3.93540×10^{-12}	1.73760×10^{-13}	657.884	3.62630×10^{-12}	1.60850×10^{-13}
646.618	3.91910×10^{-12}	1.73070×10^{-13}	658.477	3.61180×10^{-12}	1.60250×10^{-13}
647.211	3.90290×10^{-12}	1.72390×10^{-13}	659.070	3.59730×10^{-12}	1.59650×10^{-13}
647.804	3.88670×10^{-12}	1.71710×10^{-13}	659.663	3.58290×10^{-12}	1.59050×10^{-13}
648.397	3.87070×10^{-12}	1.71040×10^{-13}	660.256	3.56860×10^{-12}	1.58460×10^{-13}
648.990	3.85470×10^{-12}	1.70370×10^{-13}	660.849	3.55440×10^{-12}	1.57880×10^{-13}
649.583	3.83890×10^{-12}	1.69700×10^{-13}	661.442	3.54030×10^{-12}	1.57300×10^{-13}
650.176	3.82310×10^{-12}	1.69040×10^{-13}	662.035	3.52620×10^{-12}	1.56720×10^{-13}
650.769	3.80750×10^{-12}	1.68390×10^{-13}	662.628	3.51220×10^{-12}	1.56140×10^{-13}
651.362	3.79190×10^{-12}	1.67730×10^{-13}	663.221	3.49830×10^{-12}	1.55570×10^{-13}
651.955	3.77640×10^{-12}	1.67090×10^{-13}	663.814	3.48450×10^{-12}	1.55000×10^{-13}
652.548	3.76100×10^{-12}	1.66440×10^{-13}	664.407	3.47070×10^{-12}	1.54440×10^{-13}
653.141	3.74570×10^{-12}	1.65810×10^{-13}	665.000	3.45710×10^{-12}	1.53880×10^{-13}
653.734	3.73050×10^{-12}	1.65170×10^{-13}	...	...	...

Table A.20. SN 1997br

JD +2450000	*UVOIR* Flux	Flux error	JD +2450000	*UVOIR* Flux	Flux error
548.588	7.31270×10^{-11}	3.47410×10^{-12}	572.106	8.82650×10^{-11}	3.80250×10^{-12}
549.176	8.26520×10^{-11}	3.83010×10^{-12}	572.693	8.45490×10^{-11}	3.64150×10^{-12}
549.764	9.18670×10^{-11}	4.19760×10^{-12}	573.281	8.10270×10^{-11}	3.49010×10^{-12}
550.352	1.00540×10^{-10}	4.56290×10^{-12}	573.869	7.76990×10^{-11}	3.34810×10^{-12}
550.940	1.08630×10^{-10}	4.91870×10^{-12}	574.457	7.45620×10^{-11}	3.21520×10^{-12}
551.528	1.16160×10^{-10}	5.26210×10^{-12}	575.045	7.16120×10^{-11}	3.09110×10^{-12}
552.116	1.23210×10^{-10}	5.59250×10^{-12}	575.633	6.88430×10^{-11}	2.97540×10^{-12}
552.703	1.29800×10^{-10}	5.90910×10^{-12}	576.221	6.62490×10^{-11}	2.86780×10^{-12}
553.291	1.35970×10^{-10}	6.21110×10^{-12}	576.809	6.38230×10^{-11}	2.76780×10^{-12}
553.879	1.41720×10^{-10}	6.49650×10^{-12}	577.397	6.15560×10^{-11}	2.67500×10^{-12}
554.467	1.47040×10^{-10}	6.76280×10^{-12}	577.985	5.94400×10^{-11}	2.58890×10^{-12}
555.055	1.51890×10^{-10}	7.00700×10^{-12}	578.573	5.74670×10^{-11}	2.50910×10^{-12}
555.643	1.56230×10^{-10}	7.22600×10^{-12}	579.161	5.56260×10^{-11}	2.43510×10^{-12}
556.231	1.60030×10^{-10}	7.41650×10^{-12}	579.749	5.39090×10^{-11}	2.36650×10^{-12}
556.819	1.63240×10^{-10}	7.57550×10^{-12}	580.337	5.23060×10^{-11}	2.30260×10^{-12}
557.407	1.65820×10^{-10}	7.70040×10^{-12}	580.925	5.08090×10^{-11}	2.24320×10^{-12}
557.995	1.67750×10^{-10}	7.78940×10^{-12}	581.513	4.94080×10^{-11}	2.18760×10^{-12}
558.583	1.68990×10^{-10}	7.84130×10^{-12}	582.101	4.80940×10^{-11}	2.13560×10^{-12}
559.171	1.69550×10^{-10}	7.85580×10^{-12}	582.688	4.68590×10^{-11}	2.08660×10^{-12}
559.759	1.69420×10^{-10}	7.83320×10^{-12}	583.276	4.56960×10^{-11}	2.04030×10^{-12}
560.347	1.68630×10^{-10}	7.77500×10^{-12}	583.864	4.45950×10^{-11}	1.99640×10^{-12}
560.935	1.67220×10^{-10}	7.68330×10^{-12}	584.452	4.35510×10^{-11}	1.95440×10^{-12}
561.523	1.65220×10^{-10}	7.56090×10^{-12}	585.040	4.25560×10^{-11}	1.91410×10^{-12}
562.111	1.62700×10^{-10}	7.41110×10^{-12}	585.628	4.16050×10^{-11}	1.87520×10^{-12}
562.698	1.59710×10^{-10}	7.23780×10^{-12}	586.216	4.06900×10^{-11}	1.83750×10^{-12}
563.286	1.56300×10^{-10}	7.04470×10^{-12}	586.804	3.98080×10^{-11}	1.80070×10^{-12}
563.874	1.52540×10^{-10}	6.83570×10^{-12}	587.392	3.89530×10^{-11}	1.76460×10^{-12}
564.462	1.48450×10^{-10}	6.61440×10^{-12}	587.980	3.81210×10^{-11}	1.72900×10^{-12}
565.050	1.44060×10^{-10}	6.38410×10^{-12}	588.568	3.73090×10^{-11}	1.69390×10^{-12}
565.638	1.39420×10^{-10}	6.14800×10^{-12}	589.156	3.65140×10^{-11}	1.65910×10^{-12}
566.226	1.34580×10^{-10}	5.90880×10^{-12}	589.744	3.57330×10^{-11}	1.62460×10^{-12}
566.814	1.29600×10^{-10}	5.66920×10^{-12}	590.332	3.49640×10^{-11}	1.59020×10^{-12}
567.402	1.24550×10^{-10}	5.43190×10^{-12}	590.920	3.42060×10^{-11}	1.55590×10^{-12}
567.990	1.19520×10^{-10}	5.19910×10^{-12}	591.508	3.34580×10^{-11}	1.52180×10^{-12}
568.578	1.14560×10^{-10}	4.97280×10^{-12}	592.095	3.27200×10^{-11}	1.48790×10^{-12}
569.166	1.09740×10^{-10}	4.75430×10^{-12}	592.683	3.19910×10^{-11}	1.45410×10^{-12}
569.754	1.05070×10^{-10}	4.54460×10^{-12}	593.271	3.12710×10^{-11}	1.42060×10^{-12}
570.342	1.00580×10^{-10}	4.34430×10^{-12}	593.859	3.05620×10^{-11}	1.38730×10^{-12}
570.930	9.62840×10^{-11}	4.15380×10^{-12}	594.447	2.98630×10^{-11}	1.35440×10^{-12}
571.518	9.21770×10^{-11}	3.97320×10^{-12}	595.035	2.91760×10^{-11}	1.32190×10^{-12}

Table A.20 (cont'd)

JD +2450000	*UVOIR* Flux	Flux error	JD +2450000	*UVOIR* Flux	Flux error
595.623	2.85010×10^{-11}	1.28980×10^{-12}	619.141	1.33000×10^{-11}	5.79520×10^{-13}
596.211	2.78400×10^{-11}	1.25840×10^{-12}	619.729	1.31160×10^{-11}	5.71450×10^{-13}
596.799	2.71930×10^{-11}	1.22750×10^{-12}	620.317	1.29370×10^{-11}	5.63580×10^{-13}
597.387	2.65610×10^{-11}	1.19730×10^{-12}	620.905	1.27630×10^{-11}	5.55920×10^{-13}
597.975	2.59450×10^{-11}	1.16780×10^{-12}	621.492	1.25920×10^{-11}	5.48450×10^{-13}
598.563	2.53460×10^{-11}	1.13910×10^{-12}	622.080	1.24260×10^{-11}	5.41170×10^{-13}
599.151	2.47640×10^{-11}	1.11120×10^{-12}	622.668	1.22640×10^{-11}	5.34060×10^{-13}
599.739	2.41980×10^{-11}	1.08410×10^{-12}	623.256	1.21050×10^{-11}	5.27110×10^{-13}
600.327	2.36510×10^{-11}	1.05790×10^{-12}	623.844	1.19500×10^{-11}	5.20330×10^{-13}
600.915	2.31210×10^{-11}	1.03260×10^{-12}	624.432	1.17980×10^{-11}	5.13700×10^{-13}
601.503	2.26090×10^{-11}	1.00810×10^{-12}	625.020	1.16490×10^{-11}	5.07220×10^{-13}
602.090	2.21150×10^{-11}	9.84550×10^{-13}	625.608	1.15040×10^{-11}	5.00870×10^{-13}
602.678	2.16370×10^{-11}	9.61840×10^{-13}	626.196	1.13610×10^{-11}	4.94660×10^{-13}
603.266	2.11770×10^{-11}	9.39980×10^{-13}	626.784	1.12210×10^{-11}	4.88580×10^{-13}
603.854	2.07330×10^{-11}	9.18970×10^{-13}	627.372	1.10840×10^{-11}	4.82610×10^{-13}
604.442	2.03060×10^{-11}	8.98770×10^{-13}	627.960	1.09500×10^{-11}	4.76770×10^{-13}
605.030	1.98940×10^{-11}	8.79370×10^{-13}	628.548	1.08180×10^{-11}	4.71030×10^{-13}
605.618	1.94970×10^{-11}	8.60730×10^{-13}	629.136	1.06880×10^{-11}	4.65410×10^{-13}
606.206	1.91140×10^{-11}	8.42830×10^{-13}	629.724	1.05610×10^{-11}	4.59880×10^{-13}
606.794	1.87460×10^{-11}	8.25650×10^{-13}	630.312	1.04360×10^{-11}	4.54460×10^{-13}
607.382	1.83900×10^{-11}	8.09140×10^{-13}	630.899	1.03130×10^{-11}	4.49130×10^{-13}
607.970	1.80480×10^{-11}	7.93280×10^{-13}	631.487	1.01920×10^{-11}	4.43890×10^{-13}
608.558	1.77170×10^{-11}	7.78040×10^{-13}	632.075	1.00730×10^{-11}	4.38740×10^{-13}
609.146	1.73980×10^{-11}	7.63380×10^{-13}	632.663	9.95610×10^{-12}	4.33670×10^{-13}
609.734	1.70910×10^{-11}	7.49280×10^{-13}	633.251	9.84100×10^{-12}	4.28690×10^{-13}
610.322	1.67930×10^{-11}	7.35700×10^{-13}	633.839	9.72760×10^{-12}	4.23790×10^{-13}
610.910	1.65060×10^{-11}	7.22630×10^{-13}	634.427	9.61590×10^{-12}	4.18960×10^{-13}
611.497	1.62280×10^{-11}	7.10030×10^{-13}	635.015	9.50590×10^{-12}	4.14210×10^{-13}
612.085	1.59590×10^{-11}	6.97880×10^{-13}	635.603	9.39750×10^{-12}	4.09530×10^{-13}
612.673	1.56990×10^{-11}	6.86160×10^{-13}	636.191	9.29060×10^{-12}	4.04920×10^{-13}
613.261	1.54470×10^{-11}	6.74830×10^{-13}	636.779	9.18530×10^{-12}	4.00380×10^{-13}
613.849	1.52020×10^{-11}	6.63890×10^{-13}	637.367	9.08140×10^{-12}	3.95900×10^{-13}
614.437	1.49660×10^{-11}	6.53310×10^{-13}	637.955	8.97900×10^{-12}	3.91480×10^{-13}
615.025	1.47360×10^{-11}	6.43060×10^{-13}	638.543	8.87800×10^{-12}	3.87130×10^{-13}
615.613	1.45130×10^{-11}	6.33140×10^{-13}	639.131	8.77830×10^{-12}	3.82840×10^{-13}
616.201	1.42960×10^{-11}	6.23530×10^{-13}	639.719	8.67990×10^{-12}	3.78610×10^{-13}
616.789	1.40860×10^{-11}	6.14200×10^{-13}	640.307	8.58280×10^{-12}	3.74430×10^{-13}
617.377	1.38810×10^{-11}	6.05150×10^{-13}	640.894	8.48700×10^{-12}	3.70310×10^{-13}
617.965	1.36820×10^{-11}	5.96370×10^{-13}	641.482	8.39240×10^{-12}	3.66250×10^{-13}
618.553	1.34890×10^{-11}	5.87830×10^{-13}	642.070	8.29910×10^{-12}	3.62240×10^{-13}

Table A.20 (cont'd)

JD +2450000	*UVOIR* Flux	Flux error	JD +2450000	*UVOIR* Flux	Flux error
642.658	8.20690×10^{-12}	3.58280×10^{-13}	654.417	6.58020×10^{-12}	2.88670×10^{-13}
643.246	8.11580×10^{-12}	3.54370×10^{-13}	655.005	6.50860×10^{-12}	2.85610×10^{-13}
643.834	8.02590×10^{-12}	3.50510×10^{-13}	655.593	6.43770×10^{-12}	2.82590×10^{-13}
644.422	7.93710×10^{-12}	3.46710×10^{-13}	656.181	6.36770×10^{-12}	2.79600×10^{-13}
645.010	7.84940×10^{-12}	3.42940×10^{-13}	656.769	6.29850×10^{-12}	2.76650×10^{-13}
645.598	7.76270×10^{-12}	3.39230×10^{-13}	657.357	6.23010×10^{-12}	2.73730×10^{-13}
646.186	7.67710×10^{-12}	3.35560×10^{-13}	657.945	6.16250×10^{-12}	2.70850×10^{-13}
646.774	7.59260×10^{-12}	3.31940×10^{-13}	658.533	6.09570×10^{-12}	2.67990×10^{-13}
647.362	7.50900×10^{-12}	3.28370×10^{-13}	659.121	6.02960×10^{-12}	2.65180×10^{-13}
647.950	7.42650×10^{-12}	3.24830×10^{-13}	659.709	5.96430×10^{-12}	2.62390×10^{-13}
648.538	7.34490×10^{-12}	3.21340×10^{-13}	660.297	5.89970×10^{-12}	2.59640×10^{-13}
649.126	7.26430×10^{-12}	3.17890×10^{-13}	660.884	5.83590×10^{-12}	2.56920×10^{-13}
649.714	7.18470×10^{-12}	3.14490×10^{-13}	661.472	5.77280×10^{-12}	2.54230×10^{-13}
650.302	7.10600×10^{-12}	3.11120×10^{-13}	662.060	5.71040×10^{-12}	2.51570×10^{-13}
650.889	7.02820×10^{-12}	3.07800×10^{-13}	662.648	5.64870×10^{-12}	2.48950×10^{-13}
651.477	6.95130×10^{-12}	3.04510×10^{-13}	663.236	5.58770×10^{-12}	2.46350×10^{-13}
652.065	6.87540×10^{-12}	3.01270×10^{-13}	663.824	5.52750×10^{-12}	2.43780×10^{-13}
652.653	6.80030×10^{-12}	2.98060×10^{-13}	664.412	5.46790×10^{-12}	2.41240×10^{-13}
653.241	6.72610×10^{-12}	2.94890×10^{-13}	665.000	5.40900×10^{-12}	2.38730×10^{-13}
653.829	6.65270×10^{-12}	2.91760×10^{-13}	...	...	...

Table A.21. SN 1998aq

JD +2450000	*UVOIR* Flux	Flux error	JD +2450000	*UVOIR* Flux	Flux error
921.789	1.06590×10^{-10}	4.76850×10^{-12}	993.347	1.20190×10^{-11}	5.30780×10^{-13}
923.578	1.47580×10^{-10}	6.61710×10^{-12}	995.136	1.14730×10^{-11}	5.06470×10^{-13}
925.367	1.78910×10^{-10}	8.00020×10^{-12}	996.925	1.09710×10^{-11}	4.84200×10^{-13}
927.156	2.01300×10^{-10}	8.98010×10^{-12}	998.714	1.05090×10^{-11}	4.63700×10^{-13}
928.945	2.14950×10^{-10}	9.57940×10^{-12}	1000.50	1.00800×10^{-11}	4.44710×10^{-13}
930.734	2.19830×10^{-10}	9.79750×10^{-12}	1002.29	9.68150×10^{-12}	4.27050×10^{-13}
932.523	2.16330×10^{-10}	9.64560×10^{-12}	1004.08	9.30850×10^{-12}	4.10540×10^{-13}
934.312	2.05590×10^{-10}	9.16740×10^{-12}	1005.87	8.95840×10^{-12}	3.95050×10^{-13}
936.101	1.89460×10^{-10}	8.44030×10^{-12}	1007.66	8.62860×10^{-12}	3.80460×10^{-13}
937.889	1.70160×10^{-10}	7.56250×10^{-12}	1009.45	8.31670×10^{-12}	3.66660×10^{-13}
939.678	1.49850×10^{-10}	6.63300×10^{-12}	1011.24	8.02100×10^{-12}	3.53580×10^{-13}
941.467	1.30250×10^{-10}	5.73410×10^{-12}	1013.03	7.73970×10^{-12}	3.41150×10^{-13}
943.256	1.12490×10^{-10}	4.92200×10^{-12}	1014.81	7.47150×10^{-12}	3.29310×10^{-13}
945.045	9.71540×10^{-11}	4.22600×10^{-12}	1016.60	7.21540×10^{-12}	3.18000×10^{-13}
946.834	8.43420×10^{-11}	3.65350×10^{-12}	1018.39	6.97020×10^{-12}	3.07190×10^{-13}
948.623	7.38860×10^{-11}	3.19620×10^{-12}	1020.18	6.73530×10^{-12}	2.96840×10^{-13}
950.412	6.54620×10^{-11}	2.83750×10^{-12}	1021.97	6.50980×10^{-12}	2.86930×10^{-13}
952.201	5.86940×10^{-11}	2.55760×10^{-12}	1023.76	6.29330×10^{-12}	2.77410×10^{-13}
953.990	5.32150×10^{-11}	2.33690×10^{-12}	1025.55	6.08510×10^{-12}	2.68270×10^{-13}
955.779	4.87060×10^{-11}	2.15840×10^{-12}	1027.34	5.88490×10^{-12}	2.59490×10^{-13}
957.568	4.49050×10^{-11}	2.00840×10^{-12}	1029.13	5.69220×10^{-12}	2.51050×10^{-13}
959.357	4.16100×10^{-11}	1.87690×10^{-12}	1030.92	5.50660×10^{-12}	2.42940×10^{-13}
961.146	3.86750×10^{-11}	1.75670×10^{-12}	1032.70	5.32780×10^{-12}	2.35130×10^{-13}
962.935	3.59990×10^{-11}	1.64350×10^{-12}	1034.49	5.15550×10^{-12}	2.27610×10^{-13}
964.724	3.35210×10^{-11}	1.53510×10^{-12}	1036.28	4.98950×10^{-12}	2.20370×10^{-13}
966.513	3.12050×10^{-11}	1.43060×10^{-12}	1038.07	4.82950×10^{-12}	2.13400×10^{-13}
968.302	2.90340×10^{-11}	1.33030×10^{-12}	1039.86	4.67520×10^{-12}	2.06690×10^{-13}
970.090	2.70030×10^{-11}	1.23460×10^{-12}	1041.65	4.52630×10^{-12}	2.00220×10^{-13}
971.879	2.51120×10^{-11}	1.14450×10^{-12}	1043.44	4.38280×10^{-12}	1.93990×10^{-13}
973.668	2.33630×10^{-11}	1.06060×10^{-12}	1045.23	4.24430×10^{-12}	1.87980×10^{-13}
975.457	2.17560×10^{-11}	9.83490×10^{-13}	1047.02	4.11060×10^{-12}	1.82180×10^{-13}
977.246	2.02880×10^{-11}	9.13250×10^{-13}	1048.80	3.98170×10^{-12}	1.76590×10^{-13}
979.035	1.89550×10^{-11}	8.49830×10^{-13}	1050.59	3.85720×10^{-12}	1.71200×10^{-13}
980.824	1.77480×10^{-11}	7.92900×10^{-13}	1052.38	3.73710×10^{-12}	1.66000×10^{-13}
982.613	1.66590×10^{-11}	7.41980×10^{-13}	1054.17	3.62100×10^{-12}	1.60980×10^{-13}
984.402	1.56780×10^{-11}	6.96520×10^{-13}	1055.96	3.50900×10^{-12}	1.56140×10^{-13}
986.191	1.47930×10^{-11}	6.55910×10^{-13}	1057.75	3.40080×10^{-12}	1.51460×10^{-13}
987.980	1.39940×10^{-11}	6.19560×10^{-13}	1059.54	3.29630×10^{-12}	1.46940×10^{-13}
989.769	1.32710×10^{-11}	5.86910×10^{-13}	1061.33	3.19530×10^{-12}	1.42570×10^{-13}
991.558	1.26160×10^{-11}	5.57470×10^{-13}	1063.12	3.09770×10^{-12}	1.38360×10^{-13}

Table A.21 (cont'd)

JD +2450000	*UVOIR* Flux	Flux error	JD +2450000	*UVOIR* Flux	Flux error
1064.91	3.00340×10^{-12}	1.34280×10^{-13}	1136.46	9.19640×10^{-13}	4.36730×10^{-14}
1066.69	2.91220×10^{-12}	1.30340×10^{-13}	1138.25	8.93620×10^{-13}	4.25160×10^{-14}
1068.48	2.82400×10^{-12}	1.26540×10^{-13}	1140.04	8.68370×10^{-13}	4.13900×10^{-14}
1070.27	2.73880×10^{-12}	1.22850×10^{-13}	1141.83	8.43850×10^{-13}	4.02960×10^{-14}
1072.06	2.65630×10^{-12}	1.19290×10^{-13}	1143.62	8.20050×10^{-13}	3.92320×10^{-14}
1073.85	2.57660×10^{-12}	1.15850×10^{-13}	1145.41	7.96940×10^{-13}	3.81970×10^{-14}
1075.64	2.49940×10^{-12}	1.12510×10^{-13}	1147.20	7.74510×10^{-13}	3.71920×10^{-14}
1077.43	2.42480×10^{-12}	1.09290×10^{-13}	1148.98	7.52730×10^{-13}	3.62140×10^{-14}
1079.22	2.35250×10^{-12}	1.06160×10^{-13}	1150.77	7.31580×10^{-13}	3.52630×10^{-14}
1081.01	2.28260×10^{-12}	1.03140×10^{-13}	1152.56	7.11050×10^{-13}	3.43370×10^{-14}
1082.79	2.21490×10^{-12}	1.00210×10^{-13}	1154.35	6.91110×10^{-13}	3.34380×10^{-14}
1084.58	2.14940×10^{-12}	9.73780×10^{-14}	1156.14	6.71760×10^{-13}	3.25630×10^{-14}
1086.37	2.08590×10^{-12}	9.46320×10^{-14}	1157.93	6.52960×10^{-13}	3.17110×10^{-14}
1088.16	2.02450×10^{-12}	9.19710×10^{-14}	1159.72	6.34700×10^{-13}	3.08830×10^{-14}
1089.95	1.96500×10^{-12}	8.93920×10^{-14}	1161.51	6.16970×10^{-13}	3.00780×10^{-14}
1091.74	1.90730×10^{-12}	8.68930×10^{-14}	1163.30	5.99750×10^{-13}	2.92940×10^{-14}
1093.53	1.85150×10^{-12}	8.44710×10^{-14}	1165.08	5.83030×10^{-13}	2.85320×10^{-14}
1095.32	1.79730×10^{-12}	8.21230×10^{-14}	1166.87	5.66790×10^{-13}	2.77900×10^{-14}
1097.10	1.74490×10^{-12}	7.98460×10^{-14}	1168.66	5.51010×10^{-13}	2.70680×10^{-14}
1098.90	1.69410×10^{-12}	7.76370×10^{-14}	1170.45	5.35690×10^{-13}	2.63660×10^{-14}
1100.68	1.64480×10^{-12}	7.54960×10^{-14}	1172.24	5.20810×10^{-13}	2.56830×10^{-14}
1102.47	1.59710×10^{-12}	7.34180×10^{-14}	1174.03	5.06350×10^{-13}	2.50180×10^{-14}
1104.26	1.55080×10^{-12}	7.14020×10^{-14}	1175.82	4.92310×10^{-13}	2.43700×10^{-14}
1106.05	1.50590×10^{-12}	6.94460×10^{-14}	1177.61	4.78660×10^{-13}	2.37400×10^{-14}
1107.84	1.46240×10^{-12}	6.75480×10^{-14}	1179.40	4.65410×10^{-13}	2.31270×10^{-14}
1109.63	1.42020×10^{-12}	6.57060×10^{-14}	1181.19	4.52540×10^{-13}	2.25310×10^{-14}
1111.42	1.37930×10^{-12}	6.39180×10^{-14}	1182.97	4.40030×10^{-13}	2.19500×10^{-14}
1113.21	1.33960×10^{-12}	6.21820×10^{-14}	1184.76	4.27880×10^{-13}	2.13840×10^{-14}
1114.99	1.30110×10^{-12}	6.04970×10^{-14}	1186.55	4.16070×10^{-13}	2.08340×10^{-14}
1116.78	1.26380×10^{-12}	5.88610×10^{-14}	1188.34	4.04600×10^{-13}	2.02980×10^{-14}
1118.57	1.22760×10^{-12}	5.72720×10^{-14}	1190.13	3.93460×10^{-13}	1.97770×10^{-14}
1120.36	1.19240×10^{-12}	5.57280×10^{-14}	1191.92	3.82630×10^{-13}	1.92690×10^{-14}
1122.15	1.15830×10^{-12}	5.42290×10^{-14}	1193.71	3.72100×10^{-13}	1.87750×10^{-14}
1123.94	1.12530×10^{-12}	5.27730×10^{-14}	1195.50	3.61880×10^{-13}	1.82940×10^{-14}
1125.73	1.09320×10^{-12}	5.13590×10^{-14}	1197.29	3.51940×10^{-13}	1.78250×10^{-14}
1127.52	1.06210×10^{-12}	4.99840×10^{-14}	1199.07	3.42290×10^{-13}	1.73690×10^{-14}
1129.31	1.03180×10^{-12}	4.86490×10^{-14}	1200.86	3.32910×10^{-13}	1.69240×10^{-14}
1131.09	1.00250×10^{-12}	4.73510×10^{-14}	1202.65	3.23790×10^{-13}	1.64920×10^{-14}
1132.88	9.74070×10^{-13}	4.60900×10^{-14}	1204.44	3.14930×10^{-13}	1.60710×10^{-14}
1134.67	9.46450×10^{-13}	4.48650×10^{-14}	1206.23	3.06310×10^{-13}	1.56600×10^{-14}

Table A.21 (cont'd)

JD +2450000	*UVOIR* Flux	Flux error	JD +2450000	*UVOIR* Flux	Flux error
1208.02	2.97940×10^{-13}	1.52610×10^{-14}	1242.01	1.76700×10^{-13}	9.36690×10^{-15}
1209.81	2.89810×10^{-13}	1.48720×10^{-14}	1243.80	1.71940×10^{-13}	9.13050×10^{-15}
1211.60	2.81900×10^{-13}	1.44930×10^{-14}	1245.59	1.67310×10^{-13}	8.90020×10^{-15}
1213.39	2.74220×10^{-13}	1.41240×10^{-14}	1247.38	1.62820×10^{-13}	8.67580×10^{-15}
1215.18	2.66750×10^{-13}	1.37650×10^{-14}	1249.17	1.58440×10^{-13}	8.45710×10^{-15}
1216.96	2.59480×10^{-13}	1.34150×10^{-14}	1250.95	1.54180×10^{-13}	8.24400×10^{-15}
1218.75	2.52430×10^{-13}	1.30740×10^{-14}	1252.74	1.50050×10^{-13}	8.03640×10^{-15}
1220.54	2.45570×10^{-13}	1.27420×10^{-14}	1254.53	1.46020×10^{-13}	7.83410×10^{-15}
1222.33	2.38900×10^{-13}	1.24180×10^{-14}	1256.32	1.42110×10^{-13}	7.63690×10^{-15}
1224.12	2.32410×10^{-13}	1.21030×10^{-14}	1258.11	1.38300×10^{-13}	7.44480×10^{-15}
1225.91	2.26110×10^{-13}	1.17960×10^{-14}	1259.90	1.34600×10^{-13}	7.25760×10^{-15}
1227.70	2.19980×10^{-13}	1.14970×10^{-14}	1261.69	1.31000×10^{-13}	7.07520×10^{-15}
1229.49	2.14020×10^{-13}	1.12060×10^{-14}	1263.48	1.27490×10^{-13}	6.89740×10^{-15}
1231.28	2.08230×10^{-13}	1.09220×10^{-14}	1265.27	1.24090×10^{-13}	6.72410×10^{-15}
1233.06	2.02600×10^{-13}	1.06460×10^{-14}	1267.06	1.20770×10^{-13}	6.55530×10^{-15}
1234.85	1.97130×10^{-13}	1.03760×10^{-14}	1268.84	1.17550×10^{-13}	6.39070×10^{-15}
1236.64	1.91800×10^{-13}	1.01140×10^{-14}	1270.63	1.14420×10^{-13}	6.23030×10^{-15}
1238.43	1.86630×10^{-13}	9.85850×10^{-15}	1272.42	1.11370×10^{-13}	6.07410×10^{-15}
1240.22	1.81590×10^{-13}	9.60950×10^{-15}	1274.21	1.08400×10^{-13}	5.92170×10^{-15}

Table A.22. SN 1998bu

JD +2450000	*UVOIR* Flux	Flux error	JD +2450000	*UVOIR* Flux	Flux error
930.000	1.28560×10^{-11}	1.18410×10^{-12}	956.131	8.58360×10^{-10}	3.80670×10^{-11}
930.653	1.52660×10^{-11}	1.40600×10^{-12}	956.784	8.37060×10^{-10}	3.71230×10^{-11}
931.307	1.80040×10^{-11}	1.65820×10^{-12}	957.437	8.12610×10^{-10}	3.60390×10^{-11}
931.960	2.10990×10^{-11}	1.94330×10^{-12}	958.090	7.85460×10^{-10}	3.48330×10^{-11}
932.613	2.45810×10^{-11}	2.26400×10^{-12}	958.744	7.56110×10^{-10}	3.35280×10^{-11}
933.266	2.84800×10^{-11}	2.62310×10^{-12}	959.397	7.25140×10^{-10}	3.21480×10^{-11}
933.920	3.28260×10^{-11}	3.02320×10^{-12}	960.050	6.93120×10^{-10}	3.07170×10^{-11}
934.573	3.76510×10^{-11}	3.46690×10^{-12}	960.703	6.60610×10^{-10}	2.92620×10^{-11}
935.226	4.29940×10^{-11}	3.95640×10^{-12}	961.357	6.28110×10^{-10}	2.78020×10^{-11}
935.879	4.89060×10^{-11}	4.49380×10^{-12}	962.010	5.96090×10^{-10}	2.63590×10^{-11}
936.533	5.54560×10^{-11}	5.08040×10^{-12}	962.663	5.64900×10^{-10}	2.49480×10^{-11}
937.186	6.27340×10^{-11}	5.71730×10^{-12}	963.317	5.34860×10^{-10}	2.35850×10^{-11}
937.839	7.08450×10^{-11}	6.40500×10^{-12}	963.970	5.06200×10^{-10}	2.22800×10^{-11}
938.492	7.99090×10^{-11}	7.14340×10^{-12}	964.623	4.79080×10^{-10}	2.10410×10^{-11}
939.146	9.01830×10^{-11}	7.93220×10^{-12}	965.276	4.53600×10^{-10}	1.98760×10^{-11}
939.799	1.02390×10^{-10}	8.77100×10^{-12}	965.930	4.29830×10^{-10}	1.87880×10^{-11}
940.452	1.17610×10^{-10}	9.66340×10^{-12}	966.583	4.07800×10^{-10}	1.77810×10^{-11}
941.106	1.36540×10^{-10}	1.06240×10^{-11}	967.236	3.87480×10^{-10}	1.68550×10^{-11}
941.759	1.59160×10^{-10}	1.16750×10^{-11}	967.889	3.68840×10^{-10}	1.60090×10^{-11}
942.412	1.84740×10^{-10}	1.28310×10^{-11}	968.543	3.51810×10^{-10}	1.52430×10^{-11}
943.065	2.12870×10^{-10}	1.40880×10^{-11}	969.196	3.36330×10^{-10}	1.45540×10^{-11}
943.719	2.57830×10^{-10}	1.54750×10^{-11}	969.849	3.22280×10^{-10}	1.39380×10^{-11}
944.372	3.52030×10^{-10}	1.77590×10^{-11}	970.503	3.09580×10^{-10}	1.33900×10^{-11}
945.025	4.74410×10^{-10}	2.16890×10^{-11}	971.156	2.98090×10^{-10}	1.29040×10^{-11}
945.678	5.84160×10^{-10}	2.60040×10^{-11}	971.809	2.87690×10^{-10}	1.24750×10^{-11}
946.332	6.67910×10^{-10}	2.95750×10^{-11}	972.462	2.78260×10^{-10}	1.20950×10^{-11}
946.985	7.29270×10^{-10}	3.22630×10^{-11}	973.116	2.69660×10^{-10}	1.17570×10^{-11}
947.638	7.74950×10^{-10}	3.42790×10^{-11}	973.769	2.61740×10^{-10}	1.14520×10^{-11}
948.291	8.10100×10^{-10}	3.58390×10^{-11}	974.422	2.54380×10^{-10}	1.11730×10^{-11}
948.945	8.37930×10^{-10}	3.70800×10^{-11}	975.075	2.47430×10^{-10}	1.09120×10^{-11}
949.598	8.60220×10^{-10}	3.80820×10^{-11}	975.729	2.40770×10^{-10}	1.06620×10^{-11}
950.251	8.77920×10^{-10}	3.88820×10^{-11}	976.382	2.34290×10^{-10}	1.04160×10^{-11}
950.905	8.91480×10^{-10}	3.94980×10^{-11}	977.035	2.27880×10^{-10}	1.01690×10^{-11}
951.558	9.01080×10^{-10}	3.99370×10^{-11}	977.688	2.21480×10^{-10}	9.91570×10^{-12}
952.211	9.06790×10^{-10}	4.02000×10^{-11}	978.342	2.15010×10^{-10}	9.65400×10^{-12}
952.864	9.08590×10^{-10}	4.02860×10^{-11}	978.995	2.08450×10^{-10}	9.38180×10^{-12}
953.518	9.06430×10^{-10}	4.01940×10^{-11}	979.648	2.01780×10^{-10}	9.09870×10^{-12}
954.171	9.00290×10^{-10}	3.99240×10^{-11}	980.302	1.95010×10^{-10}	8.80570×10^{-12}
954.824	8.90170×10^{-10}	3.94770×10^{-11}	980.955	1.88160×10^{-10}	8.50460×10^{-12}
955.477	8.76140×10^{-10}	3.88550×10^{-11}	981.608	1.81290×10^{-10}	8.19810×10^{-12}

Table A.22 (cont'd)

JD +2450000	*UVOIR* Flux	Flux error	JD +2450000	*UVOIR* Flux	Flux error
982.261	1.74450×10^{-10}	7.88940×10^{-12}	1008.39	6.48330×10^{-11}	2.84030×10^{-12}
982.915	1.67690×10^{-10}	7.58200×10^{-12}	1009.04	6.38330×10^{-11}	2.79470×10^{-12}
983.568	1.61090×10^{-10}	7.27940×10^{-12}	1009.70	6.28560×10^{-11}	2.75020×10^{-12}
984.221	1.54690×10^{-10}	6.98500×10^{-12}	1010.35	6.18990×10^{-11}	2.70680×10^{-12}
984.874	1.48550×10^{-10}	6.70170×10^{-12}	1011.01	6.09630×10^{-11}	2.66450×10^{-12}
985.528	1.42710×10^{-10}	6.43170×10^{-12}	1011.66	6.00470×10^{-11}	2.62330×10^{-12}
986.181	1.37190×10^{-10}	6.17690×10^{-12}	1012.31	5.91510×10^{-11}	2.58300×10^{-12}
986.834	1.32030×10^{-10}	5.93820×10^{-12}	1012.97	5.82730×10^{-11}	2.54380×10^{-12}
987.487	1.27210×10^{-10}	5.71610×10^{-12}	1013.62	5.74140×10^{-11}	2.50560×10^{-12}
988.141	1.22750×10^{-10}	5.51070×10^{-12}	1014.27	5.65730×10^{-11}	2.46830×10^{-12}
988.794	1.18640×10^{-10}	5.32130×10^{-12}	1014.92	5.57500×10^{-11}	2.43190×10^{-12}
989.447	1.14840×10^{-10}	5.14720×10^{-12}	1015.58	5.49430×10^{-11}	2.39650×10^{-12}
990.101	1.11350×10^{-10}	4.98730×10^{-12}	1016.23	5.41540×10^{-11}	2.36190×10^{-12}
990.754	1.08140×10^{-10}	4.84040×10^{-12}	1016.88	5.33800×10^{-11}	2.32820×10^{-12}
991.407	1.05190×10^{-10}	4.70530×10^{-12}	1017.54	5.26230×10^{-11}	2.29530×10^{-12}
992.060	1.02460×10^{-10}	4.58060×10^{-12}	1018.19	5.18810×10^{-11}	2.26330×10^{-12}
992.714	9.99410×10^{-11}	4.46530×10^{-12}	1018.84	5.11550×10^{-11}	2.23200×10^{-12}
993.367	9.75980×10^{-11}	4.35800×10^{-12}	1019.50	5.04430×10^{-11}	2.20150×10^{-12}
994.020	9.54130×10^{-11}	4.25780×10^{-12}	1020.15	4.97460×10^{-11}	2.17180×10^{-12}
994.673	9.33650×10^{-11}	4.16370×10^{-12}	1020.80	4.90630×10^{-11}	2.14280×10^{-12}
995.327	9.14370×10^{-11}	4.07490×10^{-12}	1021.46	4.83940×10^{-11}	2.11450×10^{-12}
995.980	8.96130×10^{-11}	3.99070×10^{-12}	1022.11	4.77380×10^{-11}	2.08700×10^{-12}
996.633	8.78800×10^{-11}	3.91050×10^{-12}	1022.76	4.70960×10^{-11}	2.06010×10^{-12}
997.286	8.62250×10^{-11}	3.83380×10^{-12}	1023.42	4.64670×10^{-11}	2.03390×10^{-12}
997.940	8.46390×10^{-11}	3.76010×10^{-12}	1024.07	4.58500×10^{-11}	2.00830×10^{-12}
998.593	8.31150×10^{-11}	3.68920×10^{-12}	1024.72	4.52460×10^{-11}	1.98330×10^{-12}
999.246	8.16440×10^{-11}	3.62070×10^{-12}	1025.38	4.46540×10^{-11}	1.95900×10^{-12}
999.899	8.02220×10^{-11}	3.55430×10^{-12}	1026.03	4.40740×10^{-11}	1.93530×10^{-12}
1000.55	7.88440×10^{-11}	3.49000×10^{-12}	1026.68	4.35060×10^{-11}	1.91210×10^{-12}
1001.21	7.75060×10^{-11}	3.42760×10^{-12}	1027.34	4.29490×10^{-11}	1.88950×10^{-12}
1001.86	7.62050×10^{-11}	3.36690×10^{-12}	1027.99	4.24030×10^{-11}	1.86750×10^{-12}
1002.51	7.49380×10^{-11}	3.30780×10^{-12}	1028.64	4.18680×10^{-11}	1.84600×10^{-12}
1003.17	7.37050×10^{-11}	3.25030×10^{-12}	1029.30	4.13430×10^{-11}	1.82500×10^{-12}
1003.82	7.25020×10^{-11}	3.19430×10^{-12}	1029.95	4.08290×10^{-11}	1.80460×10^{-12}
1004.47	7.13280×10^{-11}	3.13980×10^{-12}	1030.60	4.03250×10^{-11}	1.78460×10^{-12}
1005.13	7.01810×10^{-11}	3.08660×10^{-12}	1031.26	3.98310×10^{-11}	1.76510×10^{-12}
1005.78	6.90620×10^{-11}	3.03480×10^{-12}	1031.91	3.93460×10^{-11}	1.74610×10^{-12}
1006.43	6.79680×10^{-11}	2.98430×10^{-12}	1032.56	3.88720×10^{-11}	1.72750×10^{-12}
1007.09	6.68990×10^{-11}	2.93510×10^{-12}	1033.22	3.84060×10^{-11}	1.70940×10^{-12}
1007.74	6.58540×10^{-11}	2.88710×10^{-12}	1033.87	3.79500×10^{-11}	1.69170×10^{-12}

Table A.22 (cont'd)

JD +2450000	*UVOIR* Flux	Flux error	JD +2450000	*UVOIR* Flux	Flux error
1034.52	3.75020×10^{-11}	1.67450×10^{-12}	1047.59	3.01430×10^{-11}	1.40190×10^{-12}
1035.18	3.70630×10^{-11}	1.65760×10^{-12}	1048.24	2.98420×10^{-11}	1.39120×10^{-12}
1035.83	3.66330×10^{-11}	1.64120×10^{-12}	1048.90	2.95470×10^{-11}	1.38080×10^{-12}
1036.48	3.62110×10^{-11}	1.62510×10^{-12}	1049.55	2.92570×10^{-11}	1.37050×10^{-12}
1037.14	3.57970×10^{-11}	1.60940×10^{-12}	1050.20	2.89730×10^{-11}	1.36050×10^{-12}
1037.79	3.53910×10^{-11}	1.59410×10^{-12}	1050.85	2.86930×10^{-11}	1.35070×10^{-12}
1038.44	3.49920×10^{-11}	1.57920×10^{-12}	1051.51	2.84190×10^{-11}	1.34100×10^{-12}
1039.09	3.46020×10^{-11}	1.56450×10^{-12}	1052.16	2.81490×10^{-11}	1.33160×10^{-12}
1039.75	3.42190×10^{-11}	1.55030×10^{-12}	1052.81	2.78850×10^{-11}	1.32240×10^{-12}
1040.40	3.38430×10^{-11}	1.53630×10^{-12}	1053.47	2.76240×10^{-11}	1.31330×10^{-12}
1041.06	3.34740×10^{-11}	1.52270×10^{-12}	1054.12	2.73690×10^{-11}	1.30440×10^{-12}
1041.71	3.31120×10^{-11}	1.50930×10^{-12}	1054.77	2.71170×10^{-11}	1.29570×10^{-12}
1042.36	3.27570×10^{-11}	1.49630×10^{-12}	1055.43	2.68710×10^{-11}	1.28720×10^{-12}
1043.02	3.24080×10^{-11}	1.48360×10^{-12}	1056.08	2.66280×10^{-11}	1.27880×10^{-12}
1043.67	3.20660×10^{-11}	1.47110×10^{-12}	1056.73	2.63900×10^{-11}	1.27060×10^{-12}
1044.32	3.17300×10^{-11}	1.45890×10^{-12}	1057.39	2.61550×10^{-11}	1.26250×10^{-12}
1044.97	3.14010×10^{-11}	1.44700×10^{-12}	1058.04	2.59250×10^{-11}	1.25460×10^{-12}
1045.63	3.10780×10^{-11}	1.43540×10^{-12}	1058.69	2.56980×10^{-11}	1.24680×10^{-12}
1046.28	3.07600×10^{-11}	1.42400×10^{-12}	1059.35	2.54760×10^{-11}	1.23920×10^{-12}
1046.94	3.04480×10^{-11}	1.41280×10^{-12}	1060.00	2.52570×10^{-11}	1.23170×10^{-12}

Table A.23. SN 1998de

JD +2451000	*UVOIR* Flux	Flux error	JD +2450000	*UVOIR* Flux	Flux error
18.6130	6.44556×10^{-13}	3.29411×10^{-14}	43.1360	1.02174×10^{-12}	5.17138×10^{-14}
19.2260	9.33930×10^{-13}	4.47563×10^{-14}	43.7490	9.63183×10^{-13}	4.86827×10^{-14}
19.8390	1.25868×10^{-12}	5.97912×10^{-14}	44.3620	9.08994×10^{-13}	4.58573×10^{-14}
20.4520	1.57020×10^{-12}	7.48792×10^{-14}	44.9750	8.59141×10^{-13}	4.32447×10^{-14}
21.0650	1.85107×10^{-12}	8.83457×10^{-14}	45.5880	8.13553×10^{-13}	4.08459×10^{-14}
21.6780	2.10084×10^{-12}	1.00069×10^{-13}	46.2010	7.72058×10^{-13}	3.86552×10^{-14}
22.2910	2.32395×10^{-12}	1.10393×10^{-13}	46.8140	7.34446×10^{-13}	3.66663×10^{-14}
22.9050	2.52370×10^{-12}	1.19612×10^{-13}	47.4270	7.00461×10^{-13}	3.48679×10^{-14}
23.5180	2.70178×10^{-12}	1.27874×10^{-13}	48.0400	6.69814×10^{-13}	3.32469×10^{-14}
24.1310	2.85808×10^{-12}	1.35188×10^{-13}	48.6530	6.42198×10^{-13}	3.17873×10^{-14}
24.7440	2.99156×10^{-12}	1.41512×10^{-13}	49.2660	6.17329×10^{-13}	3.04747×10^{-14}
25.3570	3.10112×10^{-12}	1.46795×10^{-13}	49.8790	5.94884×10^{-13}	2.92940×10^{-14}
25.9700	3.18620×10^{-12}	1.50985×10^{-13}	50.4920	5.74611×10^{-13}	2.82294×10^{-14}
26.5830	3.24716×10^{-12}	1.54108×10^{-13}	51.1060	5.56242×10^{-13}	2.72683×10^{-14}
27.1960	3.28511×10^{-12}	1.56213×10^{-13}	51.7190	5.39523×10^{-13}	2.63966×10^{-14}
27.8090	3.30037×10^{-12}	1.57302×10^{-13}	52.3320	5.24258×10^{-13}	2.56023×10^{-14}
28.4220	3.29144×10^{-12}	1.57307×10^{-13}	52.9450	5.10232×10^{-13}	2.48767×10^{-14}
29.0350	3.25471×10^{-12}	1.56004×10^{-13}	53.5580	4.97287×10^{-13}	2.42082×10^{-14}
29.6480	3.18770×10^{-12}	1.53273×10^{-13}	54.1710	4.85267×10^{-13}	2.35896×10^{-14}
30.2610	3.09338×10^{-12}	1.49200×10^{-13}	54.7840	4.74048×10^{-13}	2.30147×10^{-14}
30.8740	2.97984×10^{-12}	1.44158×10^{-13}	55.3970	4.63511×10^{-13}	2.24764×10^{-14}
31.4870	2.85637×10^{-12}	1.38604×10^{-13}	56.0100	4.53568×10^{-13}	2.19688×10^{-14}
32.1010	2.73006×10^{-12}	1.32856×10^{-13}	56.6230	4.44124×10^{-13}	2.14893×10^{-14}
32.7140	2.60434×10^{-12}	1.27098×10^{-13}	57.2360	4.35115×10^{-13}	2.10321×10^{-14}
33.3270	2.48072×10^{-12}	1.21386×10^{-13}	57.8490	4.26490×10^{-13}	2.05957×10^{-14}
33.9400	2.35985×10^{-12}	1.15786×10^{-13}	58.4620	4.18190×10^{-13}	2.01766×10^{-14}
34.5530	2.24248×10^{-12}	1.10334×10^{-13}	59.0750	4.10177×10^{-13}	1.97734×10^{-14}
35.1660	2.12921×10^{-12}	1.05066×10^{-13}	59.6880	4.02413×10^{-13}	1.93828×10^{-14}
35.7790	2.02048×10^{-12}	1.00004×10^{-13}	60.3020	3.94875×10^{-13}	1.90045×10^{-14}
36.3920	1.91639×10^{-12}	9.51523×10^{-14}	60.9150	3.87538×10^{-13}	1.86363×10^{-14}
37.0050	1.81673×10^{-12}	9.04966×10^{-14}	61.5280	3.80389×10^{-13}	1.82781×10^{-14}
37.6180	1.72122×10^{-12}	8.60191×10^{-14}	62.1410	3.73395×10^{-13}	1.79288×10^{-14}
38.2310	1.62951×10^{-12}	8.16950×10^{-14}	62.7540	3.66568×10^{-13}	1.75884×10^{-14}
38.8440	1.54139×10^{-12}	7.75036×10^{-14}	63.3670	3.59875×10^{-13}	1.72548×10^{-14}
39.4570	1.45663×10^{-12}	7.34311×10^{-14}	63.9800	3.53328×10^{-13}	1.69280×10^{-14}
40.0700	1.37521×10^{-12}	6.94729×10^{-14}	64.5930	3.46907×10^{-13}	1.66092×10^{-14}
40.6830	1.29700×10^{-12}	6.56310×10^{-14}	65.2060	3.40603×10^{-13}	1.62963×10^{-14}
41.2960	1.22239×10^{-12}	6.19174×10^{-14}	65.8190	3.34429×10^{-13}	1.59894×10^{-14}
41.9100	1.15154×10^{-12}	5.83473×10^{-14}	66.4320	3.28365×10^{-13}	1.56886×10^{-14}
42.5230	1.08456×10^{-12}	5.49409×10^{-14}	67.0450	3.22415×10^{-13}	1.53942×10^{-14}

Table A.23 (cont'd)

JD +2451000	*UVOIR* Flux	Flux error	JD +2450000	*UVOIR* Flux	Flux error
67.6580	3.16581×10^{-13}	1.51050×10^{-14}	92.1810	1.58281×10^{-13}	7.37938×10^{-15}
68.2710	3.10855×10^{-13}	1.48224×10^{-14}	92.7940	1.55703×10^{-13}	7.25532×10^{-15}
68.8840	3.05240×10^{-13}	1.45442×10^{-14}	93.4070	1.53156×10^{-13}	7.13360×10^{-15}
69.4970	2.99727×10^{-13}	1.42729×10^{-14}	94.0200	1.50662×10^{-13}	7.01401×10^{-15}
70.1110	2.94330×10^{-13}	1.40063×10^{-14}	94.6330	1.48212×10^{-13}	6.89677×10^{-15}
70.7240	2.89030×10^{-13}	1.37456×10^{-14}	95.2460	1.45804×10^{-13}	6.78169×10^{-15}
71.3370	2.83840×10^{-13}	1.34899×10^{-14}	95.8590	1.43439×10^{-13}	6.66866×10^{-15}
71.9500	2.78762×10^{-13}	1.32404×10^{-14}	96.4720	1.41118×10^{-13}	6.55782×10^{-15}
72.5630	2.73776×10^{-13}	1.29950×10^{-14}	97.0850	1.38830×10^{-13}	6.44896×10^{-15}
73.1760	2.68896×10^{-13}	1.27560×10^{-14}	97.6980	1.36597×10^{-13}	6.34218×10^{-15}
73.7890	2.64111×10^{-13}	1.25212×10^{-14}	98.3120	1.34387×10^{-13}	6.23740×10^{-15}
74.4020	2.59424×10^{-13}	1.22918×10^{-14}	98.9250	1.32232×10^{-13}	6.13451×10^{-15}
75.0150	2.54846×10^{-13}	1.20668×10^{-14}	99.5380	1.30111×10^{-13}	6.03365×10^{-15}
75.6280	2.50356×10^{-13}	1.18473×10^{-14}	100.151	1.28023×10^{-13}	5.93469×10^{-15}
76.2410	2.45956×10^{-13}	1.16323×10^{-14}	100.764	1.25981×10^{-13}	5.83755×10^{-15}
76.8540	2.41657×10^{-13}	1.14218×10^{-14}	101.377	1.23962×10^{-13}	5.74231×10^{-15}
77.4670	2.37448×10^{-13}	1.12157×10^{-14}	101.990	1.21999×10^{-13}	5.64878×10^{-15}
78.0800	2.33329×10^{-13}	1.10153×10^{-14}	102.603	1.20059×10^{-13}	5.55705×10^{-15}
78.6930	2.29291×10^{-13}	1.08181×10^{-14}	103.216	1.18152×10^{-13}	5.46702×10^{-15}
79.3070	2.25343×10^{-13}	1.06256×10^{-14}	103.829	1.16280×10^{-13}	5.37868×10^{-15}
79.9200	2.21474×10^{-13}	1.04371×10^{-14}	104.442	1.14442×10^{-13}	5.29191×10^{-15}
80.5330	2.17696×10^{-13}	1.02528×10^{-14}	105.055	1.12637×10^{-13}	5.20682×10^{-15}
81.1460	2.13986×10^{-13}	1.00723×10^{-14}	105.668	1.10865×10^{-13}	5.12318×10^{-15}
81.7590	2.10355×10^{-13}	9.89566×10^{-15}	106.281	1.09127×10^{-13}	5.04108×10^{-15}
82.3720	2.06791×10^{-13}	9.72280×10^{-15}	106.894	1.07409×10^{-13}	4.96052×10^{-15}
82.9850	2.03305×10^{-13}	9.55339×10^{-15}	107.508	1.05725×10^{-13}	4.88138×10^{-15}
83.5980	1.99885×10^{-13}	9.38753×10^{-15}	108.121	1.04068×10^{-13}	4.80354×10^{-15}
84.2110	1.96542×10^{-13}	9.22506×10^{-15}	108.734	1.02440×10^{-13}	4.72710×10^{-15}
84.8240	1.93254×10^{-13}	9.06587×10^{-15}	109.347	1.00838×10^{-13}	4.65204×10^{-15}
85.4370	1.90031×10^{-13}	8.90983×10^{-15}	109.960	9.92612×10^{-14}	4.57816×10^{-15}
86.0500	1.86872×10^{-13}	8.75691×10^{-15}	110.573	9.77111×10^{-14}	4.50565×10^{-15}
86.6630	1.83767×10^{-13}	8.60700×10^{-15}	111.186	9.61852×10^{-14}	4.43430×10^{-15}
87.2760	1.80726×10^{-13}	8.45996×10^{-15}	111.799	9.46833×10^{-14}	4.36410×10^{-15}
87.8890	1.77738×10^{-13}	8.31568×10^{-15}	112.412	9.32055×10^{-14}	4.29505×10^{-15}
88.5030	1.74802×10^{-13}	8.17426×10^{-15}	113.025	9.17508×10^{-14}	4.22716×10^{-15}
89.1160	1.71930×10^{-13}	8.03547×10^{-15}	113.638	9.03192×10^{-14}	4.16043×10^{-15}
89.7290	1.69100×10^{-13}	7.89920×10^{-15}	114.251	8.89109×10^{-14}	4.09487×10^{-15}
90.3420	1.66322×10^{-13}	7.76556×10^{-15}	114.864	8.75238×10^{-14}	4.03037×10^{-15}
90.9550	1.63596×10^{-13}	7.63445×10^{-15}	115.477	8.61605×10^{-14}	3.96695×10^{-15}
91.5680	1.60912×10^{-13}	7.50565×10^{-15}	116.090	8.48178×10^{-14}	3.90451×10^{-15}

Table A.23 (cont'd)

JD +2451000	*UVOIR* Flux	Flux error	JD +2450000	*UVOIR* Flux	Flux error
116.704	8.34971×10^{-14}	3.84327×10^{-15}	124.673	6.82383×10^{-14}	3.13824×10^{-15}
117.317	8.21987×10^{-14}	3.78304×10^{-15}	125.286	6.71957×10^{-14}	3.09031×10^{-15}
117.930	8.09229×10^{-14}	3.72383×10^{-15}	125.899	6.61691×10^{-14}	3.04308×10^{-15}
118.543	7.96677×10^{-14}	3.66564×10^{-15}	126.513	6.51571×10^{-14}	2.99664×10^{-15}
119.156	7.84334×10^{-14}	3.60860×10^{-15}	127.126	6.41581×10^{-14}	2.95075×10^{-15}
119.769	7.72211×10^{-14}	3.55250×10^{-15}	127.739	6.31721×10^{-14}	2.90563×10^{-15}
120.382	7.60289×10^{-14}	3.49733×10^{-15}	128.352	6.22001×10^{-14}	2.86105×10^{-15}
120.995	7.48580×10^{-14}	3.44333×10^{-15}	128.965	6.12419×10^{-14}	2.81717×10^{-15}
121.608	7.37080×10^{-14}	3.39016×10^{-15}	129.578	6.02987×10^{-14}	2.77393×10^{-15}
122.221	7.25769×10^{-14}	3.33803×10^{-15}	130.191	5.93716×10^{-14}	2.73144×10^{-15}
122.834	7.14654×10^{-14}	3.28672×10^{-15}	130.804	5.84640×10^{-14}	2.68995×10^{-15}
123.447	7.03721×10^{-14}	3.23642×10^{-15}	131.417	5.75805×10^{-14}	2.64968×10^{-15}
124.060	6.92966×10^{-14}	3.18690×10^{-15}	132.030	5.67277×10^{-14}	2.61071×10^{-15}

Table A.24. SN 1999aa

JD +2451000	*UVOIR* Flux	Flux error	JD +2451000	*UVOIR* Flux	Flux error
221.598	9.19840×10^{-12}	4.15430×10^{-13}	245.518	1.30360×10^{-11}	5.77450×10^{-13}
222.196	1.10350×10^{-11}	4.90400×10^{-13}	246.116	1.24490×10^{-11}	5.50740×10^{-13}
222.794	1.26580×10^{-11}	5.60510×10^{-13}	246.714	1.18880×10^{-11}	5.25220×10^{-13}
223.392	1.40510×10^{-11}	6.21830×10^{-13}	247.312	1.13560×10^{-11}	5.00980×10^{-13}
223.990	1.52550×10^{-11}	6.74850×10^{-13}	247.910	1.08530×10^{-11}	4.78080×10^{-13}
224.588	1.63130×10^{-11}	7.21320×10^{-13}	248.508	1.03810×10^{-11}	4.56570×10^{-13}
225.186	1.72590×10^{-11}	7.62830×10^{-13}	249.106	9.93800×10^{-12}	4.36480×10^{-13}
225.784	1.81170×10^{-11}	8.00480×10^{-13}	249.704	9.52550×10^{-12}	4.17820×10^{-13}
226.382	1.89010×10^{-11}	8.35000×10^{-13}	250.302	9.14250×10^{-12}	4.00570×10^{-13}
226.980	1.96190×10^{-11}	8.66760×10^{-13}	250.899	8.78850×10^{-12}	3.84730×10^{-13}
227.578	2.02750×10^{-11}	8.95950×10^{-13}	251.497	8.46230×10^{-12}	3.70250×10^{-13}
228.176	2.08710×10^{-11}	9.22620×10^{-13}	252.095	8.16290×10^{-12}	3.57100×10^{-13}
228.774	2.14070×10^{-11}	9.46750×10^{-13}	252.693	7.88880×10^{-12}	3.45210×10^{-13}
229.372	2.18820×10^{-11}	9.68260×10^{-13}	253.291	7.63850×10^{-12}	3.34530×10^{-13}
229.970	2.22930×10^{-11}	9.87020×10^{-13}	253.889	7.41020×10^{-12}	3.24970×10^{-13}
230.568	2.26390×10^{-11}	1.00290×10^{-12}	254.487	7.20210×10^{-12}	3.16450×10^{-13}
231.166	2.29160×10^{-11}	1.01580×10^{-12}	255.085	7.01230×10^{-12}	3.08860×10^{-13}
231.764	2.31240×10^{-11}	1.02560×10^{-12}	255.683	6.83870×10^{-12}	3.02090×10^{-13}
232.362	2.32600×10^{-11}	1.03220×10^{-12}	256.281	6.67900×10^{-12}	2.96030×10^{-13}
232.960	2.33230×10^{-11}	1.03550×10^{-12}	256.879	6.53100×10^{-12}	2.90540×10^{-13}
233.558	2.33120×10^{-11}	1.03550×10^{-12}	257.477	6.39250×10^{-12}	2.85500×10^{-13}
234.156	2.32280×10^{-11}	1.03220×10^{-12}	258.075	6.26130×10^{-12}	2.80770×10^{-13}
234.754	2.30700×10^{-11}	1.02560×10^{-12}	258.673	6.13520×10^{-12}	2.76220×10^{-13}
235.352	2.28420×10^{-11}	1.01580×10^{-12}	259.271	6.01220×10^{-12}	2.71740×10^{-13}
235.950	2.25450×10^{-11}	1.00300×10^{-12}	259.869	5.89060×10^{-12}	2.67200×10^{-13}
236.548	2.21830×10^{-11}	9.87190×10^{-13}	260.467	5.76870×10^{-12}	2.62520×10^{-13}
237.146	2.17620×10^{-11}	9.68680×10^{-13}	261.065	5.64540×10^{-12}	2.57620×10^{-13}
237.744	2.12850×10^{-11}	9.47670×10^{-13}	261.663	5.51980×10^{-12}	2.52460×10^{-13}
238.342	2.07590×10^{-11}	9.24420×10^{-13}	262.261	5.39140×10^{-12}	2.47010×10^{-13}
238.940	2.01900×10^{-11}	8.99210×10^{-13}	262.859	5.26010×10^{-12}	2.41280×10^{-13}
239.538	1.95860×10^{-11}	8.72350×10^{-13}	263.457	5.12590×10^{-12}	2.35280×10^{-13}
240.136	1.89530×10^{-11}	8.44130×10^{-13}	264.055	4.98940×10^{-12}	2.29050×10^{-13}
240.734	1.82980×10^{-11}	8.14880×10^{-13}	264.653	4.85110×10^{-12}	2.22650×10^{-13}
241.332	1.76290×10^{-11}	7.84900×10^{-13}	265.251	4.71190×10^{-12}	2.16140×10^{-13}
241.930	1.69510×10^{-11}	7.54490×10^{-13}	265.849	4.57270×10^{-12}	2.09570×10^{-13}
242.528	1.62720×10^{-11}	7.23940×10^{-13}	266.447	4.43440×10^{-12}	2.03010×10^{-13}
243.126	1.55970×10^{-11}	6.93510×10^{-13}	267.045	4.29800×10^{-12}	1.96510×10^{-13}
243.724	1.49310×10^{-11}	6.63440×10^{-13}	267.643	4.16420×10^{-12}	1.90130×10^{-13}
244.322	1.42800×10^{-11}	6.33950×10^{-13}	268.241	4.03390×10^{-12}	1.83920×10^{-13}
244.920	1.36470×10^{-11}	6.05230×10^{-13}	268.839	3.90760×10^{-12}	1.77910×10^{-13}

Table A.24 (cont'd)

JD +2451000	*UVOIR* Flux	Flux error	JD +2451000	*UVOIR* Flux	Flux error
269.437	3.78590×10^{-12}	1.72140×10^{-13}	293.357	1.77710×10^{-12}	7.87870×10^{-14}
270.035	3.66920×10^{-12}	1.66610×10^{-13}	293.955	1.75460×10^{-12}	7.77240×10^{-14}
270.633	3.55790×10^{-12}	1.61350×10^{-13}	294.553	1.73240×10^{-12}	7.66790×10^{-14}
271.231	3.45190×10^{-12}	1.56370×10^{-13}	295.151	1.71050×10^{-12}	7.56510×10^{-14}
271.829	3.35150×10^{-12}	1.51670×10^{-13}	295.749	1.68900×10^{-12}	7.46410×10^{-14}
272.427	3.25670×10^{-12}	1.47250×10^{-13}	296.347	1.66790×10^{-12}	7.36480×10^{-14}
273.025	3.16720×10^{-12}	1.43090×10^{-13}	296.945	1.64700×10^{-12}	7.26710×10^{-14}
273.623	3.08300×10^{-12}	1.39200×10^{-13}	297.543	1.62640×10^{-12}	7.17100×10^{-14}
274.221	3.00380×10^{-12}	1.35550×10^{-13}	298.141	1.60620×10^{-12}	7.07650×10^{-14}
274.819	2.92950×10^{-12}	1.32140×10^{-13}	298.739	1.58620×10^{-12}	6.98350×10^{-14}
275.417	2.85970×10^{-12}	1.28950×10^{-13}	299.337	1.56660×10^{-12}	6.89200×10^{-14}
276.015	2.79410×10^{-12}	1.25960×10^{-13}	299.935	1.54720×10^{-12}	6.80210×10^{-14}
276.613	2.73250×10^{-12}	1.23160×10^{-13}	300.533	1.52800×10^{-12}	6.71350×10^{-14}
277.211	2.67460×10^{-12}	1.20520×10^{-13}	301.131	1.50920×10^{-12}	6.62640×10^{-14}
277.809	2.62000×10^{-12}	1.18040×10^{-13}	301.729	1.49060×10^{-12}	6.54070×10^{-14}
278.407	2.56850×10^{-12}	1.15710×10^{-13}	302.327	1.47230×10^{-12}	6.45640×10^{-14}
279.005	2.51990×10^{-12}	1.13490×10^{-13}	302.925	1.45420×10^{-12}	6.37340×10^{-14}
279.603	2.47390×10^{-12}	1.11400×10^{-13}	303.523	1.43640×10^{-12}	6.29180×10^{-14}
280.201	2.43020×10^{-12}	1.09400×10^{-13}	304.121	1.41890×10^{-12}	6.21140×10^{-14}
280.799	2.38860×10^{-12}	1.07490×10^{-13}	304.719	1.40150×10^{-12}	6.13240×10^{-14}
281.397	2.34900×10^{-12}	1.05670×10^{-13}	305.317	1.38450×10^{-12}	6.05460×10^{-14}
281.995	2.31110×10^{-12}	1.03930×10^{-13}	305.915	1.36760×10^{-12}	5.97800×10^{-14}
282.593	2.27480×10^{-12}	1.02250×10^{-13}	306.513	1.35100×10^{-12}	5.90270×10^{-14}
283.191	2.23990×10^{-12}	1.00630×10^{-13}	307.111	1.33470×10^{-12}	5.82850×10^{-14}
283.789	2.20630×10^{-12}	9.90610×10^{-14}	307.709	1.31850×10^{-12}	5.75560×10^{-14}
284.387	2.17390×10^{-12}	9.75470×10^{-14}	308.307	1.30260×10^{-12}	5.68380×10^{-14}
284.985	2.14260×10^{-12}	9.60770×10^{-14}	308.905	1.28690×10^{-12}	5.61320×10^{-14}
285.583	2.11220×10^{-12}	9.46500×10^{-14}	309.503	1.27140×10^{-12}	5.54360×10^{-14}
286.181	2.08270×10^{-12}	9.32600×10^{-14}	310.100	1.25620×10^{-12}	5.47520×10^{-14}
286.779	2.05410×10^{-12}	9.19060×10^{-14}	310.698	1.24110×10^{-12}	5.40780×10^{-14}
287.377	2.02610×10^{-12}	9.05850×10^{-14}	311.296	1.22630×10^{-12}	5.34160×10^{-14}
287.975	1.99890×10^{-12}	8.92930×10^{-14}	311.894	1.21160×10^{-12}	5.27630×10^{-14}
288.573	1.97220×10^{-12}	8.80310×10^{-14}	312.492	1.19720×10^{-12}	5.21210×10^{-14}
289.171	1.94620×10^{-12}	8.67950×10^{-14}	313.090	1.18290×10^{-12}	5.14900×10^{-14}
289.769	1.92060×10^{-12}	8.55840×10^{-14}	313.688	1.16890×10^{-12}	5.08680×10^{-14}
290.367	1.89560×10^{-12}	8.43980×10^{-14}	314.286	1.15510×10^{-12}	5.02560×10^{-14}
290.965	1.87110×10^{-12}	8.32340×10^{-14}	314.884	1.14140×10^{-12}	4.96530×10^{-14}
291.563	1.84690×10^{-12}	8.20910×10^{-14}	315.482	1.12790×10^{-12}	4.90600×10^{-14}
292.161	1.82330×10^{-12}	8.09700×10^{-14}	316.080	1.11460×10^{-12}	4.84770×10^{-14}
292.759	1.80000×10^{-12}	7.98690×10^{-14}	316.678	1.10150×10^{-12}	4.79020×10^{-14}

Table A.24 (cont'd)

JD +2451000	*UVOIR* Flux	Flux error	JD +2451000	*UVOIR* Flux	Flux error
317.276	1.08860×10^{-12}	4.73370×10^{-14}	328.638	8.73900×10^{-13}	3.81170×10^{-14}
317.874	1.07590×10^{-12}	4.67800×10^{-14}	329.236	8.64060×10^{-13}	3.77030×10^{-14}
318.472	1.06330×10^{-12}	4.62330×10^{-14}	329.834	8.54360×10^{-13}	3.72960×10^{-14}
319.070	1.05090×10^{-12}	4.56930×10^{-14}	330.432	8.44780×10^{-13}	3.68940×10^{-14}
319.668	1.03860×10^{-12}	4.51620×10^{-14}	331.030	8.35340×10^{-13}	3.64980×10^{-14}
320.266	1.02660×10^{-12}	4.46400×10^{-14}	331.628	8.26020×10^{-13}	3.61090×10^{-14}
320.864	1.01470×10^{-12}	4.41250×10^{-14}	332.226	8.16820×10^{-13}	3.57250×10^{-14}
321.462	1.00290×10^{-12}	4.36190×10^{-14}	332.824	8.07750×10^{-13}	3.53470×10^{-14}
322.060	9.91360×10^{-13}	4.31200×10^{-14}	333.422	7.98800×10^{-13}	3.49740×10^{-14}
322.658	9.79940×10^{-13}	4.26290×10^{-14}	334.020	7.89970×10^{-13}	3.46080×10^{-14}
323.256	9.68680×10^{-13}	4.21460×10^{-14}	334.618	7.81250×10^{-13}	3.42460×10^{-14}
323.854	9.57560×10^{-13}	4.16700×10^{-14}	335.216	7.72650×10^{-13}	3.38900×10^{-14}
324.452	9.46600×10^{-13}	4.12020×10^{-14}	335.814	7.64170×10^{-13}	3.35390×10^{-14}
325.050	9.35790×10^{-13}	4.07400×10^{-14}	336.412	7.55790×10^{-13}	3.31940×10^{-14}
325.648	9.25120×10^{-13}	4.02860×10^{-14}	337.010	7.47530×10^{-13}	3.28530×10^{-14}
326.246	9.14590×10^{-13}	3.98390×10^{-14}	337.608	7.39370×10^{-13}	3.25180×10^{-14}
326.844	9.04210×10^{-13}	3.93990×10^{-14}	338.206	7.31320×10^{-13}	3.21870×10^{-14}
327.442	8.93970×10^{-13}	3.89650×10^{-14}	338.804	7.23380×10^{-13}	3.18620×10^{-14}
328.040	8.83860×10^{-13}	3.85380×10^{-14}	339.402	7.15540×10^{-13}	3.15410×10^{-14}

Table A.25. SN 1999ac

JD +2451000	*UVOIR* Flux	Flux error	JD +2451000	*UVOIR* Flux	Flux error
235.603	1.24580×10^{-11}	6.66380×10^{-13}	259.724	4.04520×10^{-11}	1.77080×10^{-12}
236.206	1.41580×10^{-11}	7.27620×10^{-13}	260.327	3.87330×10^{-11}	1.69480×10^{-12}
236.809	1.60450×10^{-11}	7.97790×10^{-13}	260.930	3.70600×10^{-11}	1.62090×10^{-12}
237.412	1.81120×10^{-11}	8.77120×10^{-13}	261.533	3.54420×10^{-11}	1.54970×10^{-12}
238.015	2.03490×10^{-11}	9.65540×10^{-13}	262.136	3.38850×10^{-11}	1.48130×10^{-12}
238.618	2.27420×10^{-11}	1.06260×10^{-12}	262.739	3.23950×10^{-11}	1.41600×10^{-12}
239.221	2.52710×10^{-11}	1.16760×10^{-12}	263.342	3.09750×10^{-11}	1.35390×10^{-12}
239.824	2.79140×10^{-11}	1.27940×10^{-12}	263.945	2.96290×10^{-11}	1.29520×10^{-12}
240.427	3.06430×10^{-11}	1.39670×10^{-12}	264.548	2.83580×10^{-11}	1.23980×10^{-12}
241.030	3.34280×10^{-11}	1.51800×10^{-12}	265.151	2.71620×10^{-11}	1.18790×10^{-12}
241.633	3.62370×10^{-11}	1.64170×10^{-12}	265.754	2.60410×10^{-11}	1.13940×10^{-12}
242.236	3.90370×10^{-11}	1.76590×10^{-12}	266.357	2.49940×10^{-11}	1.09430×10^{-12}
242.839	4.17910×10^{-11}	1.88890×10^{-12}	266.960	2.40200×10^{-11}	1.05250×10^{-12}
243.442	4.44650×10^{-11}	2.00870×10^{-12}	267.563	2.31160×10^{-11}	1.01400×10^{-12}
244.045	4.70250×10^{-11}	2.12350×10^{-12}	268.166	2.22800×10^{-11}	9.78570×10^{-13}
244.648	4.94390×10^{-11}	2.23180×10^{-12}	268.769	2.15090×10^{-11}	9.46160×10^{-13}
245.251	5.16760×10^{-11}	2.33190×10^{-12}	269.372	2.07980×10^{-11}	9.16600×10^{-13}
245.854	5.37090×10^{-11}	2.42250×10^{-12}	269.975	2.01450×10^{-11}	8.89720×10^{-13}
246.457	5.55160×10^{-11}	2.50230×10^{-12}	270.578	1.95450×10^{-11}	8.65310×10^{-13}
247.060	5.70760×10^{-11}	2.57060×10^{-12}	271.181	1.89940×10^{-11}	8.43150×10^{-13}
247.663	5.83760×10^{-11}	2.62650×10^{-12}	271.784	1.84860×10^{-11}	8.22990×10^{-13}
248.266	5.94050×10^{-11}	2.66960×10^{-12}	272.387	1.80160×10^{-11}	8.04560×10^{-13}
248.869	6.01570×10^{-11}	2.69980×10^{-12}	272.990	1.75800×10^{-11}	7.87570×10^{-13}
249.472	6.06320×10^{-11}	2.71720×10^{-12}	273.593	1.71700×10^{-11}	7.71720×10^{-13}
250.075	6.08340×10^{-11}	2.72190×10^{-12}	274.196	1.67830×10^{-11}	7.56710×10^{-13}
250.678	6.07700×10^{-11}	2.71450×10^{-12}	274.799	1.64110×10^{-11}	7.42240×10^{-13}
251.281	6.04520×10^{-11}	2.69560×10^{-12}	275.402	1.60500×10^{-11}	7.28010×10^{-13}
251.884	5.98950×10^{-11}	2.66600×10^{-12}	276.005	1.56950×10^{-11}	7.13750×10^{-13}
252.487	5.91170×10^{-11}	2.62670×10^{-12}	276.608	1.53410×10^{-11}	6.99240×10^{-13}
253.090	5.81380×10^{-11}	2.57870×10^{-12}	277.211	1.49840×10^{-11}	6.84290×10^{-13}
253.693	5.69800×10^{-11}	2.52300×10^{-12}	277.814	1.46220×10^{-11}	6.68770×10^{-13}
254.296	5.56650×10^{-11}	2.46080×10^{-12}	278.417	1.42520×10^{-11}	6.52590×10^{-13}
254.899	5.42170×10^{-11}	2.39300×10^{-12}	279.020	1.38750×10^{-11}	6.35750×10^{-13}
255.503	5.26580×10^{-11}	2.32090×10^{-12}	279.623	1.34900×10^{-11}	6.18280×10^{-13}
256.106	5.10130×10^{-11}	2.24540×10^{-12}	280.226	1.30990×10^{-11}	6.00270×10^{-13}
256.709	4.93020×10^{-11}	2.16740×10^{-12}	280.829	1.27040×10^{-11}	5.81860×10^{-13}
257.312	4.75480×10^{-11}	2.08800×10^{-12}	281.432	1.23070×10^{-11}	5.63210×10^{-13}
257.915	4.57690×10^{-11}	2.00800×10^{-12}	282.035	1.19120×10^{-11}	5.44490×10^{-13}
258.518	4.39830×10^{-11}	1.92800×10^{-12}	282.638	1.15220×10^{-11}	5.25890×10^{-13}
259.121	4.22050×10^{-11}	1.84870×10^{-12}	283.241	1.11390×10^{-11}	5.07580×10^{-13}

Table A.25 (cont'd)

JD +2451000	*UVOIR* Flux	Flux error	JD +2451000	*UVOIR* Flux	Flux error
283.844	1.07660×10^{-11}	4.89720×10^{-13}	307.965	4.62230×10^{-12}	2.03970×10^{-13}
284.447	1.04060×10^{-11}	4.72430×10^{-13}	308.568	4.55720×10^{-12}	2.01060×10^{-13}
285.050	1.00600×10^{-11}	4.55820×10^{-13}	309.171	4.49320×10^{-12}	1.98190×10^{-13}
285.653	9.73000×10^{-12}	4.39970×10^{-13}	309.774	4.43020×10^{-12}	1.95380×10^{-13}
286.256	9.41660×10^{-12}	4.24940×10^{-13}	310.377	4.36830×10^{-12}	1.92610×10^{-13}
286.859	9.12010×10^{-12}	4.10740×10^{-13}	310.980	4.30740×10^{-12}	1.89900×10^{-13}
287.462	8.84060×10^{-12}	3.97400×10^{-13}	311.583	4.24760×10^{-12}	1.87230×10^{-13}
288.065	8.57780×10^{-12}	3.84890×10^{-13}	312.186	4.18860×10^{-12}	1.84600×10^{-13}
288.668	8.33130×10^{-12}	3.73200×10^{-13}	312.789	4.13060×10^{-12}	1.82020×10^{-13}
289.271	8.10020×10^{-12}	3.62280×10^{-13}	313.392	4.07350×10^{-12}	1.79480×10^{-13}
289.874	7.88370×10^{-12}	3.52100×10^{-13}	313.995	4.01730×10^{-12}	1.76990×10^{-13}
290.477	7.68090×10^{-12}	3.42610×10^{-13}	314.598	3.96190×10^{-12}	1.74530×10^{-13}
291.080	7.49080×10^{-12}	3.33750×10^{-13}	315.201	3.90740×10^{-12}	1.72110×10^{-13}
291.683	7.31240×10^{-12}	3.25490×10^{-13}	315.804	3.85360×10^{-12}	1.69740×10^{-13}
292.286	7.14490×10^{-12}	3.17760×10^{-13}	316.407	3.80070×10^{-12}	1.67400×10^{-13}
292.889	6.98720×10^{-12}	3.10510×10^{-13}	317.010	3.74860×10^{-12}	1.65090×10^{-13}
293.492	6.83850×10^{-12}	3.03720×10^{-13}	317.613	3.69730×10^{-12}	1.62830×10^{-13}
294.095	6.69800×10^{-12}	2.97320×10^{-13}	318.216	3.64670×10^{-12}	1.60600×10^{-13}
294.698	6.56500×10^{-12}	2.91280×10^{-13}	318.819	3.59680×10^{-12}	1.58400×10^{-13}
295.302	6.43870×10^{-12}	2.85560×10^{-13}	319.422	3.54770×10^{-12}	1.56240×10^{-13}
295.905	6.31850×10^{-12}	2.80130×10^{-13}	320.025	3.49930×10^{-12}	1.54110×10^{-13}
296.508	6.20390×10^{-12}	2.74970×10^{-13}	320.628	3.45160×10^{-12}	1.52020×10^{-13}
297.111	6.09430×10^{-12}	2.70040×10^{-13}	321.231	3.40460×10^{-12}	1.49960×10^{-13}
297.714	5.98930×10^{-12}	2.65320×10^{-13}	321.834	3.35830×10^{-12}	1.47930×10^{-13}
298.317	5.88840×10^{-12}	2.60790×10^{-13}	322.437	3.31260×10^{-12}	1.45930×10^{-13}
298.920	5.79120×10^{-12}	2.56430×10^{-13}	323.040	3.26760×10^{-12}	1.43960×10^{-13}
299.523	5.69750×10^{-12}	2.52220×10^{-13}	323.643	3.22330×10^{-12}	1.42020×10^{-13}
300.126	5.60690×10^{-12}	2.48150×10^{-13}	324.246	3.17960×10^{-12}	1.40110×10^{-13}
300.729	5.51910×10^{-12}	2.44210×10^{-13}	324.849	3.13650×10^{-12}	1.38230×10^{-13}
301.332	5.43390×10^{-12}	2.40390×10^{-13}	325.452	3.09410×10^{-12}	1.36380×10^{-13}
301.935	5.35110×10^{-12}	2.36680×10^{-13}	326.055	3.05220×10^{-12}	1.34560×10^{-13}
302.538	5.27060×10^{-12}	2.33060×10^{-13}	326.658	3.01100×10^{-12}	1.32770×10^{-13}
303.141	5.19200×10^{-12}	2.29530×10^{-13}	327.261	2.97030×10^{-12}	1.31000×10^{-13}
303.744	5.11530×10^{-12}	2.26090×10^{-13}	327.864	2.93020×10^{-12}	1.29260×10^{-13}
304.347	5.04040×10^{-12}	2.22730×10^{-13}	328.467	2.89070×10^{-12}	1.27540×10^{-13}
304.950	4.96720×10^{-12}	2.19440×10^{-13}	329.070	2.85180×10^{-12}	1.25850×10^{-13}
305.553	4.89550×10^{-12}	2.16220×10^{-13}	329.673	2.81340×10^{-12}	1.24190×10^{-13}
306.156	4.82520×10^{-12}	2.13060×10^{-13}	330.276	2.77560×10^{-12}	1.22550×10^{-13}
306.759	4.75630×10^{-12}	2.09970×10^{-13}	330.879	2.73830×10^{-12}	1.20940×10^{-13}
307.362	4.68870×10^{-12}	2.06940×10^{-13}	331.482	2.70160×10^{-12}	1.19350×10^{-13}

Table A.25 (cont'd)

JD +2451000	*UVOIR* Flux	Flux error	JD +2451000	*UVOIR* Flux	Flux error
332.085	2.66540×10^{-12}	1.17780×10^{-13}	343.543	2.06690×10^{-12}	9.20710×10^{-14}
332.688	2.62960×10^{-12}	1.16240×10^{-13}	344.146	2.03970×10^{-12}	9.09070×10^{-14}
333.291	2.59440×10^{-12}	1.14720×10^{-13}	344.749	2.01280×10^{-12}	8.97600×10^{-14}
333.894	2.55970×10^{-12}	1.13230×10^{-13}	345.352	1.98640×10^{-12}	8.86290×10^{-14}
334.497	2.52550×10^{-12}	1.11750×10^{-13}	345.955	1.96030×10^{-12}	8.75150×10^{-14}
335.100	2.49180×10^{-12}	1.10300×10^{-13}	346.558	1.93450×10^{-12}	8.64170×10^{-14}
335.704	2.45860×10^{-12}	1.08870×10^{-13}	347.161	1.90920×10^{-12}	8.53350×10^{-14}
336.307	2.42580×10^{-12}	1.07460×10^{-13}	347.764	1.88420×10^{-12}	8.42680×10^{-14}
336.910	2.39350×10^{-12}	1.06070×10^{-13}	348.367	1.85950×10^{-12}	8.32160×10^{-14}
337.513	2.36160×10^{-12}	1.04700×10^{-13}	348.970	1.83520×10^{-12}	8.21800×10^{-14}
338.116	2.33020×10^{-12}	1.03350×10^{-13}	349.573	1.81120×10^{-12}	8.11580×10^{-14}
338.719	2.29930×10^{-12}	1.02020×10^{-13}	350.176	1.78750×10^{-12}	8.01510×10^{-14}
339.322	2.26880×10^{-12}	1.00710×10^{-13}	350.779	1.76420×10^{-12}	7.91580×10^{-14}
339.925	2.23870×10^{-12}	9.94240×10^{-14}	351.382	1.74120×10^{-12}	7.81790×10^{-14}
340.528	2.20900×10^{-12}	9.81530×10^{-14}	351.985	1.71860×10^{-12}	7.72150×10^{-14}
341.131	2.17980×10^{-12}	9.69000×10^{-14}	352.588	1.69620×10^{-12}	7.62630×10^{-14}
341.734	2.15100×10^{-12}	9.56660×10^{-14}	353.191	1.67420×10^{-12}	7.53260×10^{-14}
342.337	2.12260×10^{-12}	9.44500×10^{-14}	353.794	1.65240×10^{-12}	7.44010×10^{-14}
342.940	2.09450×10^{-12}	9.32520×10^{-14}	354.397	1.63100×10^{-12}	7.34900×10^{-14}

Table A.26. SN 1999aw

JD +2451000	*UVOIR* Flux	Flux error	JD +2451000	*UVOIR* Flux	Flux error
245.578	2.40764×10^{-12}	1.29230×10^{-13}	268.693	1.81597×10^{-12}	9.07538×10^{-14}
246.156	2.56163×10^{-12}	1.34253×10^{-13}	269.271	1.74286×10^{-12}	8.69617×10^{-14}
246.734	2.70411×10^{-12}	1.39559×10^{-13}	269.849	1.67354×10^{-12}	8.33608×10^{-14}
247.312	2.83082×10^{-12}	1.44726×10^{-13}	270.427	1.60803×10^{-12}	7.99563×10^{-14}
247.889	2.94139×10^{-12}	1.49541×10^{-13}	271.005	1.54638×10^{-12}	7.67479×10^{-14}
248.467	3.03798×10^{-12}	1.53914×10^{-13}	271.583	1.48863×10^{-12}	7.37370×10^{-14}
249.045	3.12273×10^{-12}	1.57868×10^{-13}	272.161	1.43457×10^{-12}	7.09193×10^{-14}
249.623	3.19750×10^{-12}	1.61428×10^{-13}	272.739	1.38414×10^{-12}	6.82943×10^{-14}
250.201	3.26354×10^{-12}	1.64631×10^{-13}	273.317	1.33726×10^{-12}	6.58557×10^{-14}
250.779	3.32186×10^{-12}	1.67480×10^{-13}	273.894	1.29386×10^{-12}	6.35988×10^{-14}
251.357	3.37256×10^{-12}	1.69981×10^{-13}	274.472	1.25364×10^{-12}	6.15161×10^{-14}
251.935	3.41573×10^{-12}	1.72138×10^{-13}	275.050	1.21655×10^{-12}	5.96004×10^{-14}
252.513	3.45123×10^{-12}	1.73917×10^{-13}	275.628	1.18242×10^{-12}	5.78440×10^{-14}
253.090	3.47881×10^{-12}	1.75313×10^{-13}	276.206	1.15107×10^{-12}	5.62397×10^{-14}
253.668	3.49803×10^{-12}	1.76297×10^{-13}	276.784	1.12236×10^{-12}	5.47784×10^{-14}
254.246	3.50859×10^{-12}	1.76854×10^{-13}	277.362	1.09601×10^{-12}	5.34502×10^{-14}
254.824	3.51030×10^{-12}	1.76975×10^{-13}	277.940	1.07189×10^{-12}	5.22454×10^{-14}
255.402	3.50300×10^{-12}	1.76638×10^{-13}	278.518	1.04989×10^{-12}	5.11556×10^{-14}
255.980	3.48645×10^{-12}	1.75838×10^{-13}	279.095	1.02974×10^{-12}	5.01704×10^{-14}
256.558	3.46075×10^{-12}	1.74574×10^{-13}	279.673	1.01128×10^{-12}	4.92797×10^{-14}
257.136	3.42605×10^{-12}	1.72859×10^{-13}	280.251	9.94340×10^{-13}	4.84725×10^{-14}
257.714	3.38267×10^{-12}	1.70697×10^{-13}	280.829	9.78732×10^{-13}	4.77388×10^{-14}
258.291	3.33098×10^{-12}	1.68119×10^{-13}	281.407	9.64284×10^{-13}	4.70700×10^{-14}
258.869	3.27149×10^{-12}	1.65132×10^{-13}	281.985	9.50814×10^{-13}	4.64533×10^{-14}
259.447	3.20476×10^{-12}	1.61783×10^{-13}	282.563	9.38161×10^{-13}	4.58802×10^{-14}
260.025	3.13174×10^{-12}	1.58094×10^{-13}	283.141	9.26167×10^{-13}	4.53411×10^{-14}
260.603	3.05290×10^{-12}	1.54115×10^{-13}	283.719	9.14654×10^{-13}	4.48267×10^{-14}
261.181	2.96930×10^{-12}	1.49891×10^{-13}	284.296	9.03486×10^{-13}	4.43275×10^{-14}
261.759	2.88191×10^{-12}	1.45449×10^{-13}	284.874	8.92524×10^{-13}	4.38355×10^{-14}
262.337	2.79141×10^{-12}	1.40857×10^{-13}	285.452	8.81633×10^{-13}	4.33434×10^{-14}
262.915	2.69884×10^{-12}	1.36138×10^{-13}	286.030	8.70696×10^{-13}	4.28453×10^{-14}
263.492	2.60500×10^{-12}	1.31351×10^{-13}	286.608	8.59604×10^{-13}	4.23343×10^{-14}
264.070	2.51068×10^{-12}	1.26535×10^{-13}	287.186	8.48274×10^{-13}	4.18055×10^{-14}
264.648	2.41663×10^{-12}	1.21723×10^{-13}	287.764	8.36623×10^{-13}	4.12542×10^{-14}
265.226	2.32365×10^{-12}	1.16953×10^{-13}	288.342	8.24591×10^{-13}	4.06791×10^{-14}
265.804	2.23239×10^{-12}	1.12255×10^{-13}	288.920	8.12118×10^{-13}	4.00756×10^{-14}
266.382	2.14312×10^{-12}	1.07664×10^{-13}	289.497	7.99191×10^{-13}	3.94434×10^{-14}
266.960	2.05656×10^{-12}	1.03201×10^{-13}	290.075	7.85778×10^{-13}	3.87827×10^{-14}
267.538	1.97293×10^{-12}	9.88838×10^{-14}	290.653	7.71888×10^{-13}	3.80932×10^{-14}
268.116	1.89267×10^{-12}	9.47305×10^{-14}	291.231	7.57531×10^{-13}	3.73751×10^{-14}

Table A.26 (cont'd)

JD +2451000	*UVOIR* Flux	Flux error	JD +2451000	*UVOIR* Flux	Flux error
291.809	7.42734×10^{-13}	3.66317×10^{-14}	314.925	3.04542×10^{-13}	1.48518×10^{-14}
292.387	7.27529×10^{-13}	3.58641×10^{-14}	315.503	3.00558×10^{-13}	1.46618×10^{-14}
292.965	7.11977×10^{-13}	3.50759×10^{-14}	316.080	2.96712×10^{-13}	1.44794×10^{-14}
293.543	6.96114×10^{-13}	3.42717×10^{-14}	316.658	2.93016×10^{-13}	1.43033×10^{-14}
294.121	6.80021×10^{-13}	3.34527×10^{-14}	317.236	2.89447×10^{-13}	1.41336×10^{-14}
294.698	6.63747×10^{-13}	3.26247×10^{-14}	317.814	2.85984×10^{-13}	1.39681×10^{-14}
295.276	6.47395×10^{-13}	3.17911×10^{-14}	318.392	2.82637×10^{-13}	1.38078×10^{-14}
295.854	6.31015×10^{-13}	3.09568×10^{-14}	318.970	2.79386×10^{-13}	1.36518×10^{-14}
296.432	6.14689×10^{-13}	3.01252×10^{-14}	319.548	2.76230×10^{-13}	1.35001×10^{-14}
297.010	5.98487×10^{-13}	2.93008×10^{-14}	320.126	2.73147×10^{-13}	1.33525×10^{-14}
297.588	5.82479×10^{-13}	2.84874×10^{-14}	320.704	2.70149×10^{-13}	1.32081×10^{-14}
298.166	5.66737×10^{-13}	2.76882×10^{-14}	321.281	2.67215×10^{-13}	1.30669×10^{-14}
298.744	5.51307×10^{-13}	2.69070×10^{-14}	321.859	2.64345×10^{-13}	1.29289×10^{-14}
299.322	5.36248×10^{-13}	2.61459×10^{-14}	322.437	2.61550×10^{-13}	1.27930×10^{-14}
299.900	5.21608×10^{-13}	2.54085×10^{-14}	323.015	2.58798×10^{-13}	1.26614×10^{-14}
300.477	5.07433×10^{-13}	2.46949×10^{-14}	323.593	2.56111×10^{-13}	1.25309×10^{-14}
301.055	4.93736×10^{-13}	2.40095×10^{-14}	324.171	2.53467×10^{-13}	1.24036×10^{-14}
301.633	4.80562×10^{-13}	2.33515×10^{-14}	324.749	2.50879×10^{-13}	1.22786×10^{-14}
302.211	4.67904×10^{-13}	2.27230×10^{-14}	325.327	2.48324×10^{-13}	1.21558×10^{-14}
302.789	4.55794×10^{-13}	2.21230×10^{-14}	325.905	2.45824×10^{-13}	1.20352×10^{-14}
303.367	4.44233×10^{-13}	2.15527×10^{-14}	326.482	2.43359×10^{-13}	1.19169×10^{-14}
303.945	4.33213×10^{-13}	2.10110×10^{-14}	327.060	2.40939×10^{-13}	1.18008×10^{-14}
304.523	4.22721×10^{-13}	2.04990×10^{-14}	327.638	2.38554×10^{-13}	1.16860×10^{-14}
305.100	4.12769×10^{-13}	2.00135×10^{-14}	328.216	2.36214×10^{-13}	1.15733×10^{-14}
305.678	4.03314×10^{-13}	1.95555×10^{-14}	328.794	2.33898×10^{-13}	1.14630×10^{-14}
306.256	3.94365×10^{-13}	1.91228×10^{-14}	329.372	2.31617×10^{-13}	1.13539×10^{-14}
306.834	3.85891×10^{-13}	1.87144×10^{-14}	329.950	2.29370×10^{-13}	1.12459×10^{-14}
307.412	3.77868×10^{-13}	1.83301×10^{-14}	330.528	2.27159×10^{-13}	1.11413×10^{-14}
307.990	3.70275×10^{-13}	1.79668×10^{-14}	331.106	2.24981×10^{-13}	1.10368×10^{-14}
308.568	3.63089×10^{-13}	1.76244×10^{-14}	331.683	2.22827×10^{-13}	1.09346×10^{-14}
309.146	3.56298×10^{-13}	1.73007×10^{-14}	332.261	2.20696×10^{-13}	1.08342×10^{-14}
309.724	3.49859×10^{-13}	1.69956×10^{-14}	332.839	2.18598×10^{-13}	1.07350×10^{-14}
310.302	3.43759×10^{-13}	1.67070×10^{-14}	333.417	2.16534×10^{-13}	1.06374×10^{-14}
310.879	3.37977×10^{-13}	1.64325×10^{-14}	333.995	2.14481×10^{-13}	1.05410×10^{-14}
311.457	3.32489×10^{-13}	1.61734×10^{-14}	334.573	2.12460×10^{-13}	1.04461×10^{-14}
312.035	3.27262×10^{-13}	1.59262×10^{-14}	335.151	2.10461×10^{-13}	1.03524×10^{-14}
312.613	3.22297×10^{-13}	1.56921×10^{-14}	335.729	2.08483×10^{-13}	1.02602×10^{-14}
313.191	3.17559×10^{-13}	1.54677×10^{-14}	336.307	2.06536×10^{-13}	1.01690×10^{-14}
313.769	3.13026×10^{-13}	1.52531×10^{-14}	336.884	2.04599×10^{-13}	1.00791×10^{-14}
314.347	3.08698×10^{-13}	1.50481×10^{-14}	337.462	2.02692×10^{-13}	9.99042×10^{-15}

Table A.26 (cont'd)

JD +2451000	*UVOIR* Flux	Flux error	JD +2451000	*UVOIR* Flux	Flux error
338.040	2.00795×10^{-13}	9.90284×10^{-15}	348.442	1.70063×10^{-13}	8.50952×10^{-15}
338.618	1.98928×10^{-13}	9.81635×10^{-15}	349.020	1.68542×10^{-13}	8.44232×10^{-15}
339.196	1.97070×10^{-13}	9.73095×10^{-15}	349.598	1.67045×10^{-13}	8.37621×10^{-15}
339.774	1.95243×10^{-13}	9.64665×10^{-15}	350.176	1.65561×10^{-13}	8.31095×10^{-15}
340.352	1.93424×10^{-13}	9.56345×10^{-15}	350.754	1.64100×10^{-13}	8.24672×10^{-15}
340.930	1.91626×10^{-13}	9.48125×10^{-15}	351.332	1.62649×10^{-13}	8.18337×10^{-15}
341.508	1.89859×10^{-13}	9.40016×10^{-15}	351.910	1.61219×10^{-13}	8.12071×10^{-15}
342.085	1.88101×10^{-13}	9.32000×10^{-15}	352.487	1.59799×10^{-13}	8.05883×10^{-15}
342.663	1.86354×10^{-13}	9.24098×10^{-15}	353.065	1.58396×10^{-13}	7.99764×10^{-15}
343.241	1.84639×10^{-13}	9.16293×10^{-15}	353.643	1.57001×10^{-13}	7.93699×10^{-15}
343.819	1.82935×10^{-13}	9.08598×10^{-15}	354.221	1.55622×10^{-13}	7.87695×10^{-15}
344.397	1.81254×10^{-13}	9.01015×10^{-15}	354.799	1.54248×10^{-13}	7.81740×10^{-15}
344.975	1.79595×10^{-13}	8.93535×10^{-15}	355.377	1.52880×10^{-13}	7.75824×10^{-15}
345.553	1.77949×10^{-13}	8.86160×10^{-15}	355.955	1.51530×10^{-13}	7.69985×10^{-15}
346.131	1.76339×10^{-13}	8.78905×10^{-15}	356.533	1.50190×10^{-13}	7.64194×10^{-15}
346.709	1.74730×10^{-13}	8.71749×10^{-15}	357.111	1.48865×10^{-13}	7.58507×10^{-15}
347.286	1.73157×10^{-13}	8.64715×10^{-15}	357.688	1.47571×10^{-13}	7.52936×10^{-15}
347.864	1.71598×10^{-13}	8.57783×10^{-15}	358.266	1.46307×10^{-13}	7.47551×10^{-15}

Table A.27. SN 1999by

JD +2450000	*UVOIR* Flux	Flux error	JD +2450000	*UVOIR* Flux	Flux error
1300.60	2.62990×10^{-11}	1.22020×10^{-12}	1324.72	2.85210×10^{-11}	1.38850×10^{-12}
1301.21	3.03550×10^{-11}	1.36860×10^{-12}	1325.33	2.73070×10^{-11}	1.32890×10^{-12}
1301.81	3.47920×10^{-11}	1.53860×10^{-12}	1325.93	2.61150×10^{-11}	1.26950×10^{-12}
1302.41	3.95300×10^{-11}	1.72670×10^{-12}	1326.53	2.49540×10^{-11}	1.21080×10^{-12}
1303.02	4.44770×10^{-11}	1.92840×10^{-12}	1327.14	2.38340×10^{-11}	1.15380×10^{-12}
1303.62	4.95330×10^{-11}	2.13850×10^{-12}	1327.74	2.27690×10^{-11}	1.09930×10^{-12}
1304.22	5.45910×10^{-11}	2.35170×10^{-12}	1328.34	2.17670×10^{-11}	1.04800×10^{-12}
1304.82	5.95410×10^{-11}	2.56280×10^{-12}	1328.94	2.08340×10^{-11}	1.00010×10^{-12}
1305.43	6.42690×10^{-11}	2.76650×10^{-12}	1329.55	1.99730×10^{-11}	9.55990×10^{-13}
1306.03	6.86660×10^{-11}	2.95760×10^{-12}	1330.15	1.91810×10^{-11}	9.15430×10^{-13}
1306.63	7.26240×10^{-11}	3.13150×10^{-12}	1330.75	1.84550×10^{-11}	8.78250×10^{-13}
1307.24	7.60440×10^{-11}	3.28370×10^{-12}	1331.36	1.77880×10^{-11}	8.44140×10^{-13}
1307.84	7.88430×10^{-11}	3.41040×10^{-12}	1331.96	1.71750×10^{-11}	8.12760×10^{-13}
1308.44	8.09520×10^{-11}	3.50870×10^{-12}	1332.56	1.66070×10^{-11}	7.83770×10^{-13}
1309.05	8.23270×10^{-11}	3.57660×10^{-12}	1333.17	1.60800×10^{-11}	7.56850×10^{-13}
1309.65	8.29460×10^{-11}	3.61320×10^{-12}	1333.77	1.55870×10^{-11}	7.31740×10^{-13}
1310.25	8.28180×10^{-11}	3.61870×10^{-12}	1334.37	1.51250×10^{-11}	7.08190×10^{-13}
1310.85	8.19750×10^{-11}	3.59450×10^{-12}	1334.97	1.46880×10^{-11}	6.86020×10^{-13}
1311.46	8.04770×10^{-11}	3.54300×10^{-12}	1335.58	1.42740×10^{-11}	6.65070×10^{-13}
1312.06	7.84040×10^{-11}	3.46720×10^{-12}	1336.18	1.38800×10^{-11}	6.45200×10^{-13}
1312.66	7.58500×10^{-11}	3.37110×10^{-12}	1336.78	1.35050×10^{-11}	6.26310×10^{-13}
1313.27	7.29210×10^{-11}	3.25870×10^{-12}	1337.39	1.31470×10^{-11}	6.08310×10^{-13}
1313.87	6.97250×10^{-11}	3.13430×10^{-12}	1337.99	1.28040×10^{-11}	5.91130×10^{-13}
1314.47	6.63690×10^{-11}	3.00210×10^{-12}	1338.59	1.24750×10^{-11}	5.74710×10^{-13}
1315.07	6.29500×10^{-11}	2.86600×10^{-12}	1339.20	1.21590×10^{-11}	5.58990×10^{-13}
1315.68	5.95530×10^{-11}	2.72930×10^{-12}	1339.80	1.18550×10^{-11}	5.43920×10^{-13}
1316.28	5.62470×10^{-11}	2.59510×10^{-12}	1340.40	1.15620×10^{-11}	5.29460×10^{-13}
1316.88	5.30870×10^{-11}	2.46550×10^{-12}	1341.01	1.12800×10^{-11}	5.15560×10^{-13}
1317.49	5.01120×10^{-11}	2.34220×10^{-12}	1341.61	1.10090×10^{-11}	5.02180×10^{-13}
1318.09	4.73460×10^{-11}	2.22640×10^{-12}	1342.21	1.07460×10^{-11}	4.89310×10^{-13}
1318.69	4.48000×10^{-11}	2.11860×10^{-12}	1342.81	1.04920×10^{-11}	4.76890×10^{-13}
1319.30	4.24770×10^{-11}	2.01920×10^{-12}	1343.42	1.02470×10^{-11}	4.64920×10^{-13}
1319.90	4.03670×10^{-11}	1.92780×10^{-12}	1344.02	1.00090×10^{-11}	4.53350×10^{-13}
1320.50	3.84570×10^{-11}	1.84420×10^{-12}	1344.62	9.77880×10^{-12}	4.42170×10^{-13}
1321.10	3.67240×10^{-11}	1.76750×10^{-12}	1345.23	9.55540×10^{-12}	4.31350×10^{-13}
1321.71	3.51420×10^{-11}	1.69680×10^{-12}	1345.83	9.33880×10^{-12}	4.20880×10^{-13}
1322.31	3.36830×10^{-11}	1.63080×10^{-12}	1346.43	9.12840×10^{-12}	4.10740×10^{-13}
1322.92	3.23170×10^{-11}	1.56820×10^{-12}	1347.04	8.92390×10^{-12}	4.00910×10^{-13}
1323.52	3.10150×10^{-11}	1.50770×10^{-12}	1347.64	8.72520×10^{-12}	3.91370×10^{-13}
1324.12	2.97540×10^{-11}	1.44810×10^{-12}	1348.24	8.53200×10^{-12}	3.82110×10^{-13}

Table A.27 (cont'd)

JD +2450000	*UVOIR* Flux	Flux error	JD +2450000	*UVOIR* Flux	Flux error
1348.84	8.34390×10^{-12}	3.73130×10^{-13}	1372.96	3.58780×10^{-12}	1.53170×10^{-13}
1349.45	8.16090×10^{-12}	3.64390×10^{-13}	1373.57	3.51560×10^{-12}	1.49970×10^{-13}
1350.05	7.98260×10^{-12}	3.55910×10^{-13}	1374.17	3.44500×10^{-12}	1.46840×10^{-13}
1350.65	7.80890×10^{-12}	3.47660×10^{-13}	1374.77	3.37590×10^{-12}	1.43790×10^{-13}
1351.26	7.63960×10^{-12}	3.39630×10^{-13}	1375.38	3.30820×10^{-12}	1.40800×10^{-13}
1351.86	7.47460×10^{-12}	3.31820×10^{-13}	1375.98	3.24210×10^{-12}	1.37890×10^{-13}
1352.46	7.31370×10^{-12}	3.24230×10^{-13}	1376.58	3.17730×10^{-12}	1.35040×10^{-13}
1353.06	7.15680×10^{-12}	3.16830×10^{-13}	1377.19	3.11400×10^{-12}	1.32260×10^{-13}
1353.67	7.00370×10^{-12}	3.09620×10^{-13}	1377.79	3.05200×10^{-12}	1.29540×10^{-13}
1354.27	6.85420×10^{-12}	3.02610×10^{-13}	1378.39	2.99130×10^{-12}	1.26890×10^{-13}
1354.87	6.70840×10^{-12}	2.95770×10^{-13}	1378.99	2.93190×10^{-12}	1.24290×10^{-13}
1355.48	6.56600×10^{-12}	2.89110×10^{-13}	1379.60	2.87380×10^{-12}	1.21760×10^{-13}
1356.08	6.42700×10^{-12}	2.82620×10^{-13}	1380.20	2.81690×10^{-12}	1.19280×10^{-13}
1356.68	6.29130×10^{-12}	2.76300×10^{-13}	1380.80	2.76130×10^{-12}	1.16860×10^{-13}
1357.29	6.15870×10^{-12}	2.70130×10^{-13}	1381.41	2.70680×10^{-12}	1.14490×10^{-13}
1357.89	6.02920×10^{-12}	2.64120×10^{-13}	1382.01	2.65350×10^{-12}	1.12180×10^{-13}
1358.49	5.90270×10^{-12}	2.58260×10^{-13}	1382.61	2.60130×10^{-12}	1.09920×10^{-13}
1359.09	5.77910×10^{-12}	2.52540×10^{-13}	1383.22	2.55020×10^{-12}	1.07710×10^{-13}
1359.70	5.65830×10^{-12}	2.46960×10^{-13}	1383.82	2.50020×10^{-12}	1.05560×10^{-13}
1360.30	5.54020×10^{-12}	2.41520×10^{-13}	1384.42	2.45130×10^{-12}	1.03450×10^{-13}
1360.91	5.42490×10^{-12}	2.36210×10^{-13}	1385.03	2.40340×10^{-12}	1.01380×10^{-13}
1361.51	5.31210×10^{-12}	2.31040×10^{-13}	1385.63	2.35640×10^{-12}	9.93670×10^{-14}
1362.11	5.20190×10^{-12}	2.25990×10^{-13}	1386.23	2.31050×10^{-12}	9.73960×10^{-14}
1362.71	5.09420×10^{-12}	2.21060×10^{-13}	1386.83	2.26560×10^{-12}	9.54690×10^{-14}
1363.32	4.98890×10^{-12}	2.16250×10^{-13}	1387.44	2.22160×10^{-12}	9.35850×10^{-14}
1363.92	4.88590×10^{-12}	2.11550×10^{-13}	1388.04	2.17850×10^{-12}	9.17430×10^{-14}
1364.52	4.78530×10^{-12}	2.06970×10^{-13}	1388.64	2.13630×10^{-12}	8.99420×10^{-14}
1365.13	4.68680×10^{-12}	2.02500×10^{-13}	1389.25	2.09500×10^{-12}	8.81810×10^{-14}
1365.73	4.59060×10^{-12}	1.98140×10^{-13}	1389.85	2.05460×10^{-12}	8.64590×10^{-14}
1366.33	4.49640×10^{-12}	1.93880×10^{-13}	1390.45	2.01500×10^{-12}	8.47750×10^{-14}
1366.94	4.40440×10^{-12}	1.89720×10^{-13}	1391.06	1.97620×10^{-12}	8.31290×10^{-14}
1367.54	4.31440×10^{-12}	1.85660×10^{-13}	1391.66	1.93830×10^{-12}	8.15180×10^{-14}
1368.14	4.22630×10^{-12}	1.81700×10^{-13}	1392.26	1.90110×10^{-12}	7.99430×10^{-14}
1368.74	4.14020×10^{-12}	1.77830×10^{-13}	1392.86	1.86470×10^{-12}	7.84020×10^{-14}
1369.35	4.05600×10^{-12}	1.74050×10^{-13}	1393.47	1.82910×10^{-12}	7.68950×10^{-14}
1369.95	3.97360×10^{-12}	1.70360×10^{-13}	1394.07	1.79410×10^{-12}	7.54210×10^{-14}
1370.55	3.89300×10^{-12}	1.66760×10^{-13}	1394.67	1.76000×10^{-12}	7.39800×10^{-14}
1371.16	3.81420×10^{-12}	1.63240×10^{-13}	1395.28	1.72650×10^{-12}	7.25690×10^{-14}
1371.76	3.73710×10^{-12}	1.59800×10^{-13}	1395.88	1.69370×10^{-12}	7.11890×10^{-14}
1372.36	3.66170×10^{-12}	1.56450×10^{-13}	1396.48	1.66160×10^{-12}	6.98390×10^{-14}

Table A.27 (cont'd)

JD +2450000	*UVOIR* Flux	Flux error	JD +2450000	*UVOIR* Flux	Flux error
1397.08	1.63010×10^{-12}	6.85190×10^{-14}	1409.15	1.11970×10^{-12}	4.72860×10^{-14}
1397.69	1.59930×10^{-12}	6.72270×10^{-14}	1409.75	1.09920×10^{-12}	4.64420×10^{-14}
1398.29	1.56910×10^{-12}	6.59620×10^{-14}	1410.35	1.07910×10^{-12}	4.56160×10^{-14}
1398.90	1.53960×10^{-12}	6.47250×10^{-14}	1410.95	1.05950×10^{-12}	4.48070×10^{-14}
1399.50	1.51060×10^{-12}	6.35140×10^{-14}	1411.56	1.04020×10^{-12}	4.40140×10^{-14}
1400.10	1.48230×10^{-12}	6.23290×10^{-14}	1412.16	1.02130×10^{-12}	4.32380×10^{-14}
1400.70	1.45450×10^{-12}	6.11700×10^{-14}	1412.76	1.00280×10^{-12}	4.24780×10^{-14}
1401.31	1.42720×10^{-12}	6.00350×10^{-14}	1413.37	9.84660×10^{-13}	4.17330×10^{-14}
1401.91	1.40060×10^{-12}	5.89240×10^{-14}	1413.97	9.66870×10^{-13}	4.10030×10^{-14}
1402.51	1.37450×10^{-12}	5.78370×10^{-14}	1414.57	9.49430×10^{-13}	4.02880×10^{-14}
1403.12	1.34890×10^{-12}	5.67730×10^{-14}	1415.18	9.32340×10^{-13}	3.95870×10^{-14}
1403.72	1.32380×10^{-12}	5.57310×10^{-14}	1415.78	9.15580×10^{-13}	3.89010×10^{-14}
1404.32	1.29920×10^{-12}	5.47120×10^{-14}	1416.38	8.99160×10^{-13}	3.82280×10^{-14}
1404.93	1.27510×10^{-12}	5.37140×10^{-14}	1416.98	8.83050×10^{-13}	3.75690×10^{-14}
1405.53	1.25160×10^{-12}	5.27360×10^{-14}	1417.59	8.67260×10^{-13}	3.69230×10^{-14}
1406.13	1.22840×10^{-12}	5.17790×10^{-14}	1418.19	8.51780×10^{-13}	3.62900×10^{-14}
1406.73	1.20580×10^{-12}	5.08430×10^{-14}	1418.79	8.36610×10^{-13}	3.56700×10^{-14}
1407.34	1.18360×10^{-12}	4.99250×10^{-14}	1419.40	8.21730×10^{-13}	3.50620×10^{-14}
1407.94	1.16190×10^{-12}	4.90270×10^{-14}	1420.00	8.07140×10^{-13}	3.44660×10^{-14}
1408.54	1.14050×10^{-12}	4.81470×10^{-14}	...	...	...

Table A.28. SN 1999dq

JD +2451000	*UVOIR* Flux	Flux error	JD +2451000	*UVOIR* Flux	Flux error
426.829	2.12850×10^{-11}	9.22820×10^{-13}	459.995	1.15320×10^{-11}	5.20410×10^{-13}
427.658	2.52610×10^{-11}	1.10310×10^{-12}	460.824	1.11730×10^{-11}	5.07100×10^{-13}
428.487	2.83070×10^{-11}	1.24070×10^{-12}	461.653	1.08360×10^{-11}	4.94660×10^{-13}
429.317	3.07000×10^{-11}	1.34780×10^{-12}	462.482	1.05160×10^{-11}	4.82670×10^{-13}
430.146	3.26380×10^{-11}	1.43380×10^{-12}	463.312	1.02050×10^{-11}	4.70780×10^{-13}
430.975	3.42400×10^{-11}	1.50450×10^{-12}	464.141	9.90000×10^{-12}	4.58670×10^{-13}
431.804	3.55700×10^{-11}	1.56300×10^{-12}	464.970	9.59690×10^{-12}	4.46170×10^{-13}
432.633	3.66560×10^{-11}	1.61090×10^{-12}	465.799	9.29380×10^{-12}	4.33170×10^{-13}
433.462	3.75110×10^{-11}	1.64860×10^{-12}	466.628	8.99000×10^{-12}	4.19680×10^{-13}
434.291	3.81380×10^{-11}	1.67650×10^{-12}	467.457	8.68590×10^{-12}	4.05770×10^{-13}
435.121	3.85370×10^{-11}	1.69450×10^{-12}	468.286	8.38260×10^{-12}	3.91590×10^{-13}
435.950	3.87110×10^{-11}	1.70260×10^{-12}	469.116	8.08190×10^{-12}	3.77280×10^{-13}
436.779	3.86620×10^{-11}	1.70110×10^{-12}	469.945	7.78570×10^{-12}	3.63030×10^{-13}
437.608	3.83990×10^{-11}	1.69020×10^{-12}	470.774	7.49610×10^{-12}	3.48990×10^{-13}
438.437	3.79320×10^{-11}	1.67040×10^{-12}	471.603	7.21450×10^{-12}	3.35300×10^{-13}
439.266	3.72730×10^{-11}	1.64210×10^{-12}	472.432	6.94260×10^{-12}	3.22050×10^{-13}
440.095	3.64370×10^{-11}	1.60610×10^{-12}	473.261	6.68120×10^{-12}	3.09330×10^{-13}
440.925	3.54410×10^{-11}	1.56300×10^{-12}	474.090	6.43120×10^{-12}	2.97160×10^{-13}
441.754	3.43010×10^{-11}	1.51360×10^{-12}	474.920	6.19270×10^{-12}	2.85580×10^{-13}
442.583	3.30370×10^{-11}	1.45870×10^{-12}	475.749	5.96580×10^{-12}	2.74600×10^{-13}
443.412	3.16700×10^{-11}	1.39910×10^{-12}	476.578	5.75050×10^{-12}	2.64200×10^{-13}
444.241	3.02250×10^{-11}	1.33600×10^{-12}	477.407	5.54630×10^{-12}	2.54380×10^{-13}
445.070	2.87300×10^{-11}	1.27040×10^{-12}	478.236	5.35300×10^{-12}	2.45110×10^{-13}
445.900	2.72150×10^{-11}	1.20370×10^{-12}	479.065	5.16990×10^{-12}	2.36370×10^{-13}
446.729	2.57080×10^{-11}	1.13700×10^{-12}	479.894	4.99660×10^{-12}	2.28150×10^{-13}
447.558	2.42350×10^{-11}	1.07160×10^{-12}	480.724	4.83260×10^{-12}	2.20410×10^{-13}
448.387	2.28200×10^{-11}	1.00850×10^{-12}	481.553	4.67730×10^{-12}	2.13130×10^{-13}
449.216	2.14790×10^{-11}	9.48600×10^{-13}	482.382	4.53030×10^{-12}	2.06280×10^{-13}
450.045	2.02230×10^{-11}	8.92390×10^{-13}	483.211	4.39100×10^{-12}	1.99830×10^{-13}
450.874	1.90570×10^{-11}	8.40270×10^{-13}	484.040	4.25900×10^{-12}	1.93760×10^{-13}
451.704	1.79850×10^{-11}	7.92440×10^{-13}	484.869	4.13390×10^{-12}	1.88040×10^{-13}
452.533	1.70050×10^{-11}	7.48930×10^{-13}	485.698	4.01520×10^{-12}	1.82640×10^{-13}
453.362	1.61140×10^{-11}	7.09680×10^{-13}	486.528	3.90260×10^{-12}	1.77540×10^{-13}
454.191	1.53080×10^{-11}	6.74520×10^{-13}	487.357	3.79570×10^{-12}	1.72720×10^{-13}
455.020	1.45820×10^{-11}	6.43260×10^{-13}	488.186	3.69410×10^{-12}	1.68150×10^{-13}
455.849	1.39300×10^{-11}	6.15640×10^{-13}	489.015	3.59760×10^{-12}	1.63810×10^{-13}
456.678	1.33450×10^{-11}	5.91370×10^{-13}	489.844	3.50580×10^{-12}	1.59700×10^{-13}
457.508	1.28200×10^{-11}	5.70100×10^{-13}	490.673	3.41840×10^{-12}	1.55780×10^{-13}
458.337	1.23480×10^{-11}	5.51460×10^{-13}	491.503	3.33520×10^{-12}	1.52050×10^{-13}
459.166	1.19210×10^{-11}	5.35040×10^{-13}	492.332	3.25580×10^{-12}	1.48490×10^{-13}

Table A.28 (cont'd)

JD +2451000	*UVOIR* Flux	Flux error	JD +2451000	*UVOIR* Flux	Flux error
493.161	3.18000×10^{-12}	1.45080×10^{-13}	526.327	1.54200×10^{-12}	6.94180×10^{-14}
493.990	3.10770×10^{-12}	1.41820×10^{-13}	527.156	1.51740×10^{-12}	6.82980×10^{-14}
494.819	3.03850×10^{-12}	1.38700×10^{-13}	527.985	1.49330×10^{-12}	6.72000×10^{-14}
495.648	2.97220×10^{-12}	1.35700×10^{-13}	528.814	1.46950×10^{-12}	6.61230×10^{-14}
496.477	2.90870×10^{-12}	1.32810×10^{-13}	529.643	1.44620×10^{-12}	6.50670×10^{-14}
497.307	2.84780×10^{-12}	1.30040×10^{-13}	530.472	1.42330×10^{-12}	6.40320×10^{-14}
498.136	2.78920×10^{-12}	1.27360×10^{-13}	531.302	1.40080×10^{-12}	6.30160×10^{-14}
498.965	2.73290×10^{-12}	1.24780×10^{-13}	532.131	1.37860×10^{-12}	6.20200×10^{-14}
499.794	2.67870×10^{-12}	1.22280×10^{-13}	532.960	1.35690×10^{-12}	6.10440×10^{-14}
500.623	2.62640×10^{-12}	1.19870×10^{-13}	533.789	1.33560×10^{-12}	6.00860×10^{-14}
501.452	2.57580×10^{-12}	1.17530×10^{-13}	534.618	1.31460×10^{-12}	5.91460×10^{-14}
502.281	2.52700×10^{-12}	1.15260×10^{-13}	535.447	1.29390×10^{-12}	5.82240×10^{-14}
503.111	2.47980×10^{-12}	1.13070×10^{-13}	536.276	1.27370×10^{-12}	5.73190×10^{-14}
503.940	2.43400×10^{-12}	1.10930×10^{-13}	537.106	1.25370×10^{-12}	5.64320×10^{-14}
504.769	2.38960×10^{-12}	1.08860×10^{-13}	537.935	1.23420×10^{-12}	5.55610×10^{-14}
505.598	2.34650×10^{-12}	1.06850×10^{-13}	538.764	1.21490×10^{-12}	5.47070×10^{-14}
506.427	2.30460×10^{-12}	1.04890×10^{-13}	539.593	1.19600×10^{-12}	5.38680×10^{-14}
507.256	2.26390×10^{-12}	1.02980×10^{-13}	540.422	1.17740×10^{-12}	5.30450×10^{-14}
508.085	2.22420×10^{-12}	1.01120×10^{-13}	541.251	1.15910×10^{-12}	5.22380×10^{-14}
508.915	2.18560×10^{-12}	9.93060×10^{-14}	542.080	1.14110×10^{-12}	5.14450×10^{-14}
509.744	2.14790×10^{-12}	9.75380×10^{-14}	542.910	1.12350×10^{-12}	5.06670×10^{-14}
510.573	2.11110×10^{-12}	9.58130×10^{-14}	543.739	1.10610×10^{-12}	4.99030×10^{-14}
511.402	2.07520×10^{-12}	9.41300×10^{-14}	544.568	1.08900×10^{-12}	4.91530×10^{-14}
512.231	2.04010×10^{-12}	9.24860×10^{-14}	545.397	1.07230×10^{-12}	4.84170×10^{-14}
513.060	2.00580×10^{-12}	9.08800×10^{-14}	546.226	1.05580×10^{-12}	4.76940×10^{-14}
513.889	1.97230×10^{-12}	8.93100×10^{-14}	547.055	1.03950×10^{-12}	4.69850×10^{-14}
514.719	1.93940×10^{-12}	8.77760×10^{-14}	547.884	1.02360×10^{-12}	4.62880×10^{-14}
515.548	1.90730×10^{-12}	8.62760×10^{-14}	548.714	1.00790×10^{-12}	4.56040×10^{-14}
516.377	1.87580×10^{-12}	8.48080×10^{-14}	549.543	9.92490×10^{-13}	4.49320×10^{-14}
517.206	1.84500×10^{-12}	8.33720×10^{-14}	550.372	9.77330×10^{-13}	4.42720×10^{-14}
518.035	1.81470×10^{-12}	8.19670×10^{-14}	551.201	9.62420×10^{-13}	4.36240×10^{-14}
518.864	1.78510×10^{-12}	8.05920×10^{-14}	552.030	9.47770×10^{-13}	4.29880×10^{-14}
519.693	1.75600×10^{-12}	7.92450×10^{-14}	552.859	9.33350×10^{-13}	4.23630×10^{-14}
520.523	1.72750×10^{-12}	7.79270×10^{-14}	553.688	9.19180×10^{-13}	4.17490×10^{-14}
521.352	1.69950×10^{-12}	7.66350×10^{-14}	554.518	9.05240×10^{-13}	4.11450×10^{-14}
522.181	1.67200×10^{-12}	7.53700×10^{-14}	555.347	8.91530×10^{-13}	4.05530×10^{-14}
523.010	1.64500×10^{-12}	7.41310×10^{-14}	556.176	8.78050×10^{-13}	3.99710×10^{-14}
523.839	1.61860×10^{-12}	7.29170×10^{-14}	557.005	8.64790×10^{-13}	3.93990×10^{-14}
524.668	1.59260×10^{-12}	7.17270×10^{-14}	557.834	8.51760×10^{-13}	3.88370×10^{-14}
525.497	1.56710×10^{-12}	7.05610×10^{-14}	558.663	8.38930×10^{-13}	3.82840×10^{-14}

Table A.28 (cont'd)

JD +2451000	*UVOIR* Flux	Flux error	JD +2451000	*UVOIR* Flux	Flux error
559.492	8.26320×10^{-13}	3.77420×10^{-14}	576.075	6.13180×10^{-13}	2.86250×10^{-14}
560.322	8.13920×10^{-13}	3.72080×10^{-14}	576.905	6.04240×10^{-13}	2.82450×10^{-14}
561.151	8.01720×10^{-13}	3.66840×10^{-14}	577.734	5.95450×10^{-13}	2.78700×10^{-14}
561.980	7.89720×10^{-13}	3.61690×10^{-14}	578.563	5.86790×10^{-13}	2.75010×10^{-14}
562.809	7.77920×10^{-13}	3.56630×10^{-14}	579.392	5.78270×10^{-13}	2.71380×10^{-14}
563.638	7.66310×10^{-13}	3.51650×10^{-14}	580.221	5.69890×10^{-13}	2.67810×10^{-14}
564.467	7.54890×10^{-13}	3.46760×10^{-14}	581.050	5.61630×10^{-13}	2.64300×10^{-14}
565.297	7.43660×10^{-13}	3.41950×10^{-14}	581.879	5.53520×10^{-13}	2.60840×10^{-14}
566.126	7.32610×10^{-13}	3.37220×10^{-14}	582.709	5.45530×10^{-13}	2.57440×10^{-14}
566.955	7.21740×10^{-13}	3.32570×10^{-14}	583.538	5.37660×10^{-13}	2.54090×10^{-14}
567.784	7.11050×10^{-13}	3.28000×10^{-14}	584.367	5.29920×10^{-13}	2.50790×10^{-14}
568.613	7.00530×10^{-13}	3.23510×10^{-14}	585.196	5.22300×10^{-13}	2.47540×10^{-14}
569.442	6.90180×10^{-13}	3.19090×10^{-14}	586.025	5.14810×10^{-13}	2.44350×10^{-14}
570.271	6.80000×10^{-13}	3.14740×10^{-14}	586.854	5.07430×10^{-13}	2.41200×10^{-14}
571.101	6.69980×10^{-13}	3.10470×10^{-14}	587.683	5.00170×10^{-13}	2.38100×10^{-14}
571.930	6.60130×10^{-13}	3.06260×10^{-14}	588.513	4.93020×10^{-13}	2.35050×10^{-14}
572.759	6.50430×10^{-13}	3.02130×10^{-14}	589.342	4.85980×10^{-13}	2.32050×10^{-14}
573.588	6.40890×10^{-13}	2.98060×10^{-14}	590.171	4.79060×10^{-13}	2.29090×10^{-14}
574.417	6.31510×10^{-13}	2.94060×10^{-14}	591.000	4.72240×10^{-13}	2.26180×10^{-14}
575.246	6.22270×10^{-13}	2.90130×10^{-14}	...	...	...

Table A.29. SN 1999ee

JD +2451000	*UVOIR* Flux	Flux error	JD +2451000	*UVOIR* Flux	Flux error
455.704	5.57300×10^{-12}	2.89010×10^{-13}	469.774	5.74010×10^{-11}	2.55840×10^{-12}
456.055	6.71550×10^{-12}	3.36420×10^{-13}	470.126	5.71220×10^{-11}	2.54600×10^{-12}
456.407	8.02330×10^{-12}	3.90800×10^{-13}	470.477	5.67810×10^{-11}	2.53090×10^{-12}
456.759	9.49050×10^{-12}	4.52050×10^{-13}	470.829	5.63820×10^{-11}	2.51330×10^{-12}
457.111	1.11050×10^{-11}	5.19790×10^{-13}	471.181	5.59290×10^{-11}	2.49340×10^{-12}
457.462	1.28500×10^{-11}	5.93440×10^{-13}	471.533	5.54270×10^{-11}	2.47130×10^{-12}
457.814	1.47070×10^{-11}	6.72260×10^{-13}	471.884	5.48790×10^{-11}	2.44720×10^{-12}
458.166	1.66560×10^{-11}	7.55460×10^{-13}	472.236	5.42880×10^{-11}	2.42130×10^{-12}
458.518	1.86760×10^{-11}	8.42190×10^{-13}	472.588	5.36580×10^{-11}	2.39360×10^{-12}
458.869	2.07480×10^{-11}	9.31620×10^{-13}	472.940	5.29910×10^{-11}	2.36430×10^{-12}
459.221	2.28560×10^{-11}	1.02300×10^{-12}	473.291	5.22900×10^{-11}	2.33340×10^{-12}
459.573	2.49820×10^{-11}	1.11550×10^{-12}	473.643	5.15570×10^{-11}	2.30120×10^{-12}
459.925	2.71130×10^{-11}	1.20870×10^{-12}	473.995	5.07950×10^{-11}	2.26760×10^{-12}
460.276	2.92370×10^{-11}	1.30180×10^{-12}	474.347	5.00060×10^{-11}	2.23280×10^{-12}
460.628	3.13410×10^{-11}	1.39430×10^{-12}	474.698	4.91920×10^{-11}	2.19690×10^{-12}
460.980	3.34150×10^{-11}	1.48590×10^{-12}	475.050	4.83560×10^{-11}	2.16000×10^{-12}
461.332	3.54500×10^{-11}	1.57600×10^{-12}	475.402	4.75000×10^{-11}	2.12210×10^{-12}
461.683	3.74380×10^{-11}	1.66420×10^{-12}	475.754	4.66260×10^{-11}	2.08350×10^{-12}
462.035	3.93690×10^{-11}	1.75020×10^{-12}	476.106	4.57360×10^{-11}	2.04410×10^{-12}
462.387	4.12350×10^{-11}	1.83350×10^{-12}	476.457	4.48330×10^{-11}	2.00410×10^{-12}
462.739	4.30290×10^{-11}	1.91380×10^{-12}	476.809	4.39200×10^{-11}	1.96360×10^{-12}
463.090	4.47430×10^{-11}	1.99070×10^{-12}	477.161	4.29980×10^{-11}	1.92280×10^{-12}
463.442	4.63690×10^{-11}	2.06390×10^{-12}	477.513	4.20710×10^{-11}	1.88170×10^{-12}
463.794	4.79010×10^{-11}	2.13290×10^{-12}	477.864	4.11390×10^{-11}	1.84040×10^{-12}
464.146	4.93330×10^{-11}	2.19750×10^{-12}	478.216	4.02070×10^{-11}	1.79900×10^{-12}
464.497	5.06590×10^{-11}	2.25730×10^{-12}	478.568	3.92760×10^{-11}	1.75770×10^{-12}
464.849	5.18750×10^{-11}	2.31220×10^{-12}	478.920	3.83490×10^{-11}	1.71650×10^{-12}
465.201	5.29770×10^{-11}	2.36190×10^{-12}	479.271	3.74270×10^{-11}	1.67560×10^{-12}
465.553	5.39630×10^{-11}	2.40630×10^{-12}	479.623	3.65140×10^{-11}	1.63500×10^{-12}
465.905	5.48330×10^{-11}	2.44540×10^{-12}	479.975	3.56110×10^{-11}	1.59490×10^{-12}
466.256	5.55850×10^{-11}	2.47910×10^{-12}	480.327	3.47200×10^{-11}	1.55520×10^{-12}
466.608	5.62220×10^{-11}	2.50750×10^{-12}	480.678	3.38420×10^{-11}	1.51620×10^{-12}
466.960	5.67450×10^{-11}	2.53070×10^{-12}	481.030	3.29810×10^{-11}	1.47780×10^{-12}
467.312	5.71590×10^{-11}	2.54900×10^{-12}	481.382	3.21360×10^{-11}	1.44020×10^{-12}
467.663	5.74680×10^{-11}	2.56250×10^{-12}	481.734	3.13110×10^{-11}	1.40330×10^{-12}
468.015	5.76760×10^{-11}	2.57150×10^{-12}	482.085	3.05050×10^{-11}	1.36740×10^{-12}
468.367	5.77890×10^{-11}	2.57630×10^{-12}	482.437	2.97200×10^{-11}	1.33230×10^{-12}
468.719	5.78120×10^{-11}	2.57710×10^{-12}	482.789	2.89570×10^{-11}	1.29810×10^{-12}
469.070	5.77520×10^{-11}	2.57420×10^{-12}	483.141	2.82160×10^{-11}	1.26500×10^{-12}
469.422	5.76130×10^{-11}	2.56780×10^{-12}	483.492	2.74990×10^{-11}	1.23280×10^{-12}

Table A.29 (cont'd)

JD +2451000	*UVOIR* Flux	Flux error	JD +2451000	*UVOIR* Flux	Flux error
483.844	2.68060×10^{-11}	1.20170×10^{-12}	497.915	1.39050×10^{-11}	6.36660×10^{-13}
484.196	2.61370×10^{-11}	1.17170×10^{-12}	498.266	1.37230×10^{-11}	6.28730×10^{-13}
484.548	2.54920×10^{-11}	1.14270×10^{-12}	498.618	1.35370×10^{-11}	6.20600×10^{-13}
484.900	2.48720×10^{-11}	1.11480×10^{-12}	498.970	1.33490×10^{-11}	6.12260×10^{-13}
485.251	2.42760×10^{-11}	1.08800×10^{-12}	499.322	1.31570×10^{-11}	6.03710×10^{-13}
485.603	2.37050×10^{-11}	1.06230×10^{-12}	499.673	1.29620×10^{-11}	5.94970×10^{-13}
485.955	2.31580×10^{-11}	1.03760×10^{-12}	500.025	1.27650×10^{-11}	5.86030×10^{-13}
486.307	2.26350×10^{-11}	1.01410×10^{-12}	500.377	1.25650×10^{-11}	5.76920×10^{-13}
486.658	2.21350×10^{-11}	9.91560×10^{-13}	500.729	1.23620×10^{-11}	5.67650×10^{-13}
487.010	2.16590×10^{-11}	9.70110×10^{-13}	501.080	1.21580×10^{-11}	5.58240×10^{-13}
487.362	2.12050×10^{-11}	9.49700×10^{-13}	501.432	1.19520×10^{-11}	5.48710×10^{-13}
487.714	2.07730×10^{-11}	9.30310×10^{-13}	501.784	1.17450×10^{-11}	5.39090×10^{-13}
488.065	2.03630×10^{-11}	9.11910×10^{-13}	502.136	1.15370×10^{-11}	5.29410×10^{-13}
488.417	1.99730×10^{-11}	8.94480×10^{-13}	502.487	1.13280×10^{-11}	5.19680×10^{-13}
488.769	1.96030×10^{-11}	8.77990×10^{-13}	502.839	1.11210×10^{-11}	5.09940×10^{-13}
489.121	1.92520×10^{-11}	8.62410×10^{-13}	503.191	1.09130×10^{-11}	5.00220×10^{-13}
489.472	1.89190×10^{-11}	8.47710×10^{-13}	503.543	1.07070×10^{-11}	4.90540×10^{-13}
489.824	1.86040×10^{-11}	8.33840×10^{-13}	503.894	1.05030×10^{-11}	4.80930×10^{-13}
490.176	1.83050×10^{-11}	8.20770×10^{-13}	504.246	1.03010×10^{-11}	4.71400×10^{-13}
490.528	1.80220×10^{-11}	8.08460×10^{-13}	504.598	1.01010×10^{-11}	4.62000×10^{-13}
490.879	1.77530×10^{-11}	7.96860×10^{-13}	504.950	9.90440×10^{-12}	4.52730×10^{-13}
491.231	1.74980×10^{-11}	7.85920×10^{-13}	505.302	9.71110×10^{-12}	4.43610×10^{-13}
491.583	1.72560×10^{-11}	7.75600×10^{-13}	505.653	9.52130×10^{-12}	4.34680×10^{-13}
491.935	1.70250×10^{-11}	7.65850×10^{-13}	506.005	9.33560×10^{-12}	4.25930×10^{-13}
492.286	1.68040×10^{-11}	7.56610×10^{-13}	506.357	9.15400×10^{-12}	4.17390×10^{-13}
492.638	1.65930×10^{-11}	7.47840×10^{-13}	506.709	8.97690×10^{-12}	4.09060×10^{-13}
492.990	1.63910×10^{-11}	7.39470×10^{-13}	507.060	8.80430×10^{-12}	4.00960×10^{-13}
493.342	1.61960×10^{-11}	7.31460×10^{-13}	507.412	8.63660×10^{-12}	3.93100×10^{-13}
493.693	1.60070×10^{-11}	7.23740×10^{-13}	507.764	8.47370×10^{-12}	3.85470×10^{-13}
494.045	1.58230×10^{-11}	7.16270×10^{-13}	508.116	8.31580×10^{-12}	3.78090×10^{-13}
494.397	1.56440×10^{-11}	7.08990×10^{-13}	508.467	8.16300×10^{-12}	3.70960×10^{-13}
494.749	1.54680×10^{-11}	7.01840×10^{-13}	508.819	8.01510×10^{-12}	3.64070×10^{-13}
495.100	1.52950×10^{-11}	6.94790×10^{-13}	509.171	7.87230×10^{-12}	3.57430×10^{-13}
495.452	1.51230×10^{-11}	6.87780×10^{-13}	509.523	7.73440×10^{-12}	3.51040×10^{-13}
495.804	1.49520×10^{-11}	6.80770×10^{-13}	509.874	7.60150×10^{-12}	3.44880×10^{-13}
496.156	1.47810×10^{-11}	6.73720×10^{-13}	510.226	7.47340×10^{-12}	3.38970×10^{-13}
496.508	1.46090×10^{-11}	6.66580×10^{-13}	510.578	7.35010×10^{-12}	3.33280×10^{-13}
496.859	1.44360×10^{-11}	6.59340×10^{-13}	510.930	7.23140×10^{-12}	3.27820×10^{-13}
497.211	1.42620×10^{-11}	6.51950×10^{-13}	511.281	7.11730×10^{-12}	3.22580×10^{-13}
497.563	1.40850×10^{-11}	6.44400×10^{-13}	511.633	7.00750×10^{-12}	3.17550×10^{-13}

Table A.29 (cont'd)

JD +2451000	*UVOIR* Flux	Flux error	JD +2451000	*UVOIR* Flux	Flux error
511.985	6.90200×10^{-12}	3.12730×10^{-13}	518.668	5.50390×10^{-12}	2.49410×10^{-13}
512.337	6.80060×10^{-12}	3.08100×10^{-13}	519.020	5.45260×10^{-12}	2.47080×10^{-13}
512.688	6.70320×10^{-12}	3.03670×10^{-13}	519.372	5.40270×10^{-12}	2.44810×10^{-13}
513.040	6.60960×10^{-12}	2.99410×10^{-13}	519.724	5.35410×10^{-12}	2.42600×10^{-13}
513.392	6.51960×10^{-12}	2.95320×10^{-13}	520.075	5.30680×10^{-12}	2.40440×10^{-13}
513.744	6.43300×10^{-12}	2.91400×10^{-13}	520.427	5.26070×10^{-12}	2.38330×10^{-13}
514.095	6.34980×10^{-12}	2.87630×10^{-13}	520.779	5.21580×10^{-12}	2.36280×10^{-13}
514.447	6.26980×10^{-12}	2.84010×10^{-13}	521.131	5.17190×10^{-12}	2.34260×10^{-13}
514.799	6.19270×10^{-12}	2.80530×10^{-13}	521.482	5.12900×10^{-12}	2.32290×10^{-13}
515.151	6.11850×10^{-12}	2.77180×10^{-13}	521.834	5.08710×10^{-12}	2.30370×10^{-13}
515.503	6.04710×10^{-12}	2.73950×10^{-13}	522.186	5.04610×10^{-12}	2.28480×10^{-13}
515.854	5.97820×10^{-12}	2.70840×10^{-13}	522.538	5.00590×10^{-12}	2.26620×10^{-13}
516.206	5.91170×10^{-12}	2.67840×10^{-13}	522.889	4.96660×10^{-12}	2.24800×10^{-13}
516.558	5.84750×10^{-12}	2.64950×10^{-13}	523.241	4.92800×10^{-12}	2.23020×10^{-13}
516.910	5.78550×10^{-12}	2.62150×10^{-13}	523.593	4.89010×10^{-12}	2.21260×10^{-13}
517.261	5.72560×10^{-12}	2.59440×10^{-13}	523.945	4.85290×10^{-12}	2.19530×10^{-13}
517.613	5.66750×10^{-12}	2.56820×10^{-13}	524.297	4.81640×10^{-12}	2.17840×10^{-13}
517.965	5.61130×10^{-12}	2.54270×10^{-13}	524.648	4.78050×10^{-12}	2.16170×10^{-13}
518.317	5.55680×10^{-12}	2.51810×10^{-13}	525.000	4.74520×10^{-12}	2.14520×10^{-13}

Table A.30. SN 1999gp

JD +2451000	*UVOIR* Flux	Flux error	JD +2451000	*UVOIR* Flux	Flux error
542.568	6.09290×10^{-12}	2.70320×10^{-13}	565.281	4.47030×10^{-12}	1.96420×10^{-13}
543.136	6.75040×10^{-12}	2.99440×10^{-13}	565.849	4.30220×10^{-12}	1.88930×10^{-13}
543.703	7.30640×10^{-12}	3.24840×10^{-13}	566.417	4.14190×10^{-12}	1.81800×10^{-13}
544.271	7.76510×10^{-12}	3.45930×10^{-13}	566.985	3.98950×10^{-12}	1.75040×10^{-13}
544.839	8.13900×10^{-12}	3.63000×10^{-13}	567.553	3.84500×10^{-12}	1.68630×10^{-13}
545.407	8.44170×10^{-12}	3.76630×10^{-13}	568.121	3.70840×10^{-12}	1.62590×10^{-13}
545.975	8.68480×10^{-12}	3.87420×10^{-13}	568.688	3.57960×10^{-12}	1.56920×10^{-13}
546.543	8.87730×10^{-12}	3.95830×10^{-13}	569.256	3.45850×10^{-12}	1.51600×10^{-13}
547.111	9.02610×10^{-12}	4.02230×10^{-13}	569.824	3.34490×10^{-12}	1.46630×10^{-13}
547.678	9.13630×10^{-12}	4.06870×10^{-13}	570.392	3.23860×10^{-12}	1.42020×10^{-13}
548.246	9.21180×10^{-12}	4.09970×10^{-13}	570.960	3.13950×10^{-12}	1.37740×10^{-13}
548.814	9.25560×10^{-12}	4.11650×10^{-13}	571.528	3.04730×10^{-12}	1.33790×10^{-13}
549.382	9.27010×10^{-12}	4.12060×10^{-13}	572.095	2.96170×10^{-12}	1.30150×10^{-13}
549.950	9.25740×10^{-12}	4.11270×10^{-13}	572.663	2.88240×10^{-12}	1.26830×10^{-13}
550.518	9.21950×10^{-12}	4.09380×10^{-13}	573.231	2.80910×10^{-12}	1.23790×10^{-13}
551.085	9.15810×10^{-12}	4.06460×10^{-13}	573.799	2.74140×10^{-12}	1.21030×10^{-13}
551.653	9.07470×10^{-12}	4.02590×10^{-13}	574.367	2.67900×10^{-12}	1.18530×10^{-13}
552.221	8.97120×10^{-12}	3.97830×10^{-13}	574.935	2.62150×10^{-12}	1.16260×10^{-13}
552.789	8.84900×10^{-12}	3.92270×10^{-13}	575.503	2.56840×10^{-12}	1.14210×10^{-13}
553.357	8.70970×10^{-12}	3.85960×10^{-13}	576.070	2.51920×10^{-12}	1.12350×10^{-13}
553.925	8.55500×10^{-12}	3.78990×10^{-13}	576.638	2.47350×10^{-12}	1.10650×10^{-13}
554.492	8.38640×10^{-12}	3.71410×10^{-13}	577.206	2.43060×10^{-12}	1.09080×10^{-13}
555.060	8.20560×10^{-12}	3.63290×10^{-13}	577.774	2.39010×10^{-12}	1.07610×10^{-13}
555.628	8.01400×10^{-12}	3.54710×10^{-13}	578.342	2.35140×10^{-12}	1.06220×10^{-13}
556.196	7.81340×10^{-12}	3.45730×10^{-13}	578.910	2.31390×10^{-12}	1.04870×10^{-13}
556.764	7.60520×10^{-12}	3.36420×10^{-13}	579.477	2.27720×10^{-12}	1.03530×10^{-13}
557.332	7.39100×10^{-12}	3.26850×10^{-13}	580.045	2.24070×10^{-12}	1.02180×10^{-13}
557.899	7.17230×10^{-12}	3.17080×10^{-13}	580.613	2.20390×10^{-12}	1.00790×10^{-13}
558.467	6.95060×10^{-12}	3.07180×10^{-13}	581.181	2.16670×10^{-12}	9.93380×10^{-14}
559.035	6.72720×10^{-12}	2.97200×10^{-13}	581.749	2.12850×10^{-12}	9.78170×10^{-14}
559.603	6.50350×10^{-12}	2.87210×10^{-13}	582.317	2.08930×10^{-12}	9.62110×10^{-14}
560.171	6.28070×10^{-12}	2.77260×10^{-13}	582.884	2.04890×10^{-12}	9.45150×10^{-14}
560.739	6.05990×10^{-12}	2.67400×10^{-13}	583.452	2.00740×10^{-12}	9.27290×10^{-14}
561.307	5.84230×10^{-12}	2.57670×10^{-13}	584.020	1.96470×10^{-12}	9.08570×10^{-14}
561.874	5.62860×10^{-12}	2.48130×10^{-13}	584.588	1.92100×10^{-12}	8.89070×10^{-14}
562.442	5.41980×10^{-12}	2.38800×10^{-13}	585.156	1.87650×10^{-12}	8.68900×10^{-14}
563.010	5.21660×10^{-12}	2.29720×10^{-13}	585.724	1.83140×10^{-12}	8.48210×10^{-14}
563.578	5.01960×10^{-12}	2.20920×10^{-13}	586.291	1.78600×10^{-12}	8.27120×10^{-14}
564.146	4.82930×10^{-12}	2.12430×10^{-13}	586.859	1.74060×10^{-12}	8.05820×10^{-14}
564.714	4.64610×10^{-12}	2.04250×10^{-13}	587.427	1.69540×10^{-12}	7.84440×10^{-14}

Table A.30 (cont'd)

JD +2451000	*UVOIR* Flux	Flux error	JD +2451000	*UVOIR* Flux	Flux error
587.995	1.65060×10^{-12}	7.63150×10^{-14}	610.709	7.51830×10^{-13}	3.36320×10^{-14}
588.563	1.60650×10^{-12}	7.42070×10^{-14}	611.276	7.42500×10^{-13}	3.31910×10^{-14}
589.131	1.56340×10^{-12}	7.21340×10^{-14}	611.844	7.33380×10^{-13}	3.27590×10^{-14}
589.698	1.52120×10^{-12}	7.01060×10^{-14}	612.412	7.24460×10^{-13}	3.23360×10^{-14}
590.266	1.48040×10^{-12}	6.81320×10^{-14}	612.980	7.15720×10^{-13}	3.19220×10^{-14}
590.834	1.44080×10^{-12}	6.62190×10^{-14}	613.548	7.07160×10^{-13}	3.15160×10^{-14}
591.402	1.40260×10^{-12}	6.43740×10^{-14}	614.116	6.98770×10^{-13}	3.11170×10^{-14}
591.970	1.36590×10^{-12}	6.26000×10^{-14}	614.683	6.90540×10^{-13}	3.07270×10^{-14}
592.538	1.33070×10^{-12}	6.08990×10^{-14}	615.251	6.82460×10^{-13}	3.03430×10^{-14}
593.106	1.29700×10^{-12}	5.92740×10^{-14}	615.819	6.74530×10^{-13}	2.99670×10^{-14}
593.673	1.26480×10^{-12}	5.77240×10^{-14}	616.387	6.66730×10^{-13}	2.95970×10^{-14}
594.241	1.23400×10^{-12}	5.62490×10^{-14}	616.955	6.59070×10^{-13}	2.92340×10^{-14}
594.809	1.20470×10^{-12}	5.48470×10^{-14}	617.523	6.51540×10^{-13}	2.88770×10^{-14}
595.377	1.17680×10^{-12}	5.35160×10^{-14}	618.090	6.44130×10^{-13}	2.85260×10^{-14}
595.945	1.15020×10^{-12}	5.22530×10^{-14}	618.658	6.36840×10^{-13}	2.81810×10^{-14}
596.513	1.12490×10^{-12}	5.10560×10^{-14}	619.226	6.29670×10^{-13}	2.78420×10^{-14}
597.080	1.10090×10^{-12}	4.99220×10^{-14}	619.794	6.22610×10^{-13}	2.75080×10^{-14}
597.648	1.07800×10^{-12}	4.88460×10^{-14}	620.362	6.15650×10^{-13}	2.71800×10^{-14}
598.216	1.05620×10^{-12}	4.78250×10^{-14}	620.930	6.08810×10^{-13}	2.68570×10^{-14}
598.784	1.03550×10^{-12}	4.68560×10^{-14}	621.497	6.02060×10^{-13}	2.65390×10^{-14}
599.352	1.01580×10^{-12}	4.59360×10^{-14}	622.065	5.95420×10^{-13}	2.62270×10^{-14}
599.920	9.96940×10^{-13}	4.50600×10^{-14}	622.633	5.88870×10^{-13}	2.59190×10^{-14}
600.487	9.78990×10^{-13}	4.42270×10^{-14}	623.201	5.82410×10^{-13}	2.56170×10^{-14}
601.055	9.61850×10^{-13}	4.34310×10^{-14}	623.769	5.76050×10^{-13}	2.53190×10^{-14}
601.623	9.45460×10^{-13}	4.26720×10^{-14}	624.337	5.69780×10^{-13}	2.50250×10^{-14}
602.191	9.29780×10^{-13}	4.19450×10^{-14}	624.905	5.63600×10^{-13}	2.47360×10^{-14}
602.759	9.14750×10^{-13}	4.12490×10^{-14}	625.472	5.57500×10^{-13}	2.44520×10^{-14}
603.327	9.00330×10^{-13}	4.05800×10^{-14}	626.040	5.51490×10^{-13}	2.41720×10^{-14}
603.894	8.86470×10^{-13}	3.99370×10^{-14}	626.608	5.45560×10^{-13}	2.38960×10^{-14}
604.462	8.73130×10^{-13}	3.93180×10^{-14}	627.176	5.39720×10^{-13}	2.36250×10^{-14}
605.030	8.60280×10^{-13}	3.87200×10^{-14}	627.744	5.33950×10^{-13}	2.33570×10^{-14}
605.598	8.47870×10^{-13}	3.81420×10^{-14}	628.312	5.28260×10^{-13}	2.30940×10^{-14}
606.166	8.35880×10^{-13}	3.75830×10^{-14}	628.879	5.22650×10^{-13}	2.28350×10^{-14}
606.734	8.24280×10^{-13}	3.70410×10^{-14}	629.447	5.17120×10^{-13}	2.25790×10^{-14}
607.302	8.13030×10^{-13}	3.65140×10^{-14}	630.015	5.11660×10^{-13}	2.23280×10^{-14}
607.869	8.02120×10^{-13}	3.60020×10^{-14}	630.583	5.06270×10^{-13}	2.20800×10^{-14}
608.437	7.91520×10^{-13}	3.55040×10^{-14}	631.151	5.00950×10^{-13}	2.18350×10^{-14}
609.005	7.81210×10^{-13}	3.50190×10^{-14}	631.719	4.95710×10^{-13}	2.15950×10^{-14}
609.573	7.71170×10^{-13}	3.45460×10^{-14}	632.286	4.90530×10^{-13}	2.13580×10^{-14}
610.141	7.61380×10^{-13}	3.40840×10^{-14}	632.854	4.85420×10^{-13}	2.11240×10^{-14}

Table A.30 (cont'd)

JD +2451000	*UVOIR* Flux	Flux error	JD +2451000	*UVOIR* Flux	Flux error
633.422	4.80380×10^{-13}	2.08940×10^{-14}	644.211	3.96020×10^{-13}	1.71040×10^{-14}
633.990	4.75400×10^{-13}	2.06670×10^{-14}	644.779	3.92120×10^{-13}	1.69320×10^{-14}
634.558	4.70490×10^{-13}	2.04440×10^{-14}	645.347	3.88270×10^{-13}	1.67620×10^{-14}
635.126	4.65640×10^{-13}	2.02240×10^{-14}	645.915	3.84470×10^{-13}	1.65940×10^{-14}
635.693	4.60860×10^{-13}	2.00070×10^{-14}	646.482	3.80720×10^{-13}	1.64300×10^{-14}
636.261	4.56140×10^{-13}	1.97930×10^{-14}	647.050	3.77010×10^{-13}	1.62670×10^{-14}
636.829	4.51480×10^{-13}	1.95820×10^{-14}	647.618	3.73350×10^{-13}	1.61070×10^{-14}
637.397	4.46870×10^{-13}	1.93750×10^{-14}	648.186	3.69740×10^{-13}	1.59480×10^{-14}
637.965	4.42330×10^{-13}	1.91700×10^{-14}	648.754	3.66170×10^{-13}	1.57930×10^{-14}
638.533	4.37850×10^{-13}	1.89680×10^{-14}	649.322	3.62640×10^{-13}	1.56390×10^{-14}
639.101	4.33420×10^{-13}	1.87690×10^{-14}	649.889	3.59160×10^{-13}	1.54870×10^{-14}
639.668	4.29050×10^{-13}	1.85740×10^{-14}	650.457	3.55720×10^{-13}	1.53380×10^{-14}
640.236	4.24730×10^{-13}	1.83800×10^{-14}	651.025	3.52320×10^{-13}	1.51900×10^{-14}
640.804	4.20470×10^{-13}	1.81900×10^{-14}	651.593	3.48970×10^{-13}	1.50450×10^{-14}
641.372	4.16270×10^{-13}	1.80020×10^{-14}	652.161	3.45660×10^{-13}	1.49020×10^{-14}
641.940	4.12120×10^{-13}	1.78180×10^{-14}	652.729	3.42380×10^{-13}	1.47610×10^{-14}
642.508	4.08020×10^{-13}	1.76350×10^{-14}	653.297	3.39150×10^{-13}	1.46210×10^{-14}
643.075	4.03970×10^{-13}	1.74560×10^{-14}	653.864	3.35960×10^{-13}	1.44840×10^{-14}
643.643	3.99970×10^{-13}	1.72780×10^{-14}	654.432	3.32810×10^{-13}	1.43480×10^{-14}

Table A.31. SN 2000E

JD +2451000	*UVOIR* Flux	Flux error	JD +2451000	*UVOIR* Flux	Flux error
570.101	1.10858×10^{-10}	5.36977×10^{-12}	620.352	1.56758×10^{-11}	7.96008×10^{-13}
571.357	1.17726×10^{-10}	5.70900×10^{-12}	621.608	1.50013×10^{-11}	7.58315×10^{-13}
572.613	1.23622×10^{-10}	6.02172×10^{-12}	622.864	1.43952×10^{-11}	7.24801×10^{-13}
573.869	1.28551×10^{-10}	6.30361×10^{-12}	624.121	1.38465×10^{-11}	6.94843×10^{-13}
575.126	1.32607×10^{-10}	6.54611×10^{-12}	625.377	1.33472×10^{-11}	6.67860×10^{-13}
576.382	1.35704×10^{-10}	6.73314×10^{-12}	626.633	1.28892×10^{-11}	6.43382×10^{-13}
577.638	1.37547×10^{-10}	6.84301×10^{-12}	627.889	1.24665×10^{-11}	6.20993×10^{-13}
578.894	1.37724×10^{-10}	6.85420×10^{-12}	629.146	1.20738×10^{-11}	6.00358×10^{-13}
580.151	1.35824×10^{-10}	6.75110×10^{-12}	630.402	1.17070×10^{-11}	5.81176×10^{-13}
581.407	1.31612×10^{-10}	6.52924×10^{-12}	631.658	1.13615×10^{-11}	5.63240×10^{-13}
582.663	1.25212×10^{-10}	6.19821×10^{-12}	632.915	1.10342×10^{-11}	5.46359×10^{-13}
583.920	1.17055×10^{-10}	5.78164×10^{-12}	634.171	1.07242×10^{-11}	5.30394×10^{-13}
585.176	1.07806×10^{-10}	5.31260×10^{-12}	635.427	1.04283×10^{-11}	5.15204×10^{-13}
586.432	9.81628×10^{-11}	4.82563×10^{-12}	636.683	1.01450×10^{-11}	5.00713×10^{-13}
587.688	8.87231×10^{-11}	4.35057×10^{-12}	637.940	9.87311×10^{-12}	4.86835×10^{-13}
588.945	7.99053×10^{-11}	3.90877×10^{-12}	639.196	9.61148×10^{-12}	4.73508×10^{-13}
590.201	7.19507×10^{-11}	3.51331×10^{-12}	640.452	9.35923×10^{-12}	4.60695×10^{-13}
591.457	6.49536×10^{-11}	3.16978×10^{-12}	641.709	9.11564×10^{-12}	4.48337×10^{-13}
592.714	5.89096×10^{-11}	2.87812×10^{-12}	642.965	8.88018×10^{-12}	4.36413×10^{-13}
593.970	5.37608×10^{-11}	2.63561×10^{-12}	644.221	8.65226×10^{-12}	4.24894×10^{-13}
595.226	4.94150×10^{-11}	2.43682×10^{-12}	645.477	8.43151×10^{-12}	4.13761×10^{-13}
596.482	4.57670×10^{-11}	2.27592×10^{-12}	646.734	8.21785×10^{-12}	4.02999×10^{-13}
597.739	4.27047×10^{-11}	2.14607×10^{-12}	647.990	8.01077×10^{-12}	3.92593×10^{-13}
598.995	4.01143×10^{-11}	2.04060×10^{-12}	649.246	7.81028×10^{-12}	3.82528×10^{-13}
600.251	3.78874×10^{-11}	1.95247×10^{-12}	650.503	7.61595×10^{-12}	3.72787×10^{-13}
601.508	3.59209×10^{-11}	1.87501×10^{-12}	651.759	7.42777×10^{-12}	3.63376×10^{-13}
602.764	3.41267×10^{-11}	1.80233×10^{-12}	653.015	7.24547×10^{-12}	3.54263×10^{-13}
604.020	3.24317×10^{-11}	1.72942×10^{-12}	654.271	7.06871×10^{-12}	3.45450×10^{-13}
605.276	3.07874×10^{-11}	1.65311×10^{-12}	655.528	6.89724×10^{-12}	3.36922×10^{-13}
606.533	2.91684×10^{-11}	1.57221×10^{-12}	656.784	6.73088×10^{-12}	3.28644×10^{-13}
607.789	2.75671×10^{-11}	1.48709×10^{-12}	658.040	6.56910×10^{-12}	3.20622×10^{-13}
609.045	2.59949×10^{-11}	1.39938×10^{-12}	659.297	6.41188×10^{-12}	3.12828×10^{-13}
610.302	2.44707×10^{-11}	1.31161×10^{-12}	660.553	6.25879×10^{-12}	3.05257×10^{-13}
611.558	2.30176×10^{-11}	1.22619×10^{-12}	661.809	6.10952×10^{-12}	2.97883×10^{-13}
612.814	2.16538×10^{-11}	1.14533×10^{-12}	663.065	5.96390×10^{-12}	2.90713×10^{-13}
614.070	2.03934×10^{-11}	1.07038×10^{-12}	664.322	5.82180×10^{-12}	2.83714×10^{-13}
615.327	1.92427×10^{-11}	1.00225×10^{-12}	665.578	5.68308×10^{-12}	2.76901×10^{-13}
616.583	1.82019×10^{-11}	9.41103×10^{-13}	666.834	5.54780×10^{-12}	2.70265×10^{-13}
617.839	1.72650×10^{-11}	8.86725×10^{-13}	668.090	5.41589×10^{-12}	2.63804×10^{-13}
619.095	1.64261×10^{-11}	8.38578×10^{-13}	669.347	5.28740×10^{-12}	2.57513×10^{-13}

Table A.31 (cont'd)

JD +2451000	*UVOIR* Flux	Flux error	JD +2451000	*UVOIR* Flux	Flux error
670.603	5.16249×10^{-12}	2.51412×10^{-13}	678.141	4.47940×10^{-12}	2.18212×10^{-13}
671.859	5.04101×10^{-12}	2.45492×10^{-13}	679.397	4.37395×10^{-12}	2.13110×10^{-13}
673.116	4.92290×10^{-12}	2.39735×10^{-13}	680.653	4.27072×10^{-12}	2.08121×10^{-13}
674.372	4.80804×10^{-12}	2.34156×10^{-13}	681.910	4.17066×10^{-12}	2.03293×10^{-13}
675.628	4.69610×10^{-12}	2.28712×10^{-13}	683.166	4.07688×10^{-12}	1.98770×10^{-13}
676.884	4.58677×10^{-12}	2.23410×10^{-13}	...	...	...

Table A.32. SN 2000cx

JD +2451000	*UVOIR* Flux	Flux error	JD +2451000	*UVOIR* Flux	Flux error
742.593	2.40000×10^{-11}	1.00810×10^{-12}	766.312	4.44970×10^{-11}	2.01780×10^{-12}
743.186	3.16310×10^{-11}	1.33260×10^{-12}	766.905	4.23750×10^{-11}	1.91880×10^{-12}
743.779	3.96270×10^{-11}	1.68820×10^{-12}	767.497	4.04010×10^{-11}	1.82610×10^{-12}
744.372	4.75440×10^{-11}	2.04720×10^{-12}	768.090	3.85740×10^{-11}	1.74000×10^{-12}
744.965	5.50930×10^{-11}	2.39150×10^{-12}	768.683	3.68890×10^{-11}	1.66050×10^{-12}
745.558	6.21140×10^{-11}	2.71160×10^{-12}	769.276	3.53430×10^{-11}	1.58740×10^{-12}
746.151	6.85350×10^{-11}	3.00310×10^{-12}	769.869	3.39290×10^{-11}	1.52060×10^{-12}
746.744	7.43300×10^{-11}	3.26480×10^{-12}	770.462	3.26390×10^{-11}	1.45990×10^{-12}
747.337	7.95030×10^{-11}	3.49730×10^{-12}	771.055	3.14610×10^{-11}	1.40490×10^{-12}
747.930	8.40650×10^{-11}	3.70150×10^{-12}	771.648	3.03840×10^{-11}	1.35510×10^{-12}
748.523	8.80320×10^{-11}	3.87850×10^{-12}	772.241	2.93950×10^{-11}	1.30990×10^{-12}
749.116	9.14230×10^{-11}	4.02940×10^{-12}	772.834	2.84780×10^{-11}	1.26850×10^{-12}
749.709	9.42530×10^{-11}	4.15520×10^{-12}	773.427	2.76170×10^{-11}	1.23010×10^{-12}
750.302	9.65380×10^{-11}	4.25700×10^{-12}	774.020	2.67970×10^{-11}	1.19400×10^{-12}
750.894	9.82930×10^{-11}	4.33560×10^{-12}	774.613	2.60020×10^{-11}	1.15920×10^{-12}
751.487	9.95340×10^{-11}	4.39200×10^{-12}	775.206	2.52200×10^{-11}	1.12510×10^{-12}
752.080	1.00280×10^{-10}	4.42700×10^{-12}	775.799	2.44400×10^{-11}	1.09090×10^{-12}
752.673	1.00540×10^{-10}	4.44170×10^{-12}	776.392	2.36550×10^{-11}	1.05620×10^{-12}
753.266	1.00340×10^{-10}	4.43680×10^{-12}	776.985	2.28610×10^{-11}	1.02080×10^{-12}
753.859	9.97070×10^{-11}	4.41340×10^{-12}	777.578	2.20590×10^{-11}	9.84670×10^{-13}
754.452	9.86550×10^{-11}	4.37230×10^{-12}	778.171	2.12520×10^{-11}	9.47950×10^{-13}
755.045	9.72130×10^{-11}	4.31470×10^{-12}	778.764	2.04460×10^{-11}	9.10970×10^{-13}
755.638	9.54140×10^{-11}	4.24180×10^{-12}	779.357	1.96480×10^{-11}	8.74130×10^{-13}
756.231	9.32910×10^{-11}	4.15470×10^{-12}	779.950	1.88650×10^{-11}	8.37880×10^{-13}
756.824	9.08810×10^{-11}	4.05510×10^{-12}	780.543	1.81050×10^{-11}	8.02620×10^{-13}
757.417	8.82270×10^{-11}	3.94440×10^{-12}	781.136	1.73730×10^{-11}	7.68720×10^{-13}
758.010	8.53700×10^{-11}	3.82440×10^{-12}	781.729	1.66740×10^{-11}	7.36440×10^{-13}
758.603	8.23570×10^{-11}	3.69690×10^{-12}	782.322	1.60100×10^{-11}	7.05960×10^{-13}
759.196	7.92290×10^{-11}	3.56360×10^{-12}	782.915	1.53850×10^{-11}	6.77390×10^{-13}
759.789	7.60300×10^{-11}	3.42640×10^{-12}	783.508	1.47970×10^{-11}	6.50730×10^{-13}
760.382	7.27980×10^{-11}	3.28690×10^{-12}	784.101	1.42470×10^{-11}	6.25950×10^{-13}
760.975	6.95710×10^{-11}	3.14660×10^{-12}	784.693	1.37320×10^{-11}	6.02960×10^{-13}
761.568	6.63780×10^{-11}	3.00680×10^{-12}	785.286	1.32520×10^{-11}	5.81670×10^{-13}
762.161	6.32480×10^{-11}	2.86880×10^{-12}	785.879	1.28030×10^{-11}	5.61950×10^{-13}
762.754	6.02030×10^{-11}	2.73340×10^{-12}	786.472	1.23830×10^{-11}	5.43670×10^{-13}
763.347	5.72610×10^{-11}	2.60170×10^{-12}	787.065	1.19910×10^{-11}	5.26690×10^{-13}
763.940	5.44370×10^{-11}	2.47430×10^{-12}	787.658	1.16240×10^{-11}	5.10910×10^{-13}
764.533	5.17410×10^{-11}	2.35180×10^{-12}	788.251	1.12790×10^{-11}	4.96200×10^{-13}
765.126	4.91820×10^{-11}	2.23460×10^{-12}	788.844	1.09560×10^{-11}	4.82460×10^{-13}
765.719	4.67660×10^{-11}	2.12320×10^{-12}	789.437	1.06520×10^{-11}	4.69580×10^{-13}

Table A.32 (cont'd)

JD +2451000	*UVOIR* Flux	Flux error	JD +2451000	*UVOIR* Flux	Flux error
790.030	1.03660×10^{-11}	4.57480×10^{-13}	813.749	4.98380×10^{-12}	2.19880×10^{-13}
790.623	1.00950×10^{-11}	4.46070×10^{-13}	814.342	4.90910×10^{-12}	2.16550×10^{-13}
791.216	9.84030×10^{-12}	4.35300×10^{-13}	814.935	4.83570×10^{-12}	2.13290×10^{-13}
791.809	9.59890×10^{-12}	4.25090×10^{-13}	815.528	4.76360×10^{-12}	2.10090×10^{-13}
792.402	9.37040×10^{-12}	4.15400×10^{-13}	816.121	4.69280×10^{-12}	2.06960×10^{-13}
792.995	9.15360×10^{-12}	4.06170×10^{-13}	816.714	4.62310×10^{-12}	2.03880×10^{-13}
793.588	8.94760×10^{-12}	3.97360×10^{-13}	817.307	4.55470×10^{-12}	2.00870×10^{-13}
794.181	8.75180×10^{-12}	3.88940×10^{-13}	817.899	4.48740×10^{-12}	1.97910×10^{-13}
794.774	8.56520×10^{-12}	3.80880×10^{-13}	818.492	4.42130×10^{-12}	1.95010×10^{-13}
795.367	8.38720×10^{-12}	3.73140×10^{-13}	819.085	4.35630×10^{-12}	1.92160×10^{-13}
795.960	8.21720×10^{-12}	3.65710×10^{-13}	819.678	4.29230×10^{-12}	1.89370×10^{-13}
796.553	8.05440×10^{-12}	3.58560×10^{-13}	820.271	4.22940×10^{-12}	1.86630×10^{-13}
797.146	7.89830×10^{-12}	3.51660×10^{-13}	820.864	4.16760×10^{-12}	1.83950×10^{-13}
797.739	7.74850×10^{-12}	3.45000×10^{-13}	821.457	4.10680×10^{-12}	1.81310×10^{-13}
798.332	7.60440×10^{-12}	3.38570×10^{-13}	822.050	4.04700×10^{-12}	1.78720×10^{-13}
798.925	7.46560×10^{-12}	3.32350×10^{-13}	822.643	3.98820×10^{-12}	1.76180×10^{-13}
799.518	7.33160×10^{-12}	3.26320×10^{-13}	823.236	3.93030×10^{-12}	1.73680×10^{-13}
800.111	7.20220×10^{-12}	3.20480×10^{-13}	823.829	3.87340×10^{-12}	1.71240×10^{-13}
800.703	7.07690×10^{-12}	3.14800×10^{-13}	824.422	3.81750×10^{-12}	1.68830×10^{-13}
801.297	6.95550×10^{-12}	3.09290×10^{-13}	825.015	3.76240×10^{-12}	1.66470×10^{-13}
801.889	6.83760×10^{-12}	3.03930×10^{-13}	825.608	3.70820×10^{-12}	1.64160×10^{-13}
802.482	6.72310×10^{-12}	2.98720×10^{-13}	826.201	3.65490×10^{-12}	1.61890×10^{-13}
803.075	6.61170×10^{-12}	2.93640×10^{-13}	826.794	3.60250×10^{-12}	1.59650×10^{-13}
803.668	6.50320×10^{-12}	2.88690×10^{-13}	827.387	3.55090×10^{-12}	1.57460×10^{-13}
804.261	6.39750×10^{-12}	2.83860×10^{-13}	827.980	3.50020×10^{-12}	1.55310×10^{-13}
804.854	6.29430×10^{-12}	2.79150×10^{-13}	828.573	3.45020×10^{-12}	1.53190×10^{-13}
805.447	6.19350×10^{-12}	2.74550×10^{-13}	829.166	3.40110×10^{-12}	1.51120×10^{-13}
806.040	6.09500×10^{-12}	2.70070×10^{-13}	829.759	3.35280×10^{-12}	1.49080×10^{-13}
806.633	5.99880×10^{-12}	2.65680×10^{-13}	830.352	3.30520×10^{-12}	1.47080×10^{-13}
807.226	5.90460×10^{-12}	2.61390×10^{-13}	830.945	3.25840×10^{-12}	1.45110×10^{-13}
807.819	5.81240×10^{-12}	2.57200×10^{-13}	831.538	3.21230×10^{-12}	1.43180×10^{-13}
808.412	5.72200×10^{-12}	2.53100×10^{-13}	832.131	3.16700×10^{-12}	1.41280×10^{-13}
809.005	5.63360×10^{-12}	2.49090×10^{-13}	832.724	3.12240×10^{-12}	1.39410×10^{-13}
809.598	5.54680×10^{-12}	2.45170×10^{-13}	833.317	3.07860×10^{-12}	1.37580×10^{-13}
810.191	5.46170×10^{-12}	2.41320×10^{-13}	833.910	3.03540×10^{-12}	1.35780×10^{-13}
810.784	5.37830×10^{-12}	2.37560×10^{-13}	834.503	2.99290×10^{-12}	1.34010×10^{-13}
811.377	5.29650×10^{-12}	2.33880×10^{-13}	835.095	2.95110×10^{-12}	1.32280×10^{-13}
811.970	5.21610×10^{-12}	2.30270×10^{-13}	835.688	2.90990×10^{-12}	1.30570×10^{-13}
812.563	5.13730×10^{-12}	2.26730×10^{-13}	836.281	2.86940×10^{-12}	1.28890×10^{-13}
813.156	5.05980×10^{-12}	2.23270×10^{-13}	836.874	2.82960×10^{-12}	1.27240×10^{-13}

Table A.32 (cont'd)

JD +2451000	*UVOIR* Flux	Flux error	JD +2451000	*UVOIR* Flux	Flux error
837.467	2.79030×10^{-12}	1.25620×10^{-13}	848.734	2.15170×10^{-12}	9.95190×10^{-14}
838.060	2.75170×10^{-12}	1.24030×10^{-13}	849.327	2.12310×10^{-12}	9.83600×10^{-14}
838.653	2.71370×10^{-12}	1.22460×10^{-13}	849.920	2.09490×10^{-12}	9.72190×10^{-14}
839.246	2.67630×10^{-12}	1.20920×10^{-13}	850.513	2.06710×10^{-12}	9.60960×10^{-14}
839.839	2.63950×10^{-12}	1.19410×10^{-13}	851.106	2.03980×10^{-12}	9.49900×10^{-14}
840.432	2.60330×10^{-12}	1.17920×10^{-13}	851.698	2.01290×10^{-12}	9.39030×10^{-14}
841.025	2.56760×10^{-12}	1.16460×10^{-13}	852.291	1.98640×10^{-12}	9.28320×10^{-14}
841.618	2.53250×10^{-12}	1.15020×10^{-13}	852.884	1.96030×10^{-12}	9.17780×10^{-14}
842.211	2.49800×10^{-12}	1.13610×10^{-13}	853.477	1.93460×10^{-12}	9.07410×10^{-14}
842.804	2.46400×10^{-12}	1.12220×10^{-13}	854.070	1.90930×10^{-12}	8.97190×10^{-14}
843.397	2.43050×10^{-12}	1.10850×10^{-13}	854.663	1.88440×10^{-12}	8.87130×10^{-14}
843.990	2.39750×10^{-12}	1.09510×10^{-13}	855.256	1.85990×10^{-12}	8.77230×10^{-14}
844.583	2.36510×10^{-12}	1.08190×10^{-13}	855.849	1.83570×10^{-12}	8.67480×10^{-14}
845.176	2.33320×10^{-12}	1.06890×10^{-13}	856.442	1.81190×10^{-12}	8.57880×10^{-14}
845.769	2.30170×10^{-12}	1.05610×10^{-13}	857.035	1.78850×10^{-12}	8.48420×10^{-14}
846.362	2.27080×10^{-12}	1.04350×10^{-13}	857.628	1.76540×10^{-12}	8.39110×10^{-14}
846.955	2.24030×10^{-12}	1.03110×10^{-13}	858.221	1.74260×10^{-12}	8.29930×10^{-14}
847.548	2.21030×10^{-12}	1.01900×10^{-13}	858.814	1.72020×10^{-12}	8.20900×10^{-14}
848.141	2.18080×10^{-12}	1.00700×10^{-13}	859.407	1.69820×10^{-12}	8.12000×10^{-14}

Table A.33. SN 2001bt

JD +2450000	*UVOIR* Flux	Flux error	JD +2450000	*UVOIR* Flux	Flux error
2055.23	1.82563×10^{-11}	1.09313×10^{-12}	2081.36	1.13659×10^{-11}	5.47709×10^{-13}
2055.88	1.99362×10^{-11}	1.14733×10^{-12}	2082.01	1.09450×10^{-11}	5.27320×10^{-13}
2056.53	2.18167×10^{-11}	1.20926×10^{-12}	2082.66	1.05652×10^{-11}	5.09178×10^{-13}
2057.19	2.36829×10^{-11}	1.27707×10^{-12}	2083.32	1.02199×10^{-11}	4.92916×10^{-13}
2057.84	2.54070×10^{-11}	1.34611×10^{-12}	2083.97	9.90294×10^{-12}	4.78147×10^{-13}
2058.49	2.69409×10^{-11}	1.41237×10^{-12}	2084.62	9.60811×10^{-12}	4.64525×10^{-13}
2059.15	2.82819×10^{-11}	1.47362×10^{-12}	2085.28	9.32952×10^{-12}	4.51711×10^{-13}
2059.80	2.94464×10^{-11}	1.52887×10^{-12}	2085.93	9.06201×10^{-12}	4.39400×10^{-13}
2060.45	3.04494×10^{-11}	1.57780×10^{-12}	2086.58	8.80103×10^{-12}	4.27333×10^{-13}
2061.10	3.12993×10^{-11}	1.61994×10^{-12}	2087.24	8.54275×10^{-12}	4.15306×10^{-13}
2061.76	3.20018×10^{-11}	1.65491×10^{-12}	2087.89	8.28434×10^{-12}	4.03177×10^{-13}
2062.41	3.25548×10^{-11}	1.68235×10^{-12}	2088.54	8.02405×10^{-12}	3.90839×10^{-13}
2063.06	3.29551×10^{-11}	1.70178×10^{-12}	2089.20	7.76089×10^{-12}	3.78269×10^{-13}
2063.72	3.31979×10^{-11}	1.71276×10^{-12}	2089.85	7.49509×10^{-12}	3.65470×10^{-13}
2064.37	3.32778×10^{-11}	1.71503×10^{-12}	2090.50	7.22751×10^{-12}	3.52506×10^{-13}
2065.02	3.31931×10^{-11}	1.70838×10^{-12}	2091.16	6.95963×10^{-12}	3.39468×10^{-13}
2065.68	3.29415×10^{-11}	1.69288×10^{-12}	2091.81	6.69367×10^{-12}	3.26466×10^{-13}
2066.33	3.25258×10^{-11}	1.66867×10^{-12}	2092.46	6.43163×10^{-12}	3.13628×10^{-13}
2066.99	3.19536×10^{-11}	1.63621×10^{-12}	2093.11	6.17607×10^{-12}	3.01071×10^{-13}
2067.64	3.12342×10^{-11}	1.59609×10^{-12}	2093.77	5.92895×10^{-12}	2.88915×10^{-13}
2068.29	3.03801×10^{-11}	1.54907×10^{-12}	2094.42	5.69219×10^{-12}	2.77261×10^{-13}
2068.95	2.94108×10^{-11}	1.49621×10^{-12}	2095.07	5.46742×10^{-12}	2.66180×10^{-13}
2069.60	2.83456×10^{-11}	1.43852×10^{-12}	2095.73	5.25547×10^{-12}	2.55747×10^{-13}
2070.25	2.72051×10^{-11}	1.37704×10^{-12}	2096.38	5.05726×10^{-12}	2.45979×10^{-13}
2070.91	2.60118×10^{-11}	1.31303×10^{-12}	2097.03	4.87293×10^{-12}	2.36900×10^{-13}
2071.56	2.47872×10^{-11}	1.24774×10^{-12}	2097.69	4.70248×10^{-12}	2.28511×10^{-13}
2072.21	2.35530×10^{-11}	1.18202×10^{-12}	2098.34	4.54543×10^{-12}	2.20771×10^{-13}
2072.86	2.23278×10^{-11}	1.11701×10^{-12}	2099.00	4.40125×10^{-12}	2.13669×10^{-13}
2073.52	2.11272×10^{-11}	1.05349×10^{-12}	2099.65	4.26903×10^{-12}	2.07156×10^{-13}
2074.17	1.99666×10^{-11}	9.92210×10^{-13}	2100.30	4.14796×10^{-12}	2.01190×10^{-13}
2074.82	1.88568×10^{-11}	9.33726×10^{-13}	2100.96	4.03698×10^{-12}	1.95707×10^{-13}
2075.48	1.78047×10^{-11}	8.78500×10^{-13}	2101.61	3.93529×10^{-12}	1.90678×10^{-13}
2076.13	1.68189×10^{-11}	8.26816×10^{-13}	2102.26	3.84162×10^{-12}	1.86052×10^{-13}
2076.78	1.59013×10^{-11}	7.78911×10^{-13}	2102.92	3.75516×10^{-12}	1.81775×10^{-13}
2077.44	1.50543×10^{-11}	7.34891×10^{-13}	2103.57	3.67497×10^{-12}	1.77796×10^{-13}
2078.09	1.42789×10^{-11}	6.94746×10^{-13}	2104.22	3.60034×10^{-12}	1.74095×10^{-13}
2078.74	1.35717×10^{-11}	6.58428×10^{-13}	2104.87	3.53042×10^{-12}	1.70620×10^{-13}
2079.40	1.29315×10^{-11}	6.25788×10^{-13}	2105.53	3.46461×10^{-12}	1.67340×10^{-13}
2080.05	1.23527×10^{-11}	5.96633×10^{-13}	2106.18	3.40229×10^{-12}	1.64234×10^{-13}
2080.70	1.18330×10^{-11}	5.70707×10^{-13}	2106.83	3.34296×10^{-12}	1.61284×10^{-13}

Table A.33 (cont'd)

JD +2450000	*UVOIR* Flux	Flux error	JD +2450000	*UVOIR* Flux	Flux error
2107.49	3.28620×10^{-12}	1.58457×10^{-13}	2133.62	1.80026×10^{-12}	8.66526×10^{-14}
2108.14	3.23162×10^{-12}	1.55733×10^{-13}	2134.27	1.77447×10^{-12}	8.54710×10^{-14}
2108.79	3.17901×10^{-12}	1.53115×10^{-13}	2134.93	1.74911×10^{-12}	8.43128×10^{-14}
2109.45	3.12798×10^{-12}	1.50569×10^{-13}	2135.58	1.72432×10^{-12}	8.31768×10^{-14}
2110.10	3.07855×10^{-12}	1.48109×10^{-13}	2136.23	1.69987×10^{-12}	8.20624×10^{-14}
2110.75	3.03030×10^{-12}	1.45713×10^{-13}	2136.89	1.67587×10^{-12}	8.09705×10^{-14}
2111.41	2.98324×10^{-12}	1.43372×10^{-13}	2137.54	1.65221×10^{-12}	7.99002×10^{-14}
2112.06	2.93740×10^{-12}	1.41097×10^{-13}	2138.19	1.62912×10^{-12}	7.88505×10^{-14}
2112.71	2.89245×10^{-12}	1.38878×10^{-13}	2138.84	1.60638×10^{-12}	7.78213×10^{-14}
2113.37	2.84841×10^{-12}	1.36693×10^{-13}	2139.50	1.58399×10^{-12}	7.68127×10^{-14}
2114.02	2.80517×10^{-12}	1.34564×10^{-13}	2140.15	1.56204×10^{-12}	7.58234×10^{-14}
2114.67	2.76284×10^{-12}	1.32481×10^{-13}	2140.80	1.54044×10^{-12}	7.48544×10^{-14}
2115.33	2.72133×10^{-12}	1.30444×10^{-13}	2141.46	1.51929×10^{-12}	7.39024×10^{-14}
2115.98	2.68051×10^{-12}	1.28441×10^{-13}	2142.11	1.49848×10^{-12}	7.29705×10^{-14}
2116.63	2.64050×10^{-12}	1.26485×10^{-13}	2142.76	1.47800×10^{-12}	7.20552×10^{-14}
2117.29	2.60108×10^{-12}	1.24563×10^{-13}	2143.42	1.45796×10^{-12}	7.11575×10^{-14}
2117.94	2.56245×10^{-12}	1.22686×10^{-13}	2144.07	1.43824×10^{-12}	7.02762×10^{-14}
2118.59	2.52440×10^{-12}	1.20843×10^{-13}	2144.72	1.41874×10^{-12}	6.94109×10^{-14}
2119.25	2.48702×10^{-12}	1.19035×10^{-13}	2145.38	1.39967×10^{-12}	6.85616×10^{-14}
2119.90	2.45032×10^{-12}	1.17259×10^{-13}	2146.03	1.38091×10^{-12}	6.77271×10^{-14}
2120.55	2.41417×10^{-12}	1.15517×10^{-13}	2146.68	1.36236×10^{-12}	6.69083×10^{-14}
2121.21	2.37857×10^{-12}	1.13808×10^{-13}	2147.34	1.34423×10^{-12}	6.61028×10^{-14}
2121.86	2.34362×10^{-12}	1.12131×10^{-13}	2147.99	1.32631×10^{-12}	6.53107×10^{-14}
2122.51	2.30921×10^{-12}	1.10487×10^{-13}	2148.64	1.30869×10^{-12}	6.45330×10^{-14}
2123.17	2.27533×10^{-12}	1.08867×10^{-13}	2149.30	1.29138×10^{-12}	6.37676×10^{-14}
2123.82	2.24197×10^{-12}	1.07281×10^{-13}	2149.95	1.27439×10^{-12}	6.30165×10^{-14}
2124.47	2.20913×10^{-12}	1.05723×10^{-13}	2150.60	1.25760×10^{-12}	6.22768×10^{-14}
2125.13	2.17682×10^{-12}	1.04194×10^{-13}	2151.26	1.24101×10^{-12}	6.15506×10^{-14}
2125.78	2.14502×10^{-12}	1.02692×10^{-13}	2151.91	1.22475×10^{-12}	6.08360×10^{-14}
2126.43	2.11373×10^{-12}	1.01217×10^{-13}	2152.56	1.20881×10^{-12}	6.01343×10^{-14}
2127.08	2.08285×10^{-12}	9.97682×10^{-14}	2153.22	1.19309×10^{-12}	5.94457×10^{-14}
2127.74	2.05249×10^{-12}	9.83463×10^{-14}	2153.87	1.17759×10^{-12}	5.87682×10^{-14}
2128.39	2.02264×10^{-12}	9.69493×10^{-14}	2154.52	1.16243×10^{-12}	5.81032×10^{-14}
2129.04	1.99321×10^{-12}	9.55771×10^{-14}	2155.18	1.14751×10^{-12}	5.74510×10^{-14}
2129.70	1.96430×10^{-12}	9.42301×10^{-14}	2155.83	1.13282×10^{-12}	5.68115×10^{-14}
2130.35	1.93580×10^{-12}	9.29071×10^{-14}	2156.48	1.11848×10^{-12}	5.61831×10^{-14}
2131.00	1.90784×10^{-12}	9.16085×10^{-14}	2157.14	1.10427×10^{-12}	5.55667×10^{-14}
2131.66	1.88019×10^{-12}	9.03344×10^{-14}	2157.79	1.09042×10^{-12}	5.49623×10^{-14}
2132.31	1.85307×10^{-12}	8.90839×10^{-14}	2158.44	1.07679×10^{-12}	5.43700×10^{-14}
2132.97	1.82650×10^{-12}	8.78563×10^{-14}	2159.09	1.06339×10^{-12}	5.37884×10^{-14}

Table A.33 (cont'd)

JD +2450000	*UVOIR* Flux	Flux error	JD +2450000	*UVOIR* Flux	Flux error
2159.75	1.05023×10^{-12}	5.32173×10^{-14}	2164.32	9.63507×10^{-13}	4.94633×10^{-14}
2160.40	1.03728×10^{-12}	5.26564×10^{-14}	2164.98	9.51762×10^{-13}	4.89557×10^{-14}
2161.05	1.02455×10^{-12}	5.21052×10^{-14}	2165.63	9.40177×10^{-13}	4.84534×10^{-14}
2161.71	1.01201×10^{-12}	5.15622×10^{-14}	2166.28	9.28767×10^{-13}	4.79608×10^{-14}
2162.36	9.99644×10^{-13}	5.10267×10^{-14}	2166.94	9.17581×10^{-13}	4.74772×10^{-14}
2163.01	9.87453×10^{-13}	5.04993×10^{-14}	2167.59	9.06691×10^{-13}	4.70075×10^{-14}
2163.67	9.75409×10^{-13}	4.99786×10^{-14}	2168.24	8.96202×10^{-13}	4.65571×10^{-14}

Table A.34. SN 2001el

JD +2450000	*UVOIR* Flux	Flux error	JD +2450000	*UVOIR* Flux	Flux error
2171.96	9.85790×10^{-11}	4.33630×10^{-12}	2198.09	1.16580×10^{-10}	5.18610×10^{-12}
2172.61	1.15540×10^{-10}	5.09070×10^{-12}	2198.74	1.11830×10^{-10}	4.97150×10^{-12}
2173.27	1.32690×10^{-10}	5.85560×10^{-12}	2199.40	1.07500×10^{-10}	4.77690×10^{-12}
2173.92	1.49790×10^{-10}	6.62040×10^{-12}	2200.05	1.03550×10^{-10}	4.60060×10^{-12}
2174.57	1.66620×10^{-10}	7.37570×10^{-12}	2200.70	9.99440×10^{-11}	4.44120×10^{-12}
2175.23	1.82980×10^{-10}	8.11250×10^{-12}	2201.36	9.66400×10^{-11}	4.29690×10^{-12}
2175.88	1.98670×10^{-10}	8.82210×10^{-12}	2202.01	9.36030×10^{-11}	4.16580×10^{-12}
2176.53	2.13520×10^{-10}	9.49570×10^{-12}	2202.66	9.07960×10^{-11}	4.04620×10^{-12}
2177.19	2.27320×10^{-10}	1.01240×10^{-11}	2203.32	8.81840×10^{-11}	3.93610×10^{-12}
2177.84	2.39900×10^{-10}	1.07000×10^{-11}	2203.97	8.57350×10^{-11}	3.83370×10^{-12}
2178.49	2.51100×10^{-10}	1.12130×10^{-11}	2204.62	8.34150×10^{-11}	3.73710×10^{-12}
2179.15	2.60770×10^{-10}	1.16570×10^{-11}	2205.28	8.11960×10^{-11}	3.64480×10^{-12}
2179.80	2.68800×10^{-10}	1.20260×10^{-11}	2205.93	7.90510×10^{-11}	3.55530×10^{-12}
2180.45	2.75100×10^{-10}	1.23160×10^{-11}	2206.58	7.69560×10^{-11}	3.46720×10^{-12}
2181.10	2.79620×10^{-10}	1.25240×10^{-11}	2207.24	7.48910×10^{-11}	3.37960×10^{-12}
2181.76	2.82370×10^{-10}	1.26500×10^{-11}	2207.89	7.28430×10^{-11}	3.29170×10^{-12}
2182.41	2.83370×10^{-10}	1.26970×10^{-11}	2208.54	7.07990×10^{-11}	3.20290×10^{-12}
2183.06	2.82690×10^{-10}	1.26680×10^{-11}	2209.20	6.87540×10^{-11}	3.11300×10^{-12}
2183.72	2.80430×10^{-10}	1.25690×10^{-11}	2209.85	6.67040×10^{-11}	3.02200×10^{-12}
2184.37	2.76740×10^{-10}	1.24050×10^{-11}	2210.50	6.46520×10^{-11}	2.93000×10^{-12}
2185.02	2.71750×10^{-10}	1.21840×10^{-11}	2211.16	6.26010×10^{-11}	2.83720×10^{-12}
2185.68	2.65640×10^{-10}	1.19140×10^{-11}	2211.81	6.05580×10^{-11}	2.74420×10^{-12}
2186.33	2.58570×10^{-10}	1.16020×10^{-11}	2212.46	5.85320×10^{-11}	2.65140×10^{-12}
2186.99	2.50730×10^{-10}	1.12560×10^{-11}	2213.11	5.65310×10^{-11}	2.55950×10^{-12}
2187.64	2.42300×10^{-10}	1.08830×10^{-11}	2213.77	5.45670×10^{-11}	2.46890×10^{-12}
2188.29	2.33450×10^{-10}	1.04910×10^{-11}	2214.42	5.26490×10^{-11}	2.38020×10^{-12}
2188.95	2.24360×10^{-10}	1.00860×10^{-11}	2215.07	5.07860×10^{-11}	2.29400×10^{-12}
2189.60	2.15170×10^{-10}	9.67460×10^{-12}	2215.73	4.89860×10^{-11}	2.21060×10^{-12}
2190.25	2.06030×10^{-10}	9.26180×10^{-12}	2216.38	4.72550×10^{-11}	2.13050×10^{-12}
2190.91	1.97030×10^{-10}	8.85200×10^{-12}	2217.03	4.56000×10^{-11}	2.05390×10^{-12}
2191.56	1.88230×10^{-10}	8.44850×10^{-12}	2217.69	4.40230×10^{-11}	1.98110×10^{-12}
2192.21	1.79660×10^{-10}	8.05330×10^{-12}	2218.34	4.25270×10^{-11}	1.91210×10^{-12}
2192.86	1.71310×10^{-10}	7.66810×10^{-12}	2219.00	4.11130×10^{-11}	1.84710×10^{-12}
2193.52	1.63170×10^{-10}	7.29430×10^{-12}	2219.65	3.97800×10^{-11}	1.78590×10^{-12}
2194.17	1.55280×10^{-10}	6.93400×10^{-12}	2220.30	3.85270×10^{-11}	1.72860×10^{-12}
2194.82	1.47700×10^{-10}	6.59000×10^{-12}	2220.96	3.73500×10^{-11}	1.67500×10^{-12}
2195.48	1.40500×10^{-10}	6.26500×10^{-12}	2221.61	3.62470×10^{-11}	1.62490×10^{-12}
2196.13	1.33760×10^{-10}	5.96130×10^{-12}	2222.26	3.52140×10^{-11}	1.57820×10^{-12}
2196.78	1.27520×10^{-10}	5.68020×10^{-12}	2222.92	3.42470×10^{-11}	1.53470×10^{-12}
2197.44	1.21800×10^{-10}	5.42200×10^{-12}	2223.57	3.33410×10^{-11}	1.49400×10^{-12}

Table A.34 (cont'd)

JD +2450000	*UVOIR* Flux	Flux error	JD +2450000	*UVOIR* Flux	Flux error
2224.22	3.24920×10^{-11}	1.45600×10^{-12}	2250.35	1.60570×10^{-11}	7.30370×10^{-13}
2224.87	3.16950×10^{-11}	1.42050×10^{-12}	2251.00	1.58120×10^{-11}	7.19610×10^{-13}
2225.53	3.09450×10^{-11}	1.38720×10^{-12}	2251.66	1.55720×10^{-11}	7.09050×10^{-13}
2226.18	3.02390×10^{-11}	1.35600×10^{-12}	2252.31	1.53350×10^{-11}	6.98690×10^{-13}
2226.83	2.95730×10^{-11}	1.32650×10^{-12}	2252.97	1.51040×10^{-11}	6.88520×10^{-13}
2227.49	2.89420×10^{-11}	1.29870×10^{-12}	2253.62	1.48760×10^{-11}	6.78540×10^{-13}
2228.14	2.83440×10^{-11}	1.27230×10^{-12}	2254.27	1.46520×10^{-11}	6.68740×10^{-13}
2228.79	2.77750×10^{-11}	1.24730×10^{-12}	2254.93	1.44320×10^{-11}	6.59120×10^{-13}
2229.45	2.72310×10^{-11}	1.22340×10^{-12}	2255.58	1.42160×10^{-11}	6.49670×10^{-13}
2230.10	2.67120×10^{-11}	1.20060×10^{-12}	2256.23	1.40040×10^{-11}	6.40400×10^{-13}
2230.75	2.62130×10^{-11}	1.17870×10^{-12}	2256.89	1.37950×10^{-11}	6.31300×10^{-13}
2231.41	2.57340×10^{-11}	1.15760×10^{-12}	2257.54	1.35910×10^{-11}	6.22360×10^{-13}
2232.06	2.52720×10^{-11}	1.13730×10^{-12}	2258.19	1.33890×10^{-11}	6.13590×10^{-13}
2232.71	2.48260×10^{-11}	1.11760×10^{-12}	2258.84	1.31920×10^{-11}	6.04980×10^{-13}
2233.37	2.43940×10^{-11}	1.09860×10^{-12}	2259.50	1.29970×10^{-11}	5.96520×10^{-13}
2234.02	2.39750×10^{-11}	1.08010×10^{-12}	2260.15	1.28060×10^{-11}	5.88220×10^{-13}
2234.67	2.35680×10^{-11}	1.06220×10^{-12}	2260.80	1.26190×10^{-11}	5.80070×10^{-13}
2235.33	2.31720×10^{-11}	1.04470×10^{-12}	2261.46	1.24350×10^{-11}	5.72070×10^{-13}
2235.98	2.27860×10^{-11}	1.02760×10^{-12}	2262.11	1.22530×10^{-11}	5.64220×10^{-13}
2236.63	2.24090×10^{-11}	1.01100×10^{-12}	2262.76	1.20750×10^{-11}	5.56500×10^{-13}
2237.29	2.20420×10^{-11}	9.94750×10^{-13}	2263.42	1.19010×10^{-11}	5.48930×10^{-13}
2237.94	2.16820×10^{-11}	9.78860×10^{-13}	2264.07	1.17290×10^{-11}	5.41490×10^{-13}
2238.59	2.13310×10^{-11}	9.63320×10^{-13}	2264.72	1.15600×10^{-11}	5.34190×10^{-13}
2239.25	2.09870×10^{-11}	9.48100×10^{-13}	2265.38	1.13940×10^{-11}	5.27020×10^{-13}
2239.90	2.06500×10^{-11}	9.33200×10^{-13}	2266.03	1.12310×10^{-11}	5.19980×10^{-13}
2240.55	2.03200×10^{-11}	9.18600×10^{-13}	2266.68	1.10700×10^{-11}	5.13070×10^{-13}
2241.21	1.99970×10^{-11}	9.04290×10^{-13}	2267.34	1.09130×10^{-11}	5.06280×10^{-13}
2241.86	1.96800×10^{-11}	8.90260×10^{-13}	2267.99	1.07580×10^{-11}	4.99610×10^{-13}
2242.51	1.93690×10^{-11}	8.76500×10^{-13}	2268.64	1.06050×10^{-11}	4.93060×10^{-13}
2243.17	1.90640×10^{-11}	8.63010×10^{-13}	2269.30	1.04560×10^{-11}	4.86630×10^{-13}
2243.82	1.87650×10^{-11}	8.49770×10^{-13}	2269.95	1.03090×10^{-11}	4.80320×10^{-13}
2244.47	1.84710×10^{-11}	8.36790×10^{-13}	2270.60	1.01640×10^{-11}	4.74120×10^{-13}
2245.13	1.81820×10^{-11}	8.24060×10^{-13}	2271.26	1.00220×10^{-11}	4.68030×10^{-13}
2245.78	1.78990×10^{-11}	8.11560×10^{-13}	2271.91	9.88210×10^{-12}	4.62040×10^{-13}
2246.43	1.76220×10^{-11}	7.99300×10^{-13}	2272.56	9.74470×10^{-12}	4.56170×10^{-13}
2247.08	1.73490×10^{-11}	7.87260×10^{-13}	2273.22	9.60960×10^{-12}	4.50390×10^{-13}
2247.74	1.70810×10^{-11}	7.75450×10^{-13}	2273.87	9.47680×10^{-12}	4.44720×10^{-13}
2248.39	1.68180×10^{-11}	7.63860×10^{-13}	2274.52	9.34620×10^{-12}	4.39150×10^{-13}
2249.04	1.65590×10^{-11}	7.52490×10^{-13}	2275.18	9.21780×10^{-12}	4.33680×10^{-13}
2249.70	1.63060×10^{-11}	7.41320×10^{-13}	2275.83	9.09160×10^{-12}	4.28310×10^{-13}

Table A.34 (cont'd)

JD +2450000	*UVOIR* Flux	Flux error	JD +2450000	*UVOIR* Flux	Flux error
2276.48	8.96750×10^{-12}	4.23030×10^{-13}	2288.24	7.05280×10^{-12}	3.42190×10^{-13}
2277.14	8.84540×10^{-12}	4.17840×10^{-13}	2288.90	6.96210×10^{-12}	3.38390×10^{-13}
2277.79	8.72540×10^{-12}	4.12740×10^{-13}	2289.55	6.87280×10^{-12}	3.34660×10^{-13}
2278.44	8.60740×10^{-12}	4.07740×10^{-13}	2290.20	6.78500×10^{-12}	3.30980×10^{-13}
2279.09	8.49130×10^{-12}	4.02810×10^{-13}	2290.85	6.69860×10^{-12}	3.27370×10^{-13}
2279.75	8.37720×10^{-12}	3.97980×10^{-13}	2291.51	6.61360×10^{-12}	3.23820×10^{-13}
2280.40	8.26490×10^{-12}	3.93230×10^{-13}	2292.16	6.52990×10^{-12}	3.20320×10^{-13}
2281.05	8.15450×10^{-12}	3.88560×10^{-13}	2292.81	6.44750×10^{-12}	3.16890×10^{-13}
2281.71	8.04590×10^{-12}	3.83970×10^{-13}	2293.47	6.36650×10^{-12}	3.13510×10^{-13}
2282.36	7.93910×10^{-12}	3.79460×10^{-13}	2294.12	6.28670×10^{-12}	3.10180×10^{-13}
2283.01	7.83400×10^{-12}	3.75030×10^{-13}	2294.77	6.20820×10^{-12}	3.06910×10^{-13}
2283.67	7.73070×10^{-12}	3.70680×10^{-13}	2295.43	6.13090×10^{-12}	3.03690×10^{-13}
2284.32	7.62900×10^{-12}	3.66400×10^{-13}	2296.08	6.05480×10^{-12}	3.00520×10^{-13}
2284.98	7.52900×10^{-12}	3.62190×10^{-13}	2296.73	5.97990×10^{-12}	2.97410×10^{-13}
2285.63	7.43060×10^{-12}	3.58050×10^{-13}	2297.39	5.90620×10^{-12}	2.94340×10^{-13}
2286.28	7.33380×10^{-12}	3.53990×10^{-13}	2298.04	5.83360×10^{-12}	2.91320×10^{-13}
2286.94	7.23860×10^{-12}	3.49990×10^{-13}	2298.69	5.76220×10^{-12}	2.88360×10^{-13}
2287.59	7.14490×10^{-12}	3.46060×10^{-13}	2299.35	5.69190×10^{-12}	2.85430×10^{-13}

Table A.35. SN 2002bo

JD +2452000	*UVOIR* Flux	Flux error	JD +2452000	*UVOIR* Flux	Flux error
345.025	2.62530×10^{-11}	1.27210×10^{-12}	371.156	7.95640×10^{-11}	3.61040×10^{-12}
345.678	3.58040×10^{-11}	1.67850×10^{-12}	371.809	7.58460×10^{-11}	3.44270×10^{-12}
346.332	4.85470×10^{-11}	2.17640×10^{-12}	372.462	7.24270×10^{-11}	3.28930×10^{-12}
346.985	6.28220×10^{-11}	2.76430×10^{-12}	373.116	6.93080×10^{-11}	3.15020×10^{-12}
347.638	7.70250×10^{-11}	3.37940×10^{-12}	373.769	6.64830×10^{-11}	3.02520×10^{-12}
348.291	9.04990×10^{-11}	3.97670×10^{-12}	374.422	6.39460×10^{-11}	2.91410×10^{-12}
348.945	1.03110×10^{-10}	4.54170×10^{-12}	375.075	6.16830×10^{-11}	2.81630×10^{-12}
349.598	1.14880×10^{-10}	5.07230×10^{-12}	375.729	5.96780×10^{-11}	2.73100×10^{-12}
350.251	1.25810×10^{-10}	5.56810×10^{-12}	376.382	5.79080×10^{-11}	2.65700×10^{-12}
350.905	1.35870×10^{-10}	6.02740×10^{-12}	377.035	5.63490×10^{-11}	2.59290×10^{-12}
351.558	1.45010×10^{-10}	6.44710×10^{-12}	377.688	5.49670×10^{-11}	2.53710×10^{-12}
352.211	1.53160×10^{-10}	6.82390×10^{-12}	378.342	5.37290×10^{-11}	2.48760×10^{-12}
352.864	1.60270×10^{-10}	7.15450×10^{-12}	378.995	5.25930×10^{-11}	2.44240×10^{-12}
353.518	1.66280×10^{-10}	7.43630×10^{-12}	379.648	5.15210×10^{-11}	2.39920×10^{-12}
354.171	1.71170×10^{-10}	7.66740×10^{-12}	380.302	5.04690×10^{-11}	2.35600×10^{-12}
354.824	1.74910×10^{-10}	7.84710×10^{-12}	380.955	4.94000×10^{-11}	2.31080×10^{-12}
355.477	1.77520×10^{-10}	7.97530×10^{-12}	381.608	4.82820×10^{-11}	2.26200×10^{-12}
356.131	1.79020×10^{-10}	8.05310×10^{-12}	382.261	4.70880×10^{-11}	2.20840×10^{-12}
356.784	1.79450×10^{-10}	8.08220×10^{-12}	382.915	4.58040×10^{-11}	2.14930×10^{-12}
357.437	1.78860×10^{-10}	8.06530×10^{-12}	383.568	4.44270×10^{-11}	2.08480×10^{-12}
358.090	1.77350×10^{-10}	8.00540×10^{-12}	384.221	4.29620×10^{-11}	2.01530×10^{-12}
358.744	1.74970×10^{-10}	7.90630×10^{-12}	384.874	4.14260×10^{-11}	1.94190×10^{-12}
359.397	1.71840×10^{-10}	7.77180×10^{-12}	385.528	3.98440×10^{-11}	1.86570×10^{-12}
360.050	1.68040×10^{-10}	7.60630×10^{-12}	386.181	3.82440×10^{-11}	1.78830×10^{-12}
360.704	1.63660×10^{-10}	7.41400×10^{-12}	386.834	3.66530×10^{-11}	1.71130×10^{-12}
361.357	1.58820×10^{-10}	7.19940×10^{-12}	387.487	3.51000×10^{-11}	1.63590×10^{-12}
362.010	1.53590×10^{-10}	6.96660×10^{-12}	388.141	3.36080×10^{-11}	1.56350×10^{-12}
362.663	1.48080×10^{-10}	6.71970×10^{-12}	388.794	3.21950×10^{-11}	1.49490×10^{-12}
363.317	1.42370×10^{-10}	6.46280×10^{-12}	389.447	3.08740×10^{-11}	1.43090×10^{-12}
363.970	1.36530×10^{-10}	6.19950×10^{-12}	390.100	2.96520×10^{-11}	1.37170×10^{-12}
364.623	1.30650×10^{-10}	5.93310×10^{-12}	390.754	2.85320×10^{-11}	1.31750×10^{-12}
365.276	1.24770×10^{-10}	5.66670×10^{-12}	391.407	2.75120×10^{-11}	1.26820×10^{-12}
365.930	1.18970×10^{-10}	5.40290×10^{-12}	392.060	2.65870×10^{-11}	1.22360×10^{-12}
366.583	1.13290×10^{-10}	5.14420×10^{-12}	392.714	2.57520×10^{-11}	1.18330×10^{-12}
367.236	1.07760×10^{-10}	4.89260×10^{-12}	393.367	2.49970×10^{-11}	1.14690×10^{-12}
367.889	1.02430×10^{-10}	4.64980×10^{-12}	394.020	2.43150×10^{-11}	1.11400×10^{-12}
368.543	9.73300×10^{-11}	4.41740×10^{-12}	394.673	2.36980×10^{-11}	1.08430×10^{-12}
369.196	9.24750×10^{-11}	4.19630×10^{-12}	395.327	2.31370×10^{-11}	1.05720×10^{-12}
369.849	8.78870×10^{-11}	3.98770×10^{-12}	395.980	2.26240×10^{-11}	1.03240×10^{-12}
370.503	8.35800×10^{-11}	3.79220×10^{-12}	396.633	2.21530×10^{-11}	1.00960×10^{-12}

Table A.35 (cont'd)

JD +2452000	*UVOIR* Flux	Flux error	JD +2452000	*UVOIR* Flux	Flux error
397.286	2.17180×10^{-11}	9.88460×10^{-13}	423.417	1.24370×10^{-11}	5.42140×10^{-13}
397.940	2.13130×10^{-11}	9.68780×10^{-13}	424.070	1.22840×10^{-11}	5.35180×10^{-13}
398.593	2.09340×10^{-11}	9.50330×10^{-13}	424.724	1.21340×10^{-11}	5.28350×10^{-13}
399.246	2.05770×10^{-11}	9.32910×10^{-13}	425.377	1.19860×10^{-11}	5.21650×10^{-13}
399.900	2.02390×10^{-11}	9.16370×10^{-13}	426.030	1.18400×10^{-11}	5.15080×10^{-13}
400.553	1.99160×10^{-11}	9.00580×10^{-13}	426.683	1.16970×10^{-11}	5.08640×10^{-13}
401.206	1.96070×10^{-11}	8.85450×10^{-13}	427.337	1.15560×10^{-11}	5.02310×10^{-13}
401.859	1.93090×10^{-11}	8.70870×10^{-13}	427.990	1.14170×10^{-11}	4.96110×10^{-13}
402.513	1.90210×10^{-11}	8.56800×10^{-13}	428.643	1.12810×10^{-11}	4.90030×10^{-13}
403.166	1.87430×10^{-11}	8.43160×10^{-13}	429.296	1.11470×10^{-11}	4.84070×10^{-13}
403.819	1.84720×10^{-11}	8.29920×10^{-13}	429.950	1.10150×10^{-11}	4.78220×10^{-13}
404.472	1.82090×10^{-11}	8.17040×10^{-13}	430.603	1.08850×10^{-11}	4.72480×10^{-13}
405.126	1.79520×10^{-11}	8.04490×10^{-13}	431.256	1.07570×10^{-11}	4.66850×10^{-13}
405.779	1.77010×10^{-11}	7.92240×10^{-13}	431.910	1.06310×10^{-11}	4.61330×10^{-13}
406.432	1.74560×10^{-11}	7.80280×10^{-13}	432.563	1.05070×10^{-11}	4.55920×10^{-13}
407.085	1.72160×10^{-11}	7.68600×10^{-13}	433.216	1.03850×10^{-11}	4.50610×10^{-13}
407.739	1.69810×10^{-11}	7.57170×10^{-13}	433.869	1.02650×10^{-11}	4.45410×10^{-13}
408.392	1.67510×10^{-11}	7.45990×10^{-13}	434.523	1.01470×10^{-11}	4.40300×10^{-13}
409.045	1.65250×10^{-11}	7.35050×10^{-13}	435.176	1.00310×10^{-11}	4.35290×10^{-13}
409.698	1.63040×10^{-11}	7.24330×10^{-13}	435.829	9.91730×10^{-12}	4.30380×10^{-13}
410.352	1.60860×10^{-11}	7.13830×10^{-13}	436.482	9.80500×10^{-12}	4.25560×10^{-13}
411.005	1.58730×10^{-11}	7.03550×10^{-13}	437.136	9.69450×10^{-12}	4.20840×10^{-13}
411.658	1.56630×10^{-11}	6.93470×10^{-13}	437.789	9.58570×10^{-12}	4.16210×10^{-13}
412.312	1.54570×10^{-11}	6.83590×10^{-13}	438.442	9.47870×10^{-12}	4.11660×10^{-13}
412.965	1.52540×10^{-11}	6.73910×10^{-13}	439.095	9.37350×10^{-12}	4.07210×10^{-13}
413.618	1.50550×10^{-11}	6.64420×10^{-13}	439.749	9.26990×10^{-12}	4.02840×10^{-13}
414.271	1.48600×10^{-11}	6.55120×10^{-13}	440.402	9.16800×10^{-12}	3.98550×10^{-13}
414.925	1.46680×10^{-11}	6.45990×10^{-13}	441.055	9.06770×10^{-12}	3.94350×10^{-13}
415.578	1.44790×10^{-11}	6.37040×10^{-13}	441.709	8.96900×10^{-12}	3.90230×10^{-13}
416.231	1.42930×10^{-11}	6.28270×10^{-13}	442.362	8.87190×10^{-12}	3.86180×10^{-13}
416.884	1.41100×10^{-11}	6.19660×10^{-13}	443.015	8.77640×10^{-12}	3.82220×10^{-13}
417.538	1.39300×10^{-11}	6.11220×10^{-13}	443.668	8.68230×10^{-12}	3.78330×10^{-13}
418.191	1.37530×10^{-11}	6.02940×10^{-13}	444.322	8.58980×10^{-12}	3.74510×10^{-13}
418.844	1.35790×10^{-11}	5.94810×10^{-13}	444.975	8.49880×10^{-12}	3.70770×10^{-13}
419.497	1.34080×10^{-11}	5.86850×10^{-13}	445.628	8.40920×10^{-12}	3.67100×10^{-13}
420.151	1.32390×10^{-11}	5.79030×10^{-13}	446.281	8.32100×10^{-12}	3.63500×10^{-13}
420.804	1.30730×10^{-11}	5.71370×10^{-13}	446.935	8.23420×10^{-12}	3.59970×10^{-13}
421.457	1.29100×10^{-11}	5.63850×10^{-13}	447.588	8.14890×10^{-12}	3.56510×10^{-13}
422.111	1.27500×10^{-11}	5.56470×10^{-13}	448.241	8.06480×10^{-12}	3.53110×10^{-13}
422.764	1.25920×10^{-11}	5.49240×10^{-13}	448.894	7.98210×10^{-12}	3.49770×10^{-13}

Table A.35 (cont'd)

JD +2452000	*UVOIR* Flux	Flux error	JD +2452000	*UVOIR* Flux	Flux error
449.548	7.90070×10^{-12}	3.46500×10^{-13}	455.427	7.22330×10^{-12}	3.19710×10^{-13}
450.201	7.82060×10^{-12}	3.43290×10^{-13}	456.080	7.15370×10^{-12}	3.17000×10^{-13}
450.854	7.74170×10^{-12}	3.40150×10^{-13}	456.734	7.08530×10^{-12}	3.14350×10^{-13}
451.508	7.66410×10^{-12}	3.37060×10^{-13}	457.387	7.01790×10^{-12}	3.11740×10^{-13}
452.161	7.58770×10^{-12}	3.34030×10^{-13}	458.040	6.95160×10^{-12}	3.09180×10^{-13}
452.814	7.51250×10^{-12}	3.31050×10^{-13}	458.693	6.88630×10^{-12}	3.06670×10^{-13}
453.467	7.43850×10^{-12}	3.28140×10^{-13}	459.347	6.82190×10^{-12}	3.04200×10^{-13}
454.121	7.36560×10^{-12}	3.25270×10^{-13}	460.000	6.75860×10^{-12}	3.01780×10^{-13}
454.774	7.29390×10^{-12}	3.22460×10^{-13}	...	...	...

Table A.36. SN 2002cx

JD +2450000	*UVOIR* Flux	Flux error	JD +2450000	*UVOIR* Flux	Flux error
2410.02	9.69327×10^{-13}	5.28631×10^{-14}	2436.16	6.88683×10^{-13}	3.40906×10^{-14}
2410.68	1.11700×10^{-12}	5.90365×10^{-14}	2436.81	6.65658×10^{-13}	3.30298×10^{-14}
2411.33	1.30683×10^{-12}	6.59800×10^{-14}	2437.46	6.45396×10^{-13}	3.20881×10^{-14}
2411.99	1.49594×10^{-12}	7.35150×10^{-14}	2438.11	6.26942×10^{-13}	3.12270×10^{-14}
2412.64	1.64890×10^{-12}	8.03214×10^{-14}	2438.77	6.09874×10^{-13}	3.04265×10^{-14}
2413.29	1.75727×10^{-12}	8.54857×10^{-14}	2439.42	5.94019×10^{-13}	2.96817×10^{-14}
2413.95	1.82706×10^{-12}	8.89049×10^{-14}	2440.07	5.79279×10^{-13}	2.89880×10^{-14}
2414.60	1.86682×10^{-12}	9.08466×10^{-14}	2440.73	5.65616×10^{-13}	2.83427×10^{-14}
2415.25	1.88444×10^{-12}	9.16343×10^{-14}	2441.38	5.52961×10^{-13}	2.77437×10^{-14}
2415.91	1.88530×10^{-12}	9.15353×10^{-14}	2442.03	5.41268×10^{-13}	2.71885×10^{-14}
2416.56	1.87359×10^{-12}	9.07554×10^{-14}	2442.69	5.30486×10^{-13}	2.66752×10^{-14}
2417.21	1.85201×10^{-12}	8.94519×10^{-14}	2443.34	5.20597×10^{-13}	2.62007×10^{-14}
2417.86	1.82256×10^{-12}	8.77476×10^{-14}	2444.00	5.11552×10^{-13}	2.57642×10^{-14}
2418.52	1.78702×10^{-12}	8.57396×10^{-14}	2444.65	5.03347×10^{-13}	2.53639×10^{-14}
2419.17	1.74660×10^{-12}	8.35098×10^{-14}	2445.30	4.95921×10^{-13}	2.49971×10^{-14}
2419.82	1.70240×10^{-12}	8.11272×10^{-14}	2445.96	4.89260×10^{-13}	2.46632×10^{-14}
2420.48	1.65540×10^{-12}	7.86468×10^{-14}	2446.61	4.83283×10^{-13}	2.43587×10^{-14}
2421.13	1.60621×10^{-12}	7.61158×10^{-14}	2447.26	4.77897×10^{-13}	2.40789×10^{-14}
2421.78	1.55560×10^{-12}	7.35716×10^{-14}	2447.92	4.72990×10^{-13}	2.38192×10^{-14}
2422.44	1.50430×10^{-12}	7.10437×10^{-14}	2448.57	4.68403×10^{-13}	2.35749×10^{-14}
2423.09	1.45255×10^{-12}	6.85539×10^{-14}	2449.22	4.63960×10^{-13}	2.33372×10^{-14}
2423.74	1.40095×10^{-12}	6.61173×10^{-14}	2449.87	4.59486×10^{-13}	2.30995×10^{-14}
2424.40	1.34998×10^{-12}	6.37476×10^{-14}	2450.53	4.54825×10^{-13}	2.28552×10^{-14}
2425.05	1.29972×10^{-12}	6.14499×10^{-14}	2451.18	4.49856×10^{-13}	2.25987×10^{-14}
2425.70	1.25047×10^{-12}	5.92278×10^{-14}	2451.83	4.44500×10^{-13}	2.23277×10^{-14}
2426.36	1.20255×10^{-12}	5.70850×10^{-14}	2452.49	4.38792×10^{-13}	2.20413×10^{-14}
2427.01	1.15598×10^{-12}	5.50193×10^{-14}	2453.14	4.32775×10^{-13}	2.17438×10^{-14}
2427.66	1.11105×10^{-12}	5.30331×10^{-14}	2453.79	4.26581×10^{-13}	2.14375×10^{-14}
2428.32	1.06772×10^{-12}	5.11233×10^{-14}	2454.45	4.20323×10^{-13}	2.11300×10^{-14}
2428.97	1.02614×10^{-12}	4.92901×10^{-14}	2455.10	4.14122×10^{-13}	2.08228×10^{-14}
2429.62	9.86408×10^{-13}	4.75353×10^{-14}	2455.75	4.08092×10^{-13}	2.05224×10^{-14}
2430.28	9.48742×10^{-13}	4.58646×10^{-14}	2456.41	4.02292×10^{-13}	2.02280×10^{-14}
2430.93	9.13804×10^{-13}	4.43045×10^{-14}	2457.06	3.96746×10^{-13}	1.99431×10^{-14}
2431.58	8.82747×10^{-13}	4.29019×10^{-14}	2457.71	3.91470×10^{-13}	1.96657×10^{-14}
2432.24	8.56392×10^{-13}	4.16978×10^{-14}	2458.37	3.86445×10^{-13}	1.93959×10^{-14}
2432.89	8.33264×10^{-13}	4.06432×10^{-14}	2459.02	3.81632×10^{-13}	1.91329×10^{-14}
2433.54	8.08919×10^{-13}	3.95450×10^{-14}	2459.67	3.76991×10^{-13}	1.88746×10^{-14}
2434.20	7.79656×10^{-13}	3.82240×10^{-14}	2460.33	3.72502×10^{-13}	1.86213×10^{-14}
2434.85	7.47010×10^{-13}	3.67451×10^{-14}	2460.98	3.68115×10^{-13}	1.83708×10^{-14}
2435.50	7.15747×10^{-13}	3.53256×10^{-14}	2461.63	3.63809×10^{-13}	1.81223×10^{-14}

Table A.36 (cont'd)

JD +2450000	*UVOIR* Flux	Flux error	JD +2450000	*UVOIR* Flux	Flux error
2462.29	3.59566×10^{-13}	1.78758×10^{-14}	2488.42	2.26274×10^{-13}	1.06272×10^{-14}
2462.94	3.55377×10^{-13}	1.76314×10^{-14}	2489.07	2.23985×10^{-13}	1.05198×10^{-14}
2463.59	3.51221×10^{-13}	1.73893×10^{-14}	2489.72	2.21742×10^{-13}	1.04151×10^{-14}
2464.25	3.47111×10^{-13}	1.71484×10^{-14}	2490.38	2.19545×10^{-13}	1.03131×10^{-14}
2464.90	3.43027×10^{-13}	1.69088×10^{-14}	2491.03	2.17394×10^{-13}	1.02135×10^{-14}
2465.55	3.38980×10^{-13}	1.66716×10^{-14}	2491.68	2.15289×10^{-13}	1.01164×10^{-14}
2466.21	3.34959×10^{-13}	1.64368×10^{-14}	2492.34	2.13229×10^{-13}	1.00216×10^{-14}
2466.86	3.30977×10^{-13}	1.62045×10^{-14}	2492.99	2.11204×10^{-13}	9.92903×10^{-15}
2467.51	3.27033×10^{-13}	1.59746×10^{-14}	2493.64	2.09223×10^{-13}	9.83854×10^{-15}
2468.17	3.23126×10^{-13}	1.57483×10^{-14}	2494.30	2.07276×10^{-13}	9.75006×10^{-15}
2468.82	3.19258×10^{-13}	1.55254×10^{-14}	2494.95	2.05373×10^{-13}	9.66344×10^{-15}
2469.47	3.15437×10^{-13}	1.53050×10^{-14}	2495.60	2.03491×10^{-13}	9.57856×10^{-15}
2470.13	3.11652×10^{-13}	1.50880×10^{-14}	2496.26	2.01653×10^{-13}	9.49539×10^{-15}
2470.78	3.07915×10^{-13}	1.48755×10^{-14}	2496.91	1.99845×10^{-13}	9.41379×10^{-15}
2471.43	3.04212×10^{-13}	1.46664×10^{-14}	2497.56	1.98059×10^{-13}	9.33364×10^{-15}
2472.08	3.00565×10^{-13}	1.44606×10^{-14}	2498.22	1.96313×10^{-13}	9.25482×10^{-15}
2472.74	2.96973×10^{-13}	1.42592×10^{-14}	2498.87	1.94587×10^{-13}	9.17740×10^{-15}
2473.39	2.93424×10^{-13}	1.40622×10^{-14}	2499.52	1.92892×10^{-13}	9.10118×10^{-15}
2474.04	2.89918×10^{-13}	1.38694×10^{-14}	2500.18	1.91215×10^{-13}	9.02612×10^{-15}
2474.70	2.86475×10^{-13}	1.36799×10^{-14}	2500.83	1.89557×10^{-13}	8.95225×10^{-15}
2475.35	2.83074×10^{-13}	1.34956×10^{-14}	2501.48	1.87930×10^{-13}	8.87944×10^{-15}
2476.00	2.79724×10^{-13}	1.33145×10^{-14}	2502.14	1.86322×10^{-13}	8.80762×10^{-15}
2476.66	2.76437×10^{-13}	1.31387×10^{-14}	2502.79	1.84744×10^{-13}	8.73679×10^{-15}
2477.31	2.73200×10^{-13}	1.29660×10^{-14}	2503.44	1.83176×10^{-13}	8.66698×10^{-15}
2477.97	2.70003×10^{-13}	1.27986×10^{-14}	2504.09	1.81640×10^{-13}	8.59811×10^{-15}
2478.62	2.66867×10^{-13}	1.26342×10^{-14}	2504.75	1.80115×10^{-13}	8.53030×10^{-15}
2479.27	2.63793×10^{-13}	1.24741×10^{-14}	2505.40	1.78622×10^{-13}	8.46340×10^{-15}
2479.93	2.60759×10^{-13}	1.23192×10^{-14}	2506.05	1.77142×10^{-13}	8.39742×10^{-15}
2480.58	2.57787×10^{-13}	1.21674×10^{-14}	2506.71	1.75686×10^{-13}	8.33240×10^{-15}
2481.23	2.54866×10^{-13}	1.20187×10^{-14}	2507.36	1.74254×10^{-13}	8.26837×10^{-15}
2481.89	2.52007×10^{-13}	1.18754×10^{-14}	2508.01	1.72835×10^{-13}	8.20525×10^{-15}
2482.54	2.49191×10^{-13}	1.17341×10^{-14}	2508.67	1.71443×10^{-13}	8.14317×10^{-15}
2483.19	2.46437×10^{-13}	1.15982×10^{-14}	2509.32	1.70075×10^{-13}	8.08190×10^{-15}
2483.84	2.43726×10^{-13}	1.14644×10^{-14}	2509.98	1.68722×10^{-13}	8.02156×10^{-15}
2484.50	2.41080×10^{-13}	1.13350×10^{-14}	2510.63	1.67393×10^{-13}	7.96212×10^{-15}
2485.15	2.38488×10^{-13}	1.12099×10^{-14}	2511.28	1.66078×10^{-13}	7.90345×10^{-15}
2485.80	2.35940×10^{-13}	1.10870×10^{-14}	2511.94	1.64775×10^{-13}	7.84548×10^{-15}
2486.46	2.33448×10^{-13}	1.09674×10^{-14}	2512.59	1.63493×10^{-13}	7.78816×10^{-15}
2487.11	2.31011×10^{-13}	1.08509×10^{-14}	2513.24	1.62221×10^{-13}	7.73141×10^{-15}
2487.76	2.28620×10^{-13}	1.07375×10^{-14}	2513.90	1.60966×10^{-13}	7.67503×10^{-15}

Table A.36 (cont'd)

JD +2450000	*UVOIR* Flux	Flux error	JD +2450000	*UVOIR* Flux	Flux error
2514.55	1.59707×10^{-13}	7.61906×10^{-15}	2517.16	1.54768×10^{-13}	7.39770×10^{-15}
2515.20	1.58463×10^{-13}	7.56333×10^{-15}	2517.81	1.53559×10^{-13}	7.34322×10^{-15}
2515.85	1.57234×10^{-13}	7.50792×10^{-15}	2518.47	1.52367×10^{-13}	7.28960×10^{-15}
2516.51	1.55998×10^{-13}	7.45260×10^{-15}	2519.77	1.50080×10^{-13}	7.18737×10^{-15}

Table A.37. SN 2002er

JD +2400000	*UVOIR* Flux	Flux error	JD +2400000	*UVOIR* Flux	Flux error
52515.6	3.50460×10^{-11}	1.57850×10^{-12}	52538.7	2.84980×10^{-11}	1.26310×10^{-12}
52516.2	3.94610×10^{-11}	1.76410×10^{-12}	52539.3	2.73060×10^{-11}	1.21020×10^{-12}
52516.7	4.37720×10^{-11}	1.95000×10^{-12}	52539.8	2.62130×10^{-11}	1.16200×10^{-12}
52517.3	4.79200×10^{-11}	2.13260×10^{-12}	52540.4	2.52150×10^{-11}	1.11810×10^{-12}
52517.9	5.18620×10^{-11}	2.30910×10^{-12}	52541.0	2.43080×10^{-11}	1.07850×10^{-12}
52518.5	5.55700×10^{-11}	2.47720×10^{-12}	52541.6	2.34850×10^{-11}	1.04300×10^{-12}
52519.0	5.90170×10^{-11}	2.63500×10^{-12}	52542.2	2.27420×10^{-11}	1.01110×10^{-12}
52519.6	6.21810×10^{-11}	2.78070×10^{-12}	52542.7	2.20720×10^{-11}	9.82730×10^{-13}
52520.2	6.50410×10^{-11}	2.91280×10^{-12}	52543.3	2.14690×10^{-11}	9.57450×10^{-13}
52520.8	6.75770×10^{-11}	3.02990×10^{-12}	52543.9	2.09240×10^{-11}	9.34880×10^{-13}
52521.4	6.97670×10^{-11}	3.13070×10^{-12}	52544.5	2.04300×10^{-11}	9.14590×10^{-13}
52521.9	7.15950×10^{-11}	3.21410×10^{-12}	52545.1	1.99770×10^{-11}	8.96080×10^{-13}
52522.5	7.30450×10^{-11}	3.27940×10^{-12}	52545.6	1.95540×10^{-11}	8.78850×10^{-13}
52523.1	7.41060×10^{-11}	3.32580×10^{-12}	52546.2	1.91520×10^{-11}	8.62380×10^{-13}
52523.7	7.47700×10^{-11}	3.35340×10^{-12}	52546.8	1.87600×10^{-11}	8.46130×10^{-13}
52524.2	7.50350×10^{-11}	3.36210×10^{-12}	52547.4	1.83680×10^{-11}	8.29630×10^{-13}
52524.8	7.49030×10^{-11}	3.35240×10^{-12}	52547.9	1.79680×10^{-11}	8.12450×10^{-13}
52525.4	7.43840×10^{-11}	3.32510×10^{-12}	52548.5	1.75530×10^{-11}	7.94290×10^{-13}
52526.0	7.34920×10^{-11}	3.28120×10^{-12}	52549.1	1.71180×10^{-11}	7.74910×10^{-13}
52526.6	7.22510×10^{-11}	3.22190×10^{-12}	52549.7	1.66600×10^{-11}	7.54240×10^{-13}
52527.1	7.06900×10^{-11}	3.14870×10^{-12}	52550.2	1.61800×10^{-11}	7.32320×10^{-13}
52527.7	6.88440×10^{-11}	3.06350×10^{-12}	52550.8	1.56810×10^{-11}	7.09300×10^{-13}
52528.3	6.67540×10^{-11}	2.96820×10^{-12}	52551.4	1.51660×10^{-11}	6.85430×10^{-13}
52528.9	6.44680×10^{-11}	2.86470×10^{-12}	52552.0	1.46420×10^{-11}	6.61010×10^{-13}
52529.4	6.20310×10^{-11}	2.75510×10^{-12}	52552.6	1.41160×10^{-11}	6.36380×10^{-13}
52530.0	5.94930×10^{-11}	2.64160×10^{-12}	52553.1	1.35930×10^{-11}	6.11890×10^{-13}
52530.6	5.69000×10^{-11}	2.52600×10^{-12}	52553.7	1.30800×10^{-11}	5.87850×10^{-13}
52531.2	5.42920×10^{-11}	2.41010×10^{-12}	52554.3	1.25830×10^{-11}	5.64530×10^{-13}
52531.8	5.17090×10^{-11}	2.29540×10^{-12}	52554.9	1.21070×10^{-11}	5.42170×10^{-13}
52532.3	4.91790×10^{-11}	2.18320×10^{-12}	52555.5	1.16540×10^{-11}	5.20940×10^{-13}
52532.9	4.67270×10^{-11}	2.07450×10^{-12}	52556.0	1.12270×10^{-11}	5.00950×10^{-13}
52533.5	4.43720×10^{-11}	1.97000×10^{-12}	52556.6	1.08270×10^{-11}	4.82270×10^{-13}
52534.1	4.21280×10^{-11}	1.87030×10^{-12}	52557.2	1.04540×10^{-11}	4.64900×10^{-13}
52534.6	4.00010×10^{-11}	1.77570×10^{-12}	52557.8	1.01080×10^{-11}	4.48830×10^{-13}
52535.2	3.79960×10^{-11}	1.68640×10^{-12}	52558.3	9.78880×10^{-12}	4.33990×10^{-13}
52535.8	3.61160×10^{-11}	1.60260×10^{-12}	52558.9	9.49350×10^{-12}	4.20320×10^{-13}
52536.4	3.43580×10^{-11}	1.52420×10^{-12}	52559.5	9.22120×10^{-12}	4.07730×10^{-13}
52537.0	3.27210×10^{-11}	1.45120×10^{-12}	52560.1	8.96990×10^{-12}	3.96120×10^{-13}
52537.5	3.12020×10^{-11}	1.38350×10^{-12}	52560.7	8.73780×10^{-12}	3.85390×10^{-13}
52538.1	2.97960×10^{-11}	1.32080×10^{-12}	52561.2	8.52300×10^{-12}	3.75460×10^{-13}

Table A.37 (cont'd)

JD +2400000	*UVOIR* Flux	Flux error	JD +2400000	*UVOIR* Flux	Flux error
52561.8	8.32390×10^{-12}	3.66240×10^{-13}	52584.9	4.62310×10^{-12}	1.92760×10^{-13}
52562.4	8.13880×10^{-12}	3.57640×10^{-13}	52585.5	4.56840×10^{-12}	1.90370×10^{-13}
52563.0	7.96610×10^{-12}	3.49600×10^{-13}	52586.1	4.51460×10^{-12}	1.88040×10^{-13}
52563.5	7.80460×10^{-12}	3.42050×10^{-13}	52586.7	4.46160×10^{-12}	1.85750×10^{-13}
52564.1	7.65290×10^{-12}	3.34930×10^{-13}	52587.2	4.40950×10^{-12}	1.83510×10^{-13}
52564.7	7.50990×10^{-12}	3.28190×10^{-13}	52587.8	4.35830×10^{-12}	1.81320×10^{-13}
52565.3	7.37460×10^{-12}	3.21800×10^{-13}	52588.4	4.30790×10^{-12}	1.79170×10^{-13}
52565.9	7.24630×10^{-12}	3.15710×10^{-13}	52589.0	4.25830×10^{-12}	1.77070×10^{-13}
52566.4	7.12400×10^{-12}	3.09880×10^{-13}	52589.5	4.20940×10^{-12}	1.75010×10^{-13}
52567.0	7.00710×10^{-12}	3.04300×10^{-13}	52590.1	4.16140×10^{-12}	1.73000×10^{-13}
52567.6	6.89500×10^{-12}	2.98940×10^{-13}	52590.7	4.11410×10^{-12}	1.71030×10^{-13}
52568.2	6.78730×10^{-12}	2.93770×10^{-13}	52591.3	4.06750×10^{-12}	1.69090×10^{-13}
52568.7	6.68350×10^{-12}	2.88790×10^{-13}	52591.9	4.02170×10^{-12}	1.67200×10^{-13}
52569.3	6.58320×10^{-12}	2.83970×10^{-13}	52592.4	3.97660×10^{-12}	1.65350×10^{-13}
52569.9	6.48610×10^{-12}	2.79310×10^{-13}	52593.0	3.93220×10^{-12}	1.63530×10^{-13}
52570.5	6.39200×10^{-12}	2.74790×10^{-13}	52593.6	3.88840×10^{-12}	1.61750×10^{-13}
52571.1	6.30050×10^{-12}	2.70400×10^{-13}	52594.2	3.84530×10^{-12}	1.60000×10^{-13}
52571.6	6.21160×10^{-12}	2.66140×10^{-13}	52594.8	3.80290×10^{-12}	1.58290×10^{-13}
52572.2	6.12490×10^{-12}	2.61990×10^{-13}	52595.3	3.76110×10^{-12}	1.56620×10^{-13}
52572.8	6.04050×10^{-12}	2.57960×10^{-13}	52595.9	3.72000×10^{-12}	1.54970×10^{-13}
52573.4	5.95810×10^{-12}	2.54040×10^{-13}	52596.5	3.67950×10^{-12}	1.53360×10^{-13}
52573.9	5.87760×10^{-12}	2.50220×10^{-13}	52597.1	3.63960×10^{-12}	1.51790×10^{-13}
52574.5	5.79900×10^{-12}	2.46490×10^{-13}	52597.6	3.60020×10^{-12}	1.50240×10^{-13}
52575.1	5.72210×10^{-12}	2.42860×10^{-13}	52598.2	3.56150×10^{-12}	1.48720×10^{-13}
52575.7	5.64680×10^{-12}	2.39320×10^{-13}	52598.8	3.52340×10^{-12}	1.47230×10^{-13}
52576.3	5.57310×10^{-12}	2.35870×10^{-13}	52599.4	3.48580×10^{-12}	1.45770×10^{-13}
52576.8	5.50100×10^{-12}	2.32500×10^{-13}	52599.9	3.44880×10^{-12}	1.44340×10^{-13}
52577.4	5.43030×10^{-12}	2.29210×10^{-13}	52600.5	3.41230×10^{-12}	1.42940×10^{-13}
52578.0	5.36100×10^{-12}	2.26000×10^{-13}	52601.1	3.37630×10^{-12}	1.41560×10^{-13}
52578.6	5.29310×10^{-12}	2.22870×10^{-13}	52601.7	3.34090×10^{-12}	1.40210×10^{-13}
52579.1	5.22650×10^{-12}	2.19810×10^{-13}	52602.3	3.30600×10^{-12}	1.38890×10^{-13}
52579.7	5.16110×10^{-12}	2.16820×10^{-13}	52602.8	3.27160×10^{-12}	1.37590×10^{-13}
52580.3	5.09690×10^{-12}	2.13900×10^{-13}	52603.4	3.23780×10^{-12}	1.36310×10^{-13}
52580.9	5.03400×10^{-12}	2.11040×10^{-13}	52604.0	3.20440×10^{-12}	1.35060×10^{-13}
52581.5	4.97210×10^{-12}	2.08250×10^{-13}	52604.6	3.17150×10^{-12}	1.33840×10^{-13}
52582.0	4.91140×10^{-12}	2.05520×10^{-13}	52605.2	3.13910×10^{-12}	1.32630×10^{-13}
52582.6	4.85170×10^{-12}	2.02860×10^{-13}	52605.7	3.10710×10^{-12}	1.31450×10^{-13}
52583.2	4.79310×10^{-12}	2.00250×10^{-13}	52606.3	3.07560×10^{-12}	1.30290×10^{-13}
52583.8	4.73550×10^{-12}	1.97700×10^{-13}	52606.9	3.04460×10^{-12}	1.29150×10^{-13}
52584.3	4.67880×10^{-12}	1.95200×10^{-13}	52607.5	3.01400×10^{-12}	1.28030×10^{-13}

Table A.37 (cont'd)

JD +2400000	*UVOIR* Flux	Flux error	JD +2400000	*UVOIR* Flux	Flux error
52608.0	2.98390×10^{-12}	1.26940×10^{-13}	52619.0	2.48580×10^{-12}	1.09430×10^{-13}
52608.6	2.95410×10^{-12}	1.25860×10^{-13}	52619.6	2.46310×10^{-12}	1.08660×10^{-13}
52609.2	2.92490×10^{-12}	1.24800×10^{-13}	52620.2	2.44070×10^{-12}	1.07900×10^{-13}
52609.8	2.89600×10^{-12}	1.23760×10^{-13}	52620.8	2.41860×10^{-12}	1.07160×10^{-13}
52610.4	2.86750×10^{-12}	1.22740×10^{-13}	52621.3	2.39680×10^{-12}	1.06420×10^{-13}
52610.9	2.83950×10^{-12}	1.21740×10^{-13}	52621.9	2.37530×10^{-12}	1.05700×10^{-13}
52611.5	2.81180×10^{-12}	1.20760×10^{-13}	52622.5	2.35410×10^{-12}	1.04990×10^{-13}
52612.1	2.78460×10^{-12}	1.19790×10^{-13}	52623.1	2.33320×10^{-12}	1.04300×10^{-13}
52612.7	2.75770×10^{-12}	1.18840×10^{-13}	52623.6	2.31260×10^{-12}	1.03610×10^{-13}
52613.2	2.73120×10^{-12}	1.17910×10^{-13}	52624.2	2.29230×10^{-12}	1.02930×10^{-13}
52613.8	2.70510×10^{-12}	1.16990×10^{-13}	52624.8	2.27220×10^{-12}	1.02270×10^{-13}
52614.4	2.67930×10^{-12}	1.16090×10^{-13}	52625.4	2.25240×10^{-12}	1.01610×10^{-13}
52615.0	2.65390×10^{-12}	1.15210×10^{-13}	52626.0	2.23290×10^{-12}	1.00970×10^{-13}
52615.6	2.62890×10^{-12}	1.14340×10^{-13}	52626.5	2.21360×10^{-12}	1.00340×10^{-13}
52616.1	2.60420×10^{-12}	1.13490×10^{-13}	52627.1	2.19460×10^{-12}	9.97120×10^{-14}
52616.7	2.57980×10^{-12}	1.12650×10^{-13}	52627.7	2.17580×10^{-12}	9.90980×10^{-14}
52617.3	2.55580×10^{-12}	1.11820×10^{-13}	52628.3	2.15730×10^{-12}	9.84930×10^{-14}
52617.9	2.53220×10^{-12}	1.11010×10^{-13}	52628.8	2.13910×10^{-12}	9.78970×10^{-14}
52618.4	2.50880×10^{-12}	1.10210×10^{-13}	52629.4	2.12100×10^{-12}	9.73100×10^{-14}

Table A.38. SN 2003du

JD +2452000	*UVOIR* Flux	Flux error	JD +2452000	*UVOIR* Flux	Flux error
750.804	6.63920×10^{-12}	4.77120×10^{-13}	782.965	2.80940×10^{-11}	1.22550×10^{-12}
751.608	8.54730×10^{-12}	5.46620×10^{-13}	783.769	2.66110×10^{-11}	1.15880×10^{-12}
752.412	1.12540×10^{-11}	6.38160×10^{-13}	784.573	2.52740×10^{-11}	1.09950×10^{-12}
753.216	1.48480×10^{-11}	7.61290×10^{-13}	785.377	2.40730×10^{-11}	1.04700×10^{-12}
754.020	1.92380×10^{-11}	9.21240×10^{-13}	786.181	2.29970×10^{-11}	1.00100×10^{-12}
754.824	2.42110×10^{-11}	1.11440×10^{-12}	786.985	2.20320×10^{-11}	9.60630×10^{-13}
755.628	2.95200×10^{-11}	1.33060×10^{-12}	787.789	2.11640×10^{-11}	9.25360×10^{-13}
756.432	3.49470×10^{-11}	1.55810×10^{-12}	788.593	2.03800×10^{-11}	8.94370×10^{-13}
757.236	4.03180×10^{-11}	1.78720×10^{-12}	789.397	1.96650×10^{-11}	8.66840×10^{-13}
758.040	4.55010×10^{-11}	2.01080×10^{-12}	790.201	1.90050×10^{-11}	8.41920×10^{-13}
758.844	5.03980×10^{-11}	2.22370×10^{-12}	791.005	1.83860×10^{-11}	8.18790×10^{-13}
759.648	5.49310×10^{-11}	2.42210×10^{-12}	791.809	1.77980×10^{-11}	7.96650×10^{-13}
760.452	5.90390×10^{-11}	2.60340×10^{-12}	792.613	1.72290×10^{-11}	7.74830×10^{-13}
761.256	6.26730×10^{-11}	2.76500×10^{-12}	793.417	1.66710×10^{-11}	7.52820×10^{-13}
762.060	6.57940×10^{-11}	2.90530×10^{-12}	794.221	1.61180×10^{-11}	7.30260×10^{-13}
762.864	6.83730×10^{-11}	3.02270×10^{-12}	795.025	1.55680×10^{-11}	7.06990×10^{-13}
763.668	7.03930×10^{-11}	3.11620×10^{-12}	795.829	1.50190×10^{-11}	6.83010×10^{-13}
764.472	7.18450×10^{-11}	3.18510×10^{-12}	796.633	1.44740×10^{-11}	6.58490×10^{-13}
765.276	7.27330×10^{-11}	3.22940×10^{-12}	797.437	1.39340×10^{-11}	6.33690×10^{-13}
766.080	7.30680×10^{-11}	3.24910×10^{-12}	798.241	1.34030×10^{-11}	6.08910×10^{-13}
766.884	7.28730×10^{-11}	3.24490×10^{-12}	799.045	1.28860×10^{-11}	5.84480×10^{-13}
767.688	7.21760×10^{-11}	3.21810×10^{-12}	799.849	1.23860×10^{-11}	5.60710×10^{-13}
768.492	7.10180×10^{-11}	3.17000×10^{-12}	800.653	1.19060×10^{-11}	5.37820×10^{-13}
769.297	6.94420×10^{-11}	3.10250×10^{-12}	801.457	1.14480×10^{-11}	5.16010×10^{-13}
770.101	6.75010×10^{-11}	3.01790×10^{-12}	802.261	1.10150×10^{-11}	4.95400×10^{-13}
770.905	6.52500×10^{-11}	2.91860×10^{-12}	803.065	1.06060×10^{-11}	4.76030×10^{-13}
771.709	6.27500×10^{-11}	2.80730×10^{-12}	803.869	1.02220×10^{-11}	4.57930×10^{-13}
772.513	6.00600×10^{-11}	2.68670×10^{-12}	804.673	9.86300×10^{-12}	4.41070×10^{-13}
773.317	5.72400×10^{-11}	2.55950×10^{-12}	805.477	9.52700×10^{-12}	4.25380×10^{-13}
774.121	5.43460×10^{-11}	2.42830×10^{-12}	806.281	9.21300×10^{-12}	4.10800×10^{-13}
774.925	5.14310×10^{-11}	2.29560×10^{-12}	807.085	8.91940×10^{-12}	3.97240×10^{-13}
775.729	4.85420×10^{-11}	2.16360×10^{-12}	807.889	8.64460×10^{-12}	3.84610×10^{-13}
776.533	4.57180×10^{-11}	2.03430×10^{-12}	808.693	8.38700×10^{-12}	3.72820×10^{-13}
777.337	4.29930×10^{-11}	1.90920×10^{-12}	809.497	8.14490×10^{-12}	3.61790×10^{-13}
778.141	4.03930×10^{-11}	1.78960×10^{-12}	810.302	7.91680×10^{-12}	3.51440×10^{-13}
778.945	3.79360×10^{-11}	1.67650×10^{-12}	811.106	7.70130×10^{-12}	3.41690×10^{-13}
779.749	3.56370×10^{-11}	1.57060×10^{-12}	811.910	7.49720×10^{-12}	3.32490×10^{-13}
780.553	3.35010×10^{-11}	1.47240×10^{-12}	812.714	7.30340×10^{-12}	3.23780×10^{-13}
781.357	3.15340×10^{-11}	1.38220×10^{-12}	813.518	7.11880×10^{-12}	3.15500×10^{-13}
782.161	2.97330×10^{-11}	1.29990×10^{-12}	814.322	6.94260×10^{-12}	3.07620×10^{-13}

Table A.38 (cont'd)

JD +2452000	*UVOIR* Flux	Flux error	JD +2452000	*UVOIR* Flux	Flux error
815.126	6.77410×10^{-12}	3.00100×10^{-13}	847.286	3.08550×10^{-12}	1.36750×10^{-13}
815.930	6.61260×10^{-12}	2.92900×10^{-13}	848.090	3.03310×10^{-12}	1.34430×10^{-13}
816.734	6.45760×10^{-12}	2.86010×10^{-13}	848.894	2.98180×10^{-12}	1.32150×10^{-13}
817.538	6.30860×10^{-12}	2.79390×10^{-13}	849.698	2.93140×10^{-12}	1.29920×10^{-13}
818.342	6.16510×10^{-12}	2.73030×10^{-13}	850.503	2.88210×10^{-12}	1.27740×10^{-13}
819.146	6.02700×10^{-12}	2.66910×10^{-13}	851.307	2.83370×10^{-12}	1.25600×10^{-13}
819.950	5.89370×10^{-12}	2.61020×10^{-13}	852.111	2.78630×10^{-12}	1.23510×10^{-13}
820.754	5.76510×10^{-12}	2.55330×10^{-13}	852.915	2.73970×10^{-12}	1.21460×10^{-13}
821.558	5.64080×10^{-12}	2.49850×10^{-13}	853.719	2.69410×10^{-12}	1.19450×10^{-13}
822.362	5.52070×10^{-12}	2.44550×10^{-13}	854.523	2.64930×10^{-12}	1.17480×10^{-13}
823.166	5.40460×10^{-12}	2.39420×10^{-13}	855.327	2.60530×10^{-12}	1.15550×10^{-13}
823.970	5.29210×10^{-12}	2.34460×10^{-13}	856.131	2.56220×10^{-12}	1.13650×10^{-13}
824.774	5.18320×10^{-12}	2.29660×10^{-13}	856.935	2.51980×10^{-12}	1.11800×10^{-13}
825.578	5.07770×10^{-12}	2.25010×10^{-13}	857.739	2.47830×10^{-12}	1.09980×10^{-13}
826.382	4.97540×10^{-12}	2.20500×10^{-13}	858.543	2.43750×10^{-12}	1.08190×10^{-13}
827.186	4.87620×10^{-12}	2.16120×10^{-13}	859.347	2.39740×10^{-12}	1.06440×10^{-13}
827.990	4.77990×10^{-12}	2.11870×10^{-13}	860.151	2.35810×10^{-12}	1.04730×10^{-13}
828.794	4.68640×10^{-12}	2.07750×10^{-13}	860.955	2.31950×10^{-12}	1.03040×10^{-13}
829.598	4.59550×10^{-12}	2.03730×10^{-13}	861.759	2.28160×10^{-12}	1.01390×10^{-13}
830.402	4.50720×10^{-12}	1.99830×10^{-13}	862.563	2.24440×10^{-12}	9.97770×10^{-14}
831.206	4.42140×10^{-12}	1.96030×10^{-13}	863.367	2.20780×10^{-12}	9.81890×10^{-14}
832.010	4.33780×10^{-12}	1.92340×10^{-13}	864.171	2.17190×10^{-12}	9.66320×10^{-14}
832.814	4.25650×10^{-12}	1.88740×10^{-13}	864.975	2.13660×10^{-12}	9.51050×10^{-14}
833.618	4.17730×10^{-12}	1.85230×10^{-13}	865.779	2.10200×10^{-12}	9.36070×10^{-14}
834.422	4.10010×10^{-12}	1.81810×10^{-13}	866.583	2.06790×10^{-12}	9.21370×10^{-14}
835.226	4.02490×10^{-12}	1.78470×10^{-13}	867.387	2.03450×10^{-12}	9.06940×10^{-14}
836.030	3.95160×10^{-12}	1.75220×10^{-13}	868.191	2.00170×10^{-12}	8.92790×10^{-14}
836.834	3.88000×10^{-12}	1.72040×10^{-13}	868.995	1.96940×10^{-12}	8.78900×10^{-14}
837.638	3.81020×10^{-12}	1.68940×10^{-13}	869.799	1.93770×10^{-12}	8.65270×10^{-14}
838.442	3.74210×10^{-12}	1.65910×10^{-13}	870.603	1.90650×10^{-12}	8.51900×10^{-14}
839.246	3.67550×10^{-12}	1.62960×10^{-13}	871.407	1.87590×10^{-12}	8.38780×10^{-14}
840.050	3.61040×10^{-12}	1.60060×10^{-13}	872.211	1.84590×10^{-12}	8.25890×10^{-14}
840.854	3.54690×10^{-12}	1.57240×10^{-13}	873.015	1.81630×10^{-12}	8.13250×10^{-14}
841.658	3.48470×10^{-12}	1.54480×10^{-13}	873.819	1.78730×10^{-12}	8.00840×10^{-14}
842.462	3.42400×10^{-12}	1.51770×10^{-13}	874.623	1.75880×10^{-12}	7.88660×10^{-14}
843.266	3.36450×10^{-12}	1.49130×10^{-13}	875.427	1.73070×10^{-12}	7.76700×10^{-14}
844.070	3.30630×10^{-12}	1.46550×10^{-13}	876.231	1.70320×10^{-12}	7.64960×10^{-14}
844.874	3.24940×10^{-12}	1.44020×10^{-13}	877.035	1.67610×10^{-12}	7.53430×10^{-14}
845.678	3.19360×10^{-12}	1.41540×10^{-13}	877.839	1.64950×10^{-12}	7.42110×10^{-14}
846.482	3.13900×10^{-12}	1.39120×10^{-13}	878.643	1.62340×10^{-12}	7.31000×10^{-14}

Table A.38 (cont'd)

JD +2452000	*UVOIR* Flux	Flux error	JD +2452000	*UVOIR* Flux	Flux error
879.447	1.59770×10^{-12}	7.20090×10^{-14}	894.724	1.18490×10^{-12}	5.45900×10^{-14}
880.251	1.57240×10^{-12}	7.09370×10^{-14}	895.528	1.16660×10^{-12}	5.38240×10^{-14}
881.055	1.54760×10^{-12}	6.98850×10^{-14}	896.332	1.14870×10^{-12}	5.30710×10^{-14}
881.859	1.52320×10^{-12}	6.88520×10^{-14}	897.136	1.13110×10^{-12}	5.23310×10^{-14}
882.663	1.49920×10^{-12}	6.78370×10^{-14}	897.940	1.11380×10^{-12}	5.16030×10^{-14}
883.467	1.47560×10^{-12}	6.68400×10^{-14}	898.744	1.09670×10^{-12}	5.08880×10^{-14}
884.271	1.45250×10^{-12}	6.58610×10^{-14}	899.548	1.08000×10^{-12}	5.01840×10^{-14}
885.075	1.42970×10^{-12}	6.49000×10^{-14}	900.352	1.06350×10^{-12}	4.94920×10^{-14}
885.879	1.40730×10^{-12}	6.39550×10^{-14}	901.156	1.04730×10^{-12}	4.88120×10^{-14}
886.683	1.38530×10^{-12}	6.30270×10^{-14}	901.960	1.03130×10^{-12}	4.81430×10^{-14}
887.487	1.36370×10^{-12}	6.21150×10^{-14}	902.764	1.01570×10^{-12}	4.74850×10^{-14}
888.291	1.34250×10^{-12}	6.12190×10^{-14}	903.568	1.00030×10^{-12}	4.68380×10^{-14}
889.095	1.32160×10^{-12}	6.03390×10^{-14}	904.372	9.85110×10^{-13}	4.62020×10^{-14}
889.899	1.30100×10^{-12}	5.94740×10^{-14}	905.176	9.70210×10^{-13}	4.55760×10^{-14}
890.703	1.28080×10^{-12}	5.86250×10^{-14}	905.980	9.55550×10^{-13}	4.49600×10^{-14}
891.508	1.26100×10^{-12}	5.77890×10^{-14}	906.784	9.41140×10^{-13}	4.43540×10^{-14}
892.312	1.24150×10^{-12}	5.69690×10^{-14}	907.588	9.26960×10^{-13}	4.37590×10^{-14}
893.116	1.22230×10^{-12}	5.61620×10^{-14}	908.392	9.13020×10^{-13}	4.31720×10^{-14}
893.920	1.20340×10^{-12}	5.53690×10^{-14}	909.196	8.99310×10^{-13}	4.25950×10^{-14}

Bibliography

Ajhar, E. A., Tonry, J. L., Blakeslee, J. P., Riess, A. G., & Schmidt, B. P. 2001, ApJ, 559, 584

Altavilla, G., Fiorentino, G., Marconi, M., Musella, I., Cappellaro, E., Barbon, R., Benetti, S., Pastorello, A., Riello, M., Turatto, M., & Zampieri, L. 2004, MNRAS, 349, 1344

Arnett, D. 1996, Supernovae and nucleosynthesis. An investigation of the history of matter, from the Big Bang to the present (Princeton series in astrophysics, Princeton, NJ: Princeton University Press)

Arnett, W. D. 1982, ApJ, 253, 785

Arnett, W. D., Branch, D., & Wheeler, J. C. 1985, Nature, 314, 337

Baade, W. & Zwicky, F. 1934, Physical Review, 46, 76

Benetti, S., Meikle, P., Stehle, M., Altavilla, G., Desidera, S., Folatelli, G., Goobar, A., Mattila, S., Mendez, J., Navasardyan, H., Pastorello, A., Patat, F., Riello, M., Ruiz-Lapuente, P., Tsvetkov, D., Turatto, M., Mazzali, P., & Hillebrandt, W. 2004, MNRAS, 348, 261

Bennett, C. L., Hill, R. S., Hinshaw, G., Nolta, M. R., Odegard, N., Page, L., Spergel, D. N., Weiland, J. L., Wright, E. L., Halpern, M., Jarosik, N., Kogut, A., Limon, M., Meyer, S. S., Tucker, G. S., & Wollack, E. 2003, ApJS, 148, 97

Benz, W. 1997, in NATO ASIC Proc. 486: Thermonuclear Supernovae, 457

Benz, W., Cameron, A. G. W., Press, W. H., & Bowers, R. L. 1990, ApJ, 348, 647

Bessell, M. S. 1983, Publications of the Astronomical Society of the Pacific, 95, 480

—. 1990, Publications of the Astronomical Society of the Pacific, 102, 1181

—. 1999, Publications of the Astronomical Society of the Pacific, 111, 1426

Bessell, M. S., Castelli, F., & Plez, B. 1998, A&A, 337, 321

Blanchard, A., Douspis, M., Rowan-Robinson, M., & Sarkar, S. 2003, A&A, 412, 35

Blinnikov, S. 2004, private communication

Böhm-Vitense, E. 1997, AJ, 113, 13

Boughn, S. & Crittenden, R. 2004a, Nature, 427, 45

Boughn, S. P. & Crittenden, R. G. 2004b, ApJ, 612, 647

Bowers, E. J. C., Meikle, W. P. S., Geballe, T. R., Walton, N. A., Pinto, P. A., Dhillon, V. S., Howell, S. B., & Harrop-Allin, M. K. 1997, MNRAS, 290, 663

Brachwitz, F., Dean, D. J., Hix, W. R., Iwamoto, K., Langanke, K., Martínez-Pinedo, G., Nomoto, K., Strayer, M. R., Thielemann, F., & Umeda, H. 2000, ApJ, 536, 934

Brahe, T. 1573, De nova et nullius aevi memoria prius visa stella, iam pridem anno a NATO Christo 1572, mense Novembri primum conspecta, contemplatio mathematica. Hafniae, Laurentius. (Kopenhagen)

Branch, D. 1992, ApJ, 392, 35

—. 1998, ARA&A, 36, 17

Branch, D., Baron, E., Thomas, R. C., Kasen, D., Li, W., & Filippenko, A. V. 2004a, Publications of the Astronomical Society of the Pacific, 116, 903

Branch, D., Fisher, A., & Nugent, P. 1993, AJ, 106, 2383

Branch, D., Thomas, R. C., Baron, E., Kasen, D., Hatano, K., Nomoto, K., Filippenko, A. V., Li, W., & Rudy, R. J. 2004b, ApJ, 606, 413

Brown, G. E. & Bethe, H. A. 1994, ApJ, 423, 659

Candia, P., Krisciunas, K., Suntzeff, N. B., González, D., Espinoza, J., Leiton, R., Rest, A., Smith, R. C., Cuadra, J., Tavenner, T., Logan, C., Snider, K., Thomas, M., West, A. A., González, G., González, S., Phillips, M. M., Hastings, N. C., & McMillan, R. 2003, Publications of the Astronomical Society of the Pacific, 115, 277

Cappellaro, E., Mazzali, P. A., Benetti, S., Danziger, I. J., Turatto, M., della Valle, M., & Patat, F. 1997, A&A, 328, 203

Cayrel, R., Faurobert-Scholl, M., Feautrier, N., Spielfieldel, A., & Thevenin, F. 1996, ARA&A, 312, 549

Cohen, M., Walker, R. G., Carter, B., Hammersley, P., Kidger, M., & Noguchi, K. 1999, AJ, 117, 1864

Colgate, S. A. & McKee, C. 1969, ApJ, 157, 623

Colgate, S. A., Petschek, A. G., & Kriese, J. T. 1980, ApJL, 237, L81

Colina, L., Bohlin, R. C., & Castelli, F. 1996, AJ, 112, 307

Contardo, G. 2001, Technische Universität München Dissertation

Contardo, G., Leibundgut, B., & Vacca, W. D. 2000, A&A, 359, 876

Deng, J., Kawabata, K. S., Ohyama, Y., Nomoto, K., Mazzali, P. A., Wang, L., Jeffery, D. J., Iye, M., Tomita, H., & Yoshii, Y. 2004, ApJL, 605, L37

Eastman, R. G. 1997, in NATO ASIC Proc. 486: Thermonuclear Supernovae, 571

Elias, J. H., Frogel, J. A., Matthews, K., & Neugebauer, G. 1982, AJ, 87, 1029

Feldmeier, J., Jacoby, G., & Phillips, M. M. 2005, in preparation

Ferrarese, L., Mould, J. R., Kennicutt, R. C., Huchra, J., Ford, H. C., Freedman, W. L., Stetson, P. B., Madore, B. F., Sakai, S., Gibson, B. K., Graham, J. A., Hughes, S. M., Illingworth, G. D., Kelson, D. D., Macri, L., Sebo, K., & Silbermann, N. A. 2000, ApJ, 529, 745

Filippenko, A. V. 1997, ARA&A, 35, 309

Filippenko, A. V., Richmond, M. W., Branch, D., Gaskell, M., Herbst, W., Ford, C. H., Treffers, R. R., Matheson, T., Ho, L. C., Dey, A., Sargent, W. L. W., Small, T. A., & van Breugel, W. J. M. 1992, AJ, 104, 1543

Freedman, W. L., Madore, B. F., Gibson, B. K., Ferrarese, L., Kelson, D. D., Sakai, S., Mould, J. R., Kennicutt, R. C., Ford, H. C., Graham, J. A., Huchra, J. P., Hughes, S. M. G., Illingworth, G. D., Macri, L. M., & Stetson, P. B. 2001, ApJ, 553, 47

Gamezo, V. N. & Khokhlov, A. M. 2004, Physical Review Letters, 92, 211102

Garcia, A. M. 1993, A&A Suppl. Ser., 100, 47

García-Senz, D., Bravo, E., & Woosley, S. E. 1999, A&A, 349, 177

Garnavich, P. M., Bonanos, A. Z., Krisciunas, K., Jha, S., Kirshner, R. P., Schlegel, E. M., Challis, P., Macri, L. M., Hatano, K., Branch, D., Bothun, G. D., & Freedman, W. L. 2004, ApJ, 613, 1120

Georgii, R., Plüschke, S., Diehl, R., Lichti, G. G., Schönfelder, V., Bloemen, H., Hermsen, W., Ryan, J., & Bennett, K. 2002, A&A, 394, 517

Gibson, B. K., Stetson, P. B., Freedman, W. L., Mould, J. R., Kennicutt, R. C., Huchra, J. P., Sakai, S., Graham, J. A., Fassett, C. I., Kelson, D. D., Ferrarese, L., Hughes, S. M. G., Illingworth, G. D., Macri, L. M., Madore, B. F., Sebo, K. M., & Silbermann, N. A. 2000, ApJ, 529, 723

Golombek, I. & Niemeyer, J. C. 2005, accepted by A&A, astro-ph/0503617

Höflich, P. 1995, ApJ, 443, 89

Höflich, P. & Khokhlov, A. 1996, ApJ, 457, 500

Höflich, P., Khokhlov, A., Wheeler, J. C., Phillips, M. M., Suntzeff, N. B., & Hamuy, M. 1996, ApJL, 472, L81

Höflich, P. A. & et al. 1997, in NATO ASIC Proc. 486: Thermonuclear Supernovae, 659

Hamuy, M. 2003, ApJ, 582, 905

Hamuy, M., Maza, J., Pinto, P. A., Phillips, M. M., Suntzeff, N. B., Blum, R. D., Olsen, K. A. G., Pinfield, D. J., Ivanov, V. D., Augusteijn, T., Brillant, S., Chadid, M., Cuby, J.-G., Doublier, V., Hainaut, O. R., Le Floc'h, E., Lidman, C., Petr-Gotzens, M. G., Pompei, E., & Vanzi, L. 2002, AJ, 124, 417

Hamuy, M., Phillips, M. M., Maza, J., Suntzeff, N. B., Schommer, R. A., & Aviles, R. 1995, AJ, 109, 1

Hamuy, M., Phillips, M. M., Suntzeff, N. B., Maza, J., González, L. E., Roth, M., Krisciunas, K., Morrell, N., Green, E. M., Persson, S. E., & McCarthy, P. J. 2003, Nature, 424, 651

Hamuy, M., Phillips, M. M., Suntzeff, N. B., Schommer, R. A., Maza, J., Antezan, A. R., Wischnjewsky, M., Valladares, G., Muena, C., Gonzales, L. E., Aviles, R., Wells, L. A., Smith, R. C., Navarrete, M., Covarrubias, R., Williger, G. M., Walker, A. R., Layden, A. C., Elias, J. H., Baldwin, J. A., Hernandez, M., Tirado, H., Ugarte, P., Elston, R., Saavedra, N., Barrientos, F., Costa, E., Lira, P., Ruiz, M. T., Anguita, C., Gomez, X., Ortiz, P., della Valle, M., Danziger, J., Storm, J., Kim, Y.-C., Bailyn, C., Rubenstein, E. P., Tucker, D., Cersosimo, S., Mendez, R. A., Siciliano, L., Sherry, W., Chaboyer, B., Koopmann, R. A., Geisler, D., Sarajedini, A., Dey, A., Tyson, N., Rich, R. M., Gal, R., Lamontagne, R., Caldwell, N., Guhathakurta, P., Phillips, A. C., Szkody, P., Prosser, C., Ho, L. C., McMahan, R., Baggley, G., Cheng, K.-P., Havlen, R., Wakamatsu, K., Janes, K., Malkan, M., Baganoff, F., Seitzer, P., Shara, M., Sturch, C., Hesser, J., Hartig, A. N. P., Hughes, J., Welch, D., Williams, T. B., Ferguson, H., Francis, P. J., French, L., Bolte, M., Roth, J., Odewahn, S., Howell, S., & Krzeminski, W. 1996, AJ, 112, 2408

Hamuy, M., Pinto, P. A., Maza, J., Suntzeff, N. B., Phillips, M. M., Eastman, R. G., Smith, R. C., Corbally, C. J., Burstein, D., Li, Y., Ivanov, V., Moro-Martin, A., Strolger, L. G., de Souza, R. E., dos Anjos, S., Green, E. M., Pickering, T. E., González, L., Antezana, R., Wischnjewsky, M., Galaz, G., Roth, M., Persson, S. E., & Schommer, R. A. 2001, ApJ, 558, 615

Hamuy, M., Suntzeff, N. B., Bravo, J., & Phillips, M. M. 1990, Publications of the Astronomical Society of the Pacific, 102, 888

Hamuy, M., Suntzeff, N. B., Heathcote, S. R., Walker, A. R., Gigoux, P., & Phillips, M. M. 1994, Publications of the Astronomical Society of the Pacific, 106, 566

Hamuy, M., Walker, A. R., Suntzeff, N. B., Gigoux, P., Heathcote, S. R., & Phillips, M. M. 1992, Publications of the Astronomical Society of the Pacific, 104, 533

Harkness, R. 1991, in Supernova 1987A and other supernovae, ESO Conference and Workshop Proceedings, Proceedings of an ESO/EIPC Workshop, Marciana Marina, Isola d'Elba, September 17-22, 1990, Garching: European Southern Observatory (ESO), |c1991, edited by I. J. Danziger, and Kurt Kjär., 447

Hayes, D. S. 1970, ApJ, 159, 165

Hayes, D. S., Pasinetti, L. E., & Philip, A. G. D., eds. 1985, Calibration of fundamental stellar quantities; Proceedings of the Symposium, Como, Italy, May 24-29, 1984

Hernandez, M., Meikle, W. P. S., Aparicio, A., Benn, C. R., Burleigh, M. R., Chrysostomou, A. C., Fernandes, A. J. L., Geballe, T. R., Hammersley, P. L., Iglesias-Paramo, J., James, D. J., James, P. A., Kemp, S. N., Lister, T. A., Martinez-Delgado, D., Oscoz, A., Pollacco, D. L., Rozas, M., Smartt, S. J., Sorensen, P., Swaters, R. A., Telting, J. H., Vacca, W. D., Walton, N. A., & Zapatero-Osorio, M. R. 2000, MNRAS, 319, 223

Hillebrandt, W. & Niemeyer, J. C. 2000, ARA&A, 38, 191

Hoyle, F. & Fowler, W. A. 1960, ApJ, 132, 565

Iben, I. & Tutukov, A. V. 1984, ApJS, 54, 335

Iwamoto, K., Brachwitz, F., Nomoto, K., Kishimoto, N., Umeda, H., Hix, W. R., & Thielemann, F. 1999, ApJS, 125, 439

Jeffery, D. 1999, astro-ph/9907015

Jeffery, D. J., Leibundgut, B., Kirshner, R. P., Benetti, S., Branch, D., & Sonneborn, G. 1992, ApJ, 397, 304

Jha, S. 2002, Harvard University Dissertation

Jha, S., Garnavich, P. M., Kirshner, R. P., Challis, P., Soderberg, A. M., Macri, L. M., Huchra, J. P., Barmby, P., Barton, E. J., Berlind, P., Brown, W. R., Caldwell, N., Calkins, M. L., Kannappan, S. J., Koranyi, D. M., Pahre, M. A., Rines, K. J., Stanek, K. Z., Stefanik, R. P., Szentgyorgyi, A. H., Väisänen, P., Wang, Z., Zajac, J. M., Riess, A. G., Filippenko, A. V., Li, W., Modjaz, M., Treffers, R. R., Hergenrother, C. W., Grebel, E. K., Seitzer, P., Jacoby, G. H., Benson, P. J., Rizvi, A., Marschall, L. A., Goldader, J. D., Beasley, M., Vacca, W. D., Leibundgut, B., Spyromilio, J., Schmidt, B. P., & Wood, P. R. 1999, ApJS, 125, 73

Jones, M. E., Edge, A. C., & Grainge, E. 2001, astro-ph/0103046, submitted to MNRAS

Khokhlov, A. M. 1991, A&A, 245, 114

Kirshner, R. P., Jeffery, D. J., Leibundgut, B., Challis, P. M., Sonneborn, G., Phillips, M. M., Suntzeff, N. B., Smith, R. C., Winkler, P. F., Winge, C., Hamuy, M., Hunter, D. A., Roth, K. C., Blades, J. C., Branch, D., Chevalier, R. A., Fransson, C., Panagia, N., Wagoner, R. V., Wheeler, J. C., & Harkness, R. P. 1993, ApJ, 415, 589

Kotak, R., Meikle, W. P. S., Adamson, A., & Leggett, S. K. 2004, MNRAS, 354, L13

Kowal, C. T. 1968, AJ, 73, 1021

Kozma, C., Fransson, C., Hillebrandt, W., Travaglio, C., Sollerman, J., Reinecke, M., Roepke, F., & Spyromilio, J. 2005, A&A, astro-ph/0504317

Krisciunas, K., Hastings, N. C., Loomis, K., McMillan, R., Rest, A., Riess, A. G., & Stubbs, C. 2000, ApJ, 539, 658

Krisciunas, K., Phillips, M. M., Stubbs, C., Rest, A., Miknaitis, G., Riess, A. G., Suntzeff, N. B., Roth, M., Persson, S. E., & Freedman, W. L. 2001, AJ, 122, 1616

Krisciunas, K., Phillips, M. M., & Suntzeff, N. B. 2004a, ApJL, 602, L81

Krisciunas, K., Phillips, M. M., Suntzeff, N. B., Persson, S. E., Hamuy, M., Antezana, R., Candia, P., Clocchiatti, A., DePoy, D. L., Germany, L. M., Gonzalez, L., Gonzalez, S., Krzeminski, W., Maza, J., Nugent, P. E., Qiu, Y., Rest, A., Roth, M., Stritzinger, M., Strolger, L.-G., Thompson, I., Williams, T. B., & Wischnjewsky, M. 2004b, AJ, 127, 1664

Krisciunas, K., Suntzeff, N. B., Candia, P., Arenas, J., Espinoza, J., Gonzalez, D., Gonzalez, S., Höflich, P. A., Landolt, A. U., Phillips, M. M., & Pizarro, S. 2003, AJ, 125, 166

Krisciunas, K., Suntzeff, N. B., Phillips, M. M., Candia, P., Prieto, J. L., Antezana, R., Chassagne, R., Chen, H., Dickinson, M., Eisenhardt, P. R., Espinoza, J., Garnavich, P. M., González, D., Harrison, T. E., Hamuy, M., Ivanov, V. D., Krzemiński, W., Kulesa, C., McCarthy, P., Moro-Martín, A., Muena, C., Noriega-Crespo, A., Persson, S. E., Pinto, P. A., Roth, M., Rubenstein, E. P., Stanford, S. A., Stringfellow, G. S., Zapata, A., Porter, A., & Wischnjewsky, M. 2004c, AJ, 128, 3034

Kurucz, R. L., Furenlid, I., & Brault, J. T. L. 1984, Solar flux atlas from 296 to 1300 nm (National Solar Observatory Atlas, Sunspot, New Mexico: National Solar Observatory, 1984)

Landolot, A. U. 1999, private communication

Landolt, A. U. 1983, AJ, 88, 439

—. 1992a, AJ, 104, 372

—. 1992b, AJ, 104, 340

Langer, N., Deutschmann, A., Wellstein, S., & Höflich, P. 2000, A&A, 362, 1046

Leibundgut, B. 2000, ARA&A, 10, 179

—. 2001, ARA&A, 39, 67

—. 2004, A&A Suppl., 290, 29

Leibundgut, B., Kirshner, R. P., Phillips, M. M., Wells, L. A., Suntzeff, N. B., Hamuy, M., Schommer, R. A., Walker, A. R., Gonzalez, L., Ugarte, P., Williams, R. E., Williger, G., Gomez, M., Marzke, R., Schmidt, B. P., Whitney, B., Coldwell, N., Peters, J., Chaffee, F. H., Foltz, C. B., Rehner, D., Siciliano, L., Barnes, T. G., Cheng, K.-P., Hintzen, P. M. N., Kim, Y.-C., Maza, J., Parker, J. W., Porter, A. C., Schmidtke, P. C., & Sonneborn, G. 1993, AJ, 105, 301

Leibundgut, B. & Pinto, P. A. 1992, ApJ, 401, 49

Leibundgut, B. & Suntzeff, N. B. 2003, LNP Vol. 598: Supernovae and Gamma-Ray Bursters, 598, 77

Li, W., Filippenko, A. V., Chornock, R., Berger, E., Berlind, P., Calkins, M. L., Challis, P., Fassnacht, C., Jha, S., Kirshner, R. P., Matheson, T., Sargent, W. L. W., Simcoe, R. A., Smith, G. H., & Squires, G. 2003, Publications of the Astronomical Society of the Pacific, 115, 453

Li, W., Filippenko, A. V., Gates, E., Chornock, R., Gal-Yam, A., Ofek, E. O., Leonard, D. C., Modjaz, M., Rich, R. M., Riess, A. G., & Treffers, R. R. 2001, Publications of the Astronomical Society of the Pacific, 113, 1178

Li, W. D., Filippenko, A. V., Riess, A. G., Treffers, R. R., Hu, J. Y., & Qiu, Y. L. 2000, in American Institute of Physics Conference Series, 91–94

Li, W. D., Qiu, Y. L., Qiao, Q. Y., Zhu, X. H., Hu, J. Y., Richmond, M. W., Filippenko, A. V., Treffers, R. R., Peng, C. Y., & Leonard, D. C. 1999, AJ, 117, 2709

Lira, P., Suntzeff, N. B., Phillips, M. M., Hamuy, M., Maza, J., Schommer, R. A., Smith, R. C., Wells, L. A., Avilés, R., Baldwin, J. A., Elias, J. H., González, L., Layden, A., Navarrete, M., Ugarte, P., Walker, A. R., Williger, G. M., Baganoff, F. K., Crotts, A. P. S., Rich, R. M., Tyson, N. D., Dey, A., Guhathakurta, P., Hibbard, J., Kim, Y.-C., Rehner, D. M., Siciliano, E., Roth, J., Seitzer, P., & Williams, T. B. 1998, AJ, 115, 234

Livingston, W. & Wallace, L. 1991, NSO Technical Report, Tucson: National Solar Observatory, National Optical Astronomy Observatory

Livio, M. 2000, in Type Ia Supernovae, Theory and Cosmology. Edited by J. C. Niemeyer and J. W. Truran. Published by Cambridge University Press, 2000., 33

Livio, M., Donahue, M., & Panagia, N. 1997, in The Extragalactic Distance Scale

Livne, E. & Arnett, D. 1995, ApJ, 452, 62

Lundmark, K. 1920, Svenska Vetenkapsakad. Handl, 60, 8

Madore, B. F. & Freedman, W. L. 1991, Publications of the Astronomical Society of the Pacific, 103, 933

Madore, B. F., Freedman, W. L., Silbermann, N., Harding, P., Huchra, J., Mould, J. R., Graham, J. A., Ferrarese, L., Gibson, B. K., Han, M., Hoessel, J. G., Hughes, S. M., Illingworth, G. D., Phelps, R., Sakai, S., & Stetson, P. 1999, ApJ, 515, 29

Marion, G. H., Höflich, P., Vacca, W. D., & Wheeler, J. C. 2003, ApJ, 591, 316

Mason, B. S., Myers, S. T., & Readhead, A. C. S. 2001, ApJL, 555, L11

Massey, P., Strobel, K., Barnes, J. V., & Anderson, E. 1988, ApJ, 328, 315

Mazzali, P. A. 2001, MNRAS, 321, 341

Mazzali, P. A., Danziger, I. J., & Turatto, M. 1995, A&A, 297, 509

Meikle, W. P. S. 2000, MNRAS, 314, 782

Meikle, W. P. S., Bowers, E. J. C., Geballe, T. R. Walton, N. A., R., L. J., & Cumming, R. J. 1997, in NATO ASIC Proc. 486: Thermonuclear Supernovae, 53

Meikle, W. P. S., Cumming, R. J., Geballe, T. R., Lewis, J. R., Walton, N. A., Balcells, M., Cimatti, A., Croom, S. M., Dhillon, V. S., Economou, F., Jenkins, C. R., Knapen, J. H., Meadows, V. S., Morris, P. W., Perez-Fournon, I., Shanks, T., Smith, L. J., Tanvir, N. R., Veilleux, S., Vilchez, J., Wall, J. V., & Lucey, J. R. 1996, MNRAS, 281, 263

Menzies, J. W. 1989, MNRAS, 237, 21P

Milne, P. A., The, L.-S., & Leising, M. D. 1999, ApJS, 124, 503

—. 2001, ApJ, 559, 1019

Minkowski, R. 1941, Publications of the Astronomical Society of the Pacific, 53, 224

Mitton, S. 1979, Crab Nebula (Simon and Schuster Adult Publishing Group)

Mochkovitch, R. 1997, in NATO ASIC Proc. 486: Thermonuclear Supernovae, 187

Modjaz, M., Li, W., Filippenko, A. V., King, J. Y., Leonard, D. C., Matheson, T., Treffers, R. R., & Riess, A. G. 2001, Publications of the Astronomical Society of the Pacific, 113, 308

Myers, S. T., Baker, J. E., Readhead, A. C. S., Leitch, E. M., & Herbig, T. 1997, ApJ, 485, 1

Nadyozhin, D. K. 1994, ApJS, 92, 527

Nomoto, K. 1980, Space Science Reviews, 27, 563

—. 1982, ApJ, 253, 798

Nomoto, K., Thielemann, F.-K., & Yokoi, K. 1984, ApJ, 286, 644

Nugent, P., Branch, D., Baron, E., Fisher, A., Vaughan, T., & Hauschildt, P. H. 1995, Physical Review Letters, 75, 394

Pankey, T. 1962, Howard University Dissertation

Parodi, B. R., Saha, A., Sandage, A., & Tammann, G. A. 2000, ApJ, 540, 634

Patat, F., Benetti, S., Cappellaro, E., Danziger, I. J., della Valle, M., Mazzali, P. A., & Turatto, M. 1996, MNRAS, 278, 111

Percival, W. J., Baugh, C. M., Bland-Hawthorn, J., Bridges, T., Cannon, R., Cole, S., Colless, M., Collins, C., Couch, W., Dalton, G., De Propris, R., Driver, S. P., Efstathiou, G., Ellis, R. S., Frenk, C. S., Glazebrook, K., Jackson, C., Lahav, O., Lewis, I., Lumsden, S., Maddox, S., Moody, S., Norberg, P., Peacock, J. A., Peterson, B. A., Sutherland, W., & Taylor, K. 2001, MNRAS, 327, 1297

Perlmutter, S., Aldering, G., Goldhaber, G., Knop, R. A., Nugent, P., Castro, P. G., Deustua, S., Fabbro, S., Goobar, A., Groom, D. E., Hook, I. M., Kim, A. G., Kim, M. Y., Lee, J. C., Nunes, N. J., Pain, R., Pennypacker, C. R., Quimby, R., Lidman, C., Ellis, R. S., Irwin, M., McMahon, R. G., Ruiz-Lapuente, P., Walton, N., Schaefer, B., Boyle, B. J., Filippenko, A. V., Matheson, T., Fruchter, A. S., Panagia, N., Newberg, H. J. M., Couch, W. J., & The Supernova Cosmology Project. 1999, ApJ, 517, 565

Perlmutter, S., Gabi, S., Goldhaber, G., Goobar, A., Groom, D. E., Hook, I. M., Kim, A. G., Kim, M. Y., Lee, J. C., Pain, R., Pennypacker, C. R., Small, I. A., Ellis, R. S., McMahon, R. G., Boyle, B. J., Bunclark, P. S., Carter, D., Irwin, M. J., Glazebrook, K., Newberg, H. J. M., Filippenko, A. V., Matheson, T., Dopita, M., Couch, W. J., & The Supernova Cosmology Project. 1997, ApJ, 483, 565

Persson, S. E., Murphy, D. C., Krzeminski, W., Roth, M., & Rieke, M. J. 1998, AJ, 116, 2475

Phillips, M. 2004, private communication

Phillips, M. M. 1993, ApJL, 413, L105

Phillips, M. M., Krisciunas, K., Suntzeff, N. B., Roth, M., Germany, L., Candia, P., Gonzalez, S., Hamuy, M., Freedman, W. L., Persson, S. E., Nugent, P. E., Aldering, G., & Conley, A. 2003, in From Twilight to Highlight: The Physics of Supernovae, 193–+

Phillips, M. M., Lira, P., Suntzeff, N. B., Schommer, R. A., Hamuy, M., & Maza, J. 1999, AJ, 118, 1766

Piersanti, L., Gagliardi, S., Iben, I. J., & Tornambé, A. 2003, ApJ, 583, 885

Pignata, G., Patat, F., Benetti, S., Blinnikov, S., Hillebrandt, W., Kotak, R., Leibundgut, B., Mazzali, P. A., Meikle, P., Qiu, Y., Ruiz-Lapuente, P., Smartt, S. J., Sorokina, E., Stritzinger, M., Stehle, M., Turatto, M., Marsh, T., Martin-Luis, F., McBride, N., Mendez, J., Morales-Rueda, L., Narbutis, D., & Street, R. 2004, MNRAS, 355, 178

Pinto, P. A. & Eastman, R. G. 2000a, ApJ, 530, 744

—. 2000b, ApJ, 530, 757

—. 2001, New Astronomy, 6, 307

Prieto, J. L., Rest, A., & Suntzeff, N. B. 2005, in preparation

Röpke, F. K. & Hillebrandt, W. 2004, A&A, 420, L1

—. 2005, A&A, 431, 635

Reese, E. D. 2004, in Measuring and Modeling the Universe, 138

Reese, E. D., Carlstrom, J. E., Joy, M., Mohr, J. J., Grego, L., & Holzapfel, W. L. 2002, ApJ, 581, 53

Regnault, N. 2000, Université Paris-Sud Dissertation

Reinecke, M., Hillebrandt, W., & Niemeyer, J. C. 2002a, A&A, 386, 936

—. 2002b, A&A, 391, 1167

Richmond, M. W., Treffers, R. R., Filippenko, A. V., van Dyk, S. D., Paik, Y., Peng, C., Marschall, L. A., Laaksonen, B. D., Macintosh, B., & McLean, I. S. 1995, AJ, 109, 2121

Riess, A. G., Filippenko, A. V., Challis, P., Clocchiatti, A., Diercks, A., Garnavich, P. M., Gilliland, R. L., Hogan, C. J., Jha, S., Kirshner, R. P., Leibundgut, B., Phillips, M. M., Reiss, D., Schmidt, B. P., Schommer, R. A., Smith, R. C., Spyromilio, J., Stubbs, C., Suntzeff, N. B., & Tonry, J. 1998, AJ, 116, 1009

Riess, A. G., Filippenko, A. V., Li, W., Treffers, R. R., Schmidt, B. P., Qiu, Y., Hu, J., Armstrong, M., Faranda, C., Thouvenot, E., & Buil, C. 1999a, AJ, 118, 2675

Riess, A. G., Kirshner, R. P., Schmidt, B. P., Jha, S., Challis, P., Garnavich, P. M., Esin, A. A., Carpenter, C., Grashius, R., Schild, R. E., Berlind, P. L., Huchra, J. P., Prosser, C. F., Falco, E. E., Benson, P. J., Briceño, C., Brown, W. R., Caldwell, N., dell'Antonio, I. P., Filippenko, A. V., Goodman, A. A., Grogin, N. A., Groner, T., Hughes, J. P., Green, P. J., Jansen, R. A., Kleyna, J. T., Luu, J. X., Macri, L. M., McLeod, B. A., McLeod, K. K., McNamara, B. R., McLean, B., Milone, A. A. E., Mohr, J. J., Moraru, D., Peng, C., Peters, J., Prestwich, A. H., Stanek, K. Z., Szentgyorgyi, A., & Zhao, P. 1999b, AJ, 117, 707

Riess, A. G., Li, W., Stetson, P. B., Filippenko, A. V., Jha, S., Kirshner, R. P., Challis, P. M., Garnavich, P. M., & Chornock, R. 2005, ApJ, 627, 579

Riess, A. G., Press, W. H., & Kirshner, R. P. 1996, ApJ, 473, 88

Ruiz-Lapuente, P., Cappellaro, E., Turatto, M., Gouiffes, C., Danziger, I. J., della Valle, M., & Lucy, L. B. 1992, ApJL, 387, L33

Ruiz-Lapuente, P., Comeron, F., Méndez, J., Canal, R., Smartt, S. J., Filippenko, A. V., Kurucz, R. L., Chornock, R., Foley, R. J., Stanishev, V., & Ibata, R. 2004, Nature, 431, 1069

Ruiz-Lapuente, P. & Spruit, H. C. 1998, ApJ, 500, 360

Saha, A., Sandage, A., Tammann, G. A., Dolphin, A. E., Christensen, J., Panagia, N., & Macchetto, F. D. 2001a, ApJ, 562, 314

Saha, A., Sandage, A., Tammann, G. A., Labhardt, L., Macchetto, F. D., & Panagia, N. 1999, ApJ, 522, 802

Saha, A., Sandage, A., Thim, F., Labhardt, L., Tammann, G. A., Christensen, J., Panagia, N., & Macchetto, F. D. 2001b, ApJ, 551, 973

Saio, H. & Nomoto, K. 1985, A&A, 150, L21

—. 2004, ApJ, 615, 444

Salvo, M. E., Cappellaro, E., Mazzali, P. A., Benetti, S., Danziger, I. J., Patat, F., & Turatto, M. 2001, MNRAS, 321, 254

Sandage, A. & Tammann, G. A. 1993, ApJ, 415, 1

Schlegel, D. J., Finkbeiner, D. P., & Davis, M. 1998, ApJ, 500, 525

Shanks, T. 2005, in Maps of the Cosmos, ASP Conf. Ser., Eds. M. Colless and L. Staveley-Smith

Smith, C. 2000, private communication

Sollerman, J., Lindahl, J., Kozma, C., Challis, P., Filippenko, A. V., Fransson, C., Garnavich, P. M., Leibundgut, B., Li, W., Lundqvist, P., Milne, P., Spyromilio, J., & Kirshner, R. P. 2004, A&A, 428, 555

Spergel, D. N., Verde, L., Peiris, H. V., Komatsu, E., Nolta, M. R., Bennett, C. L., Halpern, M., Hinshaw, G., Jarosik, N., Kogut, A., Limon, M., Meyer, S. S., Page, L., Tucker, G. S., Weiland, J. L., Wollack, E., & Wright, E. L. 2003, ApJS, 148, 175

Stanishev, V. 2005, in preparation

Stebbins, J. & Kron, G. E. 1957, ApJ, 126, 266

Stehle, M., Mazzali, P. A., Benetti, S., & Hillebrandt, W. 2005, MNRAS, 360, 1231

Stetson, P. B. & Gibson, B. K. 2001, MNRAS, 328, L1

Stritzinger, M., Hamuy, M., Suntzeff, N. B., Smith, R. C., Phillips, M. M., Maza, J., Strolger, L.-G., Antezana, R., González, L., Wischnjewsky, M., Candia, P., Espinoza, J., González, D., Stubbs, C., Becker, A. C., Rubenstein, E. P., & Galaz, G. 2002, AJ, 124, 2100

Stritzinger, M. D., Suntzeff, N. B., Hamuy, M., Challis, P., Demarco, R., Germany, L., & Soderberg, A. M. 2005, Publications of the Astronomical Society of the Pacific, 117, 810

Strolger, L.-G., Smith, R. C., Suntzeff, N. B., Phillips, M. M., Aldering, G., Nugent, P., Knop, R., Perlmutter, S., Schommer, R. A., Ho, L. C., Hamuy, M., Krisciunas, K., Germany, L. M., Covarrubias, R., Candia, P., Athey, A., Blanc, G., Bonacic, A., Bowers, T., Conley, A., Dahlén, T., Freedman, W., Galaz, G., Gates, E., Goldhaber, G., Goobar, A., Groom, D., Hook, I. M., Marzke, R., Mateo, M., McCarthy, P., Méndez, J., Muena, C., Persson, S. E., Quimby, R., Roth, M., Ruiz-Lapuente, P., Seguel, J., Szentgyorgyi, A., von Braun, K., Wood-Vasey, W. M., & York, T. 2002, AJ, 124, 2905

Suntzeff, N. B. 1996, in IAU Colloq. 145: Supernovae and Supernova Remnants, 41

Suntzeff, N. B. 2000, in American Institute of Physics Conference Series, 65–74

Suntzeff, N. B. 2003, in From Twilight to Highlight: The Physics of Supernovae, 183

Suntzeff, N. B., Hamuy, M., Martin, G., Gomez, A., & Gonzalez, R. 1988, AJ, 96, 1864

Suntzeff, N. B., Phillips, M. M., Covarrubias, R., Navarrete, M., Pérez, J. J., Guerra, A., Acevedo, M. T., Doyle, L. R., Harrison, T., Kane, S., Long, K. S., Maza, J., Miller, S., Piatti, A. E., Clariá, J. J., Ahumada, A. V., Pritzl, B., & Winkler, P. F. 1999, AJ, 117, 1175

Sutherland, P. G. & Wheeler, J. C. 1984, ApJ, 280, 282

Swartz, D. A., Sutherland, P. G., & Harkness, R. P. 1995, ApJ, 446, 766

Tammann, G. A. & Leibundgut, B. 1990, A&A, 236, 9

Tammann, G. A. & Reindl, B. 2002, A&A Suppl., 280, 165

Taylor, B. J. 1984, ApJS, 54, 259

Thielemann, F.-K., Brachwitz, F., Höflich, P., Martinez-Pinedo, G., & Nomoto, K. 2004, New Astronomy Review, 48, 605

Thim, F., Tammann, G. A., Saha, A., Dolphin, A., Sandage, A., Tolstoy, E., & Labhardt, L. 2003, ApJ, 590, 256

Thomas, R. C., Branch, D., Baron, E., Nomoto, K., Li, W., & Filippenko, A. V. 2004, ApJ, 601, 1019

Tonry, J. L., Blakeslee, J. P., Ajhar, E. A., & Dressler, A. 1997, ApJ, 475, 399

Tonry, J. L., Dressler, A., Blakeslee, J. P., Ajhar, E. A., Fletcher, A. B., Luppino, G. A., Metzger, M. R., & Moore, C. B. 2001, ApJ, 546, 681

Tonry, J. L., Schmidt, B. P., Barris, B., Candia, P., Challis, P., Clocchiatti, A., Coil, A. L., Filippenko, A. V., Garnavich, P., Hogan, C., Holland, S. T., Jha, S., Kirshner, R. P., Krisciunas, K., Leibundgut, B., Li, W., Matheson, T., Phillips, M. M., Riess, A. G., Schommer, R., Smith, R. C., Sollerman, J., Spyromilio, J., Stubbs, C. W., & Suntzeff, N. B. 2003, ApJ, 594, 1

Travaglio, C., Hillebrandt, W., Reinecke, M., & Thielemann, F.-K. 2004, A&A, 425, 1029

Turatto, M., Benetti, S., Cappellaro, E., Danziger, I. J., della Valle, M., Gouiffes, C., Mazzali, P. A., & Patat, F. 1996, MNRAS, 283, 1

Udalski, A., Wyrzykowski, L., Pietrzynski, G., Szewczyk, O., Szymanski, M., Kubiak, M., Soszynski, I., & Zebrun, K. 2001, Acta Astronomica, 51, 221

Vacca, W. D. & Leibundgut, B. 1996, ApJL, 471, L37

Vacca, W. D. & Leibundgut, B. 1997, in NATO ASIC Proc. 486: Thermonuclear Supernovae, 65

Valentini, G., Di Carlo, E., Massi, F., Dolci, M., Arkharov, A. A., Larionov, V. M., Pastorello, A., Di Paola, A., Benetti, S., Cappellaro, E., Turatto, M., Pedichini, F., D'Alessio, F., Caratti o Garatti, A., Li Causi, G., Speziali, R., Danziger, I. J., & Tornambé, A. 2003, ApJ, 595, 779

van den Bergh, S., Li, W., & Filippenko, A. V. 2005, Publications of the Astronomical Society of the Pacific, 117, 773

Vinkó, J., Csák, B., Csizmadia, S., Fürész, G., Kiss, L. L., Sárneczky, K., Szabó, G., Sziládi, K., & Bíró, I. B. 2001, A&A, 372, 824

Weaver, T. A. & Woosley, S. E. 1980, in AIP Conf. Proc. 63: Supernovae Spectra, 15

Webbink, R. F. 1984, ApJ, 277, 355

Wells, L. A., Phillips, M. M., Suntzeff, B., Heathcote, S. R., Hamuy, M., Navarrete, M., Fernandez, M., Weller, W. G., Schommer, R. A., Kirshner, R. P., Leibundgut, B., Willner, S. P., Peletier, S. P., Schlegel, E. M., Wheeler, J. C., Harkness, R. P., Bell, D. J., Matthews, J. M., Filippenko, A. V., Shields, J. C., Richmond, M. W., Jewitt, D., Luu, J., Tran, H. D., Appleton, P. N., Robson, E. I., Tyson, J. A., Guhathakurta, P., Eder, J. A., Bond, H. E., Potter, M., Veilleux, S., Porter, A. C., Humphreys, R. M., Janes, K. A., Williams, T. B., Costa, E., Ruiz, M. T., Lee, J. T., Lutz, J. H., Rich, R. M., Winkler, P. F., & Tyson, N. D. 1994, AJ, 108, 2233

Wheeler, J. C. & Harkness, R. P. 1990, Reports of Progress in Physics, 53, 1467

Wilson, O. C. 1939, ApJ, 90, 634

Woosley, S. E. 1991, in AIP Conf. Proc. 232: Gamma-Ray Line Astrophysics, 270–290

Woosley, S. E. & Weaver, T. A. 1986, ARA&A, 24, 205

—. 1994a, ApJ, 423, 371

Woosley, S. E., Weaver, T. A., & Taam, R. E. 1980, in Texas Workshop on Type I Supernovae, 96–112

Woosley, S. W. 1990, in Supernovae, ed. A. Petschek (Berlin: Springer-Verlag), 182

Woosley, S. W. & Weaver, T. A. 1994b, in Supernovae, Les Houches Session LIV, ed. J. Audouze, S. Bludman, R. Mochovitch, & J. Zinn-Justion (Amsterdam: Elsevier), 63

Yoon, S.-C. & Langer, N. 2005, A&A, 435, 967

Yoon, S.-C., Langer, N., & Scheithauer, S. 2004, A&A, 425, 217

Zwicky, F. 1935, Sci. Mon., 40, 461

—. 1939, Physical Review, 55, 726

Acknowledgments

I am grateful to my Doktorvater Wolfgang Hillebrandt for hosting me at the MPA and providing me with a three year fellowship via the International Max Planck Research School on Astrophysics at the Technische Universität München. A very special thanks goes to my supervisor Bruno Leibundgut. It has been a wonderful pleasure to work with Bruno. He is a fine gentleman and I thank him for his strong mentor-ship and steadfast support.

A warm hearted thanks to Mario Hamuy and Nicholas Suntzeff for introducing me to this exciting field of astrophysics. A part of their strong passion and excitement to research SNe has worn off on me. Thank you for sharing your time and knowledge with me.

There are number of people whom I have enjoyed critical discussions that have made many parts of this work possible and pleasurable. In Munich they include: Stephanie Walch, Gert Hütsi, Jen Chubla, Sergei Blinnikov, Paolo Mazzali and Fritz Röpke. While in Chile I appreciated helpful conversations with Mark Phillips and the flamboyant Kevin Krisciunas.

For the Landolt standard stars work I thank the coauthors of the resultant published paper. They include Nicholas Suntzeff, Mario Hamuy, Peter Challis, Ricardo Demarco, Lisa Germany, and A. M. Soderberg. A special thanks goes to Arlo Landolt for providing us updated values for the spectrophotometric standards. We acknowledge Mike Bessell, Kevin Krisciunas, Brian Schmidt, Eric Persson, and Fiorella Castelli for helpful discussions on photometry and spectrophotometry. I also acknowledge financial support for this project from the HST grant GO-07505.02-96A.

This research has made use of the NASA/IPAC Extragalactic Database (NED), which is operated by the Jet Propulsion Laboratory, California Institute of Technology, under contract with the National Aeronautics and Space Administration.

Finally I acknowledge my parents for their continuing support. They have been my guiding light.

München Deutschland, September 9th, 2005.